The Influence of Sulphidizing Attack on the Mechanism of Failure of Coated Superalloy Under Cyclic Loading Conditions

by

G. Govender

Submitted in fulfilment of the academic requirements for the degree of PHD in Mechanical Engineering in the Department of Mechanical Engineering, University of Natal, Durban.

January 1998

ABSTRACT

A systematic study of the effect of sulphidizing atmosphere on the High Temperature Low Cycle Fatigue (HTLCF) properties of coated and uncoated unidirectionally solidified MAR-M002 nickel base superalloy was performed at 870°C. The coating systems investigated were, aluminide coating, three types of platinum modified aluminide coatings, and platinum coating.

The creep-plasticity mode of the strain range partitioning method was used for creep-fatigue loading. A constant loading regime (Strain range 6.6×10^{-3}) was used to test the samples in argon, air and Ar + 5%SO_2 and a lower strain range of 3.8×10^{-3} was used to investigate the creep-fatigue properties in Ar + 5%SO_2 only. The results were analysed using scanning electron microscopy including spot analyses (SEM-EDS), Auger electron spectroscopy (AES) and X-ray diffraction (XRD) techniques.

The synergistic effect of sulphidizing environment and the creep fatigue loading (Strain range - 0.66%) resulted in accelerated failure in all the materials systems tested, except for the TYPE I platinum aluminide coated sample. This coating displayed a "self-healing" mechanism which enhanced its fatigue life under sulphidizing conditions.

In general, the coatings had an adverse effect on the fatigue properties of the material systems. This was due to the poor mechanical properties of the coating. The mechanical properties of the coating was influenced by the coating microstructure and the chemical composition. The modification of the NiAl zone with platinum in the platinum aluminide coatings improved the fatigue properties of the coating by altering the crack propagation mechanism in the NiAl zone. The higher the platinum content in this region the more brittle it became.

The platinum modified aluminide coating showed an improvement in the corrosion fatigue properties in the SO_2 containing environment at the higher strain range when compared with the uncoated, aluminide coated and platinum coated samples.

However, at the lower strain range all the coating systems performed worse than the uncoated alloy. This was mainly due to the brittle failure of the coating. The platinum modified aluminides performed the worst due to the presence of brittle platinum aluminide phases.

The interdiffusion and interaction of platinum with the substrate alloying elements, resulted in this coating being ineffective for corrosion protection. The resultant coating layer produced poor corrosion-fatigue properties.

Although the coating systems did show evidence of resistance to sulphidation and oxidation there were relatively ineffective under the combination of sulphidizing environment and fatigue loading due to their poor mechanical properties.

The mechanism of sulphidation was consistent for all the material systems tested with oxidation proceeding first and sulphidation proceeding at the corrosion scale/substrate interface. The crack propagation in the coating and substrate was controlled by the sulphidation attack at the crack tip and failure of the oxide scales formed in the cracks.

DECLARATION

I hereby declare that this thesis is my original work except where due acknowledgements have been made. It has not been submitted before for any degree or examination to any other University.

Signed : _____

G. Govender

Date : _____

ACKNOWLEDGEMENTS

I would like to thank the following people for their assistance and support:

Dr N. Comins and the CSIR for supporting the research programme.

Prof. E. Aghion for his encouragement and for supervising the project.

Ross Pennefather and those staff at the CSIR who assisted with the preparation of the samples for fatigue testing, my literature review and in obtaining a better understanding of the coating processes.

Wynand for his assistance with AES analysis done at the CSIR.

Jeff Ferreira for assisting with the experiments and his encouragement.

Paddy for the development and printing of all the photographs and for his words of encouragement when things did not go well.

Feona and Phil for their assistance with the SEM work done at UND.

Mike and Yogus for assistance with the SEM work done at UDW.

Dr Dunlevey for his assistance with the XRD analysis.

The staff at the Department of Mechanical Engineering, UND, for their assistance during the course of the degree.

Vicky for her friendship and help with the thesis.

Nalini and Diresh for providing me with a place to stay close to university for the times when I was spending long hours on the thesis.

My sisters Manogeri and Sarojini for their assistance with the thesis.

And finally my parents and family for their support, patience and encouragement during the course of the degree.

TABLE OF CONTENTS

LIST OF FIGURES

LIST OF TABLES

INTRODUCTION

The fuel-efficiency and performance of jet engines are determined by how high a temperature they can work at, however, the temperature at which these engines operate are limited by the materials available. "The turbine vanes and blades of the modern jet engines are made of metal alloys having a high melting point." [1] Nickel based superalloys are the most widely used alloys for this application because of their relatively high melting points and high temperature strength.

These alloys are required to work under one of the most demanding environments. Three essential properties are required besides the high melting point: good resistance to thermal fatigue, creep and high temperature corrosion in the form of oxidation, hot corrosion and sulphidation. The development of processing techniques, directional solidification and single crystal castings, significantly improved the high temperature properties of superalloys. However, these alloys were still found to be susceptible to high temperature corrosion, particularly hot corrosion and sulphidation. This led to the inception of surface coating systems in order to provide protection against corrosion.

Three basic coating systems were developed: diffusion coatings, overlay coatings and thermal barrier coatings (TBC). The "first" of the coating systems developed was the diffusion coatings which enriched the surface of the alloy with reactive elements chromium, aluminium and/or silicon. Of the diffusion coatings, the most commonly used was the aluminide coating. The coating provided a reservoir of aluminium which formed the protective oxide scale. The overlay coatings are more advanced and can be designed for specific environmental conditions while the TBC effectively insulated the material from the high temperature gaseous environment, resulting in the alloy operating temperature being significantly lower. Although the aluminide coating provide good resistance to oxidation it was found to be susceptible to hot corrosion environments. This resulted in the development of the modified aluminide coatings which included the silicon modified aluminides, chromium modified aluminides and platinum modified aluminides. Of the modified aluminide coatings, the platinum modified aluminides are the most popular. These coatings provide a cheaper alternative to the overlay and thermal barrier coatings.

The platinum modified aluminides have been shown to improve the high temperature oxidation and hot corrosion properties over the conventional aluminides. However, even though the coatings may be able to provide adequate resistance to corrosion, they have to maintain their structural integrity under mechanical loading. Several studies on the mechanical properties of coating systems have indicated that the coating layer displayed very brittle properties [2- 16] with the coating failing under relatively low strains. Failure of the coating due to mechanical loading resulted in the substrate being exposed to the environment and hence the coating was not performing the function it was intended to.

There are few reported studies on the effect of environment on the high temperature low cycle fatigue (HTLCF) of coated superalloys. Studies on the HTLCF of aluminide coated nickel based superalloy revealed that under low cycle loading conditions brittle fracture of the coating had occurred resulting in the premature failure of the sample [17].

Due to the lack of data on the combined effect of HTLCF and corrosive environment, a systematic study of the HTLCF of platinum aluminide coated , aluminide coated, platinum coated and uncoated unidirectionally solidified MAR-M002 nickel base superalloy in air, argon and Ar + 5% SO_2 at 870°C was undertaken.

CHAPTER 1

1. LITERATURE REVIEW

1.1 INTRODUCTION

Superalloys are the most widely used alloys for high temperature applications. These alloys can be subdivided into three categories: nickel-base, cobalt-base and iron-base superalloys [18]. Superalloys are used at a higher proportion of their melting temperature than any other alloy system. The development of superalloys was instrumental in the progress attained in jet engine performance. In turn, the need for more powerful and efficient engines has been the driving force for the development of superalloys [18].

Of the three major groups of superalloys, nickel-base superalloys are the most widely used in gas turbine engines by virtue of their excellent high temperature strength. The high temperature strength and corrosion resistance was mainly dependent on two factors, namely the composition and microstructure. This chapter shall serve to give some insight into the development of the microstructure, the effect of alloying elements on the strength and corrosion properties of nickel-base superalloys and the use of coating to improve the high temperature corrosion properties.

1.2 Nickel Base Superalloys

1.2.1 Introduction

Nickel base superalloys are the most complex and widely used alloys in the hot section of gas turbine engines [19]. Their microstructure, physical and mechanical properties are strongly dependent on the chemical composition and processing technique. The advent of vacuum melting around 1950 led to the alloys of higher purity, closer control of reactive strengthening and oxidation resistant elements; improvement in the total alloy density, and the casting of relatively complex shapes [18].

During the 1950's and 1960's [18] development of alloys flourished. However, this led to problems of hot corrosion and the precipitation of brittle phases like sigma, mu, and laves which weakened the alloy. This initiated the development of processing techniques and in the 1960's Pratt and Whitney developed directional solidified blades [18]. The directional solidification process was developed further to produce single crystal components and directionally solidified eutectics [18].

In parallel, the oxide dispersion strengthened (ODS) alloys were developed. ODS alloy systems are capable of producing usable creep strength to within 90% of their melting temperature. However, due to difficulties in processing, their application is somewhat limited [18].

1.2.2 Effects of Alloying Elements on the Phases

The chemical composition of nickel-base superalloys includes 12 to 13 important elemental constituents and "tramp" elements such as silicon, phosphorous, sulphur, oxygen, and nitrogen which must be carefully controlled by appropriate melting practices [19].

The "important" alloying elements can be divided into three major classes and two subclasses, namely, the matrix class, the γ' class, grain boundary class, the carbide subclass and oxide scale subclass [19].

The γ matrix class of elements include elements from groups V, VI and VII of the periodic table, namely, nickel, cobalt, iron, chromium, molybdenum and tungsten. The γ' forming class is comprised of elements from groups III, IV and V and include aluminium, titanium, columbium, tantalum and hafnium. Elements that segregate to the grain boundaries form the third class of alloying elements. These include elements from groups II, III, and IV of the periodic table and include boron, carbon and zirconium.

The carbide subclass consists of chromium, molybdenum, tungsten, columbium, tantalum and titanium while the oxide subclass is comprised of elements that develop adherent diffusion resistant oxides for environmental protection. Chromium and aluminium form this category [19].

1.2.3 The Microstructure of Nickel-Base Superalloys

1.2.3.1 The Gamma Matrix γ

FCC nickel-base alloys are used extensively for high temperature applications. Although they are not endowed with properties like high modulus of elasticity or low diffusivity their use for high temperature applications may be attributed to : 1) high tolerance of nickel to alloying, 2) formation of Cr_2O_3 oxide film and 3) formation of Al_2O_3 at high temperature

The most common solid solution strengthening elements in γ are Co, Fe, Cr, Mo, W, Ti and Al. These elements differ from nickel by 1-13% in atomic diameter and by 1-7% in the electron hole number (N_v) [19]. Hardening by solid solution strengthening is dependent on the atomic diameter oversize. Aluminium, usually added for precipitation strengthening is also a very potent solid solution strengthener. Of the solid solution strengthening elements mentioned above, W, Mo and Cr contribute most strongly while the others serve as weak solid solution strengtheners. The effects of solid solution strengthening persists up to temperatures of about $0.6T_M$. Above this temperature, γ strengthening is dependent on diffusion. Hence, elements which display low diffusivity, like Mo and W, are most effective.

1.2.3.2 Gamma Prime Phases (γ')

The precipitation of FCC A_3B compounds, γ', in superalloys was one of the most significant advances in superalloy microstructure development. The γ' is a unique intermetallic which provides strengthening by interaction with dislocation movement. The strength of γ', remarkably, improves with increasing temperature, and its inherent ductility prevents it from being a source of fracture.

Microstructure of γ' - The γ' morphology has changed progressively since the inception of superalloys. Initially γ' was observed as spherical precipitates and later as cubes. The shape of the γ' precipitate is dependent on the lattice mismatch. Gamma prime occurs as spheres at 0-0.2% lattice mismatches, becomes plates at mismatches around 0.5-1.0% and then becomes cuboidal at mismatches above 1.25% .

The Composition of γ' - Elements may substitute and partition in the γ' structure. From the ternary phase diagrams it has been established that cobalt will tend to substitute for nickel, while titanium, columbium, tantalum and hafnium will substitute for the aluminium position. Molybdenum, chromium and iron may substitute for nickel and aluminium [19].

The amount of titanium present in the alloy influences the amount of molybdenum that dissolves in the γ'. For high titanium-aluminium ratios the molybdenum dissolved to a lesser extent than in the case of no titanium. Molybdenum has the effect of raising the lattice parameter, solvus temperature and weight fraction of γ' [19].

Substitution of nickel with cobalt reduces the low temperature solubility of the nickel-chromium matrix for aluminium and titanium. Chromium, iron and cobalt can be added to increase the volumetric percent of γ' at given titanium-aluminium levels. This phenomena must not be confused with strength effects, since decreasing the chromium and iron content increases the alloy strength [19].

γ' Stability - Since γ' is the major strengthening phase present in nickel-base superalloys, its stability is critical to the alloy maintaining its strength at high temperature. Thermal exposure above $0.6T_M$ results in γ' ripening at significant rates which facilitates dislocation movement. Ripening of γ' may be described by equation 1.1 [19]. The composition of the alloy influences the γ_e, C_e and D terms [19]. It was found that γ' coarsening was reduced when the chromium content was raised from 10% to 37% in the Ni-Cr-Ti-Al type alloys. This was due to a decrease in C_e and also a reduction in the coherency strains which reduced $\gamma_e D$. High titanium-aluminium ratios result in increased coherency strains which in turn increases the ripening rate.

$$h^3 = \frac{64\ \gamma_e\ D\ C_e\ V_m\ t}{9\ R\ T} \qquad \ldots\ldots\ldots\ldots\ldots\ldots\ 1.1$$

where t = *time*
γ_e = *Specific γ'-γ interfacial free energy*
D = *coefficient of diffusion of γ' solutes in γ*
C_e = *equilibrium molar concentration of γ' solute in γ*
V_m = *molar volume of γ'*
R = *gas constant*
h = *particle size*

Cobalt and molybdenum and the combined addition of molybdenum and tungsten retards γ' coarsening. Columbium reduces the γ' coarsening by "partitioning completely to γ'" [19], hence, reducing C_e and D. Boron and zirconium, however, does not influence the growth rate in the Ni-Cr-Al alloys.

Cyclic overheating of superalloys revealed an automatic restoration of γ' at normal service temperature. Loss of creep resistance was dependent on the volume percent of γ'. Low volume percent γ' alloys weaken faster than high volume percent alloys [19]. Retarding γ' ripening may be achieved by (1) increasing volume percent of γ' and (2) add high partitioning, slow diffusing elements such as columbium and tantalum to the γ'.

Besides stability in terms of γ' ripening, transformation of γ' to other weakening phases/structures must be considered. γ' with high aluminium content cannot transform to other Ni_3X compounds, however, these compounds will form if tantalum, and/or titanium and/or columbium are present in sufficiently high concentrations. Stability of the Ni_3X compounds in decreasing order yields Ni_3Al and Ni_3Cb(or Ta) [19]. The aluminium in Ni_3Al can be replaced by titanium, columbium or tantalum resulting in metastable γ'.

Titanium rich metastable γ' transforms to weakening η (Ni_3Ti hexagonal close packed) phases in the alloys with fairly high titanium-aluminium ratios. The influence of η on the mechanical properties is dependent on the morphology of the η precipitates. η precipitating as cells at the grain boundaries resulted in a reduction in the notch stress rupture strength, while precipitation in a Widmanstätten fashion reduces the strength but not ductility. Precipitation of η at the grain boundaries may be retarded by addition of trace amounts of boron.

1.2.3.3 Carbides

Carbides tend to prefer locations along the grain boundaries in nickel-base superalloys. Early investigators found that certain grain boundary carbides had a detrimental effect on the ductility. However, it was found that creep life and ductility was sharply reduced with carbon

contents less than 0.03%. The consensus amongst investigators was that carbides do exert a beneficial effect on the rupture life at high temperature [19].

The three most common classes of carbides present in superalloys are the MC, $M_{23}C_6$ and M_6C [19]. The MC morphology is usually random cubic or script. $M_{23}C_6$ forms irregular blocky particles. M_6C type carbides can precipitate as blocky structures at the grain boundary and more rarely in a Widmanstätten intergranular morphology. MC carbides form during solidification, and are distributed heterogeneously throughout the alloy, both in the inter and trans granular regions. These carbides are a major source of carbon for subsequent heat treatments and service.

The primary carbides have a FCC structure [19]. Their close packed structures makes them very stable if in the pure form. Typical examples of MC carbides formed in decreasing order of stability are HfC, TaC, CbC and TiC. Alloying with Ta and Cb stabilize the MC carbides.

Substitution of M atoms in MC compounds influence the stability of these compounds. The presence of molybdenum or tungsten in the carbides results in degeneration of the MC carbides to $M_{23}C_6$. Typically, $M_{23}C_6$ stable carbides form during heat treatment processes or in service at temperatures between 760° and 980°C [19].

$M_{23}C_6$ occurs in copious amounts in alloys with medium to high chromium content. These carbides tend to form on the grain boundaries having complex cubic structures which are similar to the TCP σ phase [19].

Their presence along the grain boundaries influences the creep rupture life through interference with grain boundary sliding. However, failure can be initiated by cracking of the $M_{23}C_6$ particles or de-cohesion. The morphology of the $M_{23}C_6$ carbide plays a significant role on its effectiveness as a grain boundary strengthening mechanism. Cellular $M_{23}C_6$ carbides have been shown to reduce the rupture strength [19].

M_6C forms at slightly higher temperatures than $M_{23}C_6$, between 815 and 980°C. The composition of M_6C varies over a wider range, from approximately M_3C to $M_{13}C$. M_6C carbides are formed when molybdenum acts to replace chromium in other carbides.

1.2.3.4 Borides

Boron is added to superalloys in small quantities, 50-500 ppm. Its presence at the grain boundaries block the onset of grain boundary tearing. If boron is present in sufficiently large quantities, borides form at the grain boundaries. These are hard refractory particles which act as a supply of boron for the grain boundary [19].

1.2.3.5 TCP Phases

When the alloy composition is not controlled carefully, undesirable TCP phases can form during the heat treatments or more often during service. They appear as thin linear plates, often nucleating at grain boundary carbides. Typical TCP phases found in nickel-base alloys are σ and μ [19].

Sigma forms from the nickel matrix. Its composition is given by $(Cr,Mo)_x(Ni,Co)_y$ with x and y varying from 1 to 7. Its physical hardness and morphology make it an excellent source for crack initiation, leading to low temperature brittle failure. Because of refractory content, it depletes the alloy of these elements resulting in loss of solid solution strengthening. High temperature rupture may occur along these plates, resulting in a decrease in the rupture life. The μ phase can be formed but is not as well researched as σ [19].

1.3 Directional Solidification and Single Crystal Alloys

Directional solidification was first introduced in the early sixties [19]. The directional solidification process involves growing grains with a lower modulus of elasticity longitudinally in the aerofoil, effectively eliminating transverse grain boundaries. The next step from directional solidification was the single crystal casting process.

Directional solidification (DS) and single crystal (SC) alloys have the highest elevated temperature capabilities of any superalloy [20,21]. DS and SC alloys have excellent creep strength and superior thermal fatigue properties [21]. The superiority of single crystal over polycrystalline alloys is due to (a) their higher melting temperature which permits the γ'

microstructure to be refined via solution heat treatment, (b) the absence of grain boundaries, and (c) their low modulus ⟨001⟩ oriented solidification texture which improves the thermal fatigue properties [20]. The absence of grain boundaries eliminates the need for grain boundary strengthening elements, which reduce the melting temperature. This allows for a more complete solution heat treatment, and better refinement of the γ'.

The microstructure of the DS and SC alloys are very similar to the conventionally cast alloys with γ' precipitates in a γ matrix with a few carbides and borides as described earlier.

1.4 STRAIN RANGE PARTITIONING (SRP)

1.4.1 Introduction

With the development of high performance gas turbine engines, it became essential that a reliable technique for life prediction and material characterisation be developed for materials that worked at high temperatures for long periods of time. In the early 1970's Manson *et al* developed the strain range partitioning method for predicting high temperature low-cycle fatigue life [22]. The advantage of this method of testing stems from its high degree of generality.

The concept of the SRP method was based on the reasoning that in any stress-strain hysteresis loop there were two directions of loading and two types of inelastic strains. The two directions of loading were tension and compression; and the two types of inelastic strains were time dependent (creep) strain and time independent (plastic) strain. By combining these directions and types of strains the four strainranges were obtained, namely:

ϵ_{CP} - Tensile creep reversed by compressive plasticity

ϵ_{PP} - Tensile plasticity reversed by compressive plasticity

ϵ_{PC} - Tensile plasticity reversed by compressive creep.

ϵ_{CC} - Tensile creep reversed by compressive creep

Using these four basic strainranges complex high temperature low cycle fatigue hysteresis loops can be analysed by partitioning them into their respective inelastic strain components.

In order to apply the SRP for life predictions, the four strainrange versus life relationships must be generated experimentally. For the four pure generic strainranges, the basic life relationships follow the Manson-Coffin form: $N_{PP} = A(\Delta\epsilon_{PP})^{\alpha}$, $N_{CC} = A(\Delta\epsilon_{CC})^{\alpha}$, $N_{PC} = A(\Delta\epsilon_{PC})^{\alpha}$ and $N_{CP} = A(\Delta\epsilon_{CP})^{\alpha_2}$; where the coefficient A and exponents α are experimentally determined material constants [23]. In any hysteresis loop $\Delta\epsilon_{CP}$ and $\Delta\epsilon_{PC}$ cannot coexist; one or the other will be present.

Once the generic strainrange versus life relationships are obtained, the SRP method is applied to complex hysteresis loops by first partitioning the hysteresis loop into its inelastic strain components followed by applying a damage rule. The damage rule recommended was the interaction damage rule [22,23]. Using this damage rule the predicted life was given by the following equation:

$$\frac{1}{N_{PRED}} = \frac{F_{PP}}{N_{PP}} + \frac{F_{CC}}{N_{CC}} + \frac{F_{CP}}{N_{CP}} + \frac{F_{PC}}{N_{PC}} \qquad \ldots\ldots\ldots \quad 1.2$$

where N_{PRED} - is the predicted life for the hysteresis loop

N_{PP}, N_{CC}, ... - are the cyclic lives for the particular strainrange of interest

F_{CC}, F_{PP}, ... - are the fraction of each of the partitioned strainranges.

1.4.2 Experiments to Generate the Four Strainrange versus Life Relationships

PP type tests [22] - This test consists of plastic strain in both tension and compression. At high temperatures the frequencies must be sufficiently high (0.5 to 2.0 Hz) to preclude any creep strain. A typical stress-strain hysteresis for the PP type test is given in figure 1.1 a. At least six strainranges covering the range 50 - 50 000 cycles to failure must be used to generate the strainrange versus life relationship.

CP tests [22] - The three most common methods are the stress-hold method, strain-hold method and the low/high strainrate method. The tensile stress hold method (figure 1.1b) is the preferred method. This technique results in the greatest amount of creep strain in the least amount of time and the creep strain is easily identified. The tensile strain-hold procedure, figure 1.1c, is very similar to the PP procedure with the exception of a hold period

at the peak tensile strain. The deficiency in this method is that only a small amount of creep can be obtained which makes this procedure suitable for small strainranges only. The technique of slow/rapid strain rates, figure 1.1d, is very simple to apply. However, interpreting of results is not as straightforward as the previous two techniques. This procedure should only be used in the cases where the experimental equipment is not capable of generating the previous two strain cycles.

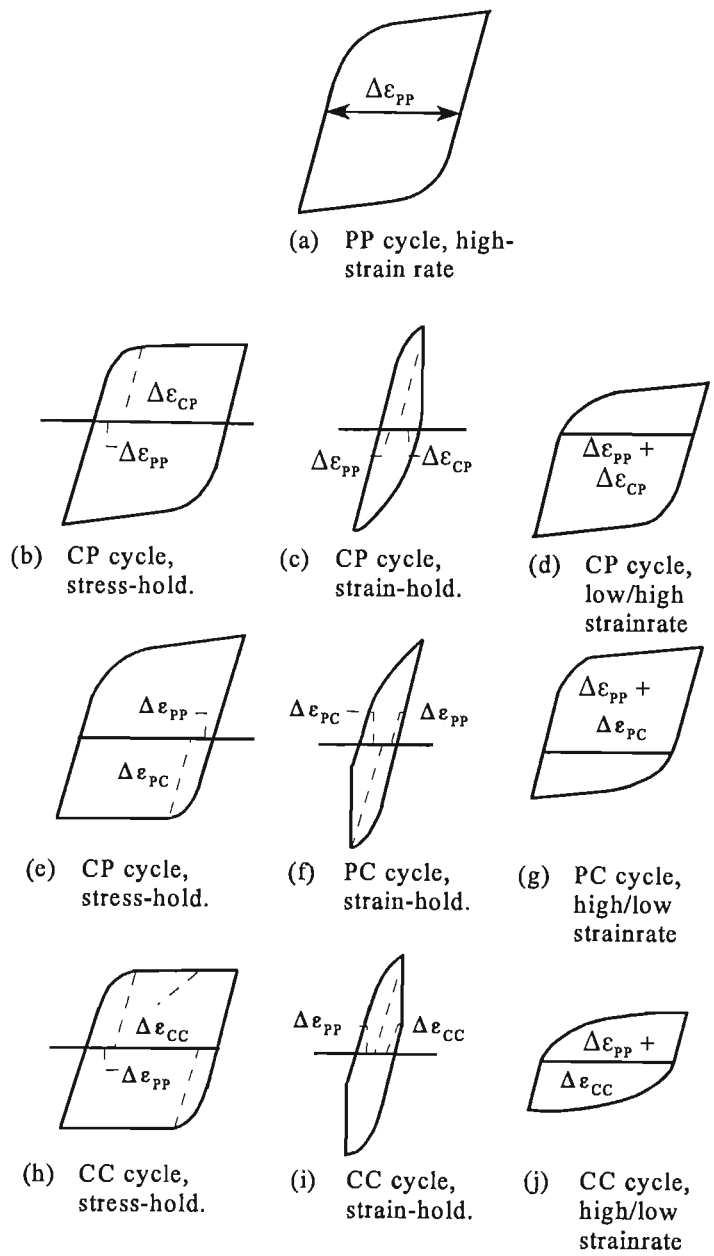

Figure 1.1 : Examples of isothermal test cycles to determine partitioned strain-range-life relationships [22].

PC type tests [22] - The PC type testing technique is simply the CP tests with the difference being the direction of the creep strain (figure 1.1e,f,g). By interchanging the tensile and compressive notation of the previous section, the techniques for PC straining can be obtained.

CC type tests [22] - There are three common techniques for generating the CC type strainranges. The first and preferred method of testing involves the use of the creep rupture type test wherein a constant tensile stress is servo-controlled until the desired strain is obtained, whereupon the stress is rapidly reversed to the equivalent compressive stress which is servo-controlled until the desired compressive strain is achieved (figure 1.1h). When the desired strain range is small the strain hold method is used. This test involves a rapid strain cycling with strain hold periods at the peak strains (figure 1.1i). If the amount of stress relaxation is the same in both tension and compression, then only CC and PP strainranges exist in the cycle. The third technique is a completely reversed strain cycle at a low frequency so that creep can occur. Again this technique is the simplest to implement but is difficult to interpret.

In all CP tests (figure 1.1b,c,d) the strainranges CP and PP also feature. While in the CC techniques the hysteresis loops are composed of CC, PP and CP or PC strains. Hence, it can be seen that there is a sequence in which the strainrange versus life relationships must be generated, namely, the PP strainrange versus life relationship first, followed by the CP and PC strainrange versus life relationships and finally the CC strainrange versus life relationship.

1.4.3 General Discussion

A review of the SRP as a life prediction technique was presented by Miller et al [23]. Characterization of several alloys indicated that the most damaging strainrange is dependent on the alloy. It was shown that for the 304 and 316 stainless steels, the most damaging cycles are the CP type strainrange with a tensile hold. For the nickel-base alloys the compressive hold cycles or the PC strainrange was most damaging. Use of strainrange partitioning as a method of life prediction indicated conflicting evidence for and against the method [23,24].

For the 1CrMoV alloy the SRP method was adequate. However, for long hold times it becomes increasingly inaccurate, indicating that the SRP cannot model time dependent effects in its standard form. The applicability of the SRP method to gas turbine alloy IN738LC, IN597 and FSX414 has been closely examined in the COST 50 programme. It was found that the tensile dwell time had a significant influence on the life. The conclusion drawn from these results was that a stress compensating factor was needed for the SRP method to produce satisfactory data. Several attempts have been made to remedy this problem by accounting for the hold time and strain rate effects, and inclusion of ductility and normalization [23,24].

Cast MAR-M002 nickel-base superalloys was characterized by the SRP method over the temperature range 750 - 1040°C by Atunes and Hancock [25]. At 850°C the PC type strain range was most damaging and the CP was least damaging. While at 1040°C the CP type strain range was most damaging. The results indicated marked temperature sensitivity.

The strain range partitioning method was developed for predicting and characterizing creep-fatigue behaviour of high temperature alloys using inelastic strains to relate to fatigue life. It was initially believed to have a high degree of generality and was relatively insensitive to various parameters like temperature, etc. However, there has been a number of conflicting opinions for and against the technique. More recently, the total strain version of the strain range partitioning method (TS-SRP), which includes the elastic as well as the nonelastic strains, has been examined [26]. The TS-SRP method incorporates an elastic component and a plastic component of strain. In order for this life prediction method to be applied the basic SRP life relationships must be be determined (using the techniques discussed earlier). This method shows promise for application to high performance jet engines [26].

1.5 Combustion Products of Jet Engine Fuel

Jet engine fuel is produced from the refinement of crude oil. Crude oil generally consists primarily of hydrocarbons and small amounts of compounds sulphur, nitrogen, oxygen and certain metallic inclusions. The density of crude oil is between 0.8 and 1.0 g/cm^3 and the typical chemical composition is shown in table 1.1 [27]. The amount of sulphur gives an indication of the "heaviness" of the crude oil. "Heavy" crude oils have a large amount of

sulphur. The presence of sulphur compounds and metallic inclusions is undesirable since they result in excessive wear of the fuel system because of their abrasive nature. The amounts of these impurities are strictly controlled by technical standards. For specification MIL-T-5624K [28], the maximum sulphur allowed is 0.4% for JP4 and JP5 (D.ENG.2494 ISSUE 8) the maximum allowable sulphur content is 0.3%. Traces of sulphur are always

Table 1.1 : Chemical Composition of Crude Oil [27]

Elements	Weight %
C	83.9 - 86.8
H_2	11.4 - 14.0
S	0.11 - 8.00
N_2	0.11 - 1.70
O_2	0.5
Metals (Fe, V, Ni, etc)	0.03

present in fuels even after careful distillation. Sulphur has important effects on the corrosion processes in the hot section of jet engines. Typical combustion products for the major groups of fuel are shown in table 1.2 [28].

In the absence of ash and for complete combustion the principle corrosion mechanisms are oxidation and sulphidation. Oxidation occurs as a result of the presence of oxygen while sulphidation due to the presence of SO_2 and SO_3. Sulphidation of the components of the turbine results in the production of low melting point sulphides like Ni_3S_2. Another type of

Table 1.2 : Composition of combustion products [28]

Fuel	Products of partial comb. (deficient-air combustion)	Products of complete comb. (excess-air combustion)
sulphur free and non ash yielding	CO_2,H_2O,CO,H_2,N_2	CO_2,H_2O,O_2,N_2
sulphurous but non-ash yielding	$CO_2,H_2O,CO,H_2,N_2,$ H_2S,S,COS,SO_2	$CO_2,H_2O,O_2,N_2,SO_2,SO_3$
sulphurous and ash yielding	$CO_2,H_2O,CO,H_2,N_2,$ H_2S,COS,SO_2,ash	$CO_2,H_2O,O_2,N_2,SO_2,SO_3$,ash

corrosion process which is extremely destructive is hot corrosion. Hot corrosion occurs when there is a deposit present on the component. This type of corrosion attack will be present typically when the ash yielding fuel is used.

From the above discussion it can be seen that the type and quality of fuel and combustion process will significantly influence the corrosion processes that occur in the hot section of jet engines.

1.6 High Temperature Corrosion

1.6.1 Oxidation

Oxygen is present in most environments where engineering alloys are used. This makes oxidation an important form of high temperature corrosion. When metals are exposed to oxygen, reaction proceeds provided the oxygen pressure is sufficiently high so as to exceed the metal-metal oxide equilibrium [29].

$$M + \frac{1}{2}O_2 = MO \qquad \ldots\ldots\ldots\ldots\ldots\ldots 1.3$$

$$(P_{O_2})^{\frac{1}{2}}_{M\text{-}MO} = \exp\left(\frac{+\Delta G_{MO}^{\circ}}{RT}\right) \qquad \ldots\ldots\ldots\ldots\ldots\ldots 1.4$$

where $(P_{O2})_{M\text{-}MO}$ - is the oxygen pressure of the metal - metal oxide

ΔG_{MO}° - standard free energy of formation of the oxide MO.

T - absolute temperature

The equilibrium oxygen pressure for metals are very small with the exception of the precious metals. Hence, the thermodynamic conditions for oxide formation in most environments are favourable. Oxide scales are therefore developed on the metals exposure to high temperature. When the oxide scale is dense and protective, the oxidation rate is given by [29]:

$$\frac{d\frac{\Delta M}{A}}{dt} = \frac{k_P}{\frac{\Delta M}{A}} \qquad \text{.....1.5}$$

Where ΔM - is the weight change

A - area of specimen

k_P - parabolic rate constant

From this expression it can be seen that the oxidation rate decreases with time since the scale acts as a barrier to further oxidation.

When the oxide scale is non-protective, the oxidation rate is given by :

$$\frac{d\frac{\Delta M}{A}}{dt} = k_l \qquad \text{.....1.6}$$

where k_l - is a constant

This equation gives a linear relationship between oxidation rate and time. There are several rate laws describing oxidation [30], however, when one is concerned primarily with oxidation resistance the parabolic and linear rate laws are sufficient [29].

When considering alloys the oxidation rate laws are modified to incorporate the different alloying elements. Upon exposure to oxygen, numerous oxide phases are formed in the initial stages. The oxide formation is controlled by the activities of the metallic components of the alloy, the oxygen pressure in the gas, and the relative affinities of the metallic elements to oxygen. "As a result of this competition between the elements in the alloy for oxygen, there is a tendency for the alloy to become covered with the most thermodynamically stable oxide." [29] The oxide scale on alloys generally consist of layers with the more stable oxides closer to the substrate. Oxidation of alloys consist of two stages; the transient stage when a variety of oxides are formed followed by a second stage where only the thermodynamically

stable oxides are formed. The dominant oxide must be most stable and lateral growth must be favoured.

When more than one element reacts with oxygen, understanding of transient oxidation becomes critical to alloy design [31]. In practice, protection of alloys at high temperature principally depends on the formation of Cr_2O_3, α-Al_2O_3 or SiO_2 layers. In order for the scale to be protective the oxide layer must develop uniformly. For high temperature application it has been found that α-Al_2O_3 is most stable. Cr_2O_3 is unstable at temperatures above 1000°C, forming gaseous CrO_3. SiO_2 suffers a similar type of problem by forming gaseous SiO at low oxygen pressures.

Having developed the oxide scale that is protective, it is important that it adheres to the substrate and does not undergo mechanical damage easily. The physical characteristics of the oxide scale and adherence are important to the development and maintenance of the scale. It has been found that a thin uniform scale is most desirable [29] since they have no grain boundaries. This eliminates the problem of short circuit oxidation. Spalling of the scale, as a result of mechanically or thermally induced stresses, may result in catastrophic oxidation of the substrate if it is not self healing. Nickel-base alloys are not as susceptible to this type of problem since the growth rate of NiO is not as high as in other alloying systems [31].

Addition of reactive elements such as Sc, Y, La, Hf, Ce and Th have been shown to greatly improve the oxide scale characteristics and hence the oxidation resistance of superalloys [32-36] through various effects:

i) promotion of selective oxidation of an element which forms a stable oxide (typically Al_2O_3 or Cr_2O_3)
ii) by reduction in the growth rate of Cr_2O_3 and NiO, and
iii) inhibition of scale failure (i.e. through thickness cracking and scale/substrate interfacial decohesion) on both Cr_2O_3 and Al_2O_3 forming alloys.

The oxidation resistance of various alloy systems (carbon steels, Cr-Mo steels, ferritic , martensitic and austenitic stainless steels, Fe-Ni-Cr and Ni-Cr-Fe alloys and iron ,nickel and cobalt based superalloys) were reviewed by George Y. Lai [37]. The corrosion resistance of steels was dependent on the formation of Cr_2O_3 scale at high temperatures. Chromium

content in excess of 18% was necessary for developing an effective oxide scale. Solid solution strengthened superalloys were resistant to oxidation at lower temperatures but were susceptible at temperature exceeding 1150°C. Superalloys strengthened with γ' were not as resistant as the solid solution strengthened alloys. This was attributed to higher titanium content of these alloys. In general, it was concluded that most alloy systems depend on the formation of chromium oxide scales for protection against oxidation. Above 1000-1100°C these scales lose their protection capabilities. At these temperatures aluminium oxide scales are significantly more effective. In order to form protective alumina scales, an alloy must have at least 4% Al.

1.6.2 Sulphidation

Sulphur is one of the most common contaminants in high temperature energy conversion systems. The sulphidation of metals and alloys is a very aggressive wastage process. The parabolic wastage rates are several magnitudes higher than that of oxidation. In particular, the present generation of high temperature alloys and superalloys are totally unsuitable for service in sulphur containing gases of low oxygen potential [38].

A typical chemical reaction that can be observed in sulphidation is [30] :

$$MS + \frac{1}{2}O_2 = MO + \frac{1}{2}S_2 \qquad \ldots\ldots\ldots \quad 1.8$$

$$2M + \frac{1}{2}S_2 + \frac{1}{2}O_2 = MO + MS \qquad \ldots\ldots\ldots \quad 1.7$$

Generally, the metal oxide phases are more stable and it is not uncommon to find corrosion scales which are composed of both oxides and sulphides. The most effective means of inhibiting sulphidation attack is by the formation of Al_2O_3 and Cr_2O_3 oxide scales. Formation of these scales are, however, dependent on the environmental conditions (temperature, oxygen pressure and sulphur pressure). Low oxygen pressures result in a discontinuous oxide scale which allows for sulphur penetration and hence higher corrosion rates [30]. Even when

protective oxide scales are formed, they may be damaged by cracking and spalling (due to thermal stresses) and the ensuing sulphidation attack proceeds rapidly.

If an oxide barrier cannot be formed then protection must be provided by a sulphide scale. However, this results in an accelerated corrosion rate. The sulphide phases formed, cracks and spalls easily resulting in the corrosion process progressing linearly [39]. Besides the problem of spalling and cracking, the formation of low melting point metal-metal sulphide eutectics further enhances the corrosion rate. Table 1.3 [39] and table 1.4 [38] show the melting temperature of metal-sulphides eutectics and metal sulphides. The presence of molten sulphide eutectics allows for the easy diffusion of sulphur through the corrosion scale to the scale-substrate interface and/or diffusion of the metal out to the gas / corrosion scale interface which results in an accelerated attack. The mechanism of sulphidation is very similar to oxidation which indicates that behaviour of the alloying elements follow a similar pattern to that in oxidation. Chromium has a higher affinity to form sulphides than nickel or many of the other alloying elements. When oxygen is present, as in the case of SO_2 and SO_3 [40] bearing atmospheres, oxides and sulphides are present in the scale. This scale provides a higher protection when compared to oxygen free environments like H_2S.

Table 1.3 : Differences between metal and sulphide eutectic melting point [39]

Metal	Metal melting Temperature °C	Metal-sulphide Eutectic Melting temperature °C
Co	1495	877
Cr	1850	1350
Cu	1083	1070
Fe	1539	985
Mn	1260	-
Ni	1455	645

Table 1.4 : Melting Temperature of Some Metal - Sulphides [38]

Sulphide	Melting temperature (°C)
Al_2S_3	1099
TiS_2	1999 - 2099
ZrS	1822
HfS	2373 - 2473
V_2S_3	1799 - 1999
TaS_2	999
Cr_2S_3	(CrS) 1550
MoS_2	1457
FeS	1189
Co_9S_8	1080
NiS	796

F. Gesmundo *et al* [40] reviewed the sulphidation behaviour of various pure metals. Titanium in pure SO_2 formed scales composed of an inner layer of sulphide and an outer layer of TiO. The reaction rate was parabolic and approximately one order of magnitude higher than in oxygen. The corrosion of chromium in pure SO_2 showed that only chromium oxides formed, however, some investigations showed that CrS was also formed in similar environments [40]. The reaction kinetics were approximately parabolic with the reaction rate being two or three orders of magnitude larger than in oxygen. Several studies of the corrosion of nickel in SO_2 containing environments [41-43] indicated that the corrosion processes of nickel was very dependent on the environment and the temperature range. Reaction of nickel in pure SO_2 in the temperature range 773-1373 K generally produces a scale that consists of an inner layer of single phase sulphide "surmounted" by a thick duplex NiO + nickel sulphide mixture [40]. The inner sulphide for T< 806K was Ni_3S_2, $Ni_{3\pm x}S_2$ for 806<T<910K and NiS liquid at higher temperatures. The corrosion scale morphology was similar in SO_2/argon mixtures. Corrosion of nickel in SO_2/O mixtures can be divided into two temperature regions. At low temperatures (T<910K), the most stable sulphide phase is solid and at high temperatures a liquid Ni-S solution forms [40]. In the low temperature range the corrosion scale consists of an inner layer of single - phase sulphide and outer duplex layer and the reaction kinetics are initially linear followed by a parabolic rate. At high temperatures the scale morphology is

the same, with the inner sulphide being a liquid. The reaction kinetics at high temperatures are approximately parabolic [40].

The kinetics of corrosion in pure and dilute SO_2 are very complex [40]. The highest rates are reported for the temperature range 873-1073K where the duplex layer is rich in sulphides. The reaction kinetics at 876K in SO_2/ argon mixtures showed an initial linear stage, a second stage of increasing rate, and a final parabolic rate [40]. At temperatures of 1273 and 1373K the kinetics in pure SO_2 was reported as protective and approximately parabolic [40]. The rates at 1373K were lower than that at 1273K due to the decrease in the diffusional contribution of the sulphide phase.

The effect of SO_2 on the oxidation behaviour of NiCrAl - based alloys in air was studied by W.J. Quadakkers et al [44]. The Ni-10wt%Cr-9wt%Al and Ni-20wt%Cr-6wt%Al alloys were exposed to synthetic air + 1vol% SO_2 and air at 1000°C. The presence of SO_2 showed a significant increase in the corrosion rates with the attack on the alloy having a lower chromium content being more pronounced. The SO_2 reacts with the oxide forming alloying elements via transport through scale imperfections and after oxide spallation. The sulphur was tied up as chromium sulphides, depleting the matrix of chromium and leading to the formation of nickel rich oxide scales in the 10% alloy. It was demonstrated that the alloys resistance to oxidation in sulphur bearing environments may be improved by increasing the chromium content [44] and by adding a relatively high amount of yttrium (0.5wt%).

Alloys exposed to SO_2 bearing atmospheres form oxides and/or sulphides, depending on the alloy composition and temperature [37]. High corrosion rates were dependent on the formation of sulphides. At higher temperatures the formation of oxides was favoured. The general consensus was that chromium was an effective alloying element for improving sulphidation resistance [37,45].

1.6.3 Hot Corrosion

While gas induced degradation is the principal means of high temperature corrosion, deposits may form on the alloy surface, as a result of ash produced during combustion and impurities ingested into the engine, which significantly influences the corrosion processes. High temperature corrosion of the hot section gas turbine components due to salt deposits (principally sodium sulphate) is known as "hot corrosion". Since its recognition as a major problem, there has been a high level of research activity and several reviews on this subject [29,37,46-56]. Sulphur from the fuel reacts with sodium chloride ingested into the combustion chamber to form sodium sulphate, which deposits on the hot section components. Sodium chloride may come from the sea water ingested and sulphur is sourced from the fuel and may also be present in sea water [47]. Hot corrosion scale morphology is typically characterized by a porous oxide layer with the alloy beneath the scale being depleted of chromium, followed by an internal chromium rich layer [37]. There are two types of hot corrosion processes that can occur, namely, type I hot corrosion which occurs at higher temperatures (800 to 950°C) and type II hot corrosion which occurs between 700 and 800°C.

Type I hot corrosion usually consists of two stages namely, stage I (incubation and initiation) and stage II (propagation) [29,48,52]. During the initiation stage the corrosion processes are very similar to that in the absence of a deposit. The corrosion rates are low and are related to the formation of a protective oxide scale. This stage is dependent on: alloy composition, fabrication condition, gas composition and velocity, salt composition, salt deposition rates, condition of the salt, temperature cycles, erosion, and specimen geometry [47]. It was obvious that in order to improve hot corrosion resistance, the alloy must be designed so as to remain in the initiation stage for as long as possible.

The propagation mode was very dependent on the deposit, and accelerated degradation was observed during this stage. There are two general classifications for the hot corrosion propagation mode in superalloys, namely, propagation modes involving fluxing reactions and the deposit component - alloy interaction mode. The salt fluxing reactions for superalloys may be acidic or basic in nature. The basic fluxing reaction mode occurs when ions from the deposit react with the oxide scales. Basic fluxing is not self-sustaining and requires a

continuous source of Na_2SO_4 to proceed indefinitely. Acidic fluxing involves the development of nonprotective reaction products on the superalloy as a result of a liquid deposit on the surface which has a deficiency of ions [48]. This effectively means that the oxide scales donates ions to the deposit. This results in degradation of the oxide scale and hence accelerated corrosion ensues. When the deposit becomes acidic due to the formation of an oxide from an element of the alloy, the reaction becomes self-sustaining. This type of propagation mode occurs when a component from the deposit reacts with alloy causing a non-protective oxide scale to be formed. Two elements that produce this effect are sulphur and chlorine. The more commonly and widely observed form of hot corrosion via this mechanism is sulphidation, ie, the reaction of sulphur with the base metal. Although sulphidation is the most common mode of hot corrosion, hot corrosion can proceed in the absence of sulphur. Hence, sulphidation cannot be used as a generalized term for hot corrosion.

1.7 Effect of the Environment on the Mechanical Properties of Uncoated Superalloys

The effect of the environment on the mechanical properties of uncoated superalloys has been studied extensively. The effect of oxidizing (air) and inert environment on the mechanical properties of superalloys [57-62] showed that the fatigue life was dependent on frequency, temperature, strain rate and microstructure. Fatigue and creep tests performed on Inconel 718 at 650°C in air and helium revealed that air accelerated the crack propagation rate and lower frequencies contributed to accelerated crack propagation [57]. The inert He atmosphere did not display sensitivity to frequency. At lower frequencies, oxygen diffusion in the grain boundaries attributed for the accelerated crack propagation. Inconel X-750 tested in air and vacuum also showed a similar behaviour [58].

The fatigue behaviour of single crystal MAR-M002 in air and vacuum was dependent on temperature [59]. Between 800 and 1400°F, the fatigue lives were not influenced due to cracks initiating internally. At 1700°F the fatigue life in air was greater than in the vacuum. Bulk oxidation of the surface initiated cracks, and the blunting mechanism of the stage II

crack growth accounted for the longer fatigue life in air. In the vacuum the stage II crack growth was enhanced resulting in accelerated failure.

In high temperature oxidizing environments, the crack propagation was slowed due to oxide induced closure and crack tip blunting [60]. Fatigue crack propagation rate in cuboidal γ' decreased when the test temperature was increased from 750 to 950°C [60] while rafted γ' showed little change. The fatigue life in air was higher for higher strain rates [61] whereas for the vacuum environment, fatigue life was insensitive to strain rates. For the higher strain rate crack propagation was transgranular while for the low strain rates the crack propagation was a mixed trans-intergranular one.

Sulphidising and hot corrosion environments have been shown to be the most severe of the corrosion processes hence their effect on the mechanical properties of superalloys has received a significant amount of attention [62-74]. Floreen and Kane [62] investigated the fatigue crack growth rate in Inconel alloy 718 samples in the following environments at 650°C :

Air	CO_2	He + 0.5% H_2S
Helium	He + 5% water vapour	He + 5% SO_2
Nitrogen	H_2 + 5% water vapour	Air + 5% SO_2
Hydrogen	Air + 5% water vapour	Air + 0.5% SO_2
Hydrogen + 2%CH_4	He + 100 ppm O_2	

The sulphur containing environments resulted in accelerated fatigue crack growth. Although some environments did not induce corrosion attack on the unloaded specimen, they resulted in a significant increase in fatigue crack growth rates. The combination of air and SO_2 decreased the crack propagation rate. Under the sulphur containing environment, low melting point nickel-sulphide (Ni_3S_2) eutectic phases were formed ahead of the propagating crack tip, enhancing the crack propagation rate. The crack propagation mode in sulphur containing environments was a mixed Mode type (transgranular and intergranular crack path). The conclusion drawn from these results were:1) the kinetic rather than the thermodynamic factors are responsible for the influence of the environment on crack propagation,
2) increasing the general corrosion resistance of the alloy does not improve the materials resistance to the combined effect of an aggressive environment and fatigue loading and

3) oxidation which takes place simultaneously with sulphidation retards the influence of sulphidation on the crack propagation rate.

Nazmy [64] evaluated the influence of sulphur containing environment on the high temperature low cycle fatigue behaviour of cast IN718 nickel-base superalloy. A corrosive deposit on the specimen surface was obtained by immersing the specimen in synthetic ash at 1123K. The tests were performed at a temperature of 1123K (temperature at which the ash melts) and the atmosphere maintained above the ash melt was air + 0.015 SO_2 + 0.015 SO_3, flowing at a constant rate of 1 litre/minute. A significant reduction in life was observed in air containing SO_2 and SO_3 compared to tests in air only. This emphasized the aggressive influence of the sulphidation process which took place. Sulphidation resulted in the formation of brittle chromium sulphide phases at the grain boundaries which resulted in crack initiation points. This consequently resulted in a reduction in the HTLCF life.

Zhang *et al* showed that sulphidation resulted in accelerated creep failure of GH33 nickel-base superalloy [65]. Creep tests performed in a gaseous mixture of SO_2 and air revealed that a Cr_2O_3 scale was formed first. Provided the scale was undamaged the corrosion proceeded in a similar manner in both air and air + SO_2 environments. Once the scale was damaged sulphidation of the base metal proceeded. The presence of low melting point sulphide phases resulted in accelerated corrosion and premature failure.

MAR-M200+Hf exposed to HTLCF + SO_2 containing environment at 975°C showed that sulphur played a decisive role in the mechanism of HTLCF . Microstructural changes at the crack tip occurred due to the sulphidation attack and mechanical relaxation [66]. HTLCF tests under Ar + 3%SO_2 environment resulted in severe blistering of the surface close to the fracture surface [67]. Addition of 20% O_2 to this environment moderated the blistering effect although the lives were similar. The blistering process was observed to occur only under the combination of mechanical loading and sulphidizing environment.

The effect of hot corrosion on the mechanical properties of nickel-base superalloys has been shown to result in a severe reduction in the mechanical properties [68-74]. Pieraggi [68] studied the creep and low cycle fatigue properties of Udimet 500 and IN-738LC at 800°C in air and Na_2SO_4 containing environment. It was found that creep does not affect the

corrosion rate, however, fatigue does affect the corrosion kinetics and growth mechanisms. The Na_2SO_4 and Na_2SO_4 +10% NaCl environments have a significant detrimental effect on both creep and fatigue properties. This was associated with grain boundary weakening by oxygen, sulphur and chlorine segregations penetrating along slip and twin planes.

The reduction in fatigue properties must be attributed mainly to corrosion induced surface changes. Corrosion facilitates crack initiation rather than propagation. A summary of the possible influences of environment on fatigue crack propagation of cast nickel-base superalloys at high temperature is given in table 1.5 [70].

Table 1.5 : The Influence of environment on the fatigue crack propagation. [70]

Environmentally induced effect	Influence on the material	Influence on fatigue crack propagation rates
dissolution of phases	change the mechanical properties at the crack tip	↑ ↓
	weakening of material	↑
	crack tip blunting	↓
crack branching	reduction of actual ΔK at crack tip	↓
grain boundary attack	weakening of grain boundaries	↑
	intergranular crack branching	↓
oxide layer	prevents rewelding	↑
	prevents resharpening of crack tip	↓
	hindrance of dislocation movement	↓
crack closure	reduction of actual ΔK at crack tip	↓

1.8 Coating Systems for High Temperature Applications

1.8.1 Introduction

Alloying element requirements for superalloys focused on strength resulting in a reduction in the corrosion resistance [75]. Therefore, the use of coatings was implemented to improve the corrosion resistance properties of these alloys. Hence, the general design philosophy is to select a material of sufficient high temperature strength followed by application of a suitable coating. Coatings can be classified into three basic groups, namely, the diffusion

coatings, overlay coatings and thermal barrier coatings [76]. The diffusion type coatings were the first coatings to be developed. These coatings included the aluminide, chromium and silicon diffusion coatings. The most popular and widely used of the diffusion coatings is the aluminide coating which is still used in present day applications. The diffusion and overlay coatings provided a surface, enriched in aluminium and chromium, which formed protective Al_2O_3 and Cr_2O_3. Thermal barrier coatings were developed to increase the working temperature of engines by reducing the temperature of the metal by as much as 200°C [78].

There are several articles that review the coating processes and their performance [75-84]. This literature review shall cover some of the coating processes, concentrating mainly on the aluminide and modified aluminide coatings as this is within the scope of the present research.

1.8.2 Aluminide Coatings

Diffusion aluminide coatings can be applied to engine components by various techniques, which include pack cementation, slurry fusion and chemical vapour deposition [82]. The most common and widely used technique for aluminide coating application is packed cementation [82,84,85,86]. This method is a type of vapour deposition process where the component and the coating reactants are contained in the same retort [82]. The coating reactant consists of aluminium powder, a chemical activator (normally a halide) and filler such as alumina. During the aluminizing process, material from the pack is transferred to the metal surface via the formation of an intermediate volatile aluminium mono-halide gas. The interdiffusion of aluminium and the substrate alloy results in the formation of an intermetallic compound/ coating. Typically, the NiAl phase is found in coatings on nickel based alloys. Due to diffusion, the coating contains most of the alloying elements to a degree.

The coating morphology and the deposition rate depends on the pack activity, temperature and processing time [87-89]. There are two classes of diffusion aluminide coatings, namely the "inward" and "outward" type coatings. When the aluminium activity is high, inward diffusion of aluminium occurs (reaction temperature between 760 and 982°C) at a higher rate than outward diffusion of nickel. A surface layer of brittle Ni_2Al_3 forms, hence a further heat treatment is required to convert this phase to NiAl. With low aluminium activity (reaction temperature between 982 and 1093°C) outward diffusion of nickel is predominant.

The properties of aluminide coatings depend upon the process method, substrate composition and subsequent heat treatments [89]. The coatings contain in excess of 30wt% Al and are between 30 -70μm thick [75]. These coatings performed well under oxidation conditions since there was sufficient reserve aluminium to form the protective alumina scales. However, under extreme hot corrosion conditions or at temperatures exceeding 1100°C the protection offered was limited. This led to the development of the modified aluminide coatings [75].

1.8.3 Modified Aluminide Coatings

Modified aluminides are aluminide coatings in which alloying elements are incorporated to improve the high temperature properties of conventional aluminides. The techniques used to fabricate these coatings are as follows [75]:

1) co-deposition of elements from the pack or slurry
2) pretreatments of the superalloy surface before pack aluminizing
3) deposition of a metallic layer by electroplating or physical vapour deposition (PVD) techniques followed by aluminizing (eg. platinum modified aluminides)

A number of additional elements have been shown to be beneficial to aluminides. The modifying elements range from silicon, chromium , the "reactive elements" (eg. Yttrium) and the noble metals such as platinum and rhodium. Doping the aluminide coating with reactive elements has been shown to improve the high temperature corrosion resistance by improving the oxide scale adhesion [90-94]. The effectiveness of reactive elements on the corrosion properties is dependent on the processing parameters [95]. Silicon modified aluminides have been used for some time. They have been shown to improve the high temperature corrosion resistance, stability of the coating and to some extent the fatigue resistance of aluminide coatings [96-97].

In chromium-modified coatings, chromium may be added to the aluminide coating by one of the following processes [98]:

1. a single step pack cementation process in which chromium and aluminium are deposited in a single step (pack codeposition) or
2. chromium is provided by either the substrate or by a previous chromizing heat treatment (two-step process).

The codeposition of chromium and aluminium simultaneously had been considered to be practically impossible due to the large differences in the diffusivity of chromium and aluminium in nickel aluminide [98]. However, by adding aluminium decelerating activators, deposition rates of chromium and aluminium of the same order could be achieved at 1100°C [98]. The coating formed consists of a chromium rich outer layer with α-Cr precipitates. "A short coming of codeposited chromium aluminide coating is that they often contain pack inclusions as a direct consequence of their outward-grown diffusion coating" [99,100]. A codeposition inclusion free coating, developed by Gleeson *et al,* has been shown to produce two types of coating structures depending on the morphology and chromium distribution [101]. The type I coating structure (figure 1.2) contains lamella α-Cr precipitates situated in the surface region, while the type II coating structure contains small spheroidal α-Cr precipitates throughout the intermediate layer [99]. Chromium enrichment of the coating occurs by metallic inclusions and possibly solid state diffusion between the pack and the specimen [102].

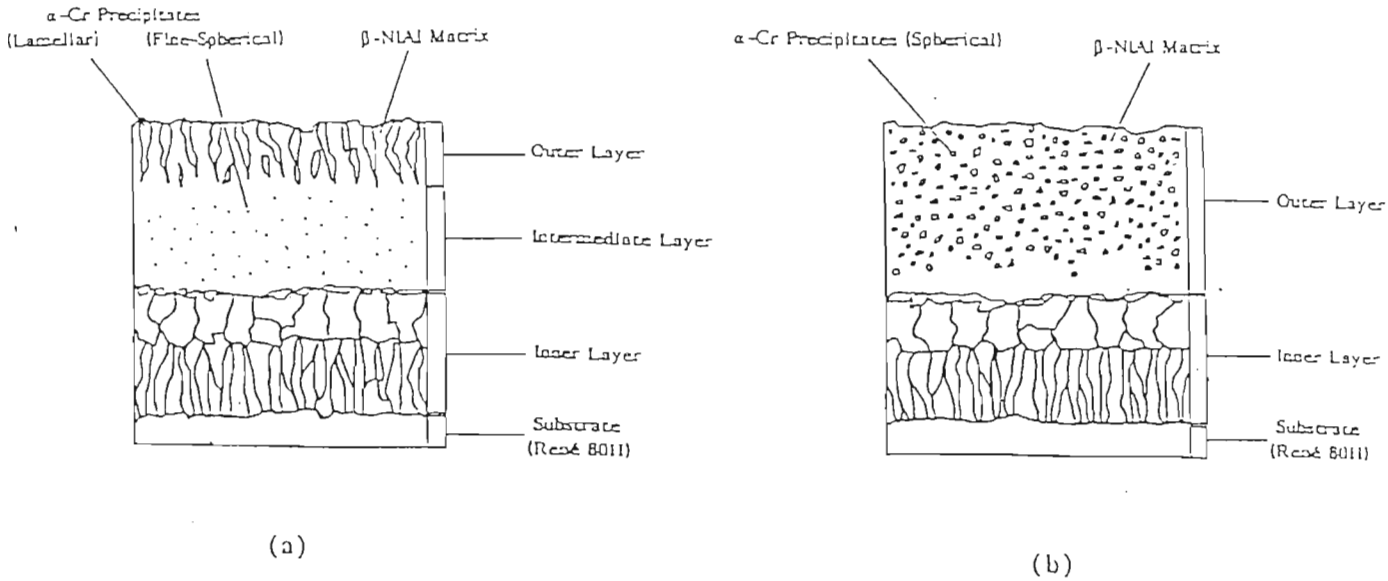

Figure 1.2 : Schematic illustration of the two types of codeposited chromium-modified aluminide coatings [99]

a) TYPE I chromium-modified aluminide coating

b) TYPE II chromium modified aluminide

In the two step chrome-aluminizing process the surface of the substrate is chromium enriched prior to aluminizing. The diffusion chromizing heat treatment may be performed by either chemical vapour deposition or pack cementation. The aluminizing heat treatment used determines the final microstructure of the coating [99,103]. The use of a high activity aluminizing post-heat treatment results in chromium enrichment of the coating by the presence of α-Cr in the outer layer. This results in a typical three zone coating. When the low activity aluminizing process is used, the outward growth of NiAl, results in the layer under the coating being rich in chromium.

1.8.4 Platinum Modified Aluminides

The concept of platinum aluminide coatings has been historically attributed to Dr Lehnert in 1970 [104,105]. Platinum modified aluminides are produced by a two step process, namely, deposition of a thin layer of platinum (≤10μm) followed by an aluminizing process. Platinum may be deposited on the substrate by electroplating, sputtering or fused salt electrolysis. The aluminizing process may be performed by pack cementation or chemical vapour deposition. The three most common commercially available platinum modified aluminides are LDC-2, RT22 and JML-1. Of these three, the LDC-2 and RT22 are produced by electroplating followed by pack aluminizing at 1030°C. In the JML-1 process the platinum is deposited by the fused salt technique followed by a low temperature (700 to 750°C) aluminizing process. This coating has to undergo a subsequent high temperature heat treatment to eliminate undesirable microstructural changes that occur [104].

The microstructural morphologies of platinum modified aluminides have been described extensively in literature [106-115]. Microstructural features depend on platinum thickness [106], prealuminizing heat treatments, the conditions and type of aluminizing process and subsequent heat treatments. The morphology and final chemistry of the coating was dependent on the initial platinum thickness [106]. With relatively thick platinum deposits (≈25μm), refractory elements from the substrate are excluded from the outer regions of the coating. Thinner platinum coatings limit the amount of refractory elements in the outer regions rather than excluding these elements. Platinum remained concentrated at the surface and acts as diffusion medium rather than a diffusion barrier for aluminium.

A typical platinum- aluminide coating consist of : i) an outer zone rich in platinum and aluminium, ii) a middle zone, in which the concentration of aluminium and platinum decrease while that of nickel increases towards the inner zone and iii) an inner zone, enriched in substrate-alloy elements, that is similar to the diffusion zone of the conventional aluminide coatings.

Boone *et al* [108] investigated the structure and hot corrosion behaviour of platinum modified aluminides produced by using different heat treatment processes and aluminizing techniques. For the HTLA process platinum exists over a wider thickness range as $PtAl_2$ dispersed in NiAl and /or platinum dissolved in low aluminium NiAl. The LTHA aluminizing process results in an external layer of either $PtAl_2$ (resulting from low interdiffusion of platinum during the prealuminizing heat treatment) or $PtAl_2$ + NiAl two phase layer (for higher diffusion rates of platinum). The layer beneath the platinum rich outer layer is essentially the normal NiAl zone. The greater amounts of substrate elements near the surface has been observed for the LTHA process coating [113].

The effects of pretreatments on the structure and oxidation behaviour of d.c sputtered platinum aluminide coatings were investigated by J.H. Sun *et al* [110]. Diffusion heat treatments produced a continuous $PtAl_2$ phase outer layer with NiAl as a second phase, a (Ni,Pt)Al inner zone (beneath the $PtAl_2$) and the interdiffusion zone. In a laser melted platinum pretreatment the outer layer consisted of $PtAl_2$ imbedded in NiAl, a (Ni,Pt)Al inner zone and the interdiffusion zone.

Deb *et al* [116] showed that the microstructure of the coating was dependent on the coating process (sequence). For the Pt-Cr-Al HTLA type process the outer layer was a three phase region consisting of α-Cr + NiAl + $PtAl_2$. The zone below this was NiAl(Cr) followed by the interdiffusion zone. The Cr-Pt-Al coating sequence resulted in a continuous $PtAl_2$ outer below which was a NiAl(Pt,Cr) zone. An intermediate zone above the interdiffusion zone consisted of α-Cr + NiAl(Cr). It was found that the coating performance was very much dependent on the coating sequence. The coating for low temperature hot corrosion resistance was obtained by the Cr-Pt-Al deposition sequence.

1.8.5 Overlay Coatings

Although aluminide and modified aluminide coatings have satisfied the majority of the high temperature applications in gas turbines, the need for a more "ideal" coating with a good balance between corrosion resistance and ductility became apparent. This stimulated the development of the overlay coatings. Overlay coatings are produced by the deposition of corrosion resistant alloy on the surface, typified by the MCrAlY series of coatings where M can be Fe, Ni, Co or a combination of these elements [29,83]. The coating alloy may be deposited by using EB-PVD [74,82], plasma spraying [117,118], electron beam alloying [119] and more recently high velocity oxygen fuel (HVOF) spraying of the coating [120]. The HVOF process was developed as a low cost alternative to low pressure plasma spraying.

Once the coating is sprayed /deposited onto the substrate a surface diffusion heat treatment is performed to bond the coating to the alloy. The coating composition is comprised essentially of the material sprayed and does not depend on diffusion of elements from the substrate [121]. Interdiffusion between the substrate and coating only occurs to a limited degree. The microstructure of overlay coatings are dependent on the coating composition and the substrate [118]. Protection is provided essentially by the formation of Al_2O_3 and Cr_2O_3 scales, as in the diffusion type coatings [82,119]. The advantage of overlay coatings stems from its flexibility in terms of coating alloy composition. The coating alloy can be designed to meet the specific needs of the designer.

1.8.6 Thermal Barrier Coatings/Ceramic Coatings

The continuing drive to improve engine performance resulted in the need for thermal barrier coatings (TBC) [122]. These coatings provide a thermal barrier to the substrate thus enabling the engine to operate at higher working temperatures (metal temperatures reduced by up to 200°C). Thermal barrier coatings have been successfully used in the flare head and primary zone section of the combustors. The main limitation of thermal barrier coatings is their low strain tolerance. The mismatch in thermal expansion coefficients of the substrate and coating leads to spalling of the coating [78].

Thermal barrier coatings are typically made up of a metallic bond coat (MCrAlY) on top of which a ceramic coat between 200-300μm thick is applied [75,78,123]. The bond coat is applied to improve the adherence of the ceramic coating to the substrate and improve the corrosion resistance since the ceramic top coat is porous. The most commonly used method to apply these coatings is plasma spraying And the most commonly applied ceramic layer is yttria stabilized zirconia [124].

A number of approaches have been investigated in order to improve the thermal shock properties and high temperatures corrosion properties of TBC [125-139]. These approaches include altering the bond coat composition, the processing techniques and composition of the ceramic coating [135-138]. The thermal fatigue properties improves with increasing density [125,126,133,136]. In a review of TBC by James and Matthews [128] it was concluded that "the optimum TBC will probably have a composite structure, consisting of a dense interfacial layer and a thick columnar layer, involving two deposition conditions".

1.9 High Temperature Corrosion of Coated Alloys

Since the inception of coatings as a means to inhibit high temperature corrosion there has been a continuing evaluation of various compositional variations and processing methods. Most coatings for high temperature corrosion resistance rely on the formation of stable chromia, alumina or silica surface scales.

Aluminides coatings at present are the most widely used coatings for gas turbines. Simple aluminides have been shown to improve the oxidation properties of alloys but were susceptible to hot corrosion conditions [82]. The effectiveness of aluminide coatings have been shown to be dependent on the coating/substrate compatibility [140,141]. In a study of various coatings on single crystal SX60A, SRR99,CMSX-2, CMSX-6, MMT143 and DS MAR-M002 [140] it was shown that although aluminide coatings in general improved the high temperature oxidation and hot corrosion properties, it was most effective on MAR-M002. The overlay coatings tested showed an improvement in hot corrosion resistance when compared with the aluminide coatings. The degree of protection offered by the overlay

coating was dependent on the composition of the coating. Coatings which relied on Cr_2O_3 for protection performed poorly above 1000°C because of the formation of volatile chromia.

High temperature corrosion of aluminide coatings on IN783-LC and MAR-M002 at 700°C and 830°C was investigated by Rhys-Jones and Swindells [142]. Corrosion tests on commercial aluminides were performed in the following environments: 1) O_2 , 2) O_2 + 0.1vol% SO_x, and 3)$Na_2SO_4 + O_2 + 0.1$ vol% SO_x . The aluminide coating provided excellent resistance to in oxidation environments but only limited resistance to sulphidation environments. The degree of degradation in the sulphidation environments was higher at the lower test temperatures. The addition of Na_2SO_4 deposit resulted in a marked increase in degradation. The corrosion process followed two steps, namely, an incubation period followed by rapid degradation of the coating.

Due to the susceptibility of aluminide coatings to high temperature sulphidation and hot corrosion a number of modified aluminides have been developed. The corrosion/oxidation resistance of several modified aluminides have been reported extensively in literature [143-147]. Six coating systems; conventional aluminides, chromium modified aluminides, silicon modified aluminides, platinum-modified nickel aluminide and platinum/rhodium-modified nickel aluminides, applied to turbine blades were investigated by S.G. Russo[143]. After 2500 hours of engine operation the coating performance ranked from best to worse was as follows: platinum/rhodium modified aluminide > platinum modified aluminide > silicon-modified aluminides > conventional aluminide (type a) > conventional aluminide (type b) > chromium-modified aluminide [143]. Even though chromium -modified aluminides fared worse than the conventional aluminides in aviation and marine environments, it has been shown to offer an improvement on aluminides in burner rig studies simulating the industrial environment [148]. Godlewski and Godlewska [149], reported that chromium had a beneficial effect on the oxidation and hot corrosion properties of aluminides. The processing parameters were also important with the high activity pack process offering better resistance than the low activity pack.

The platinum modified aluminides have been the most effective in terms of improving the high temperature corrosion properties over the conventional aluminides [150-156]. The

evaluation of the cyclic oxidation and hot corrosion of diffusion aluminides and CoCrAlY overlay coatings on nickel-base superalloys showed that platinum aluminides produced a substantial improvement of the cyclic oxidation and high temperature hot corrosion properties but had little influence on the low temperature hot corrosion properties [150,152,153]. The corrosion resistance of platinum modified aluminide coatings is dependent on the substrate, coating morphology, and the coating process. The HTLA type platinum aluminides offer better corrosion properties than the LTHA platinum aluminides due to the rapid diffusion of aluminium to the coating surface [152]. Platinum aluminide phases close to the surface promotes the selective oxidation of aluminium and reduces the effect of other alloying elements [153]. Alloys with high molybdenum and tungsten content reduce the protective properties of coatings [157].

Wu *et al* [158] performed electrochemical corrosion measurements with platinum aluminides and platinum free aluminides in Na_2So_4 hot corrosion environments. Platinum improved the resistance of the coating to basic fluxing , however, there was no significant improvement for acidic fluxing conditions. The platinum modified coating had a broader passive region and the corrosion rates were significantly lower as well. The reasons for the higher corrosion resistance of platinum aluminides were attributed to the high corrosion resistance of the platinum rich layer and an increase in the Al_2O_3 content in the scale.

The improved high temperature corrosion properties of platinum aluminides may be ascribed to the following effects of platinum :

i) improved oxide adhesion over the conventional aluminides in cyclic oxidation tests [154,155]
ii) improved stability of the coating [159,160]
iii) promotes diffusion of aluminium to the surface which enhances the formation of protective oxides
iv) inhibits the cracking and spalling of the α-Al_2O_3 scale [156].

MCrAlY type overlay coatings have been designed specially for the protection of turbine hot section components against hot corrosion induced by molten salts and aggressive environments. These coatings offered good protection under high temperature burner rig

tests. High aluminium levels in MCrAlY systems generally improve the high temperature oxidation resistance, however, with the penalty of reduced ductility [83]. Under low and intermediate temperature corrosion conditions, 650-850°C, MCrAlY coatings do not perform so well [83]. By altering/developing new overlay composition the "low" temperature marine and industrial application may be improved. The evaluation of a composite coating of MCrAlY + Al + Pt + Cr has proved beneficial to the properties of the coating system [161]. Although overlay coatings have been shown to have excellent high temperature corrosion properties the modified aluminides has received increased interest as a low cost alternative to these coatings.

1.10 Mechanical Properties of Coatings

The primary function of coatings was to offer environmental protection from the ability to form thin continuous protective oxide scales. In order for this function to be fulfilled the coating must not be breached due to mechanical loading or thermally induced cracking.

The ductile to brittle transition temperature (DBTT) for various aluminides is shown in table 1.6 [10]. The coating ductility is dependent on the coating type, thickness and temperature range over which the maximum strains have to tolerated.

Table 1.6 : DBTT temperature various aluminides [10]

Aluminide	Estimated DBTT Range
NiAl	868°-1060°C
CoAl	878°-1070°C
$PtAl_2$	870°-1070°C
Ni_3Al	730°-900°C
Ni_2Al_3	570°-710°C

Hancock *et al* [9,162] showed that the DBTT varies between 750 and 950°C with increasing coating thickness. Diffusion aluminides are metastable by nature and their composition, structure and mechanical properties will vary with thermal exposure, hence, influencing their DBTT [10]. Extensive formation of γ' at 1100°C [163-166], due to the depletion of

aluminium as a result of oxidation and diffusion into the substrate, results in an increase in the coating fracture strain from 0.52-0.65% to 5-8% [163].

Coating composition and processing methods also play an important role in the coating mechanical properties. Chromium and silicon modified aluminides are more brittle than conventional aluminides [16]. However, the crack morphology in aluminium and Al-Cr systems where similar, with cracks being discontinuous and branched. Codeposition of aluminium and chromium instead of the two step process produced better mechanical properties.

The creep-rupture and fatigue life of alloys were shown to be reduced due to the presence of coatings [2-4,18,13]. Although coatings reduced the fatigue life, the fatigue penalty was small compared to the effect of the environment on the alloy fatigue characteristics [4]. The degree to which coatings affected creep and fatigue properties depended on the coating system and substrate. Schneider *et al* [2] showed that while aluminium coatings reduced the creep life, chromized alloys experienced an increase in creep life. Coatings have a much larger influence on the directionally solidified (DS) alloys than the conventionally cast alloys [8]. The rupture life of the DS alloy was reduced even though the rupture ductility was not reduced. Higher operating temperature reduced the effects of coating on the mechanical properties. The creep rupture properties were controlled by micro cracking of the coating [8].

Thermo-mechanical fatigue properties of coated superalloys were also reduced due to coatings. Aluminide coatings reduce the thermal fatigue lives of high temperature alloys for strains less than 0.8%, however, for strains greater than 0.8% the coating has little or no influence on the thermo-mechanical fatigue behaviour [16]. This behaviour was due to the different failure mechanisms that occur above and below this critical strain value.

Thermo-mechanical fatigue tests performed on aluminide and Co-Cr-Al-Y overlay coatings by Scneider *et al* [2] revealed the inherent brittleness of coatings. For a strain of 0.25% the aluminide coating failed after only 10 cycles while the overlay coating was significantly better, failing after 500 cycles. It was also demonstrated that increasing the aluminium content of the overlay coating significantly impairs the thermo-mechanical fatigue properties

due to the formation of brittle CoAl. A comparative study on the thermo-mechanical fatigue of aluminide coated and uncoated unidirectionally solidified MAR-M002 revealed that the number of cycles to first crack was in the order of 5 to 8 times faster for the coated alloy compared to the uncoated alloy.

Wood and Restall [167] showed that the HCF properties of overlay coated single crystal nickel-base superalloy were dependent on the DBTT of the coating and the thermal expansion coefficient mismatch between the coating and the substrate. Higher temperatures (1000°C) produced lives similar to the bare alloy since the DBTT was exceeded and thermally induced stresses were less significant.

In summary the crack initiation during thermo-mechanical fatigue is dependent on [15]: i) the thermo-mechanical strain range, ii) coating ductility or fracture strain, iii) peak tensile strain temperature (peak tensile strain may occur below the DBTT of the coating), iv) the maximum temperature and v) coating/substrate thermal expansion mismatch strain.

1.11 Effect of Environment on the Mechanical Properties of Coated Superalloys

Although the effect of coatings on the mechanical properties of superalloys has received much attention, the effect of environment on the mechanical behaviour of coated alloys has been less studied.

Holmes and McClintock [168] investigated the influence of thermal fatigue strain history on the hot corrosion attack of a nickel-aluminide coating. Coatings were applied by packed cementation to stepped-disk specimens machined from Rene N4 nickel-base superalloy. The disks were then thermally cycled to simulate the severe thermal and strain transients experienced by gas turbines. Hot corrosion was studied by applying Na_2SO_4 to the specimen and controlling the partial pressure of O_2, SO_2 and SO_3 in the test environment. It was found that the hot corrosion attack was dependent on the strain history. For high strains the coating was completely penetrated by sulphides whereas for low strains only minor surface oxidation

was observed. At higher strain levels the surface oxides cracked, hence, allowing the Na_2SO_4 to react directly with the coating/substrate.

The effect of HTLCF on the failure of coated nickel-base superalloy in H_2S containing atmosphere at 650°C was investigated by Aghion *et al* [169]. Aluminide coated directionally solidified MAR-M002 was subjected to creep-fatigue loading in air, argon and Ar + 0.05% H_2S. The H_2S environment was shown to be very aggressive and resulted in an accelerated failure compared to air and argon atmospheres. The crack growth rate was controlled by the combined effect of mechanical loading and environmental interaction ahead of the crack tip.

Czech *et al* [171] reviewed the effect of environment on the mechanical properties of coated superalloys and gas turbine blades. The coating performance depended on the coating thickness, process and type of coating. Fatigue tests performed on various aluminium based coatings on IN100 at 950°C in a hot gas environment with tensile stresses of 254 and 300 MPa revealed that coatings which are less than 50μm thick improved the fatigue life compared to uncoated alloys. The heat treatment processes by which coatings were applied can also influence the creep rupture properties in hot gas environments due to changes in the microstructure. Although Cr-Al coatings protected the alloy under corrosive conditions, the times to rupture at high stresses (170 MPa) did not show an improvement over the uncoated material [171]. This was as a result of cracks in the coating which propagated to the substrate. However, at lower stresses (140 MPa) the coating did provide protection in hot salt corrosion. After 700 hours the chrome aluminide coating was completely consumed under these conditions. The MCrAlY type coatings, however, did offer better protection. Even under high stresses this coating underwent ductile deformation over cracks in the substrate [171].

Low cycle and high cycle fatigue of RT22 coated and uncoated Udimet 720 in air and hot corrosion conditions at 732 and 704°C were also studied [171]. Udimet 720 in the salt containing environment had a far lower low cycle fatigue strength than in air due to pitting which leads to crack initiation. The effectiveness of the coating depended on strain. For $\Delta\epsilon_t$ > 1% the coating failed resulting in the salt environment being able to attack the substrate. For low strain ranges $\Delta\epsilon_t$ < 1% the low cycle fatigue lifetime in air was matched in the hot

corrosion environment. This led to the conclusion that the protective coating must have a low enough DBTT for it to follow an alternating stress under operating conditions.

For the high cycle fatigue tests the performance of the coated alloy was dependent on the stress levels [171]. For low stress levels the RT22 coating did provide an improvement in the fatigue life in the corrosive salt environment. The coating reduces the fatigue life in air slightly but had no effect on the endurance limit. In the corrosive environment the cracks had initiated mainly from pits that formed along the gauge length.

The corrosion attack may be either general or specific, depending on the level of mechanical or thermal stress and the corrosive environment. In the case of general corrosion the cross-section of the component was measurably reduced resulting in an increase in stress and creep rate. Selective corrosion occurred when cracks were initiated and penetrated the coating. Corrosion attack proceeds along these cracks. Hence, when selecting a coating the designer must ensure that coating must have adequate resistance to corrosive environment, and a sufficiently high ductility so that cracks do not initiate readily in the coating.

CHAPTER TWO

2. EXPERIMENTAL PROCEDURE

MAR-M002 Nickel-base superalloy was received in the form of unidirectionally solidified bars. Creep-fatigue specimens were machined form the bars and disc samples were prepared for the corrosion tests. Coating and heat treatment procedures were then performed on the samples. High temperature creep-fatigue tests were performed on the fatigue samples at 870°C under a constant loading regime in air, argon and Ar + 5 vol% SO_2 environments. Corrosion tests were conducted on unloaded disc samples in air, argon and Ar + 5 vol% SO_2 at 870°C for five hours. The results were analysed using the scanning electron microscope with EDS analysis, X-ray diffraction analysis and auger electron spectroscopy.

2.1 Test Specimens

2.1.1 Fatigue Specimens

Fatigue specimens were turned from the bars with the configuration shown in figure 2.1. The design of the specimen took into account the capabilities of the experimental system, the specific testing conditions, and the dimensions of the bars received.

Due to the limitations on the loading capacity of the hydraulic loading system the diameter of the specimen neck was limited to 4mm. The gauge length had a hour glass shape. It was designed such that the control environment was confined in this region and to minimize the possibility of buckling [172] of the specimen. The collars were used to attach the linear variable differential/displacement transducer (LVDT) to the specimen neck in order to measure the strain across the gauge length. The thicker constant diameter sections on either end were included for shock absorption when the strain cycle was reversed. The threaded sections were used to attach the specimen to the grips.

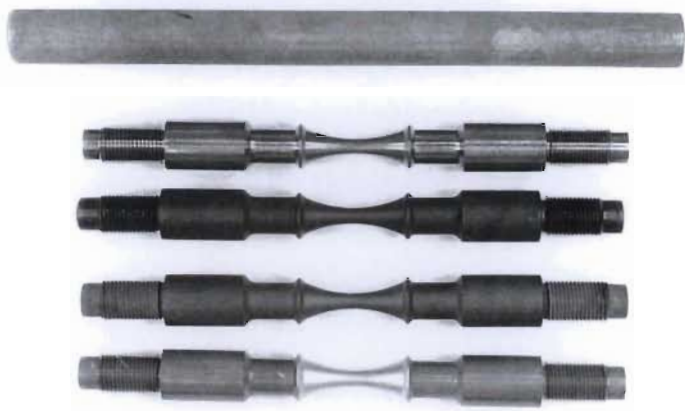

a

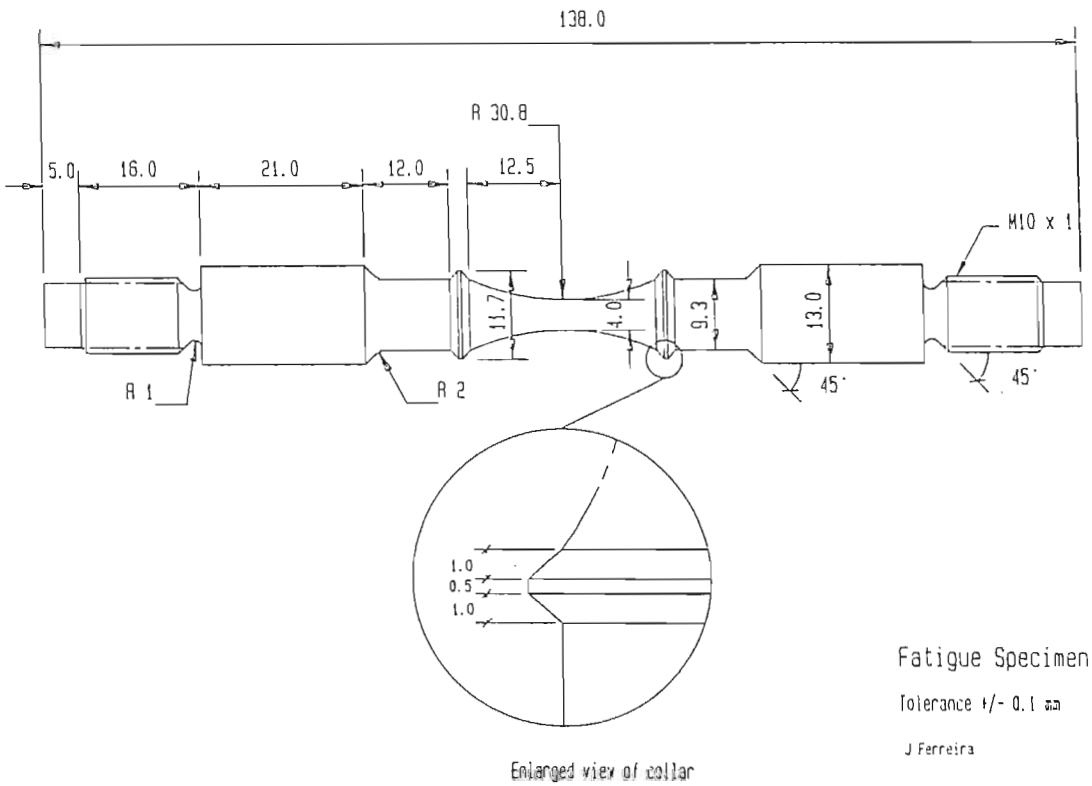

b

Figure 2.1: a) Directionally solidified bar and the coated fatigue specimens
b) Actual dimensions of the fatigue specimen

2.1.2 Corrosion Disc Specimen

Corrosion disc samples were prepared in order to perform exposure tests on the unloaded material. The dimensions of the corrosion disc samples had to comply with the requirements of the X-ray diffraction apparatus sample holder. The diameter of the disc sample was approximately 13mm and the thickness of the sample was less than 2 mm (figure 2.2). For these specimens the dimensions of the specimen were not critical as the tests were of qualitative and only gave an indication of the corrosion product present as a result of exposure to the various environments. The specimens were polished to a surface finish of 6μm. This was followed by the coating processes and heat treatments.

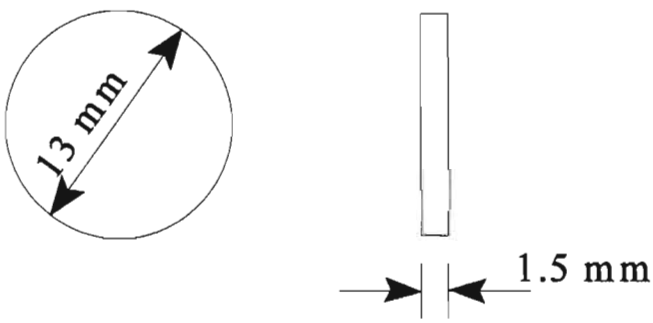

Figure 2.2 : Dimensions of disc samples used for high temperature exposure tests

2.2 Coating Procedures

Three coating systems were investigated, namely; aluminide coating, platinum coating and platinum aluminide coating.

2.2.1 Chrome-aluminide Coating

The chrome-aluminide coating was applied using the packed cementation process *(Note that the chrome-aluminide coating will be referred to as an aluminide coating from here on for ease of discussion)*. The pack powder was composed of alumina, chromium, aluminium, nitrogen (trace amounts) and ammonium chloride activator. The ammonium chloride

activator was added to the powder just before the coating process. The pack powder was then thoroughly mixed prior to the coating process in order to obtain the correct homogeneity.

Application of the coating involves four steps, namely, the surface preparation, installation of the sample onto the treatment cases, the diffusion treatment and finally unloading and cleaning of the coated parts.

2.2.1.1 Surface Preparation

The parts are subjected to sand blasting within 15 hours prior to being placed in the treatment boxes. After sand-blasting the samples were handled with care (using gloves) to avoid contamination of the surface.

2.2.1.2 Installation into the Treatment Cases

A batch of several cases can be treated at the same time. The samples were laid into the cases and progressively filled with the pack powder. It was ensured that the parts did not touch each other or the case sides (figure 2.3). The case is then covered with a non-sealing lid. The top layer of the powder was at least 10mm thick.

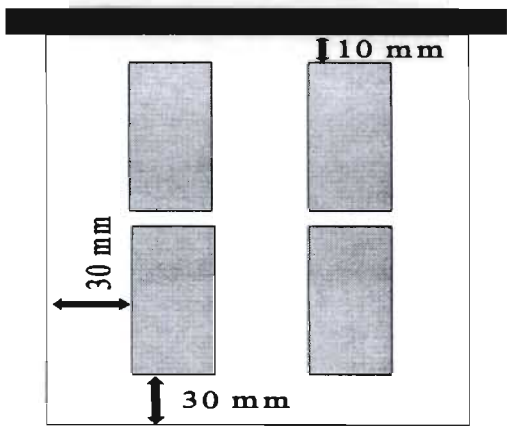

Figure 2.3: Installation of samples into the treatment cases

2.2.1.3 Diffusion Treatment

The cases were placed in a sealed enclosure (figure 2.4). The enclosure was purged with argon and then introduced into the furnace. The enclosure was continuously purged with argon up to a temperature of ±800°C. Above 800°C purging was continued with hydrogen for the duration of the coating treatment.

The coating treatment was performed at 1030°C for 12 hours. The purging process was maintained throughout the heating cycle and during the cooling cycle the purging sequence was simply the reverse of the heating sequence. In order to prevent interaction with ambient air, the cases were opened when the pack temperature was no greater than 50°C.

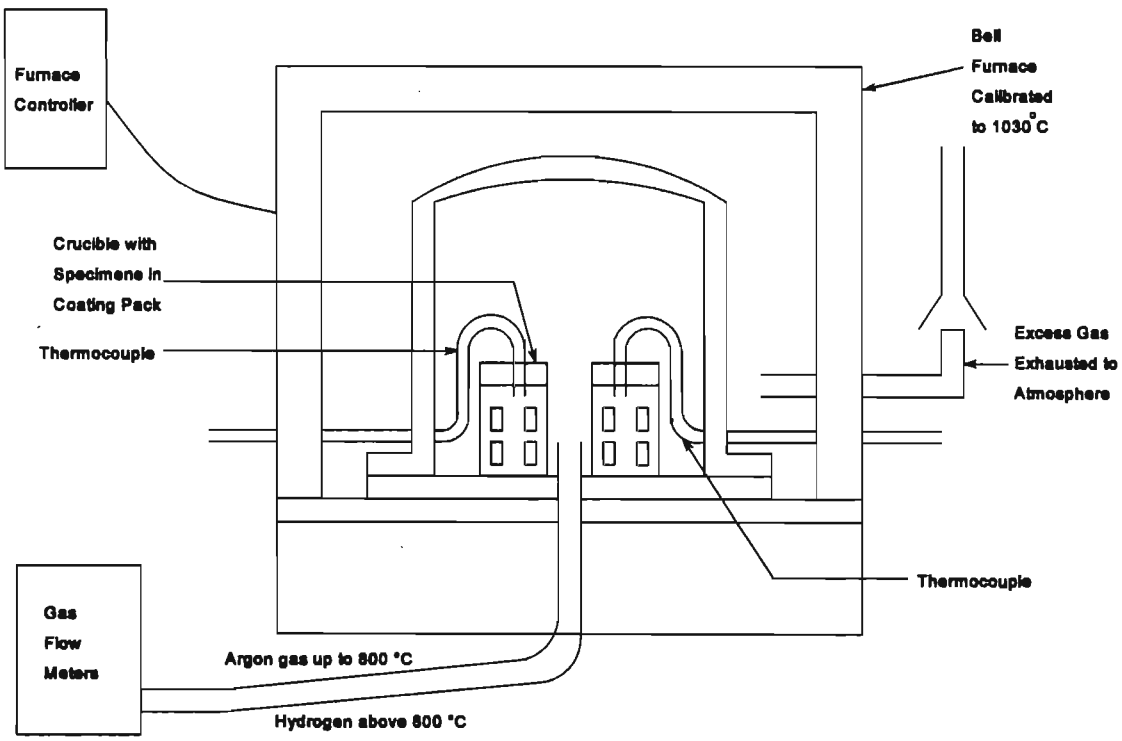

Figure 2.4 : Schematic illustration of the coating process apparatus

2.2.1.4 Unloading and Cleaning

The parts were carefully unloaded and sandblasted lightly to eliminate any trace of pack-powder. If sand-blasting was not carried out on the same day , the specimens were washed in luke warm water after removal from the oven.

2.2.2 Platinum Coating

Platinum was deposited on the specimens by electroplating. The coating thickness that could have been achieved depended on the age and quality of the electrolytic bath.

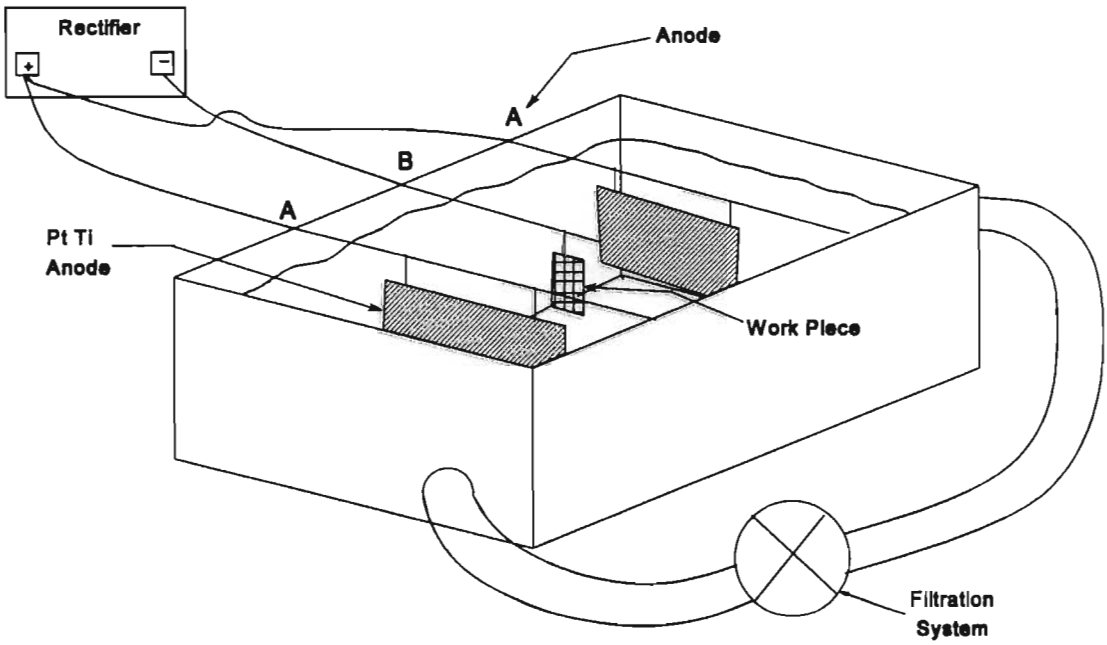

Figure 2.5 : Schematic illustration of the platinum electroplating process

The samples were first cleaned using an organic solvent. This process can be performed at either room temperature or at some higher temperature. The second step involved degreasing in a "mixture of chemicals", which was alkaline with NaOH as the major constituent (the exact composition of the mixture was not revealed by the source). Mineral acid was used for the activation step. This step removed the surface oxide layer and makes the surface more reactive. A thin coating of nickel was then applied, by the nickel strike process, to improve

the adhesion. Approximately 2μm of nickel was then deposited onto the surface by a standard electrolysis nickel process at 85-90°C. This step improved the base by covering inhomogeneities on the surface. The surface was then coated with a thin layer of gold (gold flash) to improve the adherence between the platinum and nickel. The final step was the application of the platinum layer using a standard electrolytic bath (figure 2.5) at 55-65°C.

The first batch of samples received (which were used to produce the TYPE I platinum aluminide coating) had a coating thickness of between 8 and 10μm. However, due to the age of the electrolytic bath, the samples that were coated with platinum only had a coating thickness between 4 and 6μm. A few samples with an initial platinum thickness of 2 μm were also produced for aluminizing.

2.2.3 Platinum Aluminide Coating

The platinum aluminide coating was produced by a two step process. Firstly, a platinum layer was electroplated on the specimen surface using the procedure described in the previous section. This was followed by the application of the aluminide coating via the packed cementation process described in section 2.2.1. It must be noted that the prealuminizing treatment was not performed.

2.3 Heat Treatment Procedure

The coated and uncoated samples underwent subsequent heat treatments. The uncoated, aluminide and platinum aluminide samples underwent an aging heat treatment in a vacuum furnace at 870°C for 16 hours. The pure platinum coated samples were subjected to a simulated coating heat treatment at 1030°C for 12 hours followed by the aging heat treatment at 870°C for 16 hours.

2.4 The Experimental Setup

A schematic illustration of the thermo-mechano-chemical system is shown in figure 2.6. The experimental apparatus was composed of two subsystems : the creep-fatigue loading apparatus and the gas mixing system. The complete experimental setup (figure 2.7) was capable of supplying the required atmosphere and loading conditions.

2.4.1 The creep-fatigue loading apparatus

The creep-fatigue loading system consisted of the split oven furnace and a standard electronically controlled servo hydraulic MTS testing system. The MTS machine consists of the electronic control unit and the servo hydraulic loading system (figure 2.8). The specimen was loaded onto the loading frame using austenitic stainless steel grips shown in

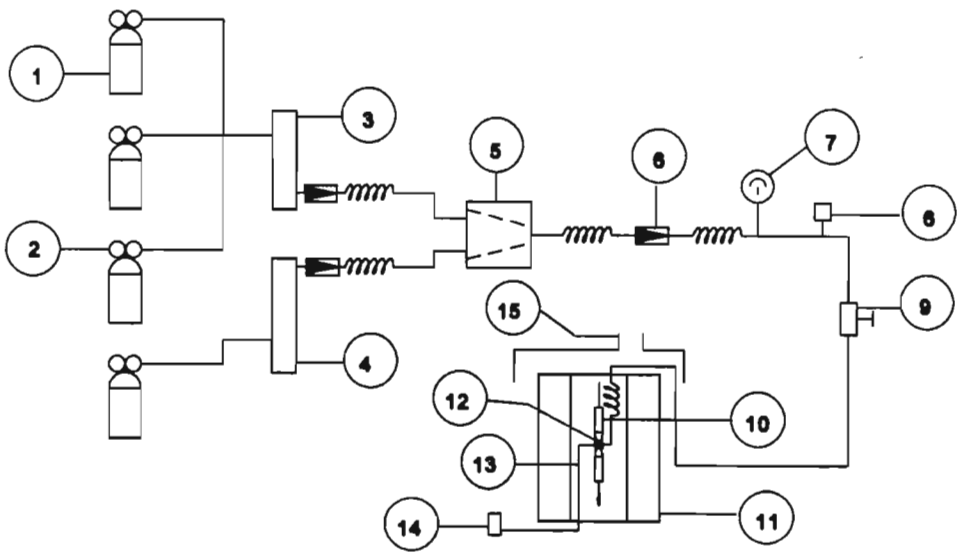

Key

1. Gas cylinders
2. Regulators
3. Gas flow meter for argon
4. Gas flowmeter for SO_2
5. Conical mixing chamber
6. Unidirectional valve
7. Pressure gauge
8. Safety valve
9. Shut-off valve
10. Fatigue specimen
11. Split oven furnace
12. Corrosion chamber
13. Type K thermocouple
14. Fluke thermometer
15. Exhaust system

Figure 2.6 : Schematic illustration of the thermo-mechanical loading system

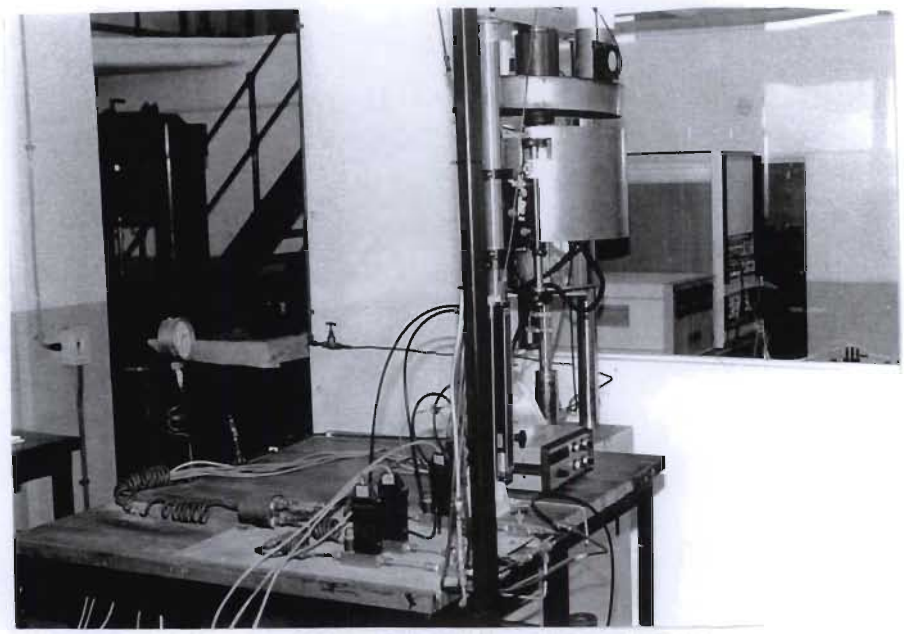

Figure 2.7 : The thermo-mechano-chemical experimental system

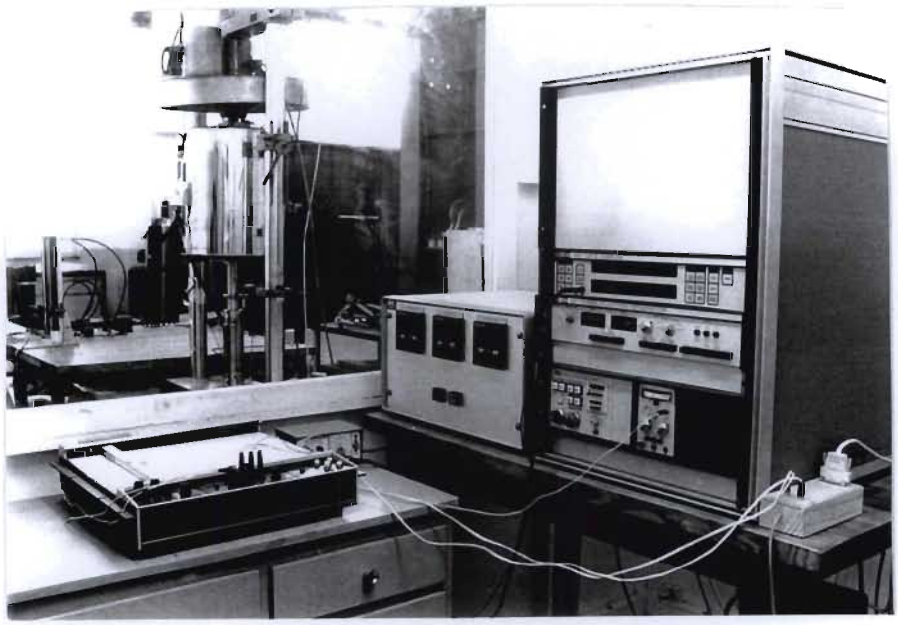

Figure 2.8 : The MTS loading frame and electronic control system

figure 2.9a. Loading of the fatigue sample was achieved via an hydraulic piston which could be controlled by either load feedback or displacement feedback which was obtained from the LVDT fitted to the piston.

A three zone Severn split oven furnace (Model SF 114/40/32/F) (Figure 2.9b) was used. The furnace had a core diameter of 114mm, outer case diameter of 300mm and length of 400mm.

The heat was produce by electrical heating coils situated in three zones, namely, the top, centre and bottom zones. Control of the temperature was achieved using a three-zone electronic control unit (Model CU3ZC/815S) fitted with three Eurotherm 815S closed loop controllers (figure 2.8). Each zone could be controlled independently. Ceramic insulation blocks were used to seal the open ends of the furnace to ensure that there was no excessive heat losses. The furnace was capable of 1100 °C ± 1°C. Due to inherent heat loses around the sealing blocks, the core temperature of the furnace was between 50°C and 100°C below the temperature measured close to the coils.

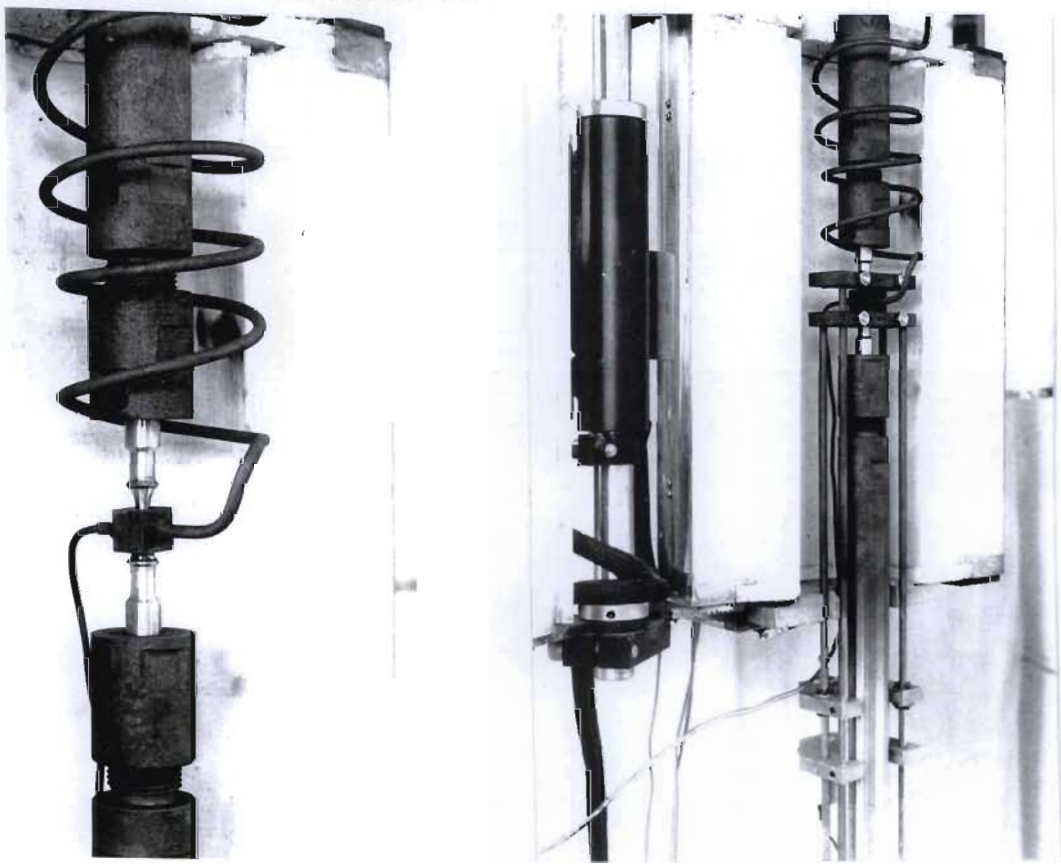

a **b**

Figure 2.9 : a) Specimen mounted in load frame using austenitic stainless steel grips with corrosion chamber in place.
b) Specimen attached to the loading frame with the LVDT in place.

Strain was measured using a SANGAMO type AES linear variable differential transducer (LVDT). Strain transfer rods attached to the collars on either end of the fatigue specimen gauge length was used to transmit the strain to the LVDT situated outside the furnace (figure 2.9b). The LVDT was cooled using a fan to avoid excessive heating of the device as a result of heat radiated from the furnace. The signal was conditioned and amplified using an

electronic LVDT signal amplifier to produce an output of ± 10V. The strain measuring range of the LVDT assembly was ± 1mm. Before performing the fatigue tests the LVDT was calibrated using a micrometer with an accuracy of ± 0.005 mm. The output from the LVDT was connected to a X-Y plotter and the data display unit of the MTS control panel. The load feedback was relayed from the MTS controller to the X-Y plotter. This enabled continuous monitoring of the load and strain. Stress-strain hysteresis loops were produced using the X-Y plotter.

In order to ensure that the specimen was exposed to the required temperature, the temperature close to the neck was measured using type K (chrome alumel) thermocouple. The thermocouple was attached to a Fluke digital temperature meter (model 51) which was used to monitor the temperature continuously.

2.4.2 Gas mixing and delivery system

The gas mixing system (figure 2.10) was capable of supplying a controlled gaseous environment to the neck of the specimen with a slight overpressure to ensure that the environment was not contaminated by air.

Figure 2.10 : The gas mixing system

The gas cylinders supplying the required gaseous environments were stored outside the laboratory (figure 2.11) as a safety precaution. Only argon (99.999% pure) and SO_2 (99.98 pure) were used in this research. Regulators were fitted to the cylinders to monitor the amount of gas in the cylinders and to regulate the gas flow out of the cylinder.

The gas mixing system was capable of mixing up to four gases in various proportions. Four flowmeters were used namely: two Matherson MFTV-33 electronic flow regulators and two Brooks rotameters (figure 2.10). For the current research only two flow meters were required. It was found that the electronic flowmeters were sensitive to the corrosive gases, especially the SO_2, hence, the rotameters were used for all the tests. The electronic flow meters were installed as a backup to the rotameters in the case of problems encountered with these flow meters during a test. The rotameters consisted of two different types, differentiated by their flowrate capacities. The one flowmeter was capable of approximately 30 l/min while the second was capable of approximately 3 l/min. The flowmeter with a flowrate of 30 l/min was used to control the flowrate of argon while the 3 l/min rotameter was used to measure the SO_2 flowrate since it was more accurate with the lower flowrates. Flow rate calibration curves were obtained for the rotormeters which took into the account the different physical properties of the gases to ensure an accurate control of the volumetric flow rate of the gases. The fittings and float in the rotameters were manufactured from stainless steel in order to avoid problems with corrosion.

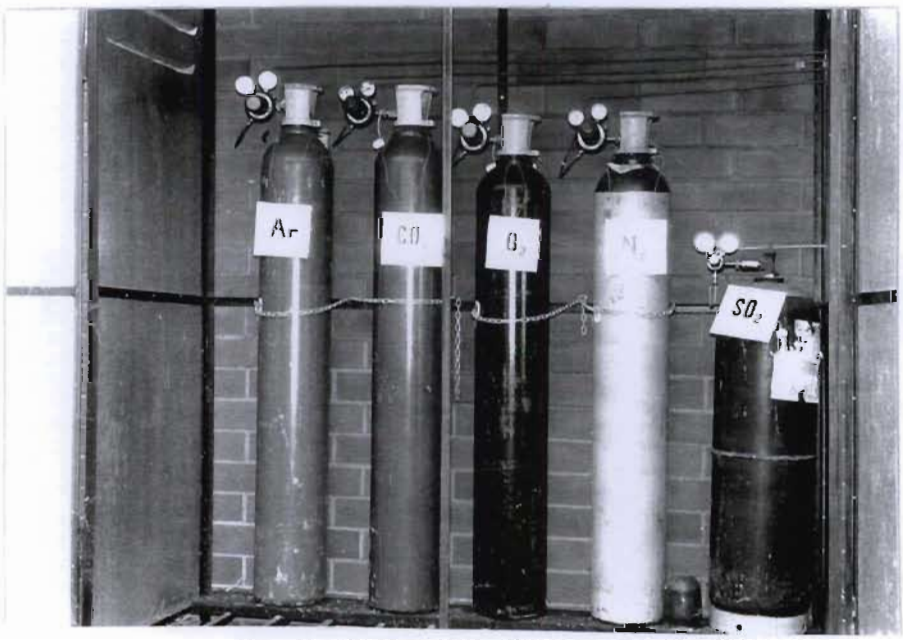

Figure 2.11 : Storage facility for the gas cylinders outside the laboratory

The measured gas flowed through coils and a one way valve before entering a conical mixing chamber. The coils present before the mixing chamber caused the flow to become turbulent and hence ensures thorough mixing of the gas in the mixing chamber. A venturi pipe design was used to measure the back pressure of the system. A one way valve ensured that there was unidirectional flow of gas. In order to protect the gas flowmeters in the case of clogging of the piping in the furnace, a safety valve was fitted in the system.

The mixed gaseous environment was conducted to the neck of the specimen (figure 2.9a) via stainless steel piping. The pipe was coiled in the furnace to ensure preheating of the gas before it entered the region around the neck of the specimen. The hot gas was confined to the neck of the specimen using a split corrosion shell (figure 2.9a) which fitted loosely around the neck. The gas entered the corrosion shell through a centrally located hole (figure 2.9a) on one half of the shell. A type K (chrome-alumel) thermocouple was inserted into a centrally positioned hole on the second half of the shell in order to measure the temperature close to the neck of the specimen. The excess gas flowing out from the corrosion shell was collected by a stainless steel hood and expelled from the laboratory via a exhaust system (figure 2.12). An extractor fan was used to force the gas out of the laboratory.

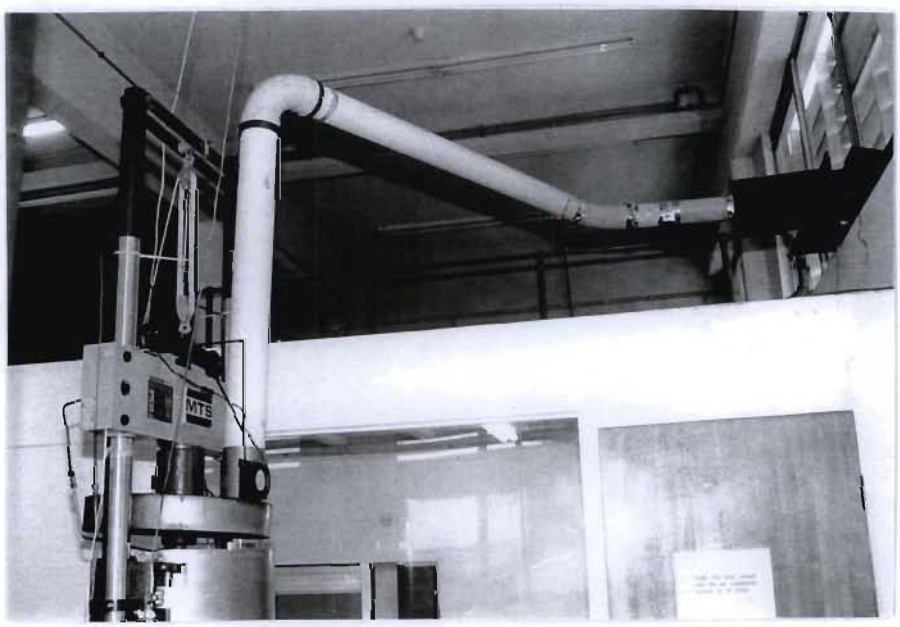

Figure 2.12 : Gas exhaust system

2.4.3 Corrosion chamber

Corrosion tests were performed on unloaded disk samples using the corrosion chamber shown in figure 2.13. The corrosion chamber was manufactured from 316 stainless steel and was capable of maintaining a positive pressure. The specimen was held in a specimen holder such that it was exposed directly to the incoming gas (figure 2.13b). The control atmosphere was fed in through a centrally located hole and a thermocouple was inserted through a hole directly opposite the gas inlet to measure the temperature in the corrosion chamber. Excess gas was exhausted through a hole drilled in the roof of the corrosion chamber as indicated in figure 2.13b. This ensured that there was always a fresh supply of gas in the chamber and there was no excessive build up of pressure in the corrosion chamber.

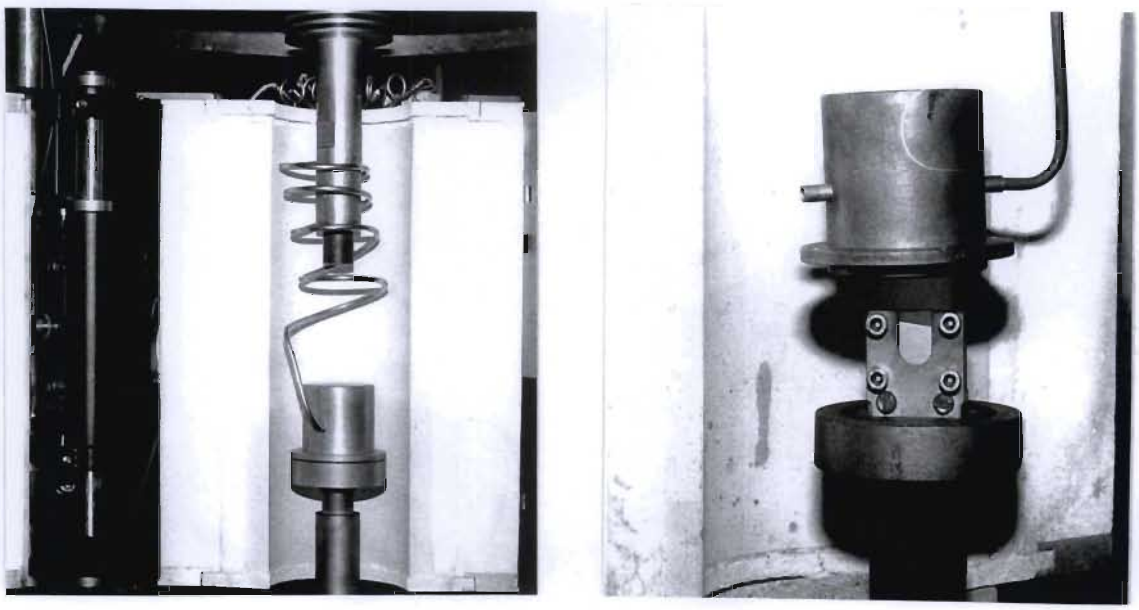

a **b**

Figure 2.13 : a) Corrosion chamber
b) Corrosion chamber open showing specimen location

2.5 The Parameters Selected for the Creep-Fatigue Loading

The strain range partitioning method of testing was adopted for the high temperature low cycle fatigue tests (HTLCF). The creep-plasticity mode of the SRP method [22] was selected because it contained creep in tension which exerts a significant influence on the failure processes in HTLCF. There are several techniques of producing creep tension and plastic

compression, namely; the tensile stress hold method, tensile strain hold method and the low/high strain rate method [22]. Of theses three methods the low/high strain rate method was selected because the MTS control system could not generate the more complex loading cycles.

A constant strain range of 0.66% was maintained across the neck of the specimen. The strain cycle constituted a tensile strain rate of 2.64×10^{-4} /sec and a compressive strain rate of 6.6×10^{-3} /sec (figure 2.14). The slow tensile strain rate ensured creep in tension and rapid

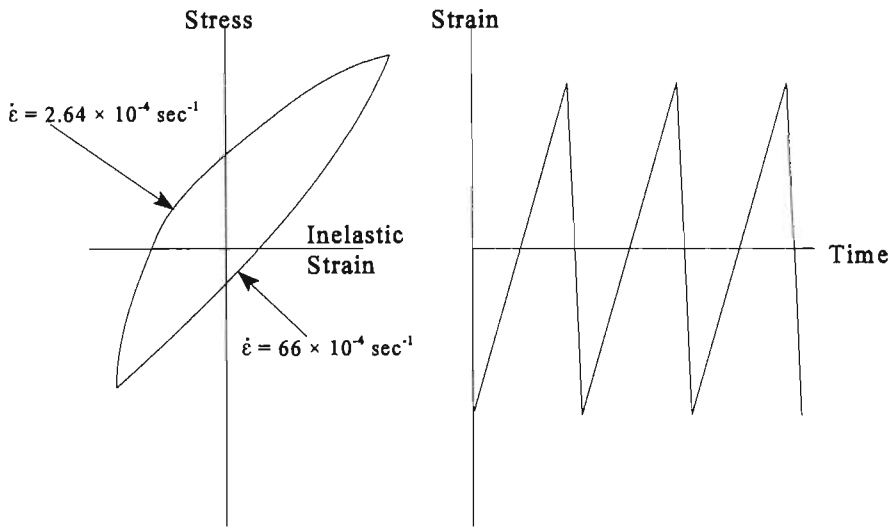

Figure 2.14 : The stress-strain loading cycle used

compressive strain rate ensured plastic compression. The strain range selected wassuch that the time to failure was sufficient to give an indication of the effect of the environment on the failure mechanism of the material and the time to failure was sufficiently low due to availability of the test apparatus. Although this strain range would result in a tensile strain (0.33%) very close to the fracture strain of aluminide coatings (0.03% to 0.45% -dependent on coating thickness[7]), it was within the strain ranges used for thermo-mechanical fatigue and low cycle fatigue reported in literature (as low as 0.25% [2] to S.R. > 0.66% [16, 17, 171]). The test environments were air, argon and Ar+5%SO_2. The high concentration of SO_2 used was selected to magnify the effect of sulphur bearing atmospheres on the fatigue failure. The argon and air environments were investigated for comparative purposes. All fatigue tests were performed at 870°C. The temperature selected took into account the capabilities of the furnace and was comparable with corrosion and fatigue tests presented in the available literature.

Due to severe cracking of the coating it was decided to perform further fatigue tests at a lower strain range in order to avoid pure mechanical failure of the coating. The environment selected for these tests was the sulphur containing atmosphere since it was basis of this study. Tests in air and argon atmospheres were not performed at this strain range because of the time constraints and the availability of material. Initial tests were performed at 0.44% strain range and 0.38% strain range (table 2.1) on aluminide coated MAR-M002 in Ar + 5%SO_2 in order to establish a suitable strain range for further tests.

Table 2.1: Strain ranges investigated for the low strain range tests.

Strain range	# of cycles to failure	Time to Failure (Hrs)
0.44%	1333	9.6
0.38%	6769	48.8

The 0.38% strain range was selected for further tests. The test temperature was maintained at 870°C and only the Ar + 5%SO_2 environment was investigated. These conditions were selected in order to establish an indication of the comparative performance of the various coating systems under the combination of sulphidizing environment and fatigue loading.

Corrosion tests were performed on unloaded disc samples in air and Ar + 5%SO_2 at 870°C in order to determine the corrosion products formed due to the environment. The corrosion specimens were exposed to the environments for 5 hours . The exposure time selected was deemed sufficient to obtain a representative evaluation of the corrosion products obtained.

2.6 Methods of Metallurgical Analysis

The creep-fatigue fracture samples and corrosion samples were analysed using the scanning electron microscope (SEM) with EDS analysis, Auger electron spectroscopy (AES) and x-ray diffraction. Preparation of the creep-fatigue samples involved preparing one of the fracture surfaces for fractography, EDS analysis and AES. The second fracture surface was cut longitudinally and metallographic samples of the longitudinal and transverse cross-sections were prepared. The samples were polished and then etched. A 10% phosphoric acid electrolytic etchant, with a dc voltage of 2V was used. The metallographic samples were analysed using the SEM and EDS analysis. X-ray diffraction analysis was performed on the corrosion samples in order to establish the corrosion products obtained.

2.6.1 Scanning electron microscopy (SEM) with energy dispersive spectroscopy (EDS) detector

Two makes of scanning electron microscopes were used, namely, the Hitachi 520 and the Joel JSM 6100 with a Noran EDS detector. The Hitachi 520 was used for photography of the fracture surface and metallographic samples only. The Joel was used for chemical analysis and photography of the metallographic samples. The Hitachi was fitted with secondary electron and backscatter detectors.

The Joel SEM was fitted with a secondary electron, backscatter and EDS detectors. The EDS detectors was capable of detecting elements down to boron. The analysis of the EDS spectrums were performed using the Voyager spectrum analysis program. This system was capable of spot chemical analysis, line scans and X-ray mapping. In order to optimize the resolution of the image and to ensure that the X-ray emission was of the expected phase an acceleration voltage of 25kV and working distance of 15 to 17mm was used. Electron beam spot size was approximately 10nm while excited volume had a diameter of approximately 1μm, hence, the minimum particle size that could be analysed was approximately 1μm in diameter.

2.6.2 X-ray diffraction Analysis (XRD)

X-ray diffraction analysis of the corrosion disc samples were performed to determine the phases present in the corrosion product. A Philips x-ray diffraction Analysis system with a cobalt K_α X-ray gun was used. The samples were scanned between angle 2θ of 20° and 100°. The x-ray diffraction spectrums obtained were analysed using the diffraction data tables available. The x-ray results obtained were purely of a qualitative nature, giving an indication of the phases present on the sample.

2.6.3 Auger electron spectroscopy (AES)

Auger electron spectroscopy was performed on the fractured samples in order to determine the presence and amounts of light elements present. The auger spectrum was acquired and processed by a computer package developed by the CSIR, Pretoria , South Africa.

AES Analysis was performed on the fractography samples only. Part of the fracture surface of the samples was ground at a angle of 10° (Figure 2.15) and polished. Polishing of the angled surface was done in order to obtain a more accurate analysis of this region. The fracture surface was not polished as analysis of the corrosion product on the surface was required. Due to irregular surface the analyses of this region was not as accurate as a polished surface, however , it served to give an indication of the elements present and their relative quantities. Point analyses were performed on the fracture surface (figure 2.15, point F), just below the fracture surface (figure 2.15, point I) and of the bulk material (figure 2.15, point B).

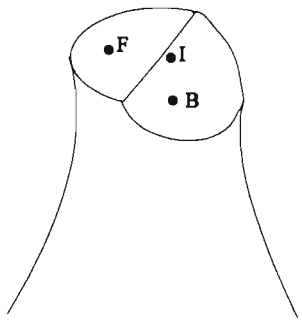

Figure 2.15 : Schematic illustration of fracture samples prepared for AES Analysis

The results obtained using an acceleration voltage of 5kV produced spectra with excessive noise. Using an acceleration voltage of 10kV instead produced acceptable results. Another problem encountered was the presence of contaminants on the specimen surface which resulted in excessive noise and unacceptable amounts of carbon in the analysis. Sputtering the surface for longer periods and sputtering during the acquisition of the spectrum solved this problem to a large degree, however, there are a few results which displayed excessive amounts of carbon.

The AES spectra obtained were analysed qualitatively and quantitatively using the standard spectra for the various elements. Due to the overlapping of the oxygen and chromium peaks, the quantitative analysis of the spectrum had to be adapted to accommodate this problem. The technique used was as follows (Consider the standard spectra of oxygen and chromium in figure 2.16):

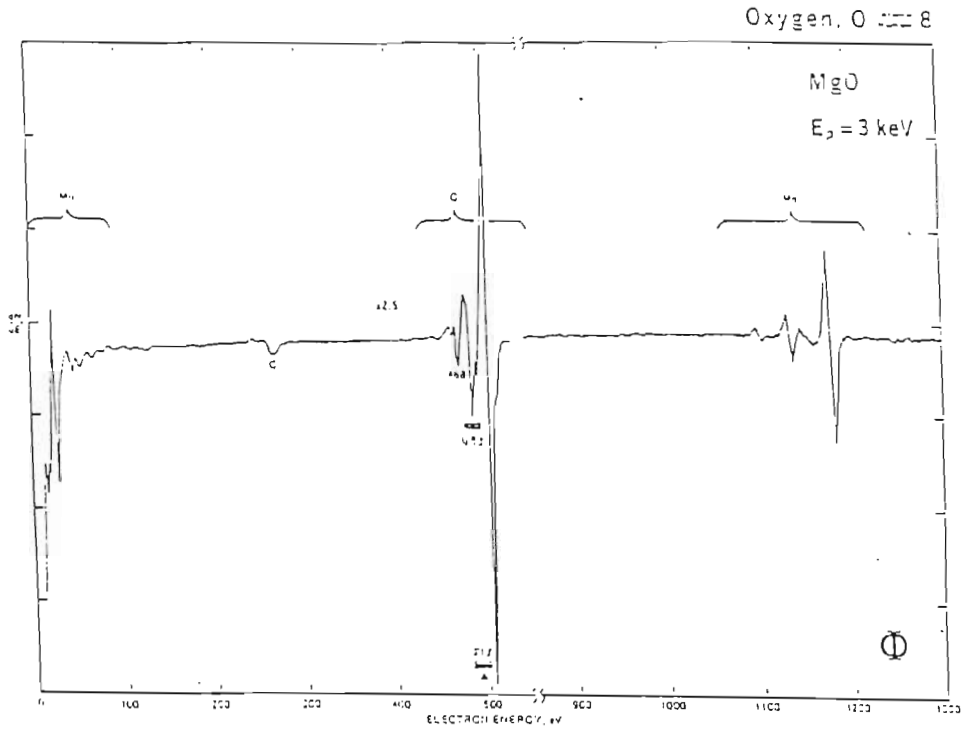

a

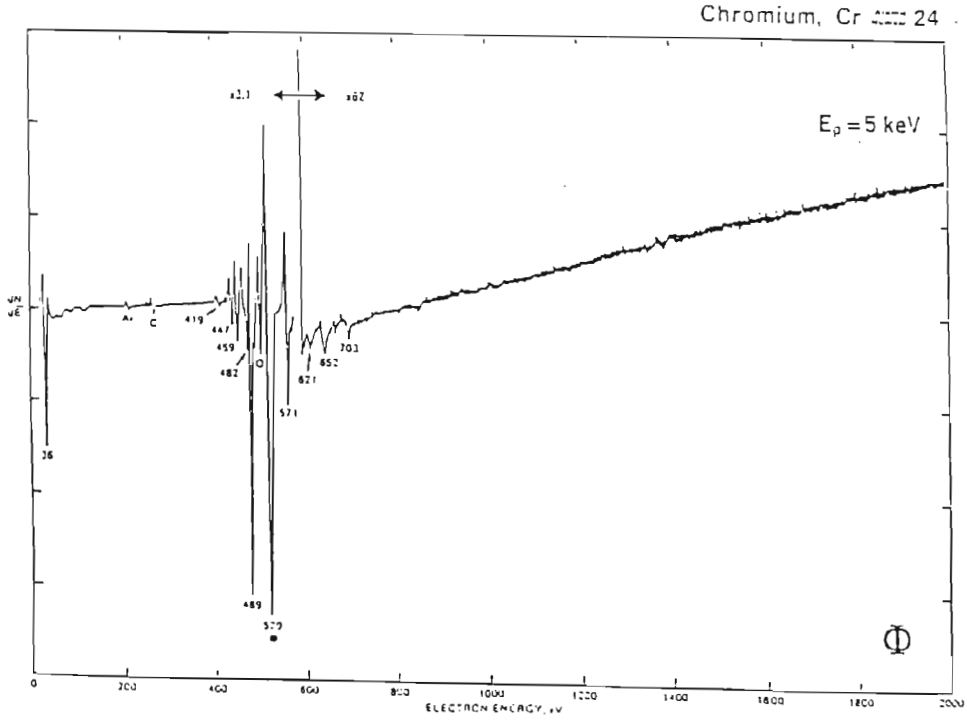

b

Figure 2.16 : a) AES spectrum for oxygen

b) AES spectrum for chromium

2. since the "lower half" of the peaks are relatively unaffected by the overlap of the spectra, the "lower half" of the acquired spectra are measured.
3. the measured "lower half" of the spectrum generated were then multiplied by the ratio, T/B, to obtained a corrected value for the "top half" of the chromium and oxygen peaks.
4. The measured lower and calculated upper peaks were summed to obtain the net peak to peak values for the oxygen and chromium peaks.

The atomic weight percent of the elements were obtained using the following equation

$$\text{ATOMIC WEIGHT \% OF ELEMENT X} = \frac{\frac{I_x}{S_x}}{\Sigma \frac{I_i}{S_i}} \qquad 2.1$$

where I_x - was the peak to peak intensity of the element x

S_x - was the relative elemental sensitivity factor of element x

There are several inherent flaws with this method of quantitative Analysis. These are : (1) the matrix effect on electron escape depths and backscatter factors, (2) chemical effects on peak shapes, and (3) surface topography. Hence, the results obtained using this analytical technique will give a qualitative indication of the amounts of elements present.

CHAPTER 3

3. RESULTS

3.1 CHARACTERIZATION OF THE MATERIAL SYSTEMS

3.1.1 Uncoated MAR-M002

MAR-M002 nickel base superalloy was received as unidirectionally solidified bars. The chemical composition (Table 3.1) of the material was determined for comparison with nominal composition of the alloy.

Table 3.1: The chemical composition in weight percent of MAR-M002 nickel-base superalloy

	Ni	Cr	Co	W	Ta	Al	Ti	C	Zr	Hf	Others
Material as Received	59	8.9	10.4	10.2	1.8	5.2	1.35	0.35	0.23	1.9	0.16Fe,0.1Nb
Nominal composition as per reference 173	61	9.0	10.0	10.0	2.5	5.5	1.5	0.14	0.05	1.5	0.015B

In order to establish the consistency of the mechanical properties, Vickers hardness tests were performed on several samples. A nominal hardness value of 414 HV was obtained. Metallographic examination of cross-sectional samples revealed a dendritic type microstructure with dendrites growing in the direction of solidification (figure 3.1).

The interdendritic zone (figure 3.1b) was composed of γ-γ' eutectic and grain boundary carbides. The larger carbide particles were made up of mainly Hf, Ta, Ti, and W with Hf and Ta making up the major constituents. The smaller blocky carbides were made up of mainly Hf with smaller amounts of Ta, W and Zr. From the analyses of the different regions in the interdiffusion zone it was evident that Hf and Zr were concentrated in this

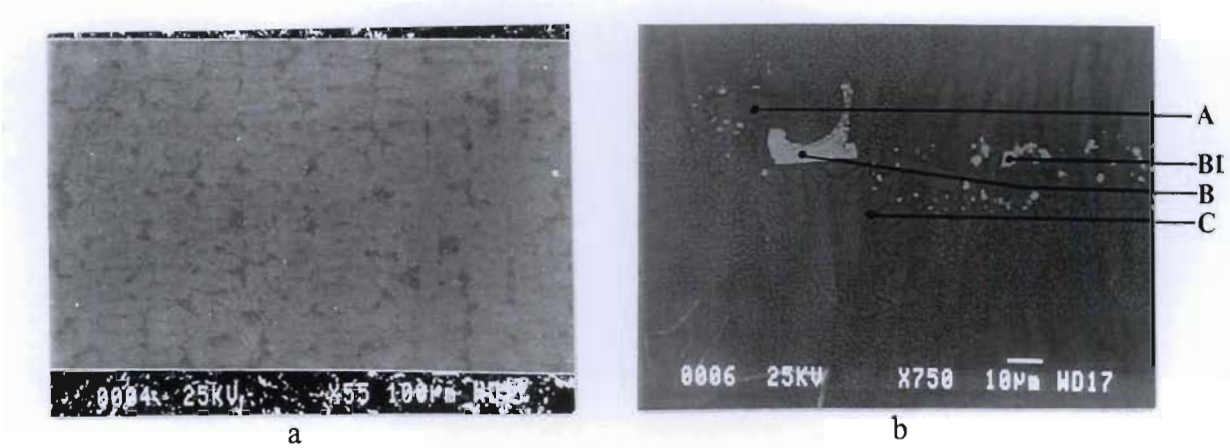

a b

Element	Weight Percent					
	A	B	B1	C	Dendritic Grain	General Analysis
Al	7.63	0.00	0.00	6.52	6.43	6.67
Ti	2.78	10.75	0.58	2.26	1.45	1.57
Cr	3.34	0.45	0.59	4.45	6.34	6.68
Co	7.69	0.52	0.68	8.04	8.06	8.29
Ni	67.77	2.14	4.94	65.83	60.20	61.48
Zr	0.21	0.00	1.42	0.00	0.49	0.00
Hf	2.24	38.24	78.62	2.91	0.92	1.56
Ta	1.58	37.88	10.33	2.80	2.46	3.10
W	6.75	10.01	2.83	7.20	13.66	10.64

Figure 3.1 : Metallographic examination of directionally solidified MAR-M002 as received.

a) Overall picture showing dendrites in the direction of solidification.

b) The interdendritic segregation zone.

region when compared with the analysis of the dendritic grain. The dendritic grain was made up of a high volume fraction of γ'. This region showed a higher concentration of the solid solution strengthening elements Cr, Co and W.

The X-ray diffraction analysis of an uncoated sample after aging at 870°C for 16 hours (figure 3.2) revealed that $Ni_3(Al,Ti)$ γ' formed the major constituent in the alloy. Smaller amounts of Ni_3Ta, Ni_3Al and Ni_3Ti γ' were also present.

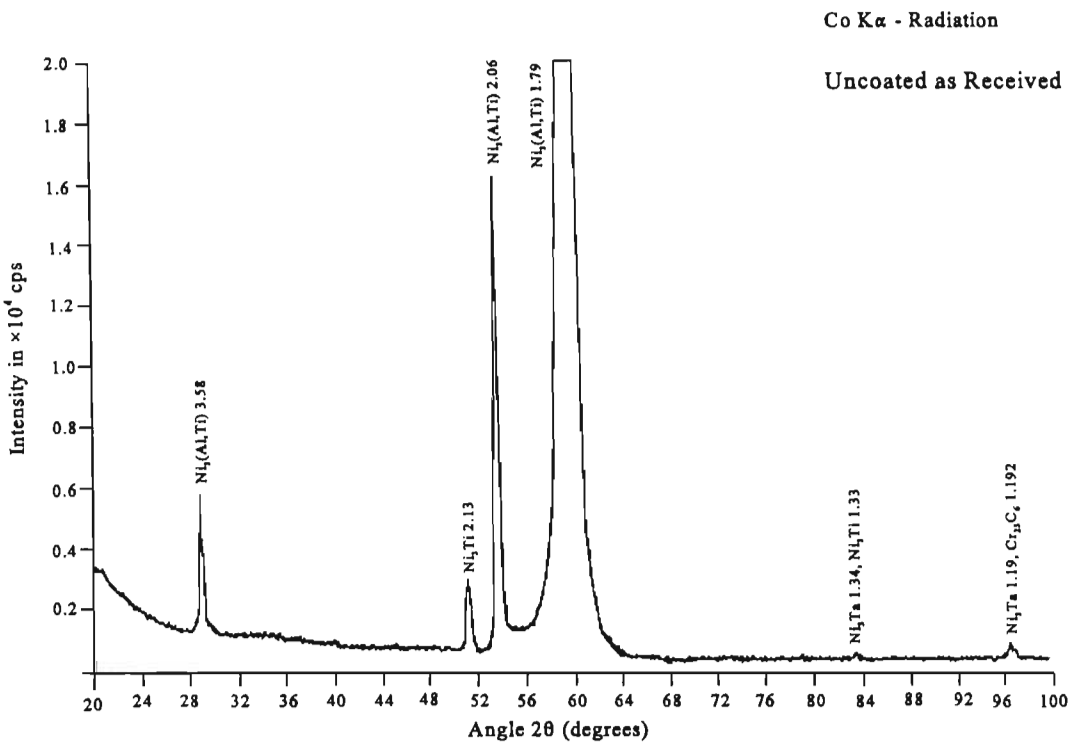

Figure 3.2 : X-ray diffraction analysis of uncoated MAR-M002 after aging at 870 °C for 16 hours.

3.1.2 Aluminide Coated MAR-M002

A high temperature low activity process was used to produce an aluminide coating with the microstructure shown in figure 3.3. The coating had a typical two zone structure, consisting of the coating (NiAl) layer and interdiffusion zone.

The coating layer was enriched in nickel and aluminium with relatively "small" traces of the substrate elements. The interdiffusion zone showed a higher concentration of the substrate alloying elements, namely, W, Cr, Ta and Co. The tungsten content in the interdiffusion zone was substantially higher than that in the substrate and the coating layer.

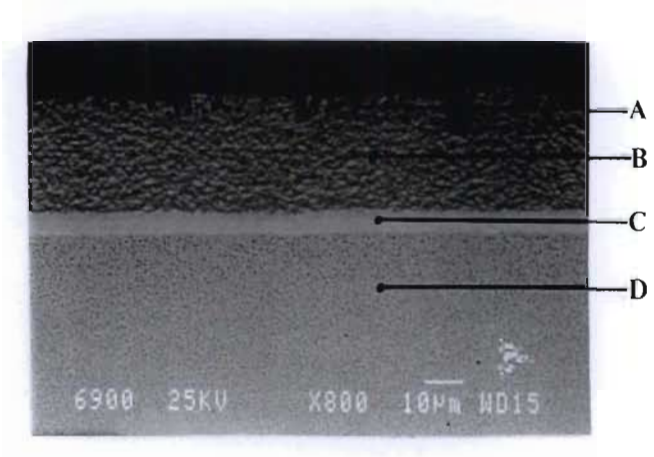

Elements	Weight Percent			
	A	B	C	D
Al	26.57	26.06	9.21	6.07
W	5.06	6.45	16.15	9.87
Ti	0.71	0.63	2.08	1.55
Cr	5.99	5.65	10.58	6.62
Co	7.48	8.59	10.18	9.33
Ni	50.63	51.93	46.55	61.85
Hf	1.55	0.14	1.08	0.12
Ta	2.02	0.55	2.36	2.35
Zr	0.00	0.00	1.81	2.27

Figure 3.3 : Cross-section showing morphology of aluminide coating as received with EDS analysis

The chemical composition of the substrate was comparable with that of the nominal composition of the alloy. The coating thickness (i.e. coating + interdiffusion zone) was approximately 30µm, 6µm of which was the interdiffusion zone.

X-ray diffraction analysis of an aluminide coated sample as received (figure 3.4) showed NiAl as the principal phase in the coating layer. A significant amount of Al_2O_3 and Cr_2O_3 was also present which is the protection mechanism of aluminide coating.

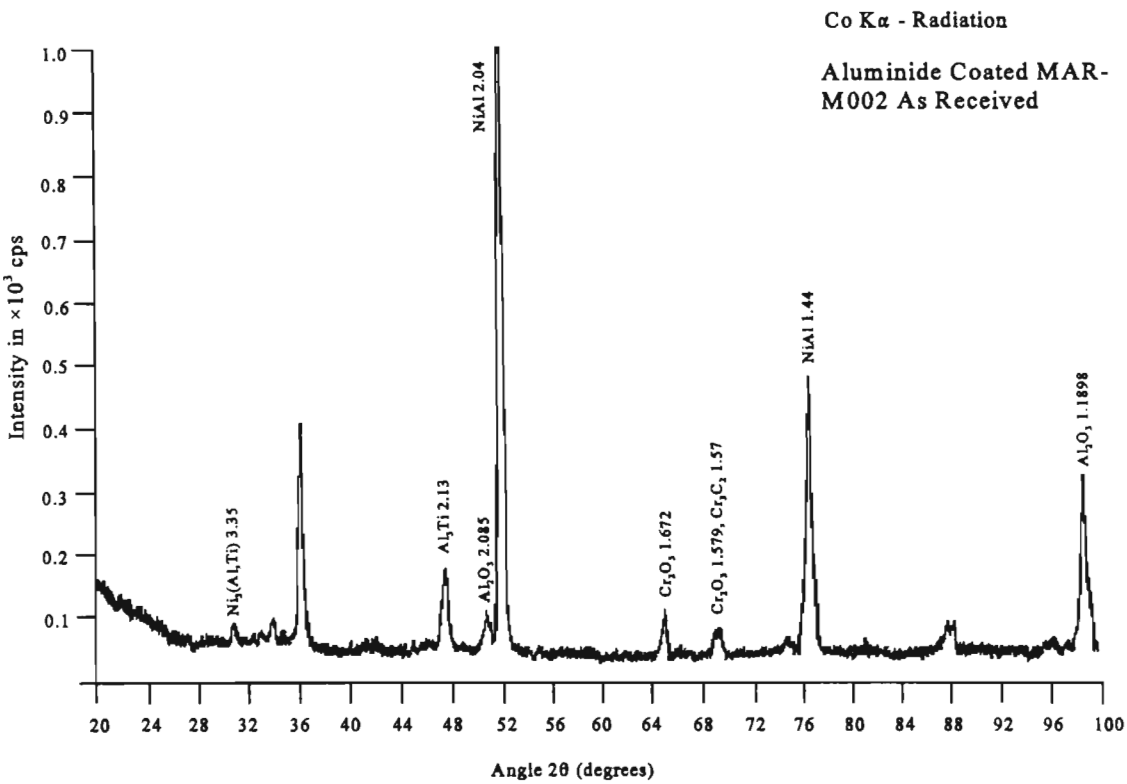

Figure 3.4 : X-ray diffraction analysis of aluminide coated MAR-M002 as received

3.1.3 TYPE I Platinum Aluminide Coated MAR-M002

The TYPE I platinum aluminide coating revealed a microstructure (figure 3.5) very similar to the conventional aluminide type coating structure. The coating system was composed of the coating/NiAl layer, the interdiffusion zone and the base metal. The coating layer displayed a "single" phase structure with relatively large amounts of pack particles imbedded close to the external surface. EDS of these particles (figure 3.5) showed that the "lighter" particles were composed primarily of chromium and the "dark" particles were effectively Al_2O_3. The coating was rich in nickel and aluminium with the platinum content being highest close to the external surface. Although significant amounts of platinum were detected in the coating, no distinctive platinum phases were observed.

EDS analysis of the coating showed significant variation of the platinum content in different regions, figure 3.5. Figure 3.5a showed an area where platinum was detected in significant quantities in the external surface with the platinum content decreasing towards the substrate. Figure 3.5b shows a region where the platinum content was significantly

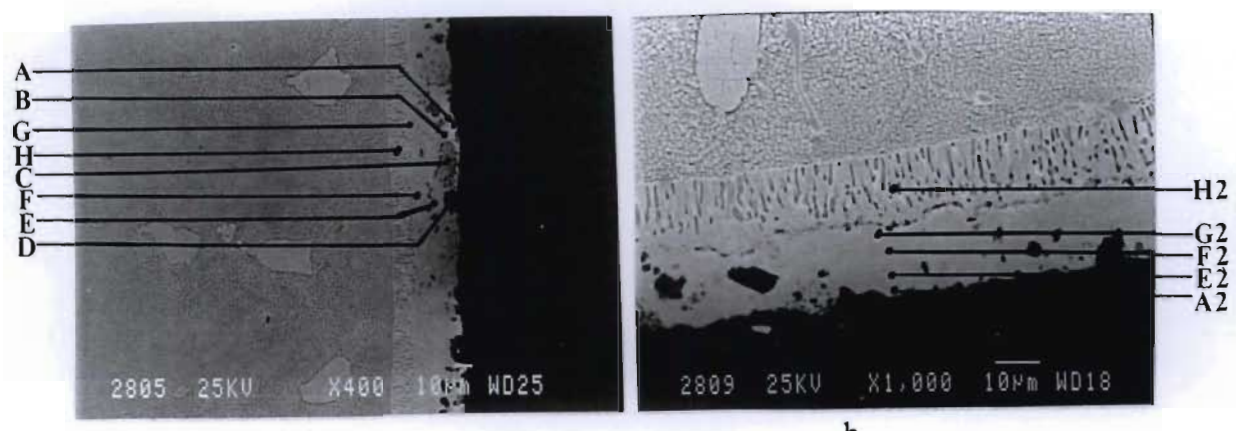

a b

Element	Weight Percent								Weight Percent				
	A	B	C	D	E	F	G	H	A2	E2	F2	G2	H2
Al	22.64	21.26	18.77	59.29	20.22	16.29	18.12	13.92	24.89	24.37	21.40	7.71	14.16
Zr	0.00	0.00	0.00	0.33	0.00	0.00	0.00	0.00	0.47	0.35	0.09	0.00	0.00
Cr	1.68	3.39	46.70	0.15	5.02	5.42	5.00	6.60	1.78	2.14	4.97	58.94	10.17
Co	4.17	9.84	6.02	0.14	11.72	12.49	14.06	12.85	9.62	11.30	13.22	7.24	14.48
Ni	47.41	52.58	24.87	1.36	57.74	54.70	54.40	49.01	61.19	61.35	56.83	19.58	50.70
Pt	**21.87**	**12.65**	**3.22**	**0.89**	**3.31**	**3.90**	**0.39**	**9.08**	**1.33**	**0.15**	**0.99**	**0.68**	**1.54**
Hf	0.00	0.00	0.00	0.00	0.57	2.30	0.00	0.00	0.00	0.00	0.50	0.09	0.00
Ta	0.00	0.00	0.00	0.17	0.00	0.56	0.83	0.00	0.00	0.00	0.01	0.70	0.00
W	2.14	0.00	0.00	0.00	0.00	0.67	0.00	3.29	0.55	0.00	0.00	0.14	3.71
Ti	0.10	0.28	0.43	0.00	1.43	3.67	5.20	5.26	0.16	0.33	2.00	4.92	5.24
O	0.00	0.00	0.00	40.67	0.00	0.00	0.00	0.00	0.00	0.00	0.00	0.00	0.00

Figure 3.5 : TYPE I platinum aluminide coated MAR-M002 microstructure

a) Region with high platinum content

b) Region with low platinum content

lower and was more uniformly distributed through the coating. There was notable amounts of platinum present in the interdiffusion zone as well. The interdiffusion zone also showed a very different morphology to that observed in the aluminide coated sample; a more columnar structure was obtained. The absence of refractory element Ta and the relatively low W content also was a significant difference from the aluminide coated sample.

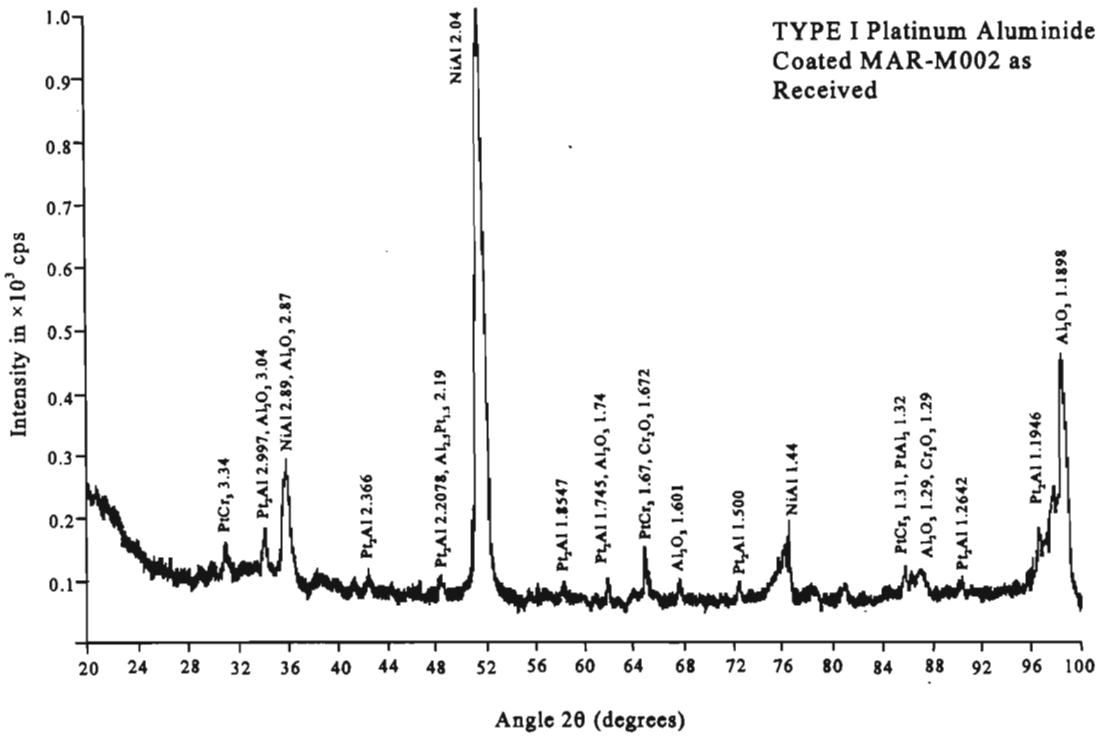

Figure 3.6 : X-ray diffraction analysis of TYPE I platinum aluminide coated MAR-M002 as received

The x-ray diffraction spectrum of the "TYPE I" platinum aluminide coating (Figure 3.6) revealed the main constituent phase to be NiAl. Small amounts of the platinum phases, $PtAl_2$ and Pt_2Al were detected. The presence of Al_2O_3 and Cr_2O_3 was also evident as in the case of the aluminide coating. The platinum phases did not manifest themselves as distinct structures but were "dissolved" in the NiAl matrix of the coating.

3.1.4 TYPE II Platinum Aluminide Coated MAR-M002

The TYPE II platinum aluminide coating was produced by a similar technique as that which was used to produce the TYPE I coating, however, there was a distinct difference in the microstructure obtained (figure 3.7). The coating morphology can be described in terms of a "three" zone type structure, the platinum rich outer zone, the NiAl zone and the interdiffusion zone. The coating layer was composed of an outer zone which was rich in platinum and aluminium (represented by the white phase); and the inner NiAl zone which was composed mainly of nickel and aluminium. High magnification of the outer zone

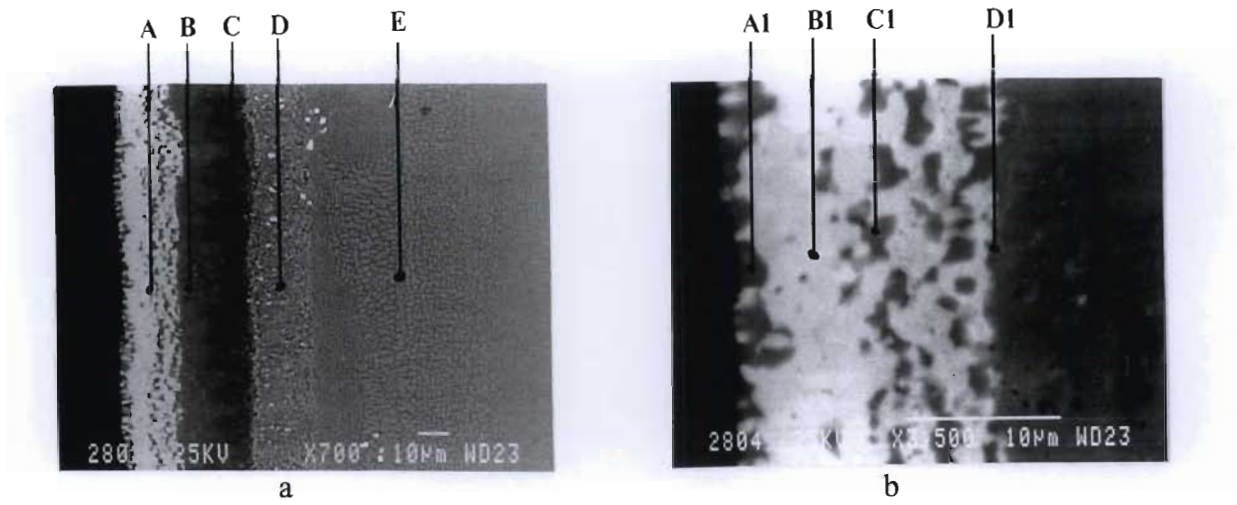

a b

Elements	Weight percent				
	A	B	C	D	E
Al	26.97	27.75	26.33	15.46	6.32
Cr	4.13	0.64	2.87	11.46	7.30
Co	1.47	6.23	10.08	9.08	9.11
Ni	24.4	51.22	52.11	42.80	57.02
Pt	**41.01**	**9.34**	**1.64**	**0.00**	**0.00**
Ti	0.12	0.07	1.06	2.27	1.58
Zr	0.00	0.02	3.85	0.72	1.02
Hf	0.69	0.60	0.30	1.47	0.22
Ta	0.96	1.77	0.00	2.39	2.43
W	0.27	2.35	1.77	14.34	15.01

Elements	Weight percent			
	A1	B1	C1	D1
Al	22.28	18.42	27.67	26.66
Cr	1.46	6.67	1.41	1.75
Co	2.39	0.32	3.02	4.46
Ni	53.63	5.21	46.13	46.72
Pt	**19.94**	**68.51**	**20.07**	**13.52**
Ti	0.00	0.17	0.21	1.32
Zr	0.00	0.00	0.24	0.00
Hf	0.10	0.36	0.00	1.16
Ta	0.20	0.00	0.00	0.55
W	0.00	0.34	1.24	3.86

Figure 3.7 : Morphology of TYPE II platinum aluminide coated MAR-M002 as received

a) Low magnification showing overall coating structure

b) High magnification of the Pt_2Al layer

revealed that it was composed of two distinct regions namely "white" and "grey" regions. The "white" region consisted mainly of aluminium and platinum with small amounts of chromium and nickel. The "grey" region was mainly composed of Pt, Al and Ni of which Ni was the major constituent. In the inner zone of the coating, the main constituents are Ni and Al, with Pt decreasing markedly as the interdiffusion zone was approached. The

interdiffusion zone showed a composition similar to that observed in the aluminide coating. The amounts of refractory elements W and Ta were significantly higher than in the TYPE I platinum aluminide coating. No Pt was detected in the interdiffusion zone.

X-ray diffraction analysis indicated that the outer layer was made up principally of Pt phases namely $PtAl_2$, Pt_2Al and Cr_3Pt (Figure 3.8). The most prominent of these phases was the $PtAl_2$ phase. A significant amount of NiAl was also present as would be expected for a modified aluminide coating. As for the aluminide and TYPE I platinum aluminide coating, Al_2O_3 was detected on the coating surface.

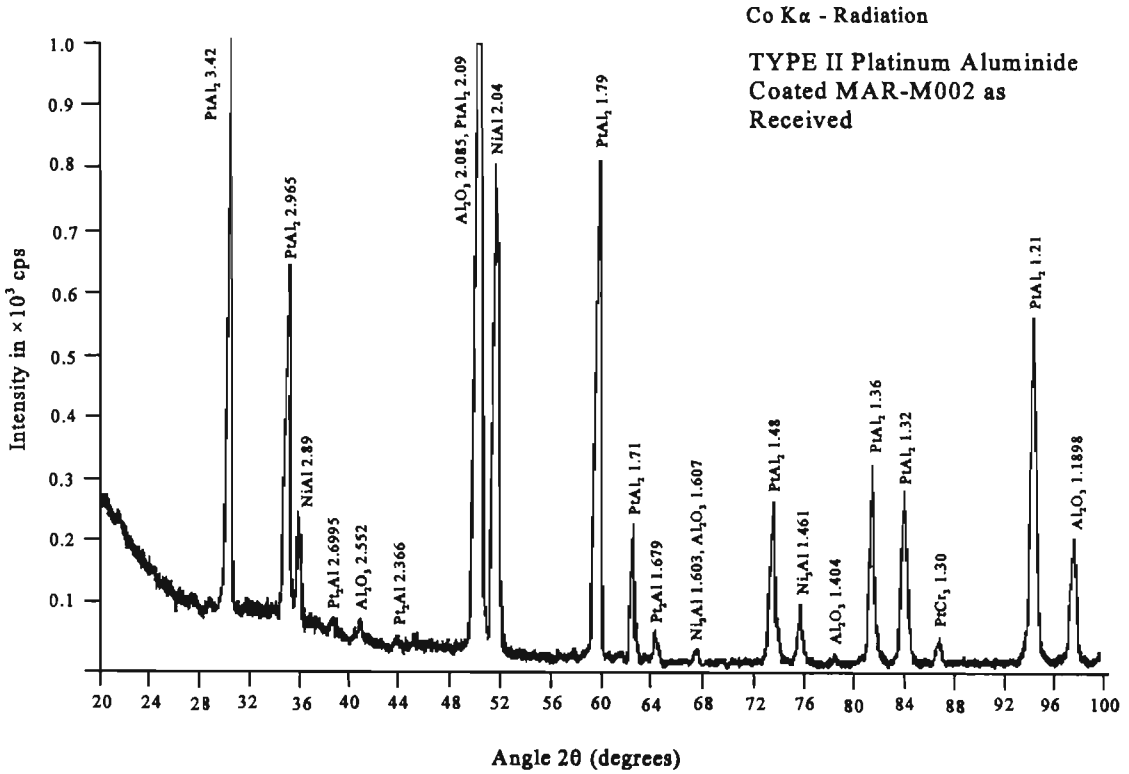

Figure 3.8 : X-ray diffraction analysis of TYPE II platinum aluminide coated MAR-M002 nickel based superalloy as received

3.1.5 2μm Platinum Aluminide Coated MAR-M002

The 2μm platinum aluminide coating was produced by applying a 2μm thick platinum layer followed by aluminizing, resulting in a coating morphology very similar to that of the TYPE II platinum aluminide coating (Figure 3.9). The coating consisted of three zones, namely, the outer zone which was rich in platinum, a middle zone which was made up of essentially nickel and aluminium with small amounts of platinum dissolved in it (essentially a NiAl uniphase layer) and the interdiffusion zone which was composed of the elements similar to that found in the aluminide coating interdiffusion zone.

The outer platinum rich zone was significantly thinner than the that observed in the TYPE II platinum aluminide coating and showed a very different morphology. The structure indicated that this zone was a mixture of NiAl and platinum rich phases, namely, Pt_2Al and $PtAl_2$. Refractory elements W, Ta and Zr were virtually excluded from the coating. The coating thickness was approximately 35μm, 15μm of which made up the interdiffusion zone and the platinum rich zone made up 5μm. The NiAl middle zone showed a significantly lower platinum content and a higher presence of the substrate alloying elements.

The interdiffusion zone was composed of mainly Al, Cr, Ni, Wand Co. The W and Ta content was very much larger than that observed in the NiAl layer. The presence of pack particles in the coating layer was evident in small quantities. These were made up of mainly small particles of aluminium oxide.

The X-ray diffraction analysis of the 2μm platinum aluminide coated MAR-M002 sample in the as received condition indicated (figure 3.10) that the initial platinum coating thickness played an important role in the phases formed in the coating. The amount of platinum intermetallics formed was significantly lower, with NiAl aluminium showing up as the major constituent of the coating. The platinum rich zone was made up of Pt_2Al.

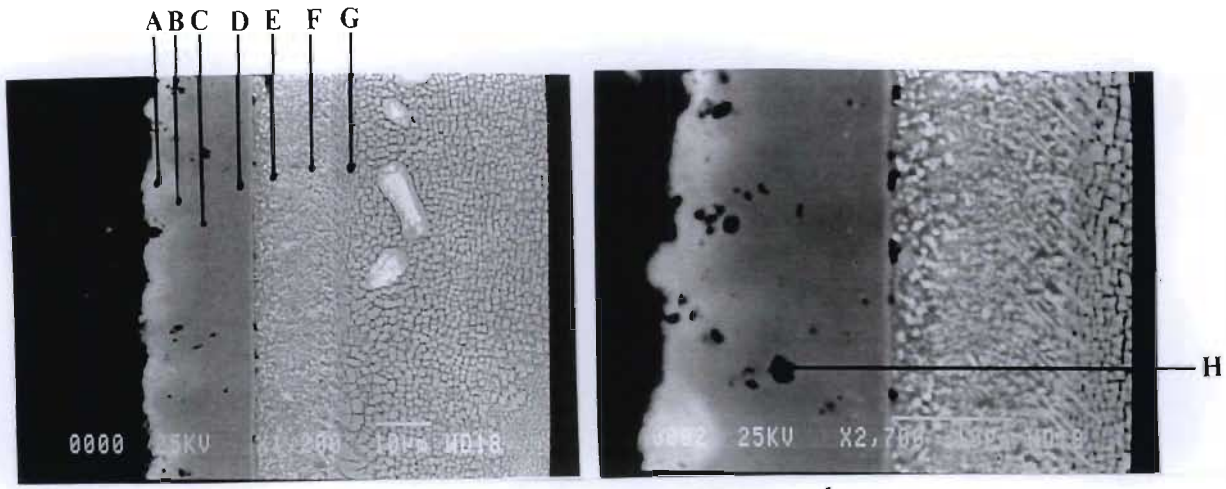

Elements	Weight percent							
	A	B	C	D	E	F	G	H
Al	21.07	25.58	25.96	21.48	13.25	9.97	7.18	32.77
Cr	1.67	1.18	1.58	4.13	10.87	14.98	6.22	1.43
Ni	39.46	52.78	58.44	56.69	41.08	33.10	59.55	34.35
Pt	**34.62**	**17.53**	**4.67**	**2.62**	**2.24**	**1.13**	**0.00**	**1.63**
Ti	0.00	0.00	0.11	1.51	1.20	1.46	1.56	0.23
Zr	0.00	0.00	0.00	0.00	0.00	0.71	0.14	0.00
Hf	0.78	0.00	0.36	1.09	0.00	0.89	1.04	0.24
Ta	0.63	0.00	0.00	1.23	1.00	3.56	2.09	0.00
W	0.00	0.00	1.32	2.59	20.47	23.06	13.84	0.56
Co	1.78	2.92	7.55	8.68	9.89	11.15	8.38	5.88
O	0.00	0.00	0.00	0.00	0.00	0.00	0.00	22.91

Figure 3.9 : 2μm Platinum aluminide coated MAR-M002 as received

a) Low magnification showing overall coating morphology

b) High magnification showing structure of outer platinum rich layer

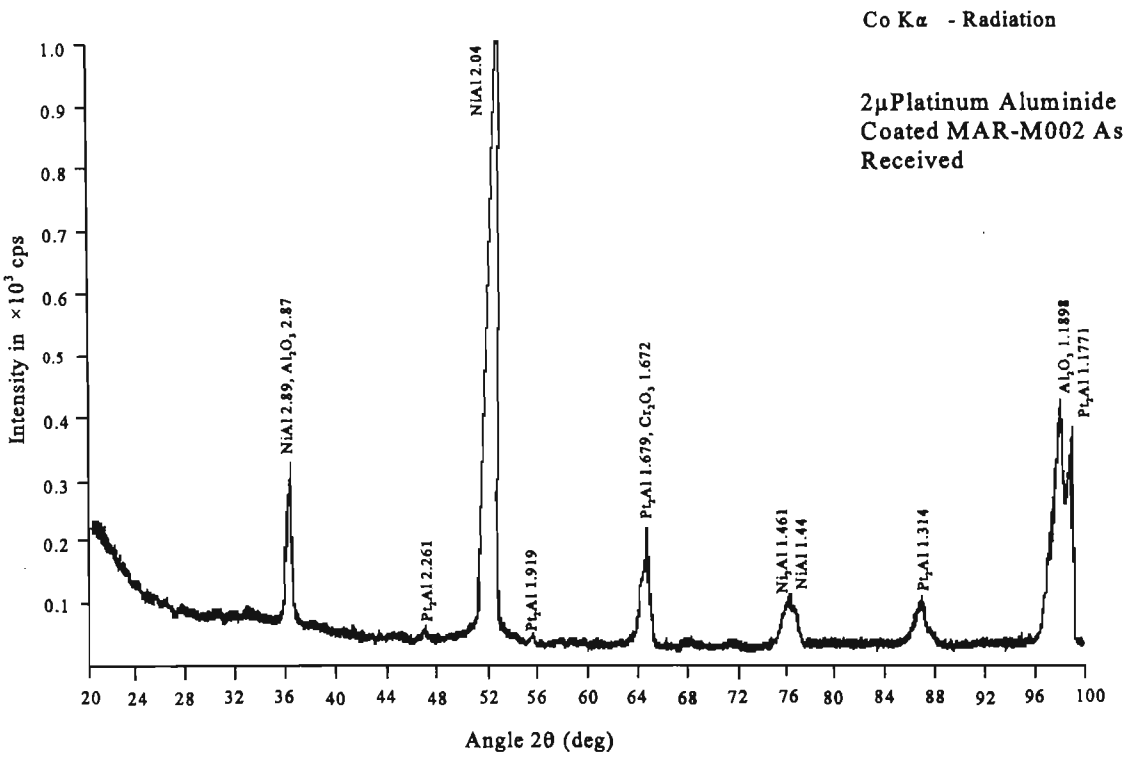

Figure 3.10 : X-ray diffraction of 2μm platinum aluminide coated MAR-M002 as received

3.1.6 Platinum Coated MAR-M002

The cross-sectional analysis of a platinum coated sample (figure 3.11) revealed a coating thickness of approximately 17μm. The coating thickness was found to be non-uniform. There was no distinct interdiffusion zone as observed in the aluminide coatings. In the region adjacent to the coating there was some degree of interaction between the substrate and platinum coating. The cuboidal γ' had been "dissolved", resulting in a γ' denuded zone. The density of γ' decreases from the substrate to the coating; with the region immediately adjacent to the coating layer showing complete dissolution of the γ'. Extensive porosity was observed between the coating and the substrate.

EDS analyses traversing the coating layer showed that the coating layer was composed of mainly nickel and platinum. The white phases observed were essentially composed of platinum and nickel with small amounts of Al, Ti, Cr and Co. The grey regions

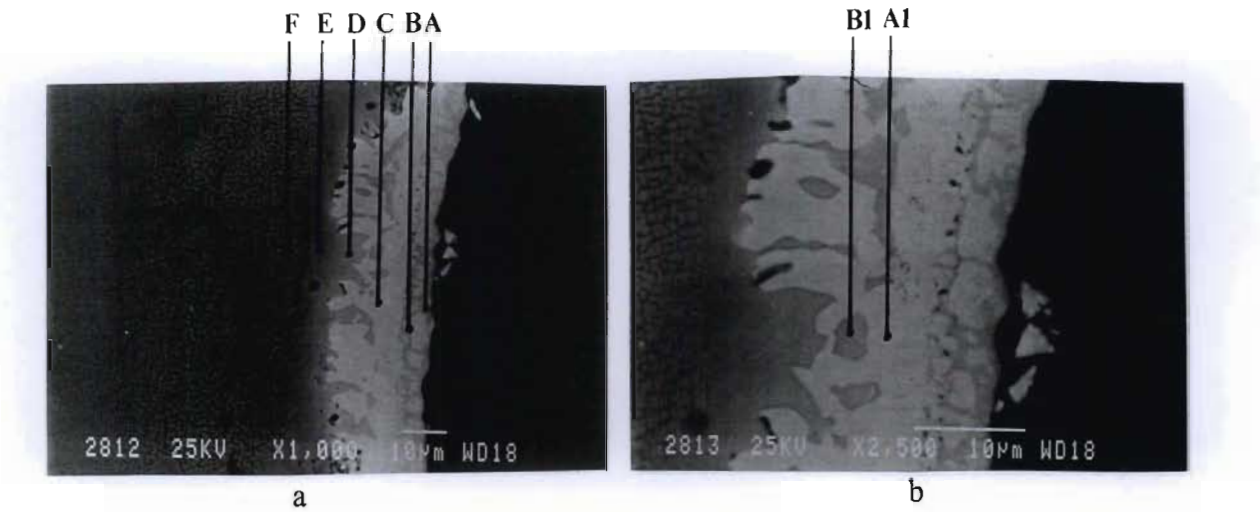

Elements	Weight percent					
	A	B	C	D	E	F
Al	0.85	2.19	3.83	2.16	5.21	5.60
Ti	1.22	2.51	4.57	1.57	5.00	4.75
Cr	9.56	8.03	2.63	10.59	7.75	8.86
Co	12.55	8.55	5.25	13.46	13.98	15.24
Ni	36.00	33.04	35.39	42.94	64.23	63.96
Zr	0.00	0.00	0.58	3.77	0.00	0.29
Hf	0.00	1.17	0.00	0.15	0.42	0.39
Ta	0.87	1.48	0.36	0.58	0.00	0.00
W	1.45	2.27	0.00	0.00	1.28	0.23
Pt	37.5	40.75	47.39	24.78	2.12	0.68

Elements	Weight percent	
	A1	B1
Al	3.72	1.89
Ti	4.61	1.92
Cr	2.27	9.23
Co	4.57	10.86
Ni	32.88	36.31
Zr	0.00	0.00
Hf	0.61	0.63
Ta	0.00	1.21
W	0.00	0.88
Pt	51.33	37.07

Figure 3.11 : Microstructure of platinum coated MAR-M002 as received

a) Overall coating structure

b) High magnification of the coating

were basically composed of platinum and nickel but showed a higher substrate alloying element content with significant amounts of Cr and Co and smaller amounts of Al and Ti. The main difference between the two regions was that the Pt, Al and Ti content in the white region was greater than that observed in the grey region while the grey region showed a higher Ni, Cr and Co content. The refractory elements such as W and Ta have been virtually excluded from the coating and the region adjacent to the coating. It was noted that

as the platinum content decreased the γ' phase became more prominent; transforming from an irregular structure to a more cuboidal structure. Close to the external surface the presence of chromium and cobalt became more significant.

The x-ray diffraction spectrum of a platinum coated (figure 3.12) sample revealed that the coating was made up of platinum phases containing Zr, Ti, Ta, Cr, Al and Co. The peaks were generally wide which may be ascribed to incomplete transformation of phases or the presence of large amounts of dissolved elements in the crystal structure. The widening of the peaks also was as a result of peaks of the different crystal structures formed, overlapping which contributed to the broadening of the peaks. Only small amounts of the γ', Ni_3Al and $Ni_3(Al, Ti)$ phases were detected indicating that the γ' was "dissolved" in the region of the coating.

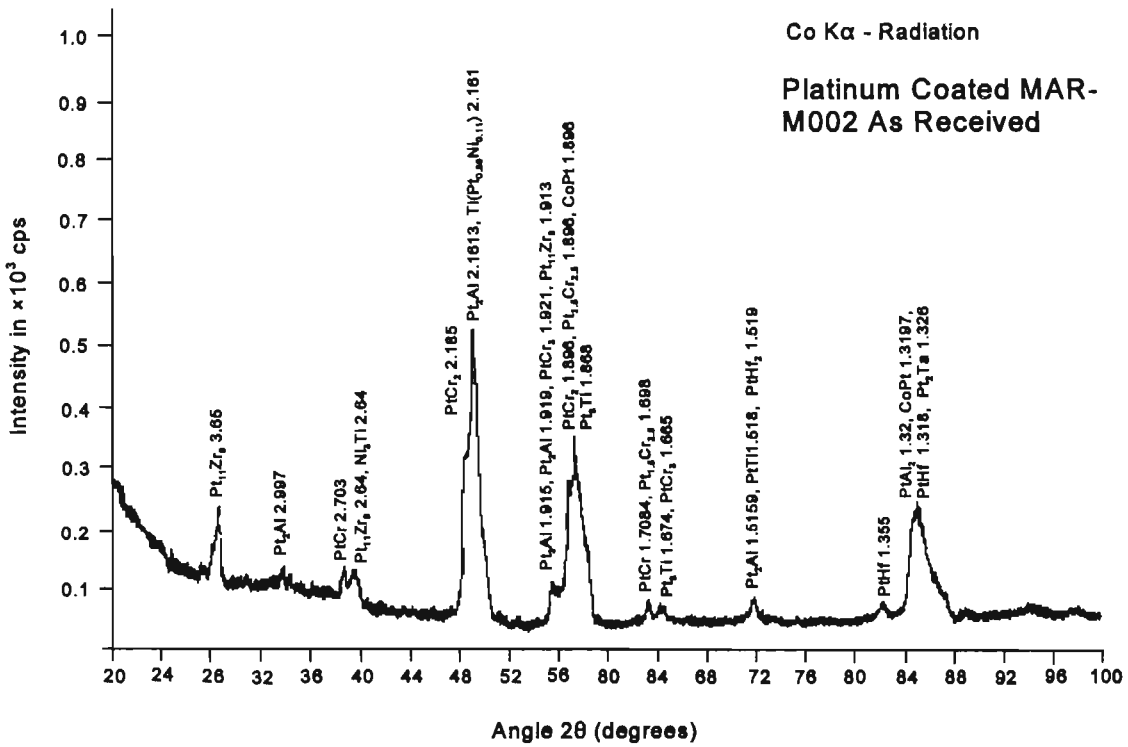

Figure 3.12 : X-ray diffraction Analysis of platinum coated MAR-M002 as received

3.2 CHARACTERIZATION OF THE MATERIALS SYSTEMS AFTER HTLCF FAILURE

3.2.1 HTLCF in Argon Atmosphere

3.2.1.1 Uncoated MAR-M002

HTLCF tests performed on uncoated MAR-M002 nickel based superalloy in argon atmosphere produced a life of 2188 cycles. Typical stress-strain hysteresis loops produced

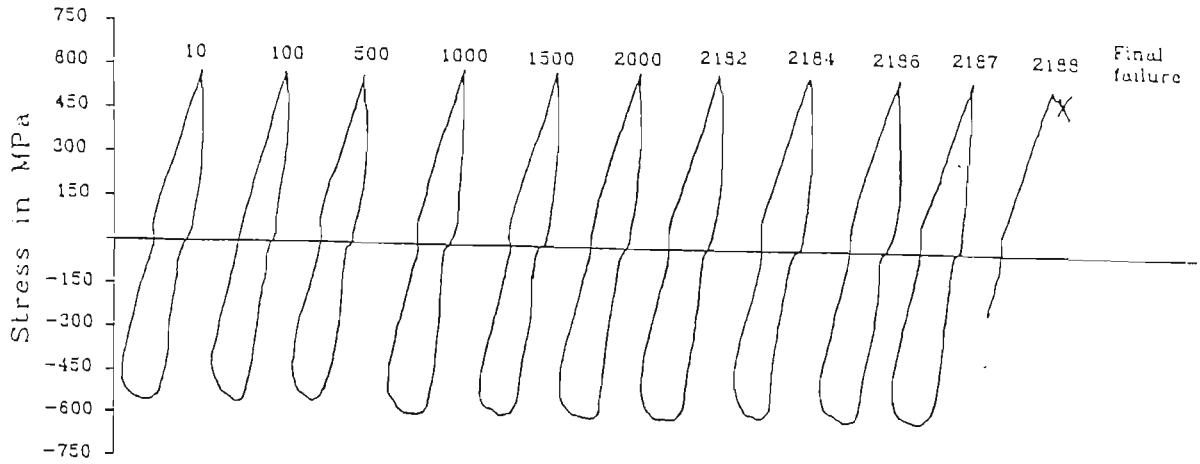

Figure 3.13 : Typical stress-strain hysteresis loops for HTLCF tests performed in argon atmosphere

are shown in figure 3.13. The final failure of the sample occurred at a fairly high tensile load and in brittle manner. Once the critical crack length was reached, crack propagation to failure was relatively fast.

The fracture surface, figure 3.14a, showed no evidence of environmental interaction. Chemical analysis of the fracture surface showed no evidence of corrosion product , with the chemical composition being similar to the nominal composition of the alloy. An analysis with oxygen was performed in order to demonstrate that there was an insignificant amount of oxidation. The relatively small amount of oxygen detected could have been as a result of minor oxidation when the specimen was being removed from the furnace on completion of the fatigue test. The external surface close the fracture (figure 3.14b) indicated the presence of fine discontinuous cracks. The cracks were, in general, perpendicular to the direction of loading.

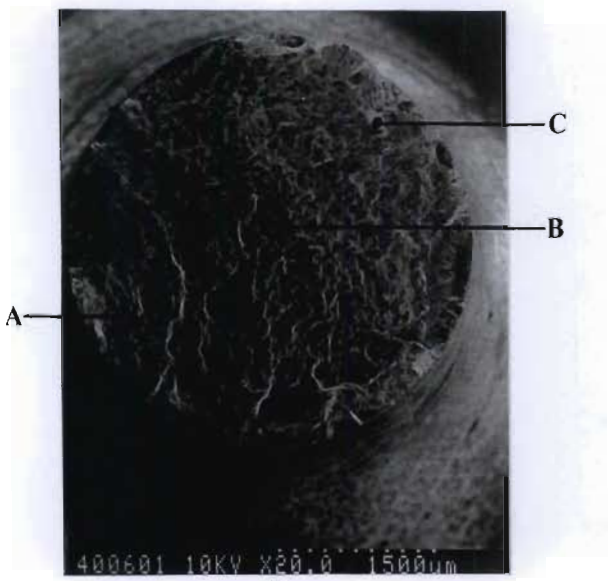

a

b

Elements	Weight percent			
	A	B	C	Analysis with O
Al	4.99	3.16	5.34	4.80
Ti	2.69	2.04	1.95	1.78
Cr	8.32	7.58	8.23	7.57
Co	9.87	8.59	9.51	8.76
Ni	58.60	53.61	58.36	53.87
W	7.80	11.39	7.56	6.74
Ta	3.80	7.78	2.48	2.29
Hf	3.87	4.45	6.18	5.71
Zr	0.63	1.39	0.39	0.35
O	0.00	0.00	0.00	8.14

Figure 3.14 : a) Fracture surface of uncoated MAR-M002 after HTLCF in argon atmosphere at 870°C

b) Fractography of uncoated MAR-M002 after HTLCF in argon atmosphere showing the external region close to the fracture surface

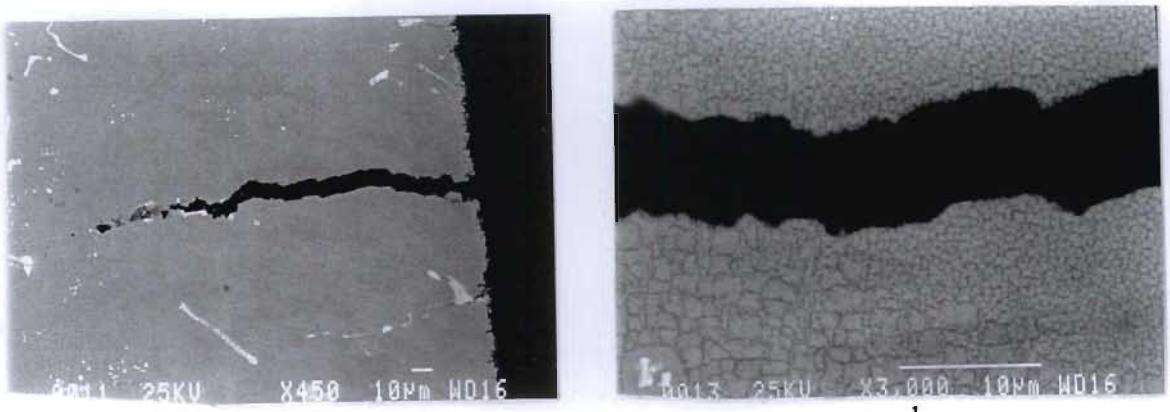

a b

Figure 3.15 : Micrographs of the cross-section of a fatigue sample after HTLCF in argon

Several cracks were observed on the metallographic sample of the longitudinal cross-section (figure 3.15a&b). The crack propagation was relatively "straight" with no evidence of environmental interaction and branching. EDS analysis of the crack edge and of the bulk alloy (table 3.2) shows little variation in the chemical compositions between these regions indicating the absence of corrosion reactions. The evidence indicated that the mode of crack propagation was transdendritic and the failure was due to pure mechanical loading.

Table 3.2 : Chemical analysis of the fatigue crack edge and bulk for a fatigue sample that had failed in argon atmosphere

	Elements (Weight percent)								
	Al	**Ti**	**Cr**	**Co**	**Ni**	**Zr**	**Hf**	**Ta**	**W**
Crack Edge	4.45	1.37	8.85	10.55	58.78	5.16	0.43	1.84	8.58
Bulk Alloy	5.74	1.22	7.87	9.71	59.02	2.66	1.23	1.14	11.42

3.2.1.2 Aluminide Coated MAR-M002

The fracture surface of aluminide coated MAR-M002 after HTLCF in inert argon atmosphere is shown in figure 3.16. The number of cycles to failure was 859 cycles. The final failure occurred, as in the uncoated sample, at a relatively high tensile load.

The fracture surface (figure 3.16b) revealed a clean surface devoid of any environmental

interaction. Micro probe analysis of the fracture surface showed no evidence of interaction with the environment. The external surface close the fracture (figure 3.16a) displayed severe cracking of the coating (around the circumference) perpendicular to the direction of loading. Cracks parallel to the loading direction were also apparent from figure 3.17. The nature of the cracks indicated a very brittle type failure of the coating.

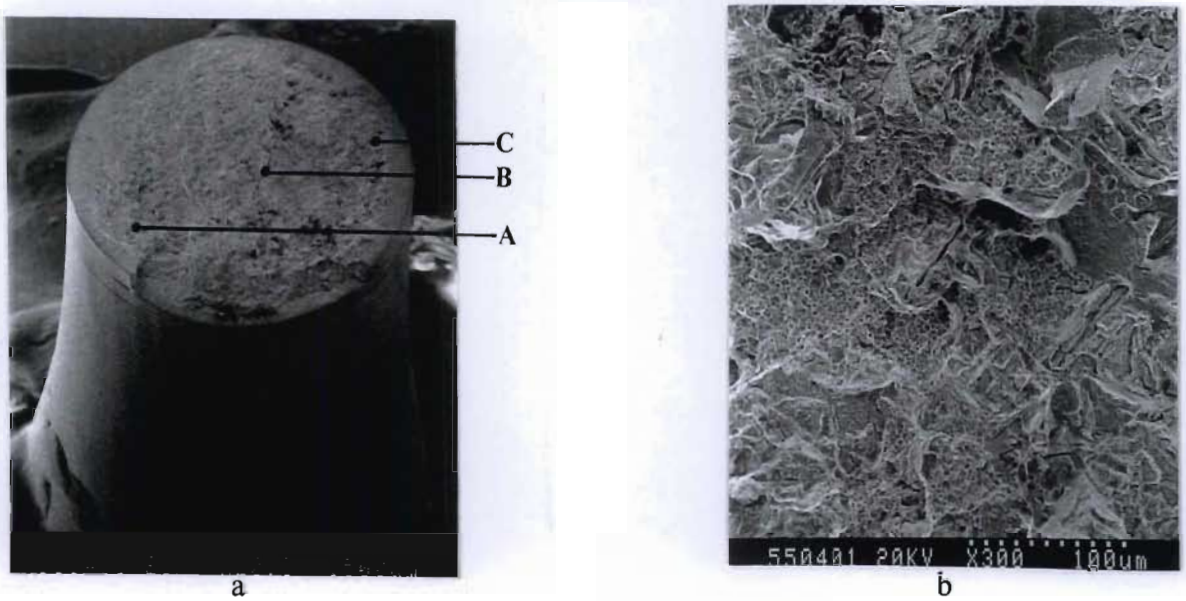

a b

Elements	Weight percent		
	A	B	C
Al	5.29	5.47	6.08
Ti	1.37	2.51	1.46
Cr	8.45	6.78	8.51
Co	9.33	8.16	10.07
Ni	59.23	55.57	56.94
W	12.01	10.32	10.63
Ta	2.46	7.18	4.00
Hf	1.87	3.77	2.29
Zr	0.00	0.23	0.02

Figure 3.16 : Fracture surface of aluminide coated MAR-M002 after HTLCF in argon atmosphere

a) Overall fracture surface

b) High magnification of the fracture surface

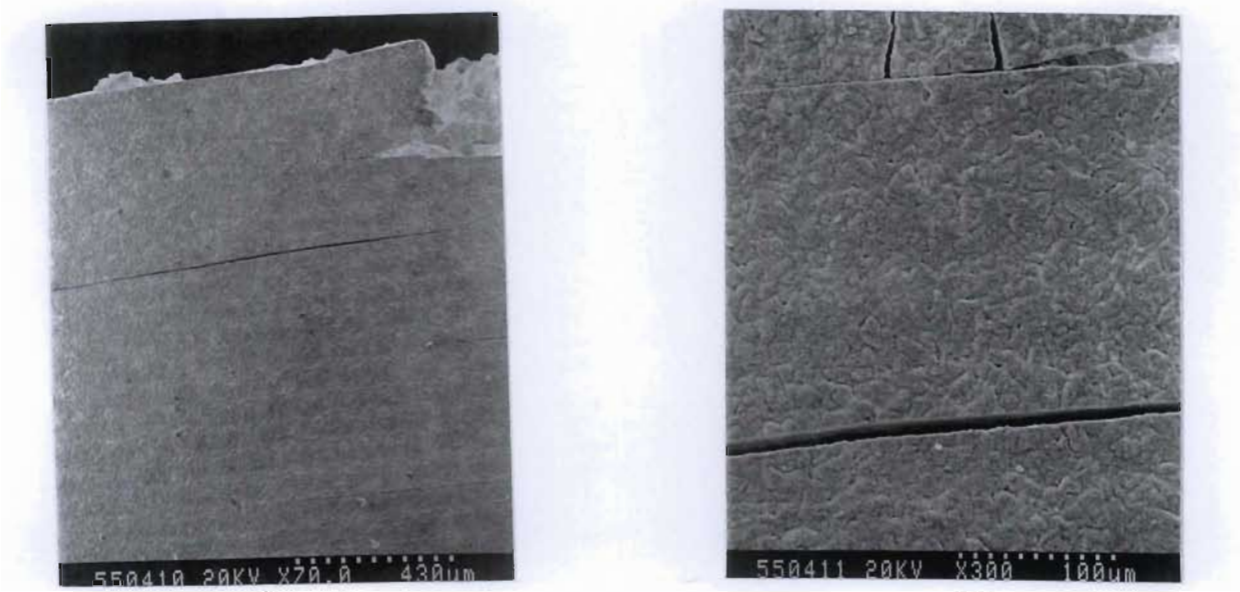

a b

Figure 3.17 : Cracking of the coating near the fracture surface after HTLCF in argon atmosphere

Examination of a cross-section of the fatigue sample revealed severe cracking of the coating (figure 3.18). The cracks in the coating showed no evidence of environmental interaction. Crack propagation in the substrate was transdendritic, perpendicular to the direction of loading. The crack was relatively "straight" with no indication of environmental interaction.

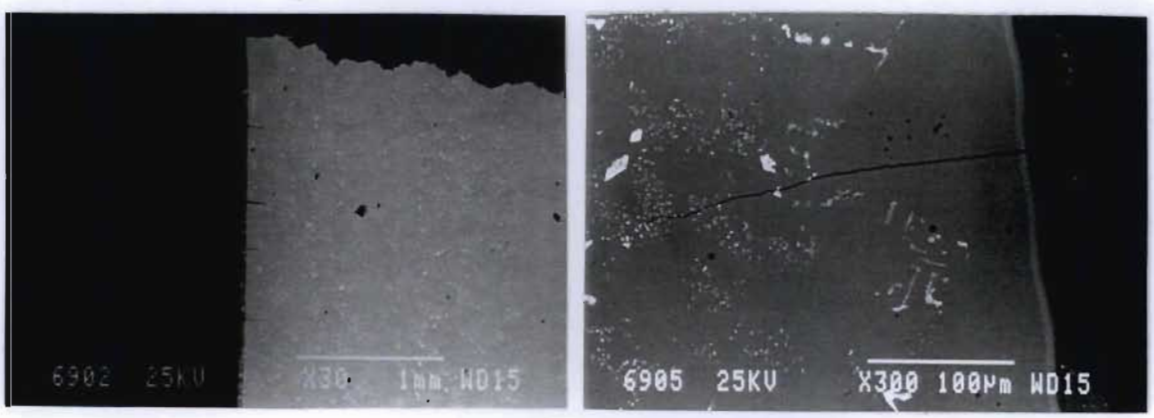

a b

Figure 3.18 : Cross-sectional analysis showing cracking of the coating.

3.2.1.3 TYPE I Platinum Aluminide Coated MAR-M002

HTLCF of TYPE I platinum aluminide coated MAR-M002 in argon atmosphere resulted in a life of 1119 cycles. Fractography analysis uncovered a region that showed minor environmental interaction, due to the corrosion chamber around the neck splitting during the test (figure 3.19a). Interaction with the environment was confirmed by the significant amount of oxygen detected in the EDS (figure 3.19) and AES (figure 3.20) analyses. It was noted that only part of the fracture surface was exposed to air.

Examination of the external region close to the fracture exhibited cracking of the coating (figure 3.19b). The cracking of the coating was as a result of the mechanical loading. The cracks in the coating were very fine and were only visible at relatively high magnifications. A significant feature was that the cracking of the coating was not as severe as that observed in the unmodified aluminide coating.

Examination of the longitudinal section after HTLCF in argon revealed several branched cracks in the coating (fig 3.21& 3.22). A significant feature in figure 3.21 was that the cracks in the coating had propagated to various degrees indicating that crack propagation through the coating occurred over a number of cycles. Crack propagation in the substrate was transdendritic and relatively straight. Figure 3.21a&b shows that there was some environmental interaction due to contamination of the argon atmosphere during the test.

However, the cross-section of the fracture surface, figure 3.22, shows no environmental interaction. This indicates that for the major part of the test the environment was not contaminated. The secondary crack observed at the fracture surface interface also shows no evidence of environmental interaction. The secondary crack was parallel to the direction of loading and occurred in the interdendritic zone.

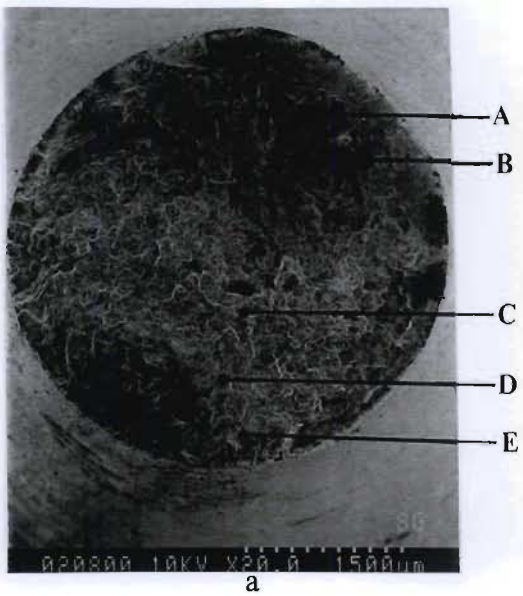

a

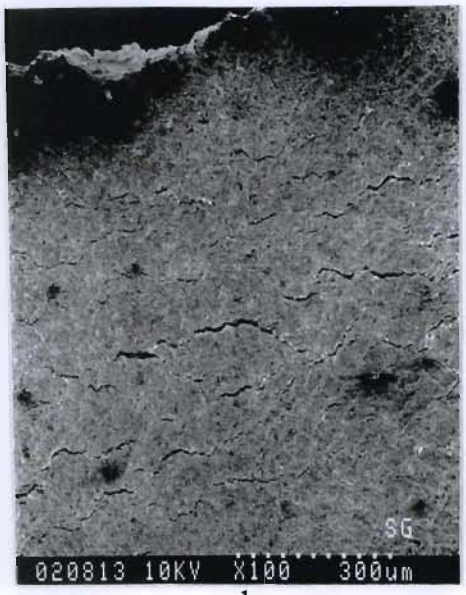

b

Elements	Weight percent				
	A	B	C	D	E
Al	4.95	4.49	5.59	5.16	5.32
Ti	1.48	2.29	1.34	2.29	1.52
Cr	6.45	6.43	7.33	6.23	7.74
Co	8.21	7.18	7.98	7.07	7.56
Ni	55.13	48.51	52.07	46.35	41.76
Zr	0.38	0.00	0.20	0.22	0.02
Ta	5.87	8.23	3.33	7.13	1.93
Hf	2.00	5.87	4.56	2.78	2.16
W	10.33	9.71	7.26	9.04	8.69
O	5.20	7.29	10.35	13.72	23.30

Figure 3.19 : Fractography of TYPE I platinum aluminide coated MAR-M002 after HTLCF in an argon environment

a) Fracture surface

b) Cracking of the coating close to the fracture surface

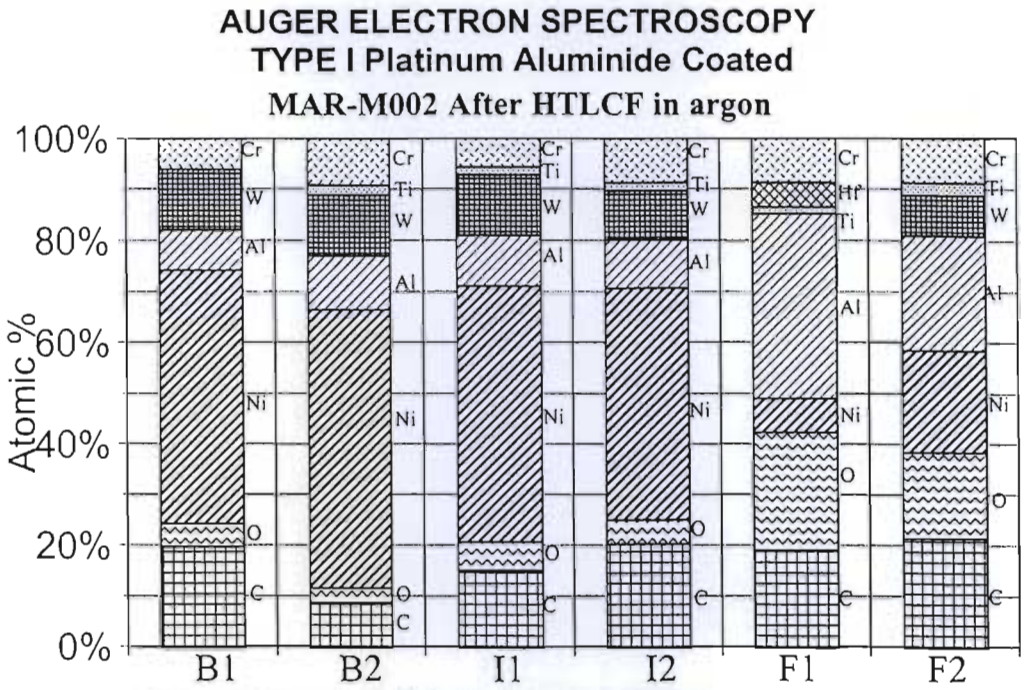

Figure 3.20 : AES analysis of TYPE I platinum aluminide coated MAR-M002 after HTLCF in argon atmosphere

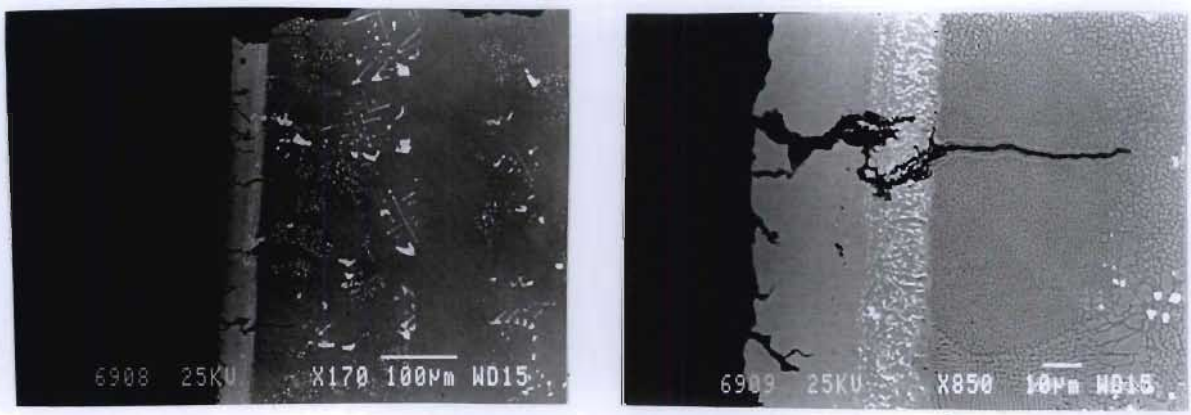

a b

Figure 3.21 : a) Longitudinal cross-section showing cracking of the coating after HTLCF in argon atmosphere

b) Cracking of the coating plus environmental interaction

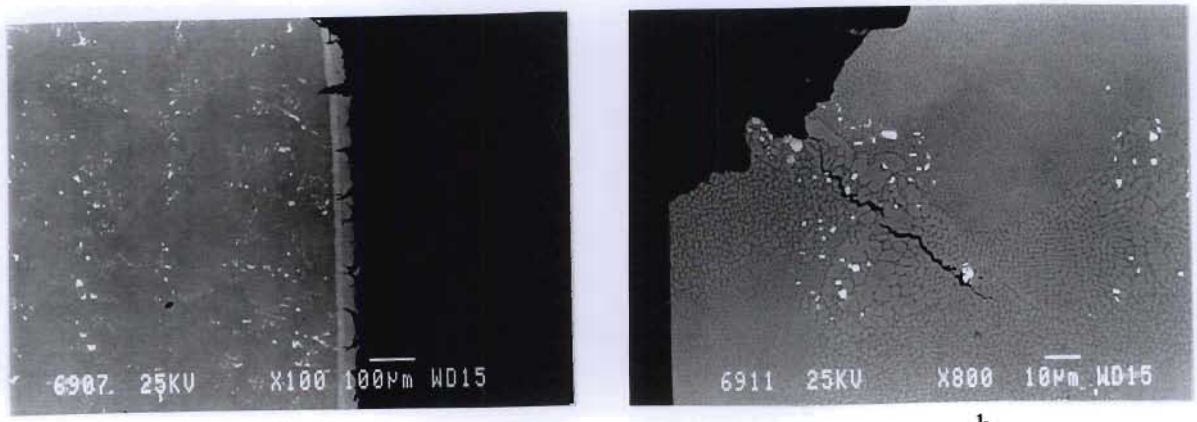

a b

Figure 3.22 : Longitudinal cross-section after HTLCF in argon atmosphere

a) Cracks in the coating with no evidence of environmental interaction

b) Secondary cracking along the fracture surface showing no environmental interaction

3.2.1.4 TYPE II Platinum Aluminide Coated MAR-M002

HTLCF of TYPE II platinum aluminide coated MAR-M002 in inert argon atmosphere produced a life of 1442 cycles. There was no evidence of any environmental interaction on the fracture surface (figure 3.23a). EDS analysis of the fracture surface, showed no significant change in the chemical composition when compared to the nominal composition of the alloy. Final failure of the fatigue sample, again occurred at a relatively high tensile load, indicating a brittle type of failure.

The external region close to the fracture, figures 3.23b & 3.24, revealed "eroding" of coating, i.e., regions where the Pt_2Al layer had delaminated. The cracking in general was random, forming a "network" of cracks. However, figure 3.24 shows a series of parallel cracks at approximately 45° to the loading direction over half the circumference while the cracks were circumferential over the other half. It must be noted that cracking of the coating, in general, occurred randomly in relation to the direction of loading. The most severe cracking was observed perpendicular to the loading direction and at the 45° angle to the loading direction.

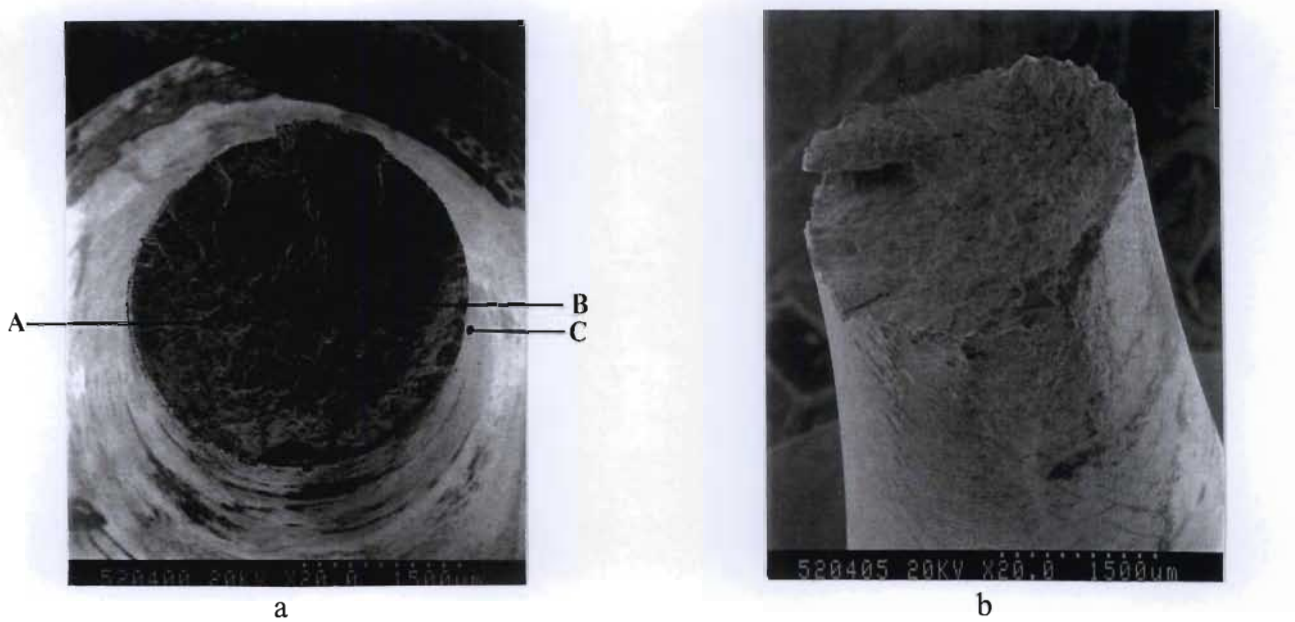

a b

Elements	Weight percent		
	A	B	C
Al	2.30	2.62	25.07
Ti	1.59	2.37	0.05
Cr	7.07	6.71	1.20
Co	9.03	8.05	0.50
Ni	49.17	48.67	2.98
Zr	0.00	0.00	0.00
Ta	5.92	8.11	1.43
Hf	2.90	4.53	0.49
W	8.43	14.59	0.71
Pt	0.00	0.00	24.34
O	3.58	4.35	43.22

Figure 3.23 : Fractography of TYPE II platinum aluminide coated MAR-M002 after HTLCF in argon atmosphere

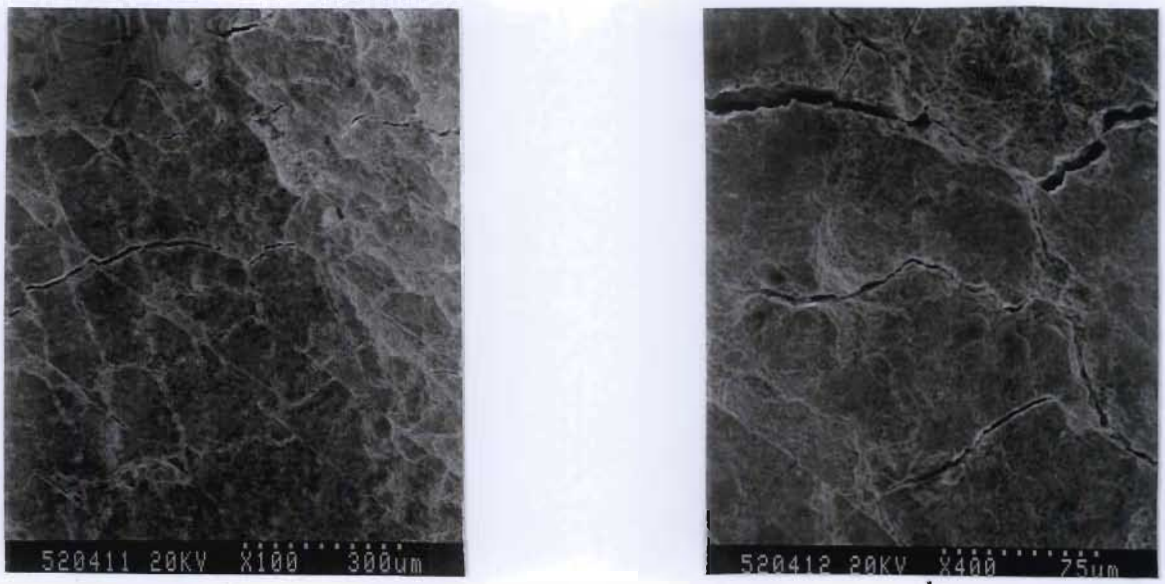

a b

Figure 3.24 : Cracking of TYPE II platinum aluminide coating near the fracture surface after HTLCF in argon atmosphere

Cross-sectional analysis of the TYPE II platinum aluminide coated sample after HTLCF in argon showed severe cracking of the coating (Figure 3.25). It was evident that the $PtAl_2$ layer was prone to brittle failure and delamination from the NiAl sub-layer (Figure 3.25d). The NiAl region exhibited a higher resistance to cracking while the substrate was the most resistant to crack initiation (Figure 3.25b). A number that of cracks that had propagated through the coating stopped at the coating-substrate interface, with the crack propagation in this region being parallel to the loading direction. The crack propagation through the base metal was transdendritic (Figures 3.25c) . The crack was "straight" with no environmental interactions at the propagating crack tip.

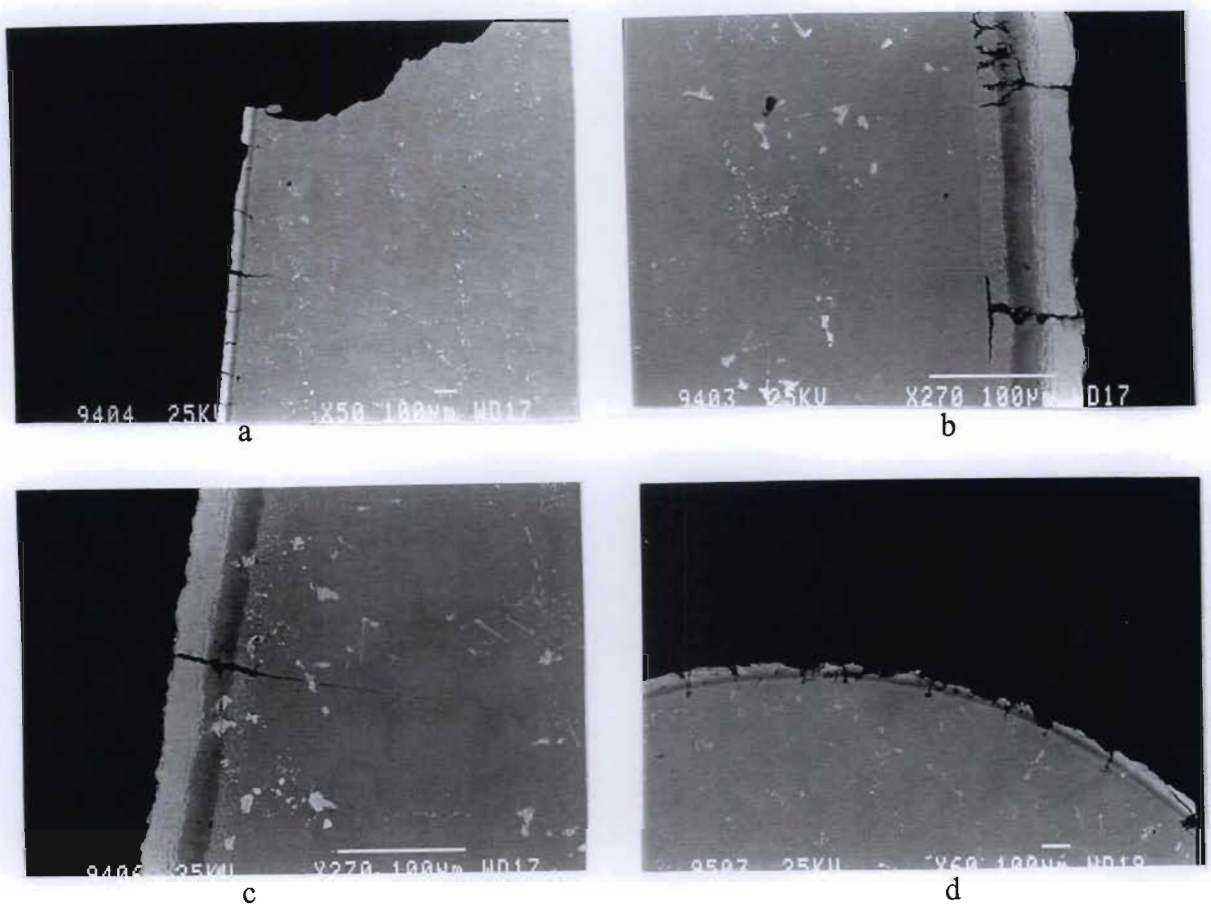

Figure 3.25 : Cross-sectional analysis of TYPE II platinum aluminide coated MAR-M002 after HTLCF in argon atmosphere showing a very coating

a) Longitudinal cross-section showing cracks in coating
b) Longitudinal cross-section showing branching of cracks in the NiAl zone
c) Crack propagation in the substrate
d) Transverse cross-section showing spalling of the $PtAl_2$ layer

3.2.1.5 Platinum Coated MAR-M002

HTLCF of platinum coated MAR-M002 in argon atmosphere resulted in a life of 1518 cycles. Fractography of the failed fatigue sample indicated a "clean" fracture surface. The absence of environmental interaction was manifested by the chemical analysis of the fracture surface (Figure 3.26a). Delamination/peeling of the coating from the substrate was evident

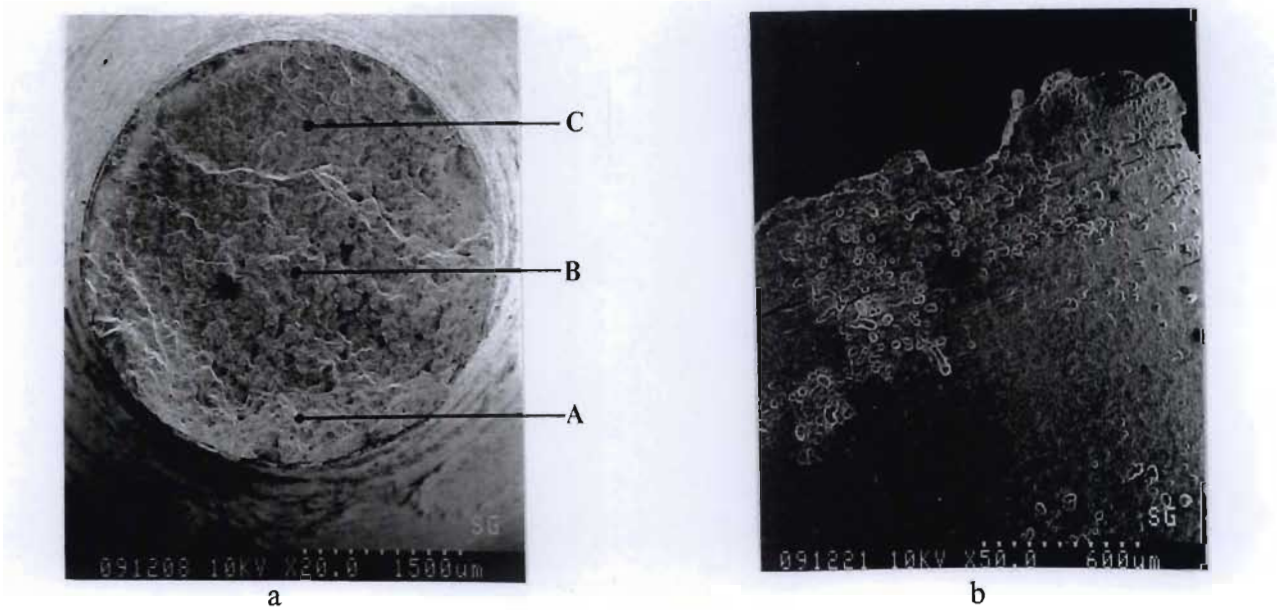

a b

Elements	Weight percent		
	A	B	C
Al	4.79	5.16	4.60
W	9.64	10.93	10.07
Ti	1.71	1.54	1.79
Cr	8.89	8.30	7.85
Co	9.24	9.20	9.27
Ni	56.39	55.42	52.43
Zr	0.26	0.03	3.76
Hf	4.65	3.89	1.81
Ta	4.36	5.53	2.81
Pt	0.00	0.00	5.60

Figure 3.26 : a) Fracture surface of a platinum coated sample after HTLCF in argon atmosphere

b) Fractography showing the coating close to the fracture surface

Fine, discontinuous circumferential cracks were observed on the coating (Figure 3.26b). The more severe cracks were most prominent in the region adjacent to the fracture surface. The "bubble" like features present on the coating, figure 3.26b, was a feature of the coating and not the due to environmental interaction.

Cross-sectional analysis of the fatigue sample revealed two important features: i) the cracking of the coating layer and ii) porosity at the coating substrate interface (figure 3.27). The thickness of the coating had increased significantly, varying from 50μm to 60μm compared to approximately 17μm in the as received sample. The cross-section of the coating-fracture interface, figure 3.27, indicated that a piece of the coating had "peeled" off the substrate.

The coating layer consisted of two regions, namely, the "white" regions and "grey" regions. The crack propagation in the coating had occurred through the "grey" regions predominantly, indicating that the "white" regions were more resistant to cracking. Porosity had occurred in the regions where the crack had penetrated the coating (in the interdiffusion zone or γ' depleted zone). This factor was instrumental in the delamination of the coating during the fatigue test.

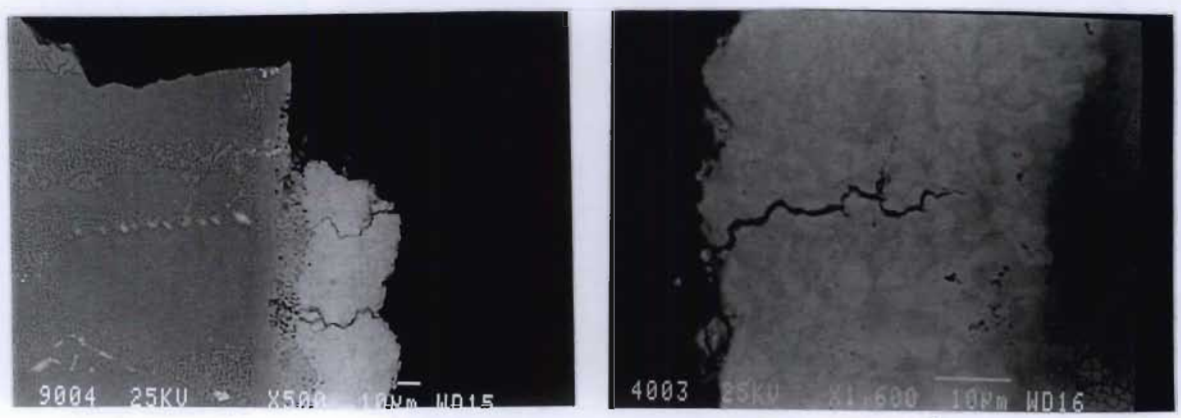

a b

Figure 3.27 : Cross-sectional analysis of platinum coated MAR-M002 after HTLCF in argon atmosphere showing peeling of the coating and crack propagation through the coating.

Crack propagation in the substrate was relatively "straight" (figure 3.28) and the crack tip was relatively sharp showing no indication of environmental effects. Chemical analysis along the crack edge and the bulk material, figure 3.28, showed little variation in the chemical composition.

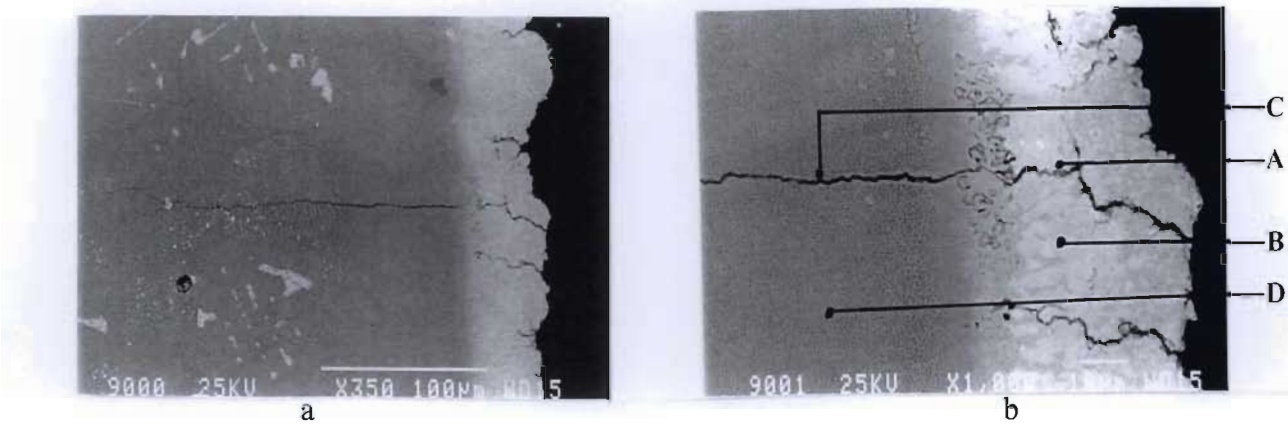

Elements	Weight percent				
	A	B(white region)	B(grey region)	C	D
Al	5.69	3.93	1.74	6.79	6.65
Ti	0.99	1.83	0.52	1.85	1.62
Cr	7.20	1.64	5.63	5.18	5.31
Co	4.84	2.82	6.77	7.80	8.47
Ni	29.88	28.65	35.81	63.28	62.20
Pt	42.05	53.15	40.79	0.73	0.00
Hf	2.65	1.55	0.00	0.00	2.92
Ta	1.31	2.08	0.81	1.80	0.00
W	5.39	4.36	7.92	11.74	13.03
Zr	0.00	0.00	0.00	0.83	0.79

Figure 3.28 : EDS analysis of the crack through the coating of a platinum coated MAR-M002 fatigue sample after HTLCF in argon

3.2.2 HTLCF in Air Atmosphere

3.2.2.1 Uncoated MAR-M002

HTLCF tests performed on uncoated MAR-M002 in air atmosphere produced a life of 2412 cycles. The final failure occurred at a relatively high tensile load and in a very brittle manner. The fracture surface (figure 3.29) showed evidence of oxidation. Oxidation of the fracture surface was manifested by the high oxygen content detected (figure 3.29) Fine cracks were observed on the external surface close to the fracture (figure 3.29b). There was a build up of corrosion product around the lip of the cracks. The corrosion product was made up of mainly Cr, Ni, Al and oxygen.

γ' depletion/coarsening was observed along the external surface exposed to the environment (figure 3.30) and along the fatigue crack edges. Several cracks had initiated on the surface of the fatigue sample but had not propagated further. It was evident from the cross-sectional analysis that crack propagation had occurred preferentially along the interdendritic segregation zone. This indicated that the dendritic grain was more resistant to fatigue crack initiation and propagation under oxidation conditions. Chemical analysis of the corrosion product filling these cracks (figure 3.30b) showed that it was made up of mainly Cr, Ni, and oxygen with small amounts of Al, Ti, Co and Ta. The γ' denuded region was depleted of the reactive elements (in particular aluminium). The secondary crack shown in figure 3.30a was branched and the crack tip was relatively "blunt". There was evidence of environmental interaction along the crack edges and the presence of corrosion product within the crack.

Analysis of the crack tip (figure 3.30c) revealed that the corrosion product at the crack tip was made up primarily of nickel oxides. The "porous" region adjacent to the crack exhibited a high oxygen and Ni content with significant amounts of the alloying elements. This layer was produced due to internal oxidation of the crack edge. The γ' denuded region showed a reduction in Al, Cr and Ti content when compared to the base material indicating that these elements were consumed in the oxidation reaction.

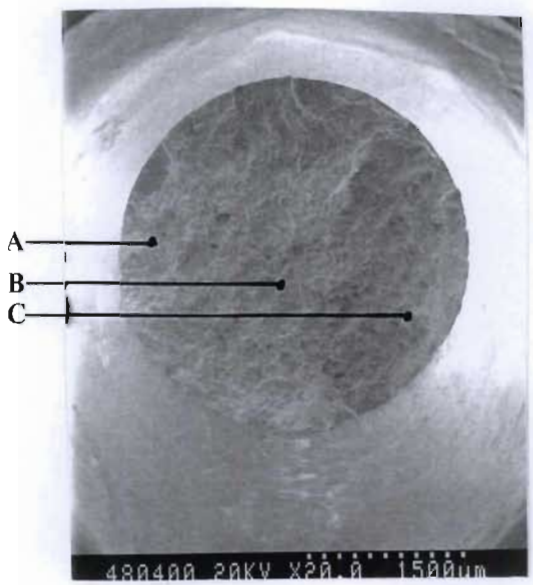

a

b

Elements	Weight percent				
	A	B	C	External Surface	Corrosion Product
Cr	6.91	9.60	7.58	12.71	21.96
Co	7.11	9.49	8.08	4.82	5.85
Ni	42.81	50.02	47.57	22.15	22.15
Zr	0.00	0.06	0.22	0.18	0.12
Hf	4.47	1.95	1.99	3.34	5.49
Ta	5.95	1.40	2.54	1.83	3.11
W	10.80	4.88	5.00	3.58	4.32
Ti	1.99	1.80	1.85	2.72	3.74
Al	3.92	1.47	1.89	14.96	7.05
O	16.00	19.32	23.28	33.71	25.96

Figure 3.29 : a) Fracture surface of uncoated MAR-M002 after HTLCF in air

b) External surface close to the fracture showing cracks and oxidation of the cracks

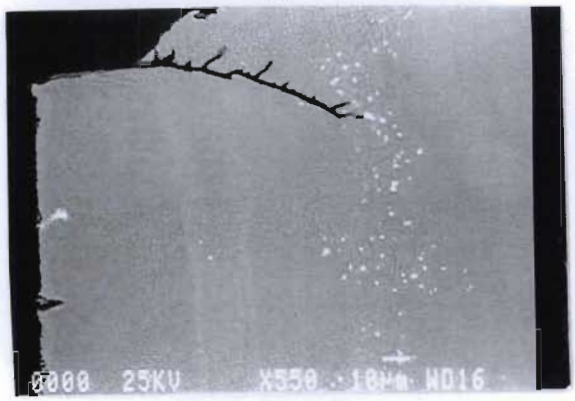

a

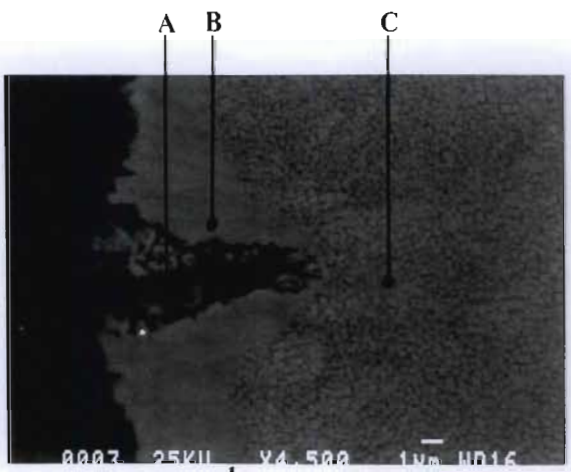

b

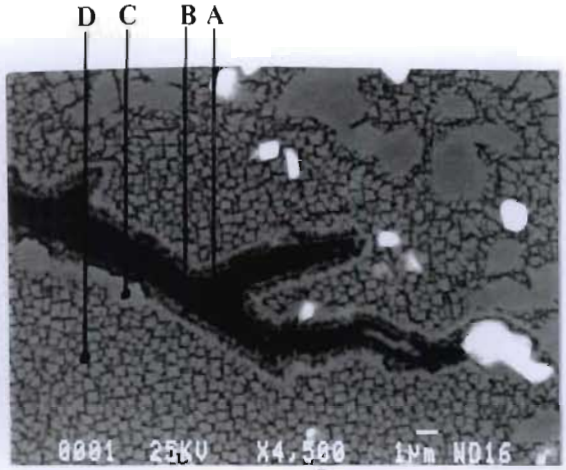

c

Elements	Weight percent		
	A	B	C
O	28.15	0.00	0.00
Ti	2.64	0.29	1.41
Cr	23.98	6.87	7.35
Co	4.16	11.38	8.99
Ni	19.77	65.91	58.35
Al	5.04	1.90	6.57
Zr	0.44	0.00	0.42
Ta	4.91	1.83	2.63
Hf	4.62	0.10	2.51
W	6.29	11.72	11.77

Elements	Weight percent			
	A	B	C	D
O	23.29	18.11	0.00	0.00
Ti	0.50	1.59	0.76	1.66
Cr	3.29	8.96	7.06	8.34
Co	5.51	7.87	9.47	9.43
Ni	32.10	42.15	62.12	58.58
Al	3.34	5.46	4.12	5.67
Zr	0.00	3.99	1.07	0.00
Ta	0.13	1.51	2.50	1.73
Hf	0.08	1.32	1.14	0.81
W	1.13	9.05	11.76	13.77

Figure 3.30 : a) Cross-section of uncoated MAR-M002 after HTLCF in air.

b) High magnification of crack on the external surface with EDS

c) Chemical analysis of the corrosion product at the crack tip

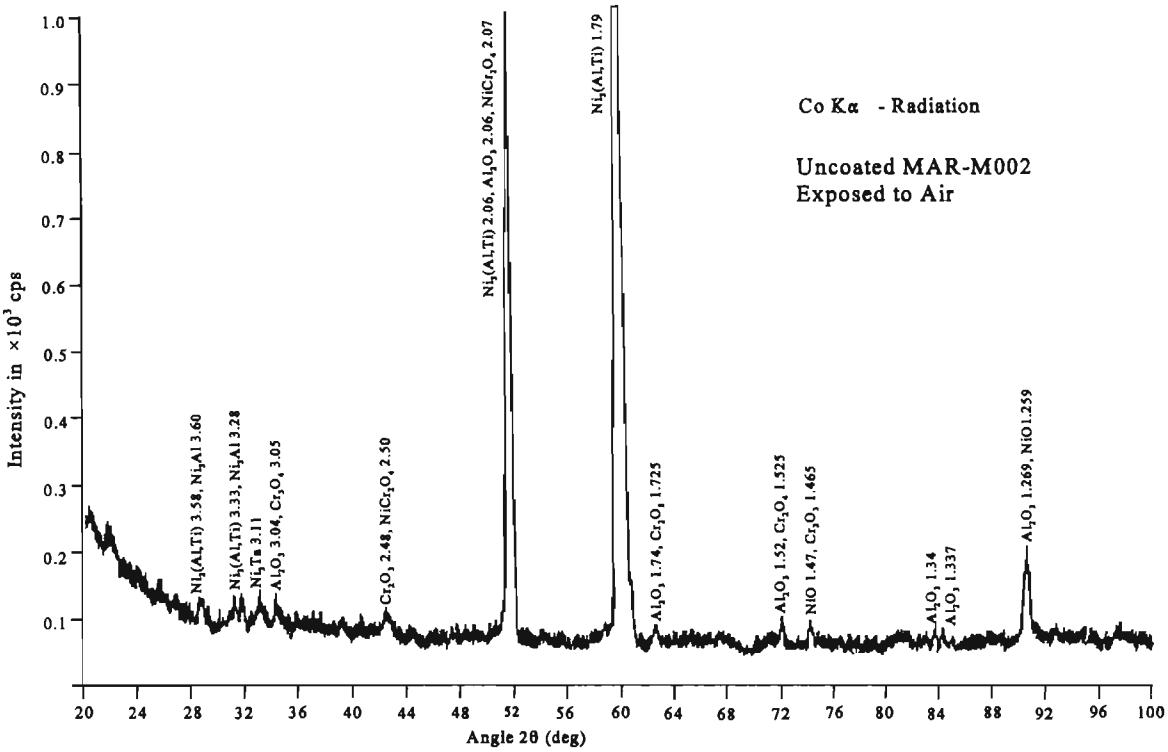

Figure 3.31 : X-ray diffraction analysis of an uncoated disc sample exposed to air environment at 870° for 5 hours

X-ray diffraction analysis of an uncoated MAR-M002 disc sample exposed to air at 870°C for five hours (figure 3.31) revealed the following oxide phases produced as result of the oxidation process: Cr_2O_3, Al_2O_3 and NiO. The corrosion tests were performed on unstressed samples, hence, the results obtained only give an indication of the type of oxide phases that will be present. It was evident from the XRD analysis that the oxides of Al and Cr are most prominent. The EDS analysis at the crack tip indicates that the corrosion product was made up of mainly nickel oxides. This was due to the combination of oxidation and the fatigue loading.

3.2.2.2 Aluminide Coated MAR-M002

Aluminide coated MAR-M002 fatigue samples exposed to creep-fatigue loading in air at 870° produced a life of 826 cycles. The final failure occurred at a fairly high tensile load and occurred in a brittle manner. The fracture surface showed clear evidence of environmental interaction (figure 3.32a). EDS analysis revealed a high oxygen and Ni content indicating the presence of mainly Ni oxides. The chemical analysis was very similar to that of the uncoated samples.

The external surface close to the fracture showed that the coating had a rippled effect due to the sample not being polished after the machining process. This, however, did not affect the fatigue life significantly. "Fine" circumferential cracks were observed in the coating (figure 3.32b). The cracks in the coating were perpendicular to the direction of loading.

Figure 3.33 shows a crack that has propagated through the coating and into the substrate. It was evident that the coating failed in brittle manner (figure 3.33) very early in the fatigue test. The coating showed no evidence of oxidation in the crack, indicating a high resistance to oxidation. The substrate, however, showed a higher susceptibility to oxidation. Crack propagation through the substrate was transdendritic and branched. High magnification of the crack tip shows a relatively "blunt" crack tip with corrosion product filling the crack (figure 3.33). The corrosion product in the crack was made up of mainly Ni oxides.

Chemical analysis of the corrosion product in the crack close to the coating indicated relatively high Al, Cr, Co and Ni content, figure 3.33b. The external surface of the coating exposed to the environment was depleted of Al due to the formation of Al_2O_3 scales on the external surface.

X-ray diffraction analysis of an aluminide coated disc sample exposed to air at 870°C for five hours is shown in figure 3.34. There was a significant increase in the amount of Al_2O_3 and Cr_2O_3 phases detected. These are the principal oxide phases formed on the external surface of the coating. This result will only represent the corrosion products that are formed due to

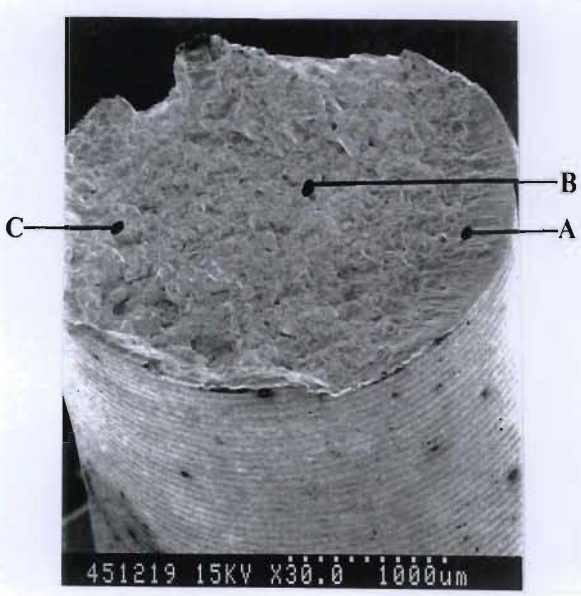

a

b

Elements	Weight percent		
	A	B	C
O	26.41	19.11	19.95
Al	1.43	3.66	4.34
W	5.04	5.26	5.37
Ti	1.25	2.13	1.87
Cr	7.60	6.60	6.67
Co	9.38	7.01	7.08
Ni	43.64	44.04	42.64
Ta	3.31	6.68	6.26
Hf	1.95	5.48	5.52
Zr	0.00	0.04	0.29

Figure 3.32 : a) Fracture surface of aluminide coated MAR-M002 after HTLCF in air atmosphere at 870°C

b) Cracking of the aluminide coating close to the fracture surface

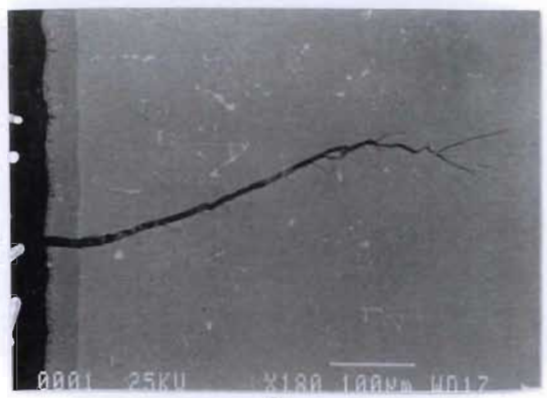

a

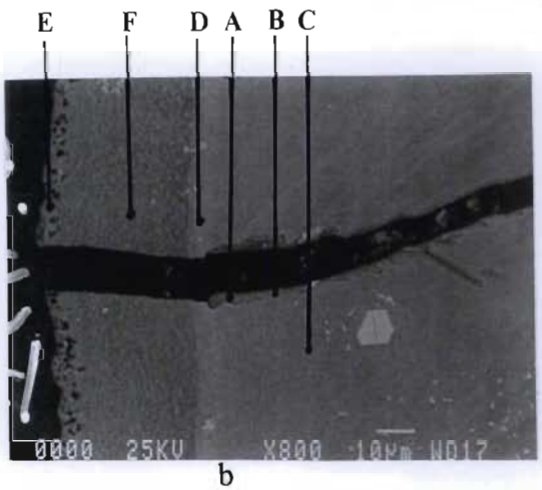

b

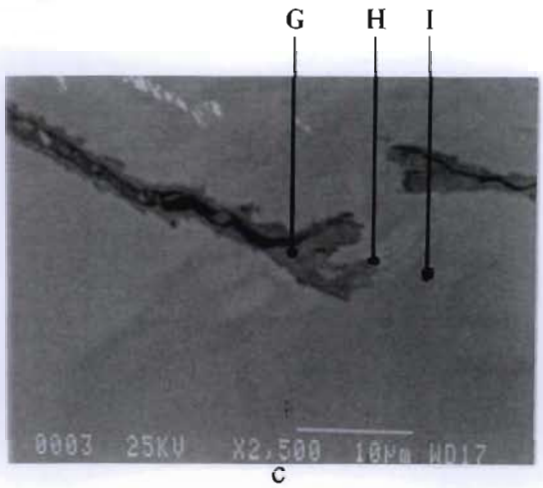

c

Elements	Weight percent						Elements	Weight percent		
	A	B	C	D	E	F		G	H	I
Al	8.61	7.86	6.27	15.18	13.67	25.27	Al	2.15	6.42	4.96
Ti	2.66	2.72	1.83	2.81	1.57	0.92	Ti	0.73	1.41	1.11
Cr	14.66	11.82	6.65	9.84	8.44	5.18	Cr	3.99	11.09	9.11
Co	13.70	8.70	8.79	10.10	6.27	7.16	Co	11.66	6.68	9.60
Ni	30.79	47.25	65.19	44.86	48.64	51.40	Ni	59.70	42.07	57.68
Zr	0.00	2.26	0.00	0.00	2.25	0.00	Zr	0.00	2.59	2.34
Hf	1.53	0.95	1.44	1.57	0.28	2.87	Hf	0.30	1.04	1.30
W	4.97	11.78	8.47	8.81	0.00	5.95	W	6.00	13.96	11.55
Ta	5.12	6.66	1.36	6.83	18.89	1.25	Ta	1.45	1.51	2.35
O	19.96	0.00	0.00	0.00	0.00	0.00	O	14.02	13.24	0.00

Figure 3.33: a) Longitudinal section of aluminide coated MAR-M002 after HTLCF in air.

b) High magnification of the crack in the coating with EDS analysis of the corrosion product.

c) Chemical analysis of the crack tip.

corrosion of the coating. In order to establish the typical phases in the corrosion product in the crack propagating in the substrate, the corrosion test performed on the uncoated sample must be considered.

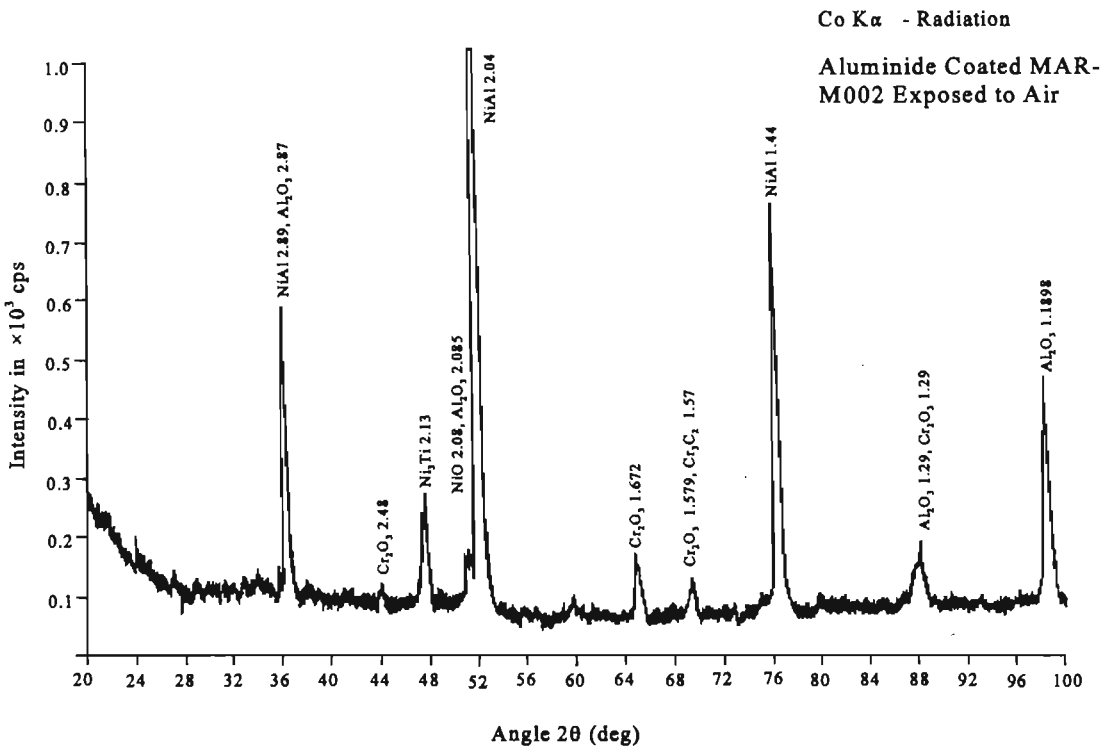

Figure 3.34 : X-ray diffraction analysis of an aluminide coated disc sample exposed to air at 870°C for 5 hours

3.2.2.3 TYPE I Platinum Aluminide Coated MAR-M002

The hysteresis loops produced for a TYPE I platinum aluminide coated sample exposed to HTLCF in air (figure 3.35) revealed that the final failure occurred at a relatively high tensile load. The number of cycles to failure was 1149 cycles. The fracture surface, figure 3.36, showed evidence of oxidation. EDS analysis of the fracture surface revealed a relatively high oxygen content. The corrosion product was made up of mainly Ni oxides. AES analysis of the fracture surface (figure 3.37) showed a relatively high oxygen content confirming the EDS analysis. The oxide composition again indicated that it was made up of mainly nickel oxides in some areas and a mixture of oxides in other areas. Fine circumferential cracks in the coating was observed close to the fracture surface (figure 3.38). In most instances they

were neither parallel nor perpendicular to the loading direction. High magnification of the cracks showed that the cracks were branched with the major cracks occurring perpendicular to the loading direction.

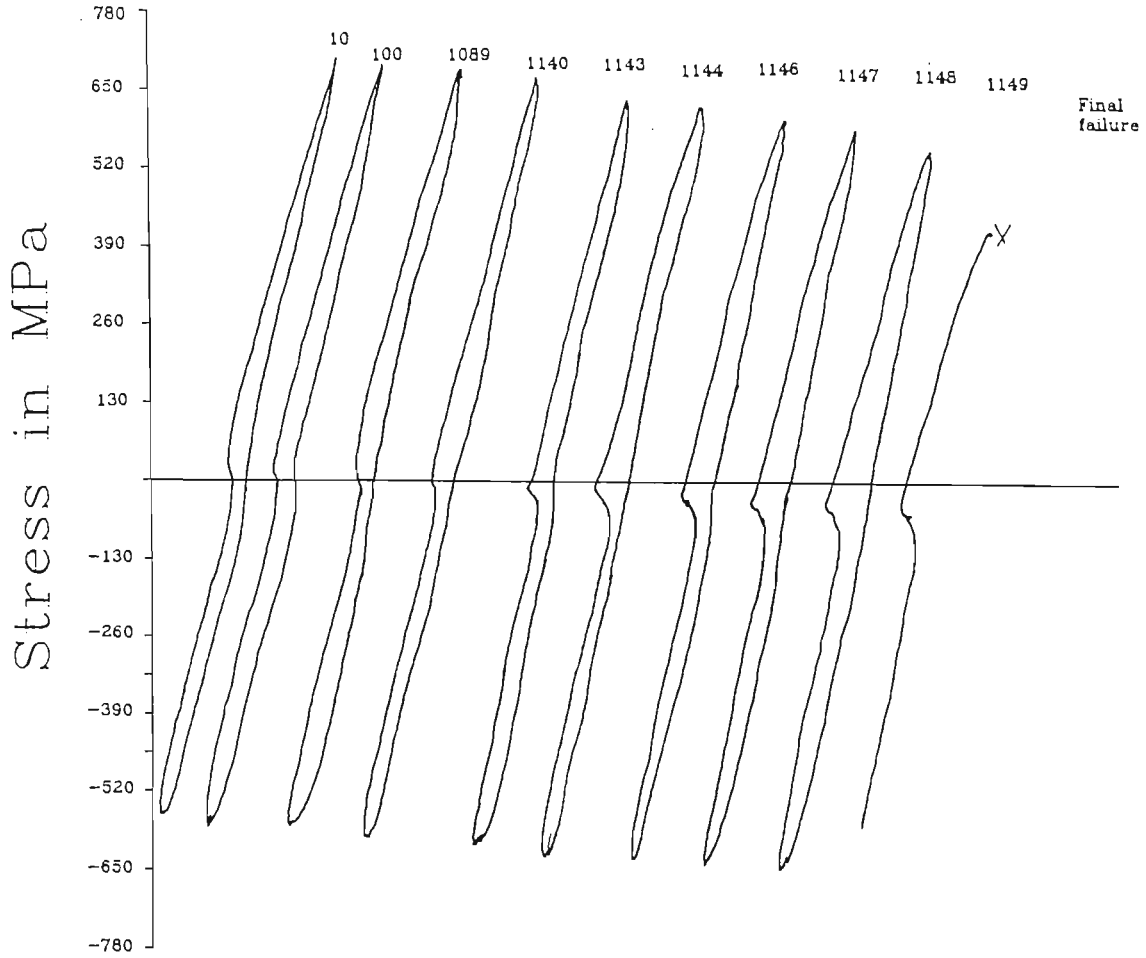

Figure 3.35 : Stress-strain hysteresis loops for TYPE I platinum aluminide coated MAR-M002 after HTLCF in air

Cross-sectional examination revealed severe cracking of the coating (figure 3.39). A significant feature was that the cracks in the coating were branched and did not follow a "straight" path through the coating. This was also observed in the fatigue tests performed in argon which indicated that this due to the mechanical properties of the coating. A number of the cracks had stopped at the coating substrate interface (interdiffusion zone) indicating that the substrate was more resistant to crack propagation. The presence of Cr rich and alumina particles interfered with the crack propagation through the coating (figure 3.39 and 3.40).

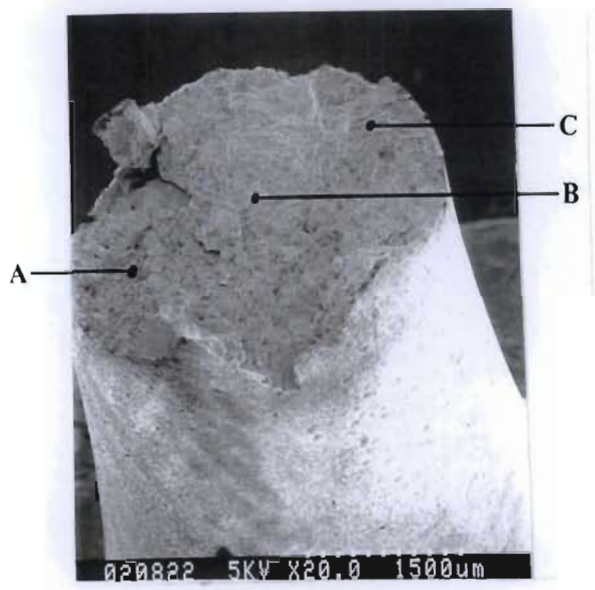

Elements	Weight percent		
	A	B	C
Al	2.74	0.73	1.05
Ti	1.69	1.91	1.39
Cr	6.02	6.26	6.61
Co	7.72	7.31	8.08
Ni	40.41	44.38	45.04
W	8.27	8.47	7.19
Ta	6.42	6.88	3.37
Hf	3.43	4.11	2.30
Zr	2.15	0.00	1.89
Fe	0.15	0.13	0.17
Pt	0.00	0.32	0.00
O	21.00	19.50	22.92

Figure 3.36 : Fractography of TYPE I platinum aluminide coated MAR-M002 after HTLCF in air

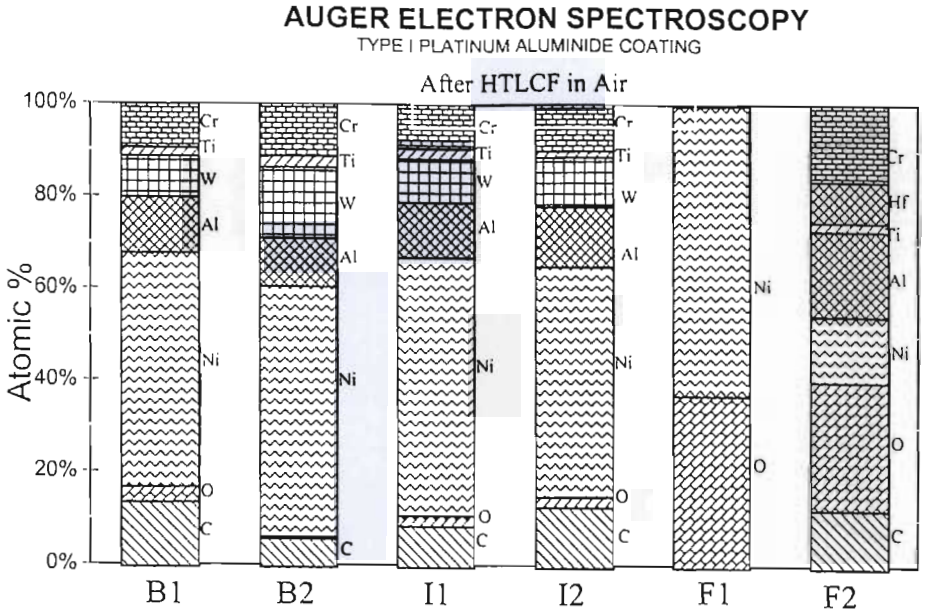

Figure 3.37 : AES analysis of the fracture surface of TYPE I platinum coated MAR-M002 after HTLCF in air

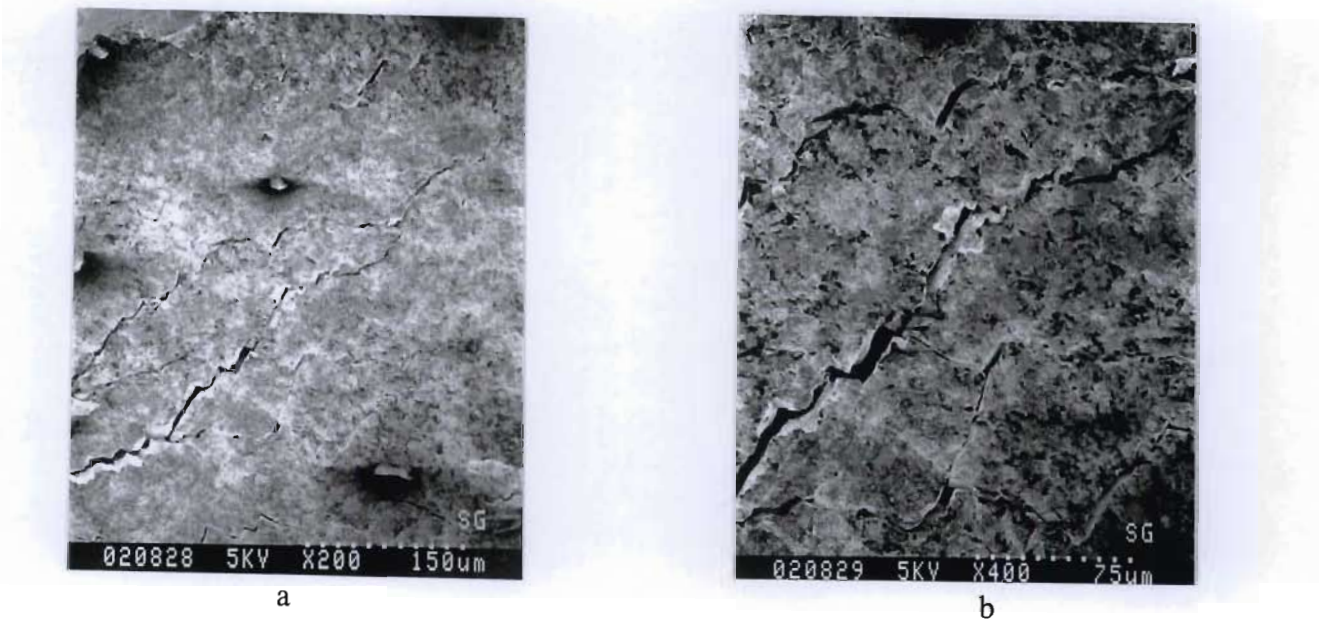

a b

Figure 3.38 : Brittle cracking of the TYPE I platinum aluminide coating close to the fracture surface due to the HTLCF loading in air atmosphere

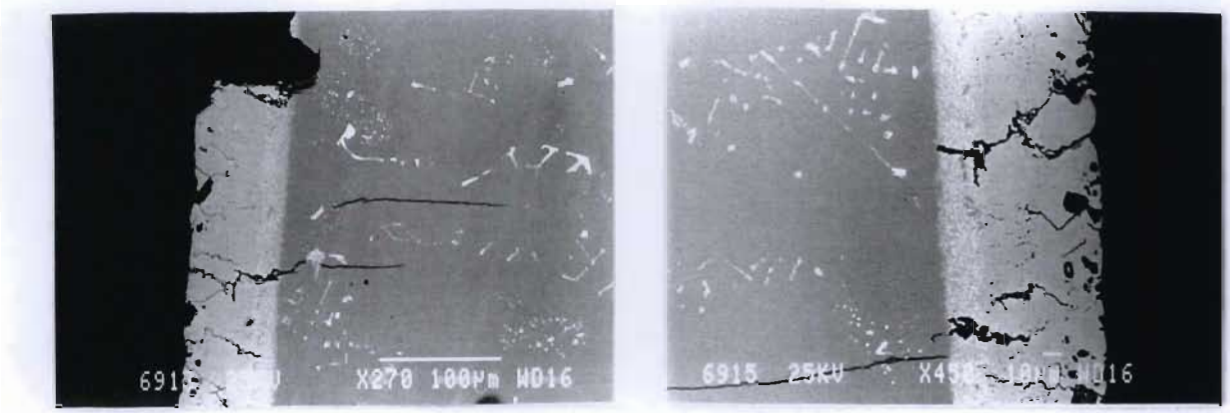

a b

Figure 3.39 : Cross-sectional analysis of TYPE I platinum aluminide coated MAR-M002 after HTLCF in air atmosphere showing cracking of the coating.

Chemical analysis in the crack, adjacent to the crack and away from the crack in the coating (figure 3.40) showed that there was no severe environmental interaction. Crack propagation through the substrate was the characteristic branched cracking observed for fatigue tests performed in air. A high magnification of the crack tip shows evidence of oxidation of the substrate (figure 3.40). The corrosion product in the crack was made up of Ni,Cr, Co, W, Al, Ta and oxygen with Ni and Cr making up the major constituents.

X-ray diffraction analysis of an unloaded disc sample exposed to air at 870°C for 5 hours revealed that the coating was resistant to oxidation (figure 3.41). Stable Al_2O_3 and Cr_2O_3 were present in significant quantities which provides effective protection against oxidation. This analysis gives the typical oxide phases that would form on the coating after exposure to oxygen at high temperature. The corrosion product formed on the fracture surface and at the crack tip was more accurately represented by the corrosion test performed on the uncoated alloy.

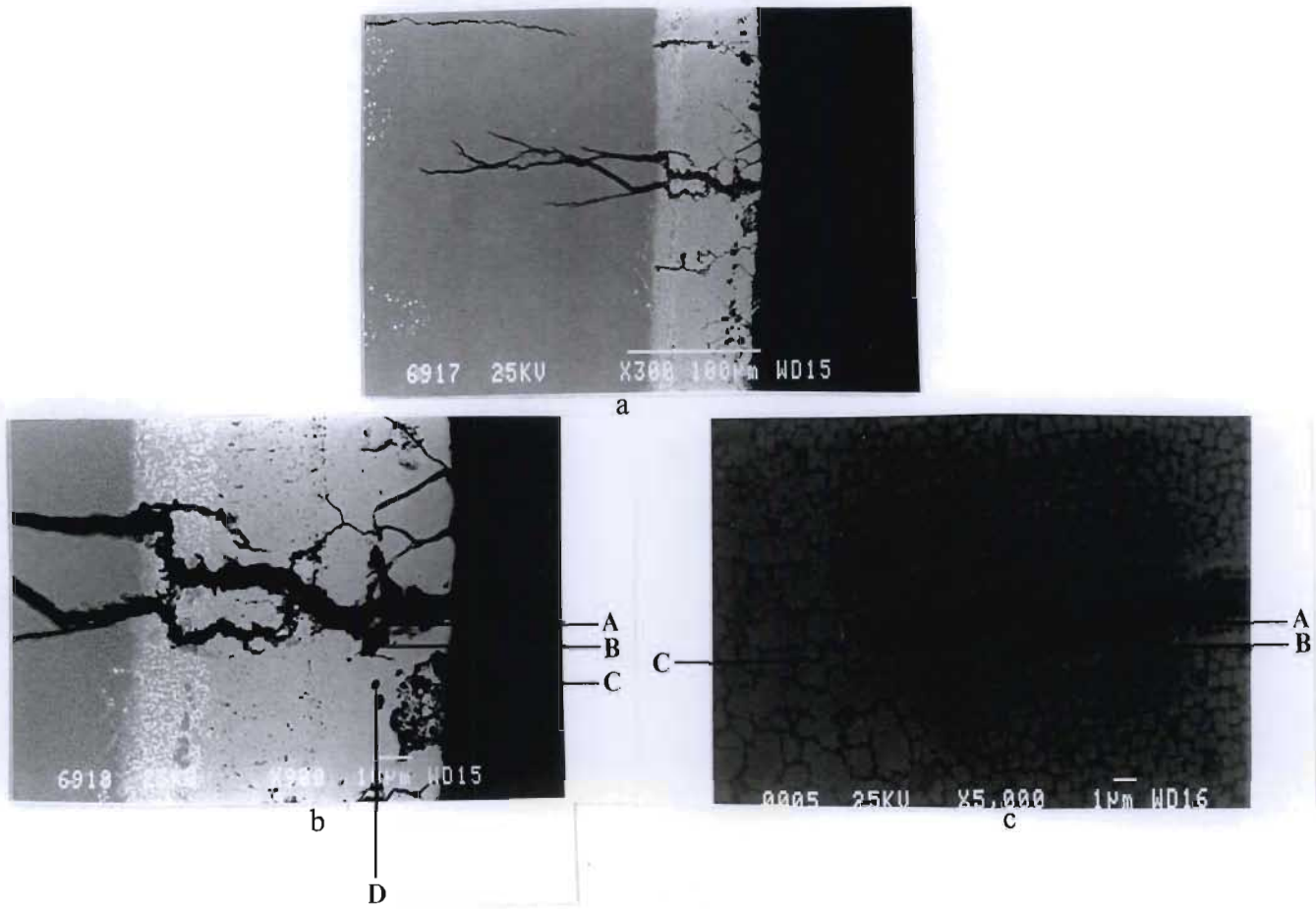

Elements	Weight percent			
	A	B	C	D
Al	27.18	25.89	36.96	16.12
Cr	1.51	2.14	1.42	4.21
Co	1.84	2.45	1.43	2.86
Ni	20.72	20.14	18.86	26.68
Pt	33.42	36.79	40.41	45.63
O	12.71	10.55	0.00	0.00
Ti	0.09	0.00	0.13	0.13
Zr	0.00	0.87	0.37	3.71
Hf	0.85	0.46	0.41	0.48
Ta	1.43	0.44	0.00	0.18
W	0.24	0.00	0.00	0.00

Elements	Weight percent		
	A	B	C
Al	4.20	5.78	4.94
Cr	15.16	9.10	8.77
Co	7.98	7.18	9.93
Ni	40.72	44.38	59.54
Pt	0.00	0.00	0.00
O	18.63	11.40	0.00
Ti	1.56	1.14	1.45
Zr	0.32	2.92	0.00
Hf	0.55	0.96	1.08
Ta	2.40	3.58	1.78
W	8.47	13.56	12.51

Figure 3.40 : Analysis of the a crack in a TYPE I platinum aluminide coated MAR-M002 fatigue sample after HTLCF in air.

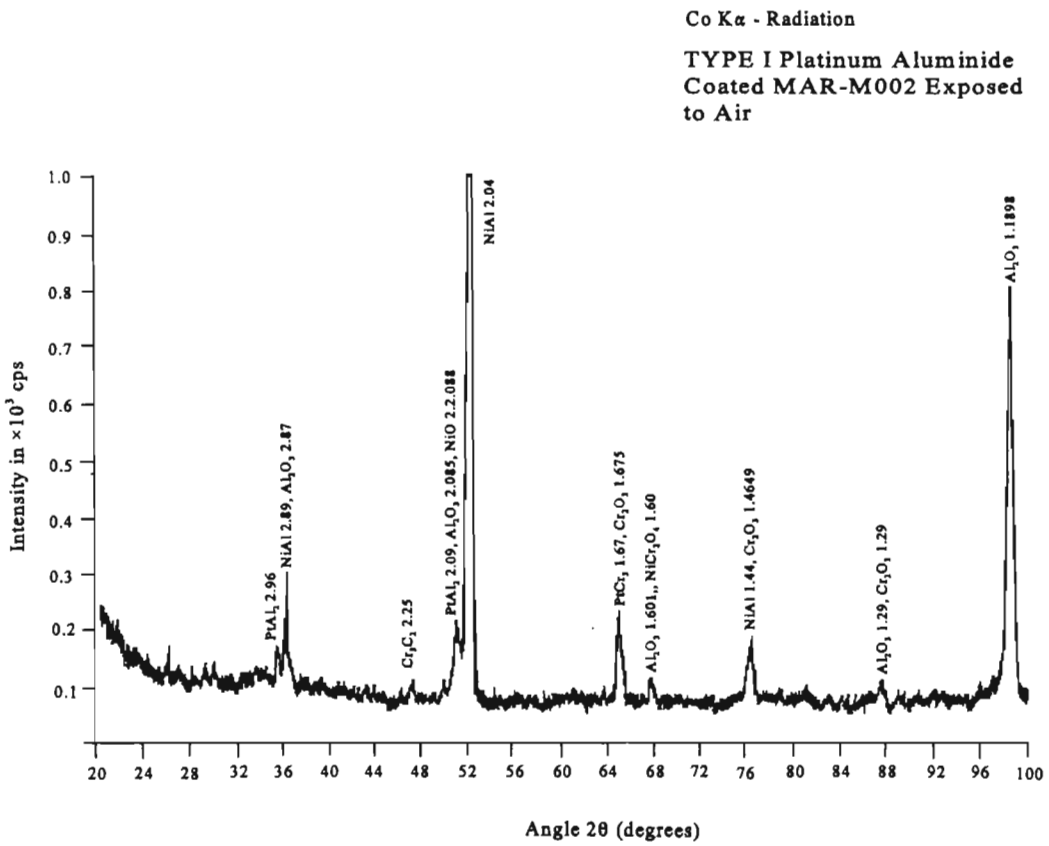

Figure 3.41 : X-ray diffraction of TYPE I platinum aluminide coated MAR-M002 exposed to air at 870°C for 5 hours

3.2.2.4 Platinum Coated MAR-M002

Platinum coated MAR-M002 exposed to HTLCF and air atmosphere at 870°C failed after 1238 cycles. The fracture surface (figure 3.42) showed evidence of oxidation. As in all the fatigue tests performed in air, the evidence obtained from the EDS analysis indicates that the corrosion product on the fracture surface was made up of principally nickel and oxygen, with smaller amounts of aluminium and chromium. AES analysis of the fracture surface indicated that corrosion product was made up of mainly nickel and oxygen (figure 3.43). There was evidence of internal oxidation and a slight reduction in the aluminium content just below the fracture surface (figure 3.43).

The external surface close to the fracture (figure 3.42b) revealed fine cracks in the coating. The cracks were composed of mainly circumferential cracks, perpendicular to the direction of loading. Figure 3.44&45 shows cross-sectional images of platinum coated MAR-M002

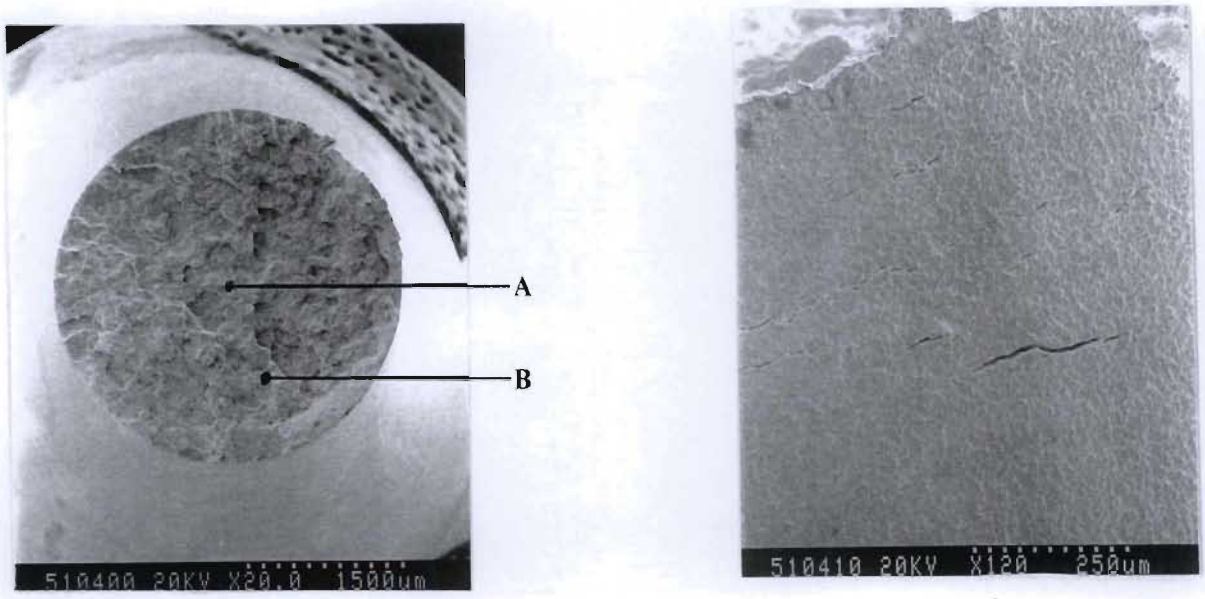

a b

Elements	Weight percent		
	A	B	External Surface
Al	2.49	2.16	10.02
Ti	2.14	2.78	1.03
Cr	6.24	5.20	5.59
Co	7.25	6.11	3.47
Ni	46.87	41.38	19.63
O	13.68	12.76	34.23
Zr	0.00	0.00	0.00
Hf	8.21	4.82	1.35
Ta	7.16	13.40	1.05
W	5.96	11.49	3.29
Pt	0.00	0.00	20.34

Figure 3.42 : Fractography of platinum coated MAR-M002 after HTLCF in air

a) Fracture Surface

b) Cracking of the coating close to the fracture.

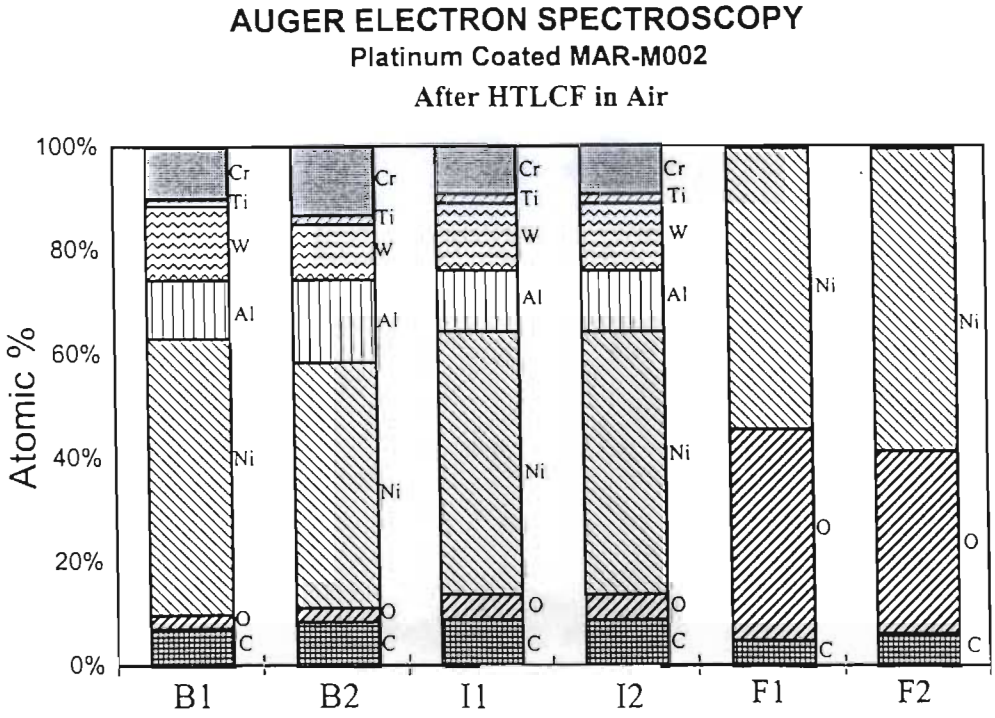

Figure 3.43 : AES analysis of the fracture surface of platinum coated MAR-M002 after HTLCF in air at 870°C

after HTLCF in air. There was evidence of a number of cracks that had initiated on the coating surface but which have not propagated all the way through the coating layer. Cracks in the coating showed a preference to propagate in the grey regions (figure 3.44b). The thickness of the coating had increased from 15μm to 30μm during the test due to the interdiffusion of platinum and alloying elements. The propagation of the fatigue crack through the substrate was branched and transdendritic. The crack tip, figure 3.44c, was "blunt" due the oxidation attack ahead of the propagating crack tip.

High magnification of the fatigue crack in the coating (figure 3.45) gave an indication of the oxidation resistance of the different regions: i) the coating was most resistant; ii) the γ' depleted zone was least resistant; and iii) the substrate was more resistant than the γ' depleted zone but less resistant than the coating layer. The corrosion product in the coating layer was made up of mainly Ni, Co, Cr, Pt and oxygen. This result indicated that the

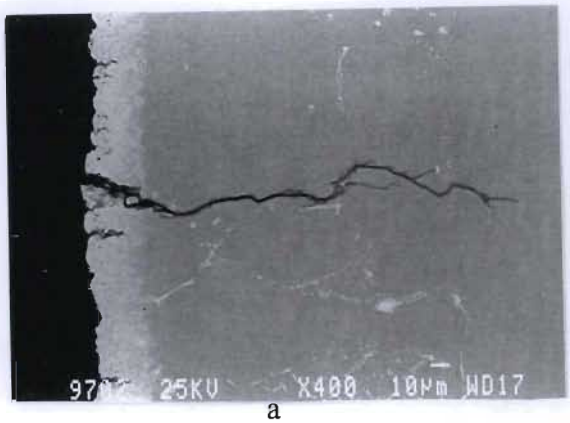

a

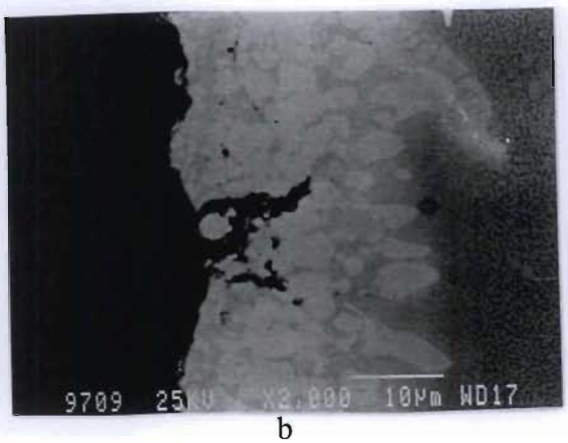

b

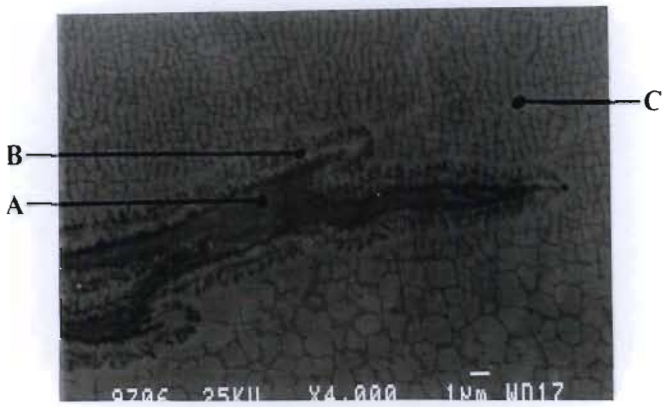

c

Elements	Weight percent		
	A	B	C
Al	2.33	7.19	4.84
Cr	7.99	4.37	7.91
Ni	50.22	53.59	60.90
Pt	0.00	0.81	0.00
Co	8.17	8.33	9.88
Ti	1.32	0.39	1.34
Zr	0.00	0.00	0.21
Hf	0.95	1.49	1.05
Ta	1.01	1.26	2.10
W	3.71	12.38	11.77
O	24.28	10.21	0.00

Figure 3.44 : a) Fatigue crack propagation in platinum coated MAR-M002 after HTLCF in air

b) Fatifue crack propagation in the coating

c) High magnification of the crack tip in the substrate

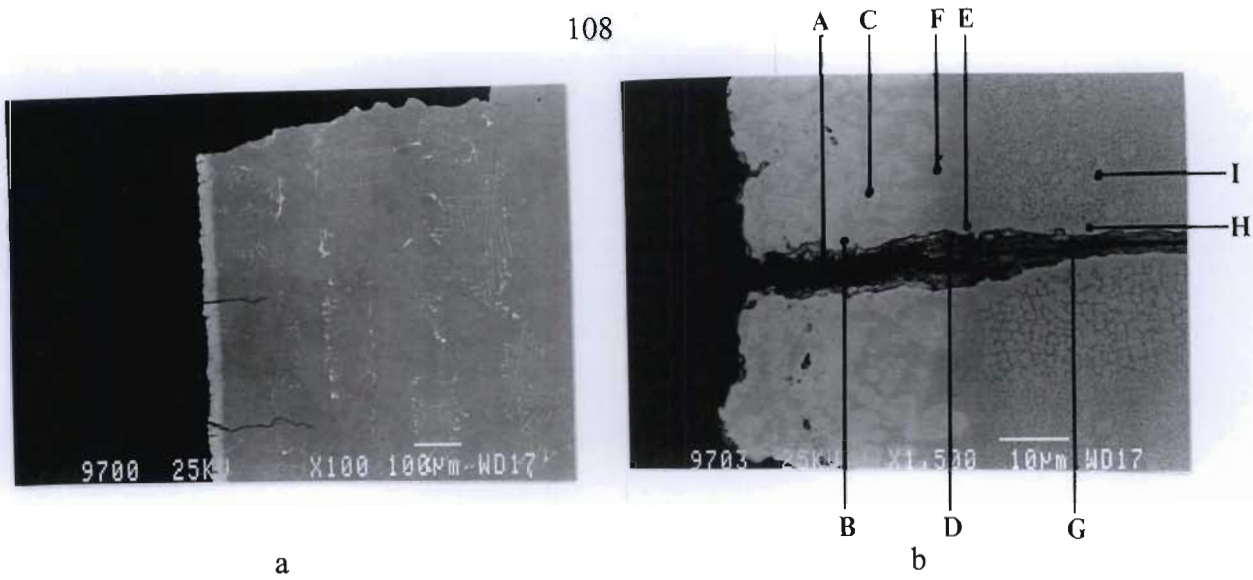

a b

Elements	Weight Percent										
	A	Bw	Bg	Cw	Cg	D	E	F	G	H	I
Al	2.25	3.93	1.31	4.00	2.18	6.68	3.37	3.20	8.31	5.36	5.72
Cr	8.42	1.87	6.87	1.99	8.97	4.68	6.50	8.32	11.34	7.50	7.88
Ni	44.16	30.51	39.41	32.52	37.09	40.22	60.76	58.23	23.64	61.70	61.14
Pt	17.47	48.25	32.41	46.57	29.44	0.32	0.00	2.66	0.09	0.35	0.00
Co	8.89	3.29	8.91	3.46	8.61	9.95	8.92	10.70	8.72	9.23	8.88
Ti	0.91	1.06	0.28	1.55	0.39	1.51	0.99	0.82	2.80	1.37	1.35
Zr	0.00	0.00	0.00	0.00	0.00	0.19	0.00	0.00	0.00	0.00	0.00
Hf	0.00	0.66	0.09	0.58	0.32	1.21	0.96	1.00	1.47	1.03	0.96
Ta	0.75	1.99	0.69	1.98	1.18	2.75	4.94	2.49	3.03	2.59	1.73
W	3.00	8.44	10.03	7.34	11.81	6.84	13.56	12.57	12.97	10.87	12.33
O	14.15	0.00	0.00	0.00	0.00	25.65	0.00	0.00	27.64	0.00	0.00

Figure 3.45 : Chemical analysis of the crack through the platinum coating after HTLCF in air

electron beam spot size was too large and part of the coating was incorporated in the analysis. The analysis of the region adjacent to the crack edge and away from the crack for the white regions in the coating, did not show a significant variation in the composition, however, in the grey regions there was significant decrease in the Cr and Al content along the crack edge. The corrosion product in the γ' depleted zone was made up of mainly Ni, Co, and oxygen with small amounts of Cr and Al. The corrosion product of the crack in the

substrate was made up of a mixture of alloying elements and oxygen. The corrosion product in the crack tip was made up of essentially Ni, Cr and oxygen (figure 3.44). The region adjacent to the crack edge showed evidence of internal oxidation. Small amounts of oxygen were detected in this region with a slight increase in the aluminium content when compared to the base material.

X-ray diffraction analysis of a platinum coated disc sample exposed to air at 870°C for five hours shows the typical oxides formed on the platinum coating (figure 3.46). Typical oxides formed are Cr_2O_3, Al_2O_3, Ti_2O_3, NiO and $NiCr_2O_4$. The oxides formed at the propagating crack tip in the substrate must be characterized using the results obtained for the uncoated disc samples.

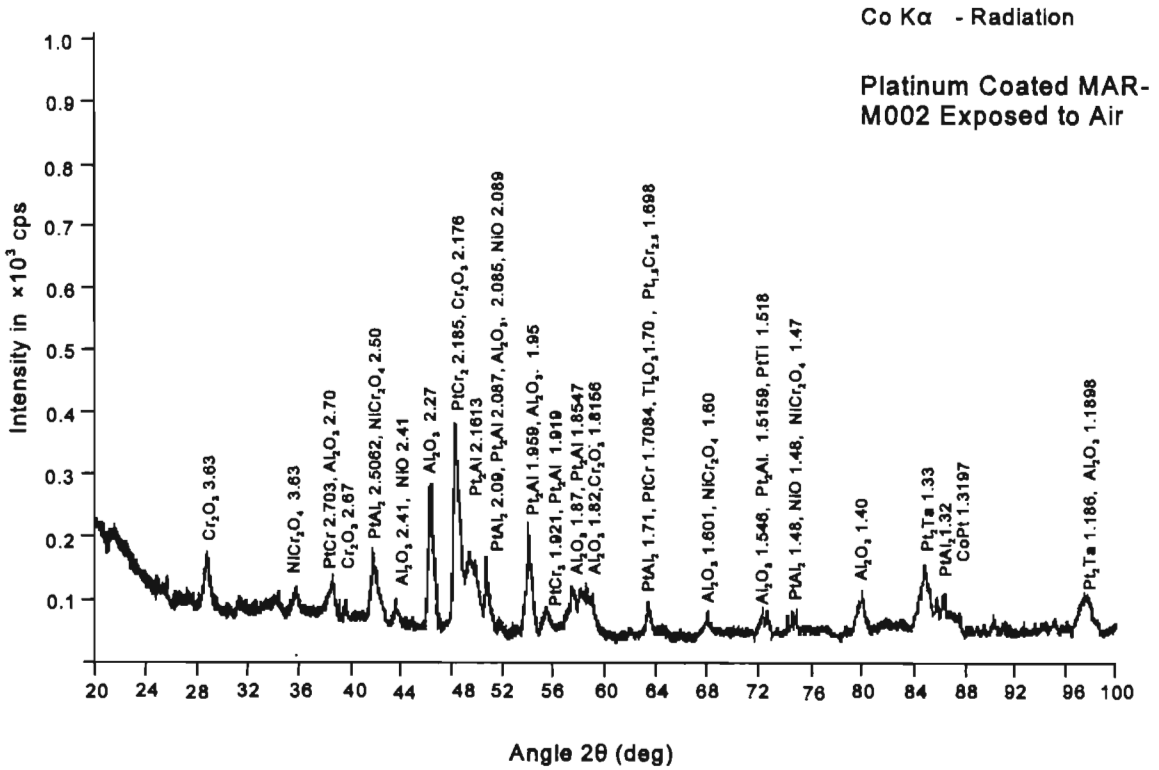

Figure 3.46 : X-ray diffraction of a platinum coated disc sample after exposure to air at 870°C for 5 hours

3.2.3 HTLCF in Ar + 5%SO_2 (Strain Range 0.66%)

3.2.3.1 Uncoated MAR-M002

Uncoated MAR-M002 failed after 335 cycles due to the combination of HTLCF and Ar + 5%SO_2 environment at 870°C. Sulphidation attack of the fracture surface was very evident (figure 3.47). The fatigue crack had initiated around the circumference and propagated perpendicular to the loading direction. Final failure had occurred at the centre of the sample; showing a very brittle final failure. EDS analysis of the fracture surface showed that the corrosion product was composed of mainly Ni, Cr, oxygen and sulphur.

The external surface close to the fracture exhibited evidence of severe sulphidation attack (figure 3.48a). The corrosion product had blistered, (figure 3.48b) and spalled off in areas (figure 3.48c). The nature of the corrosion product (figures 3.48b &d) indicated that it was most probably in the molten state at the test temperature due to the formation of low melting point nickel sulphides.

Cross-sectional examination of the fatigue sample after HTLCF in Ar + 5%SO_2 showed severe sulphidation attack of the fracture surface and the external surface (figure 3.49a). The corrosion product had spalled off in regions. Beneath the corrosion product was a "porous" region showing internal sulphidation of the substrate. The corrosion product on the fracture surface and external surface was found to consist of three distinctive layers (figures 3.49 & 3.50): black inner layer, light grey intermediate layer and dark grey outer layer. The chemical composition of the dark grey outer layer showed that it was made up mainly of Cr, Ni, S, and oxygen. This indicated that it was composed of a mixture of sulphides and oxides of Cr and Ni. The intermediate light grey layer was more complex with Ta, Ti and oxygen being the dominant elements with small amounts of Cr, Ni and sulphur compared to the dark grey layer.

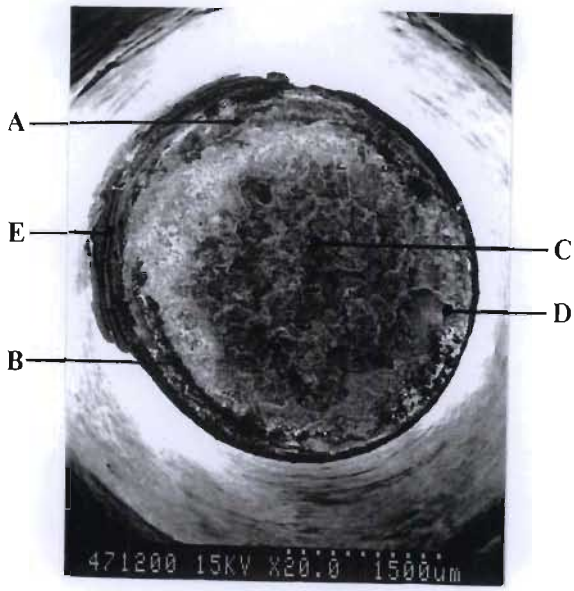

Elements	Weight percent				
	A	B	C	D	E
O	8.28	8.89	13.47	12.41	30.03
S	2.40	17.80	4.04	9.29	7.36
Cr	1.41	14.95	8.85	12.47	38.20
Co	10.15	5.61	5.61	6.50	2.82
Ni	52.38	50.42	35.54	41.25	18.60
Zr	0.55	0.00	0.12	0.06	0..08
Hf	0.63	0.57	6.01	2.15	0.28
Ta	1.28	0.49	10.83	4.89	0.72
W	18.88	0.77	8.70	2.69	0.17
Ti	0.69	0.44	2.81	3.26	1.73
Al	3.35	0.05	4.02	5.05	0.08

Figure 3.47 : Fracture surface of uncoated MAR-M002 after HTLCF in Ar + 5%SO_2 at a strain range of 0.66%

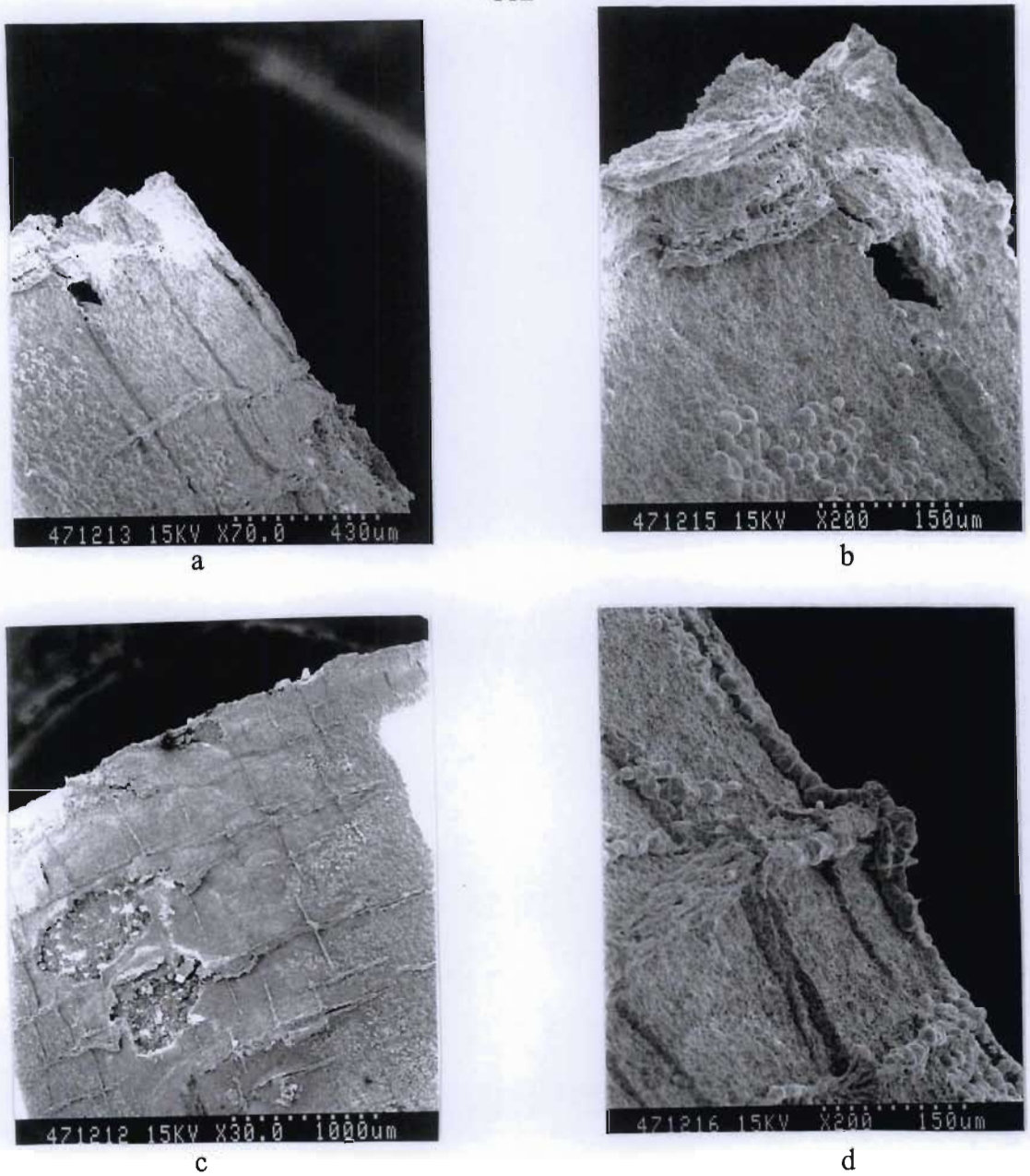

Figure 3.48 : Fractography of uncoated MAR-M002 after HTLCF in SO_2 bearing atmosphere.

The "black" layer was made up of mainly Al, Ni, S and oxygen. This region consisted of predominantly aluminium oxides and relatively small amounts of sulphides. It was also significant that this layer formed at the corrosion scale-substrate interface.

Chemical analysis of the "porous" γ' depleted region showed a significantly lower aluminium and chromium content compared to the base alloy. The dark corrosion product found in the "pores" in this region was composed of Ni, Cr, Co, Al and S with Ni and S making up the major constituents.

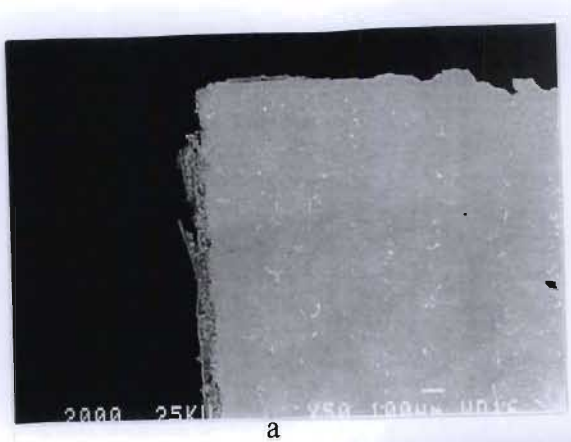

a

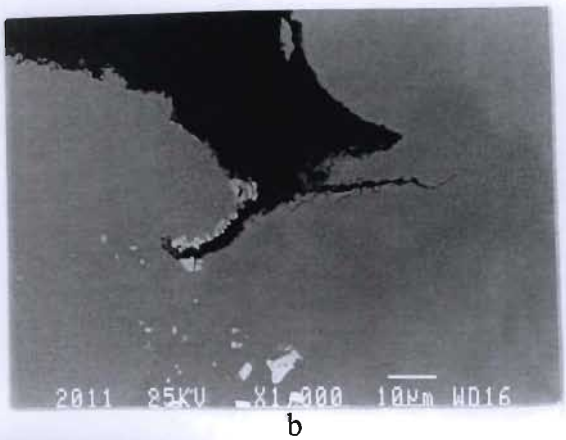

b

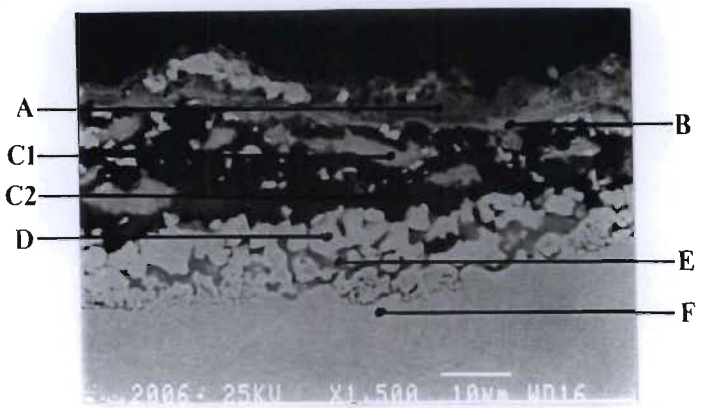

c

Elements	Weight percent						
	A	B	C1	C2	D	E	F
Al	1.13	2.20	4.91	31.63	1.53	0.53	6.09
S	6.18	6.84	3.46	7.09	0.42	33.00	0.38
Cr	34.91	6.80	5.18	2.26	0.63	25.58	8.94
Co	1.47	1.67	1.25	2.55	12.85	7.74	9.08
Ni	12.47	13.12	12.67	17.98	64.79	29.61	60.60
Ti	2.15	14.03	13.28	0.46	0.19	0.19	1.50
Zr	0.28	0.00	0.03	0.26	0.30	0.00	0.34
Hf	0.72	2.45	1.78	0.05	0.00	1.13	2.00
Ta	1.14	25.18	29.48	1.77	0.00	0.00	0.49
W	0.97	0.00	0.00	0.23	19.30	2.20	10.59
O	38.60	27.70	27.97	35.73	0.00	0.00	0.00

Figure 3.49 : a) Cross-sectional analysis of uncoated MAR-M002 after HTLCF in SO_2 containing environment

b) Secondary cracking on the fracture surface

c) Chemical analysis of the corrosion product on the fracture surface

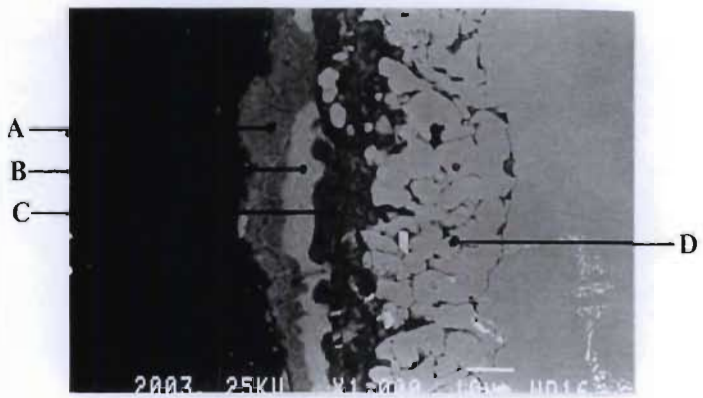

Elements	Weight percent				
	A	B	C	D (solid)	D (pores)
Al	0.11	0.29	28.99	2.26	6.82
S	13.31	2.56	7.99	0.20	28.08
Cr	23.24	9.39	3.78	0.18	9.01
Co	4.03	0.89	2.40	11.65	8.60
Ni	29.65	8.71	18.37	71.26	44.61
Ti	0.25	15.54	0.51	0.03	0.18
Zr	0.18	0.00	0.22	0.25	0.36
Hf	0.00	1.41	0.13	0.56	0.00
Ta	0.10	36.31	1.29	0.00	0.58
W	0.19	0.00	0.64	13.61	1.76
O	28.94	24.89	35.69	0.00	0.00

Figure 3.50 : Morphology of the corrosion product on the external surface of and uncoated fatigue sample after HTLCF in Ar + 5% SO_2

X-ray diffraction analysis of an uncoated disc sample after exposure to Ar + 5%SO_2 at 870°C showed that the typical phases present in the corrosion product as a result of the sulphidation attack were Ni_7S_6, Cr_5S_8, TiO_2, Cr_3S_4, CrS, Al_2O_3, Cr_2O_3, Ni_3S_2 and NiO (figure 3.51). A significant feature of the corrosion product was that it was a combination of oxides and sulphides.

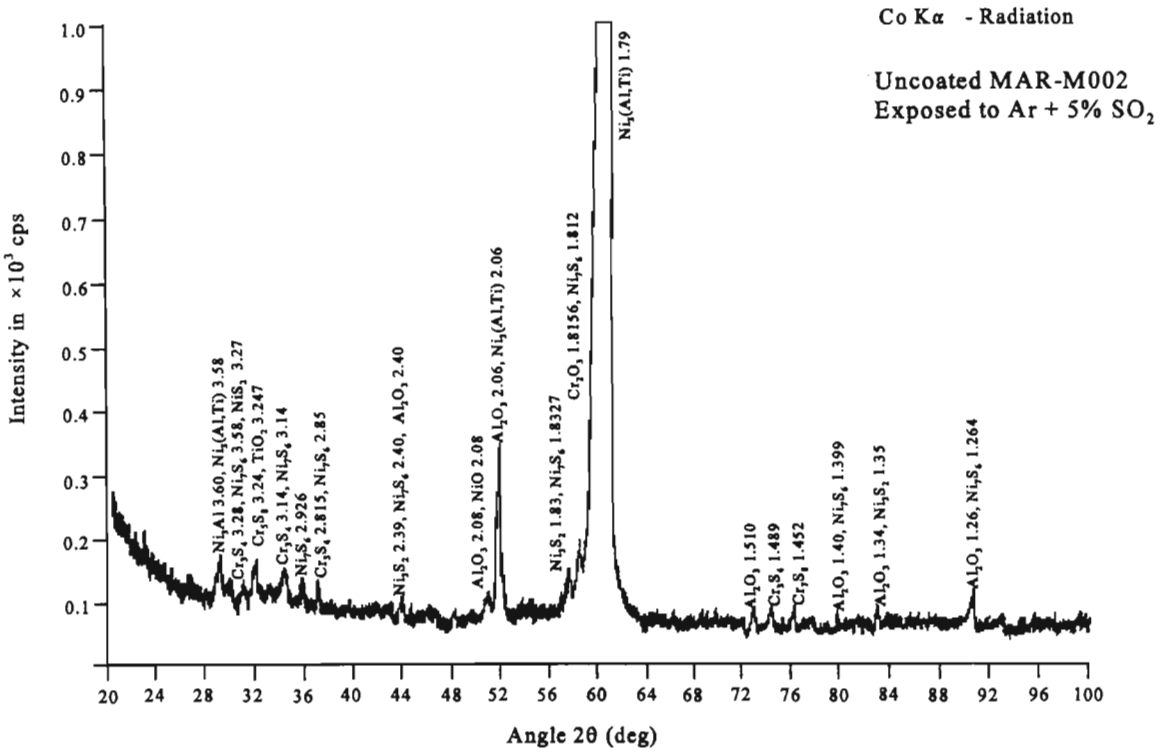

Figure 3.51 : X-ray diffraction of uncoated MAR-M002 exposed to Ar + 5%SO_2 at 870°C for 5 hours

3.2.3.2 Aluminide Coated MAR-M002

The aluminide coated MAR-M002 fatigue sample exposed to HTLCF and Ar + 5%SO_2 environment experienced an accelerated failure due to the highly corrosive SO_2 containing environment. The number of cycles to failure was 161. Sulphidation attack was manifested by dark sulphide and oxide phases on the fracture surface (figure 3.52). The corrosion product on the fracture surface was made up of principally Ni, Cr, S and oxygen (figure 3.52). This was similar to the chemical analysis of the corrosion product on the fracture surface of the uncoated sample. Analysis of the corrosion product close to the edge of the fracture surface revealed a higher nickel and aluminium content with significant amounts of oxygen and sulphur also present. AES analysis confirmed the presence of oxides in the corrosion product (figure 3.53) and showed that it consisted of a mixture of oxides and sulphides. The prominent substrate alloying elements present were Cr, Hf, Al and Ni.

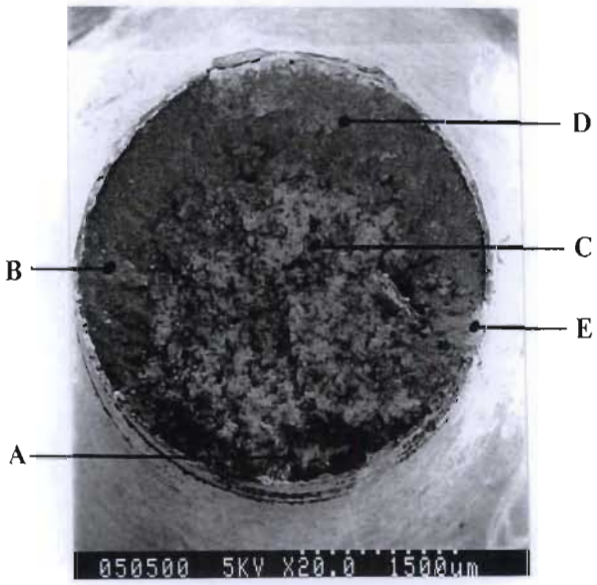

Elements	Weight percent				
	A	B	C	D	E
O	30.33	28.09	27.84	28.45	16.42
Al	0.38	0.60	1.53	2.70	13.94
Ni	25.24	27.76	28.21	28.28	46.58
Cr	25.19	25.92	17.70	18.00	3.04
Co	3.37	4.12	4.40	4.27	6.53
W	1.13	0.72	2.24	2.00	1.19
Ta	1.89	1.35	3.41	2.38	1.30
Ti	1.84	1.54	2.28	1.60	0.67
Zr	0.63	0.00	0.61	1.12	0.08
Hf	0.73	0.68	2.00	1.41	0.00
Fe	0.05	0.00	0.07	0.14	0.85
S	8.91	9.23	9.71	9.67	9.41

Figure 3.52 : Fractography of aluminide coated MAR-M002 after HTLCF in Ar + 5%SO_2 environment at a strain range of 0.66%

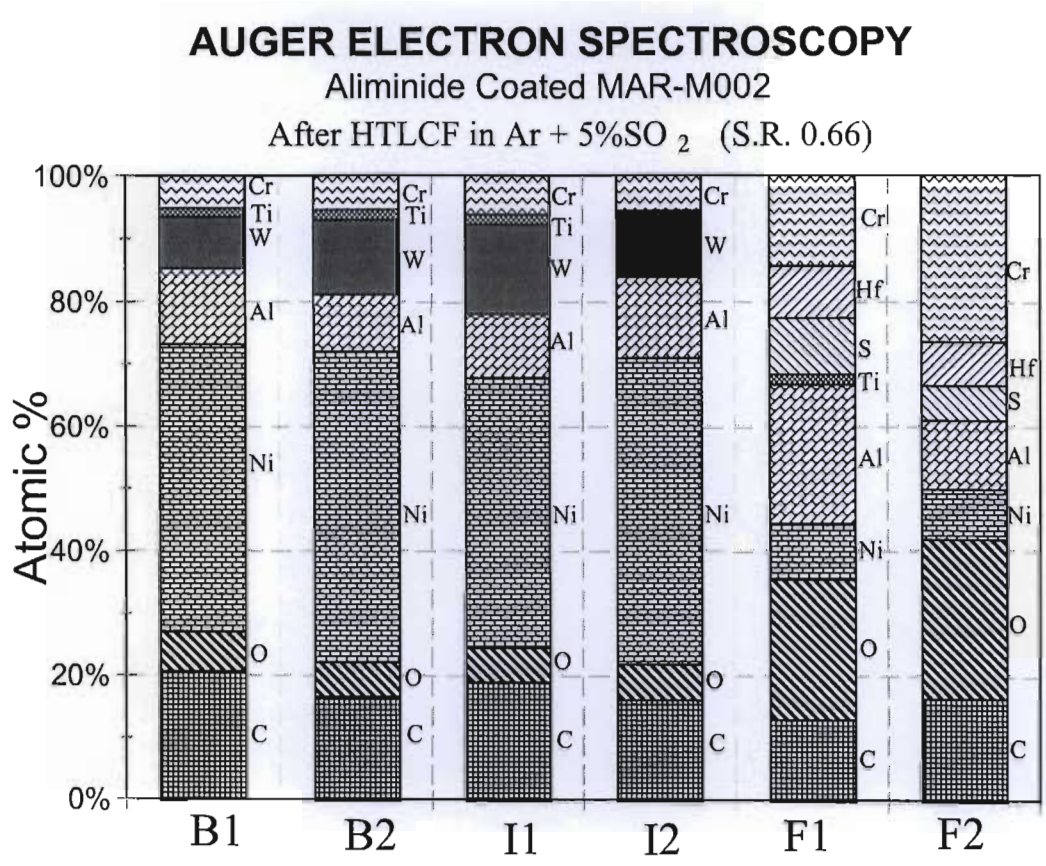

Figure 3.53 : AES analysis of the fracture surface of aluminide coated MAR-M002 after HTLCF failure in SO_2 bearing atmosphere

a b

Figure 3.54 : Cracking of the coating close to the fracture surface due to HTLCF IN Ar + 5%SO_2 (S.R. 0.66%)

Examination of the coating adjacent to the fracture surface revealed two modes of cracking (figure 3.54): the one mode was circumferential cracks perpendicular to the direction of loading and the second was cracks approximately 45° to the loading direction. The nature of the cracks indicated a very brittle type of failure. The build-up of corrosion product around the crack lip indicated that the presence of defects enhanced the corrosion process.

Cross-sectional examination (figure 3.55) revealed severe cracking of the coating. The cracks in the coating were filled with corrosion product. High magnification of a crack showed that the outer edges of crack in the coating was vulnerable to sulphidation and the corrosion process proceeded "laterally" on the external surface. The substrate also showed some resistance to crack initiation and was "protected" from sulphidation by the corrosion product filling the crack. Sulphidation and cracking also proceeded preferentially along the substrate-interdiffusion zone interface instead of into the substrate. This indicated that the interdiffusion zone was more susceptible to sulphidation.

The corrosion product in the crack was composed of two regions, namely, a dark region down the centre of the crack and a region which was a mixture of dark and light phases along the crack edge (figure 3.56). The dark region down the centre was composed of mainly Al, Ni, oxygen and sulphur. From the quantitative analysis of this region it can be seen that it was made up mainly of aluminium oxides with smaller amounts of sulphides. The "mixed" region showed a significantly higher sulphur and tungsten content. The higher sulphur content clearly indicates the presence of a higher quantity of sulphide phases in this region. The region adjacent to the corrosion product/coating interface shows a slight depletion of aluminium when compared to the normal composition of the coating. Analysis of the crack tip showed that the corrosion product was essentially Al, Ni, oxygen and sulphur. The region adjacent to the crack tip in the interdiffusion zone revealed a depletion of aluminium and tungsten as a result of the corrosion process.

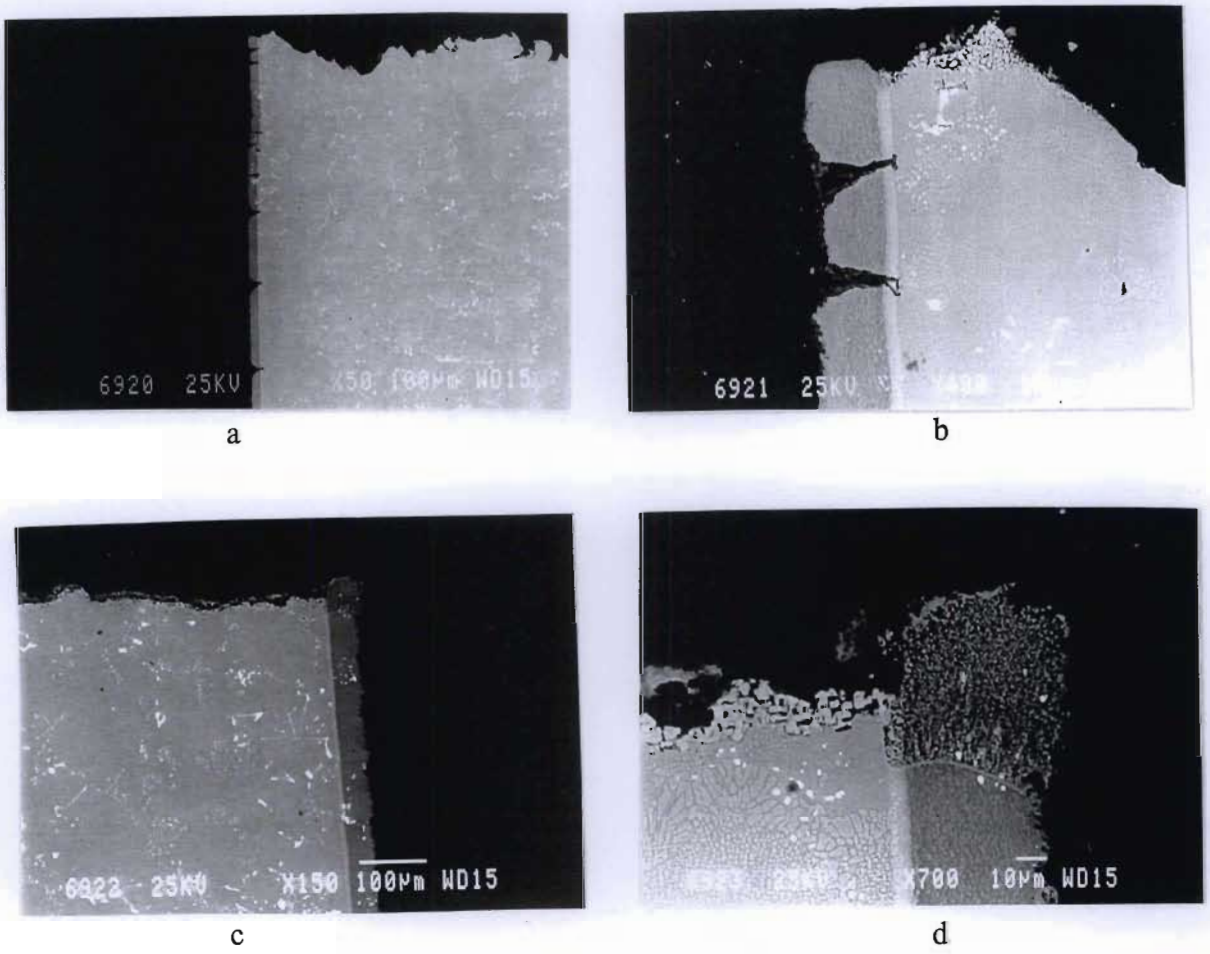

Figure 3.55 : Cross-sectional analysis of aluminide coated MAR-M002 after HTLCF in Ar + 5%SO_2

Al_2O_3, NiO, Cr_3S_4, Ni_3S_2, Ni_7S_6, Cr_3S_8, Cr_3S_7, NiS and CrS were some of the typical sulphide and oxide phases detected on an aluminide coated disc sample exposed to Ar +5%SO_2 for five hours at 870°C (figure 3.57). These phases made up the corrosion product on the coating and within the cracks in the coating. From figure 3.57, it can be seen that the oxides of Al and Cr made up a significant proportion of the corrosion product. The corrosion product on the fracture surface and the crack tip would be similar to that obtained for the uncoated sample.

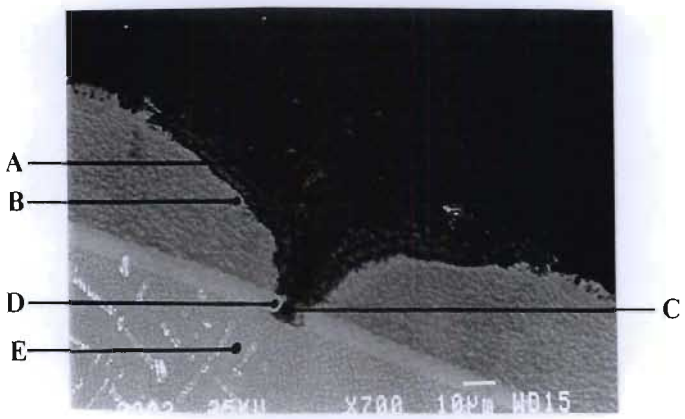

Elements	Weight percent							
	A (dark)	A (light)	B	C	D	E	Interdif fusion	Coating
O	41.49	31.21	0.00	30.62	0.00	0.00	0.00	0.00
Al	33.45	26.42	21.90	25.24	9.37	6.67	15.12	29.65
W	1.38	8.74	11.15	2.92	15.86	7.30	18.66	6.70
S	6.60	15.94	0.89	11.88	3.01	0.02	0.00	0.00
Cr	0.60	3.74	2.43	3.82	2.36	6.86	14.48	5.30
Co	2.11	1.24	5.31	2.99	10.38	8.25	9.92	7.30
Ni	13.17	9.05	56.99	11.23	51.26	58.55	34.50	46.85
Ti	0.14	0.94	0.47	3.67	0.83	1.79	2.03	0.93
Ta	0.00	0.53	0.00	4.86	3.79	8.81	3.22	2.05
Hf	0.21	1.15	0.80	1.74	2.44	1.38	1.55	1.18
Zr	0.86	1.03	0.05	1.04	0.70	0.36	0.52	0.03

Figure 3.56 : Chemical analysis of the crack in aluminide coated MAR-M002 after HTLCF in SO_2 containing environment (S.R. 0.66%)

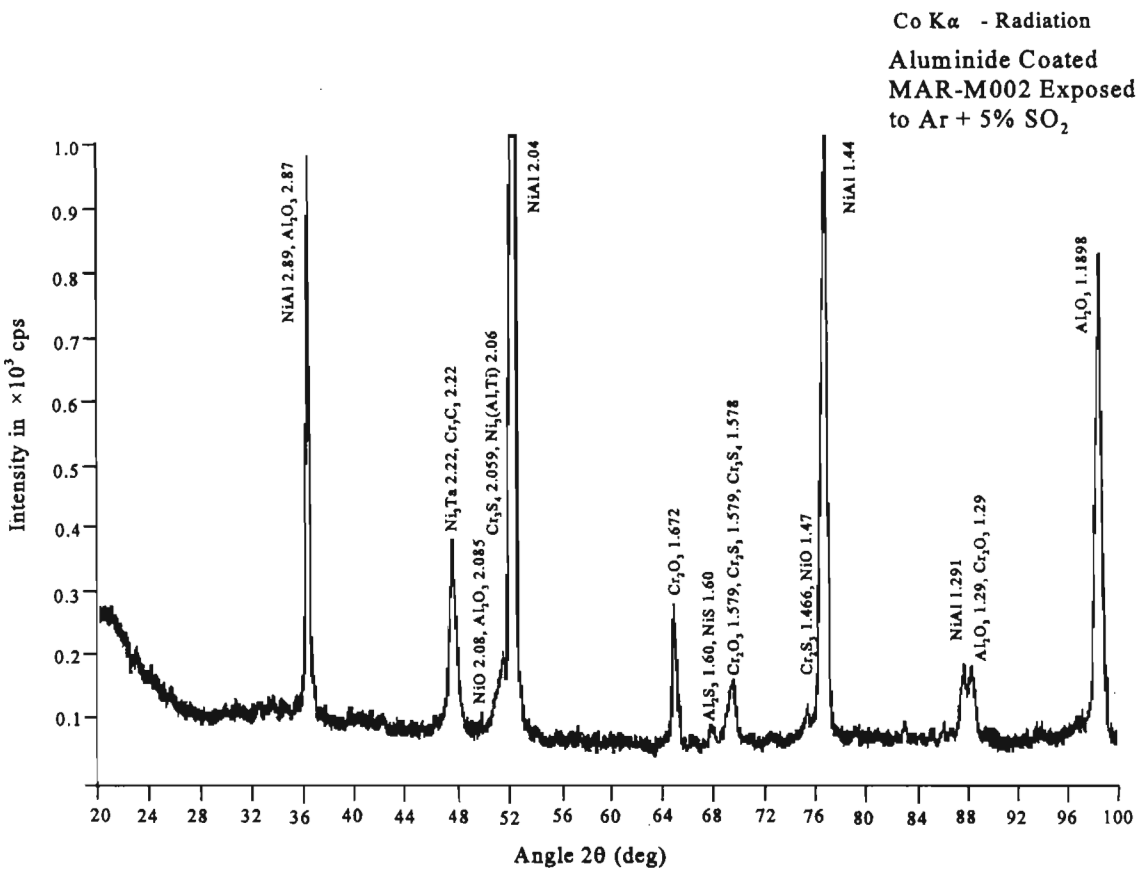

Figure 3.57 : X-ray diffraction analysis of aluminide coated MAR-M002 after exposure to Ar + 5%SO_2 for 5 hours at 870°C

3.2.3.3 TYPE I Platinum Aluminide Coated MAR-M002

The fracture surface of a TYPE I platinum aluminide coated fatigue sample after HTLCF in Ar + 5%SO_2, figure 3.58, showed evidence of severe sulphidation. The number of cycles to failure was 1377, which was a significant improvement over the aluminide coated and uncoated MAR-M002 materials systems. There were two distinct regions, namely, a "smooth" region where crack propagation occurred and a "coarse" region where final failure occurred. The external surface close to the fracture (figure 3.58&59) had a "fish scale" type of appearance. This occurred as a result of the combined effect of sulphidation attack and mechanical loading. A number of fine cracks were present in the coating. The cracks were in general perpendicular to the direction of loading with "dark" corrosion product build-up along the crack edge (figure 3.59).

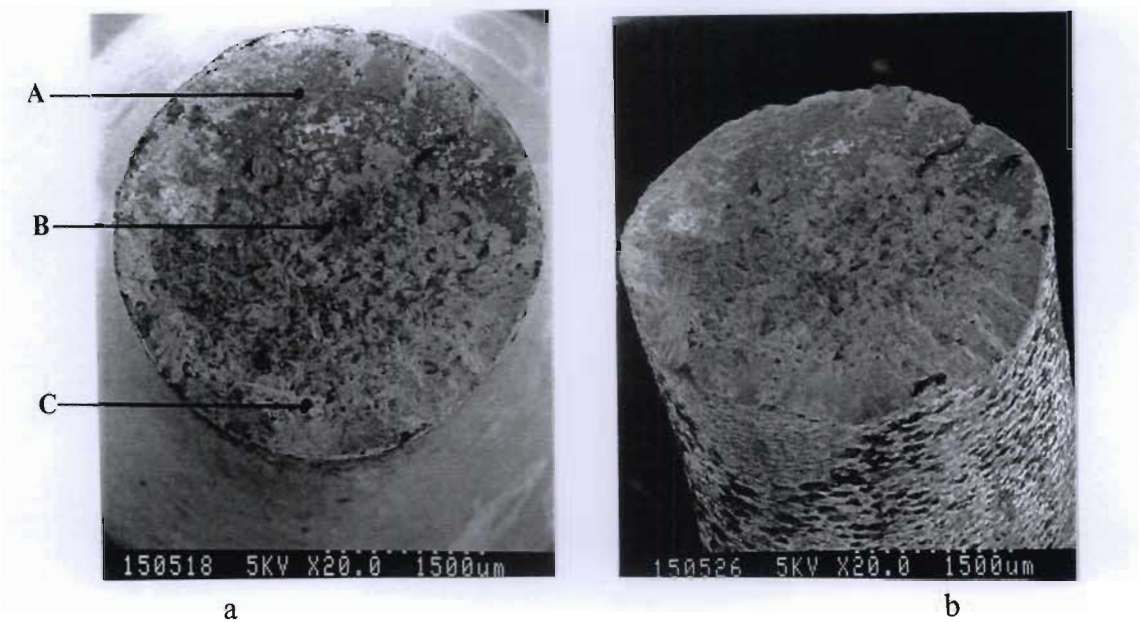

a b

Elements	Weight percent		
	A	B	C
Al	0.25	2.47	2.08
Ti	1.15	3.40	3.34
Cr	26.52	7.56	7.54
Co	3.53	5.44	4.87
Ni	29.00	35.65	32.49
W	0.24	9.26	9.78
Ta	0.69	7.79	12.03
Hf	0.61	3.33	3.93
Zr	0.03	2.26	3.97
Fe	0.43	0.23	0.32
S	9.45	3.94	1.69
O	28.08	18.67	17.95

Figure 3.58 : Fractography of TYPE I platinum aluminide coated MAR-M002 after HTLCF in Ar + 5% SO_2 (S.R. 0.66%)

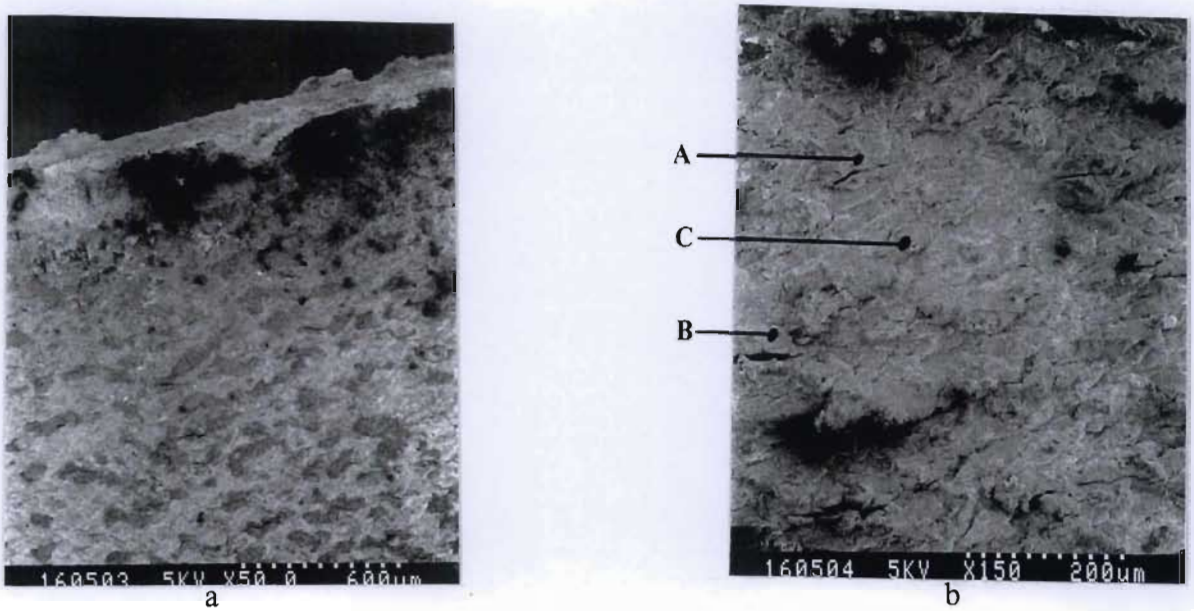

a b

Elements	Weight percent			
	A	B	C	Area Analysis
O	45.05	45.38	42.88	40.68
Al	36.59	37.60	31.43	32.71
S	0.68	4.52	5.41	4.19
Ti	0.50	0.00	0.37	0.38
Cr	5.99	2.94	7.02	10.47
Co	1.88	0.41	1.30	2.26
Ni	8.09	4.93	4.54	7.23
Ta	0.00	0.00	0.00	0.00
Pt	0.00	3.31	0.90	2.07
W	0.00	0.00	0.00	0.00
Fe	0.84	0.48	0.77	0.00
Si	0.39	0.44	0.29	0.00

Figure 3.59 : Chemical analysis of the external surface close to the fracture surface of TYPE I platinum aluminide coated MAR-M002 after HTLCF in SO_2 bearing atmosphere (S.R. 0.66%)

Chemical analysis of the fracture surface (figure 3.58) revealed a high sulphur, oxygen, Cr and Ni content in the corrosion product. This indicated that the corrosion product was rich in the sulphides and oxides of Ni and Cr. In the region where final failure had occurred, the sulphur and Ni content were significantly lower.

Chemical analysis of the regions around the cracks in the coating (figure 3.59) showed that the corrosion products on the lips of the crack was composed of essentially Al and oxygen, indicating that these areas were composed of mainly aluminium oxides. The other regions analysed showed small but significant amounts of sulphur. A significant feature was that the major constituents were Al and oxygen in all the regions analysed.

Cross-sectional examination of the TYPE I platinum aluminide coated sample exposed to SO_2 and HTLCF showed several cracks in the coating (figure 3.60). The cracks in the coating were branched indicating that the cracking of the coating occurred over a significant number of cycles. Corrosion product build-up on the coating was evident. It was noted that when the corrosion product had covered the crack, no corrosion proceeded within the crack. However, in the regions where the corrosion product was cracked, extensive corrosion of the coating was observed. The sulphidation attack was concentrated at the lip of the crack showing that the coating was most vulnerable in this region. The degradation proceeded

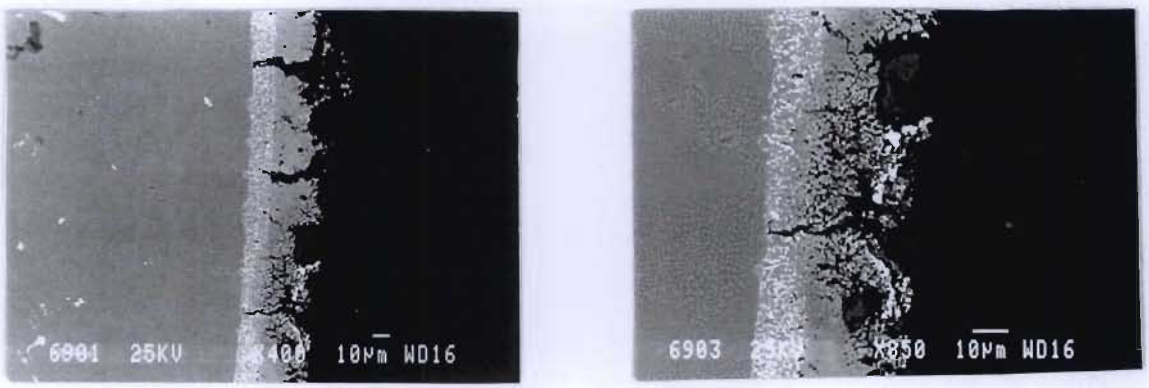

a b

Figure 3.60 : Cross-sectional analysis of TYPE I platinum aluminide coated MAR-M 002 after HTLCF in SO_2 showing the "self healing" properties (S.R 0.66%)

most rapidly along the coating surface and at a slower rate inwards. Chemical analysis of the corrosion product is shown in figure 3.61. The corrosion scale was composed of light and dark regions. Overall analysis of the corrosion product showed that it was made up mainly of Al and Cr oxides and sulphides. The dark region was found to be essentially Al and oxygen with relatively small amounts of S, Cr and Ni detected. The light regions were found to be composed mainly of Cr, Al, oxygen and S with smaller amounts of Ni, Ti, and Co. The Al content was significantly lower than that observed in the dark regions. At the coating-corrosion scale interface, a more complex structure was obtained with a relatively high Al, Cr, Ni, Pt, S and oxygen content. The sulphur content in this region was significantly higher as well. This indicated that the scale at this point was composed of the sulphides and oxides of Al, Cr and Ni with platinum "dissolved" in it. Analysis of the coating adjacent to corrosion scale indicated that this region was depleted of Al. There was also evidence of sulphur diffusing into the coating resulting in internal sulphidation attack. The corrosion product in the crack in the coating revealed that it was composed of mainly Al, Ni, S and oxygen with Ti and Cr being more significant in the interdiffusion zone. The sulphur content was highest at the crack tip.

Figure 3.62 shows the X-ray analysis of a TYPE I platinum aluminide coated MAR-M002 disc sample exposed Ar + 5% SO_2 at 870°C. Typical sulphide and oxide phases produced as a result of the sulphidation attack is shown in Table 3.3. The corrosion product consisted of the oxides and sulphides of Al, Cr and Ni.

Table 3.3 : Typical oxides and sulphides formed on TYPE I platinum aluminide coated MAR-M002 after exposure to SO_2 bearing atmosphere at 870°

Oxides	**Sulphides**
Al_2O_3	Ni_3S_2
Cr_2O_3	Ni_7S_6
NiO	Al_2S_3
	Cr_2S_4
	Cr_3S_4
	NiS
	Ni_3S_4

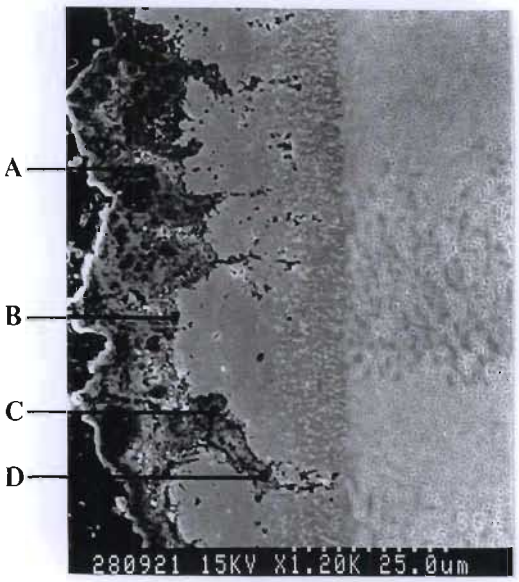

Elements	Weight percent						
	A (dark)	A (light)	B	B (coating)	C	D	D (coating)
Al	44.06	20.74	19.17	9.40	27.10	21.34	10.35
S	4.98	14.14	15.54	0.44	9.15	11.72	0.99
Ti	0.22	5.65	0.96	0.29	3.38	8.37	0.55
Cr	4.33	20.29	9.70	1.49	5.89	7.56	1.12
Co	1.10	4.12	4.44	7.07	1.97	2.31	6.14
Ni	2.20	7.75	17.88	72.66	11.43	9.96	72.66
Zr	0.00	0.27	0.00	1.22	0.25	0.73	0.00
Hf	0.38	0.19	0.35	0.51	2.65	4.53	1.34
Ta	0.44	0.05	0.70	0.00	1.42	1.28	1.27
W	0.00	0.00	0.10	2.12	1.04	0.17	1.74
Pt	0.00	0.07	10.28	4.80	1.16	0.80	3.83
O	42.28	25.72	20.87	-	34.56	31.50	-

Figure 3.61 : Chemical analysis of the corrosion product on the surface of TYPE I platinum aluminide coated MAR-M002 after HTLCF in SO_2 bearing atmosphere (S.R. 0.66%)

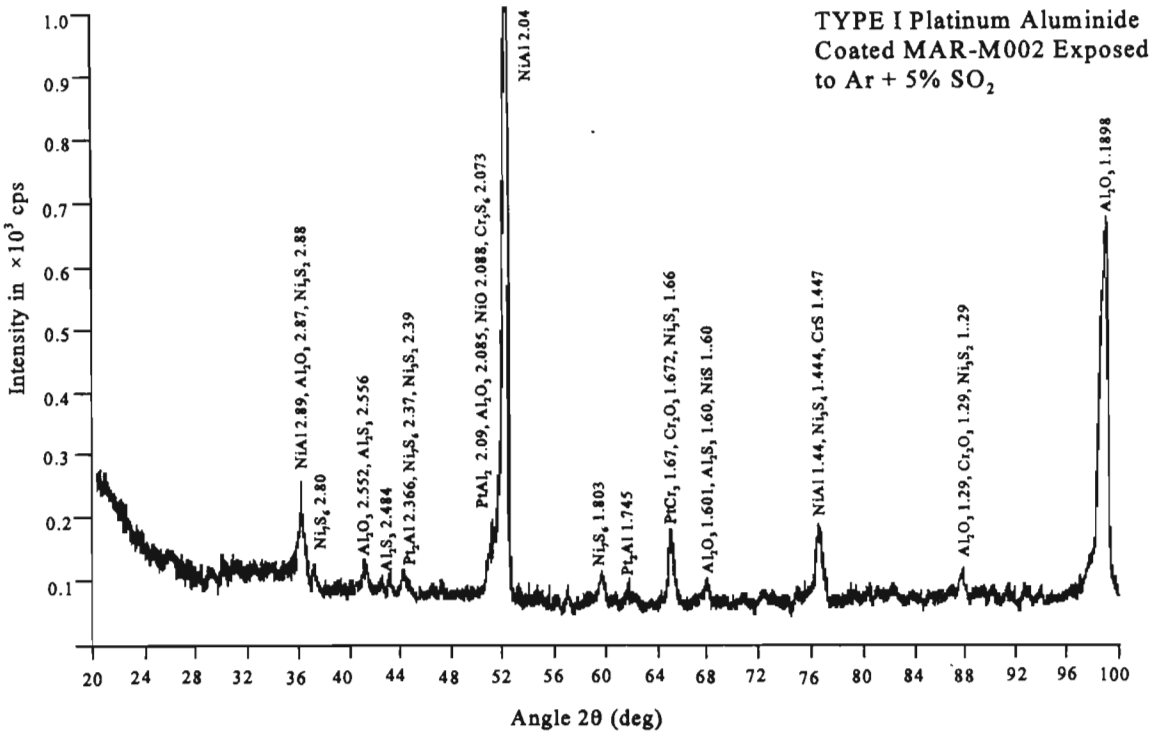

Figure 3.62 : X-ray diffraction of TYPE I platinum aluminide coated MAR-M002 after exposure to Ar + 5%SO_2 at 870°C for 5 hours

3.2.3.3 TYPE II Platinum Aluminide Coated MAR-M002

HTLCF tests performed on TYPE II platinum aluminide coated MAR-M002 in Ar + 5% SO_2 resulted in an accelerated failure. However, it did show a notable improvement over the uncoated sample tested under similar conditions. The number of cycles to failure was approximately 540 which was about one third that obtained for a similar sample tested in argon atmosphere. As in all the fatigue tests performed, the final failure occurred at a high tensile load.

The fracture surface showed extensive sulphidation attack (figure 3.63) and the coating displayed severe cracking (figure 3.63 & 64). Two types of cracks were observed: cracks perpendicular to the direction of loading and cracks at approximately 45° to the direction of loading. The morphology of the cracks indicated that the coating was forced outward by corrosion processes occurring beneath the outer layer of the coating. The coating had fractured around the lip of the cracks in certain areas, figure 3.64a, due to the presence of the brittle platinum aluminide outer layer.

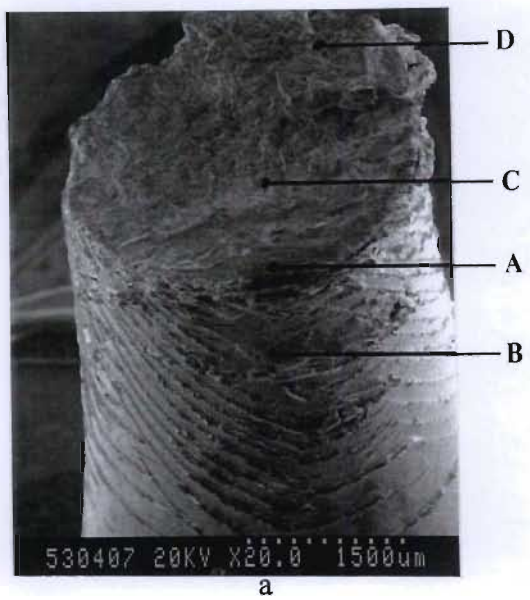

a

b

Elements	Weight percent			
	A	B	C	D
O	35.55	25.03	20.27	4.70
Al	26.13	26.46	1.95	3.19
S	4.21	0.66	5.09	8.62
Ti	0.15	0.04	0.92	2.41
Cr	10.22	2.91	27.19	7.67
Co	3.31	1.09	6.11	8.12
Ni	19.11	19.77	27.94	49.12
Zr	0.00	0.00	0.00	0.00
Hf	0.73	0.15	1.74	1.34
Ta	0.58	0.44	2.17	7.79
W	0.00	0.00	6.62	7.03
Pt	0.00	23.46	0.00	0.00

Figure 3.63 : Fractography of TYPE II platinum aluminide coated MAR-M002 after HTLCF in Ar + 5%SO_2 environment (S.R. 0.66%)

a) Fracture surface

b) Profile of fracture surface showing cracking of the coating.

Chemical analysis of the fracture surface (figure 3.63) indicated that the corrosion product was composed of essentially Ni and Cr oxides and sulphides. The corrosion scales in the lip of the crack (figure 3.63 pt A) was made up mainly of Cr, Al, Ni, oxygen and S. The region between the cracks (figure 3.63 pt B) showed very little evidence of sulphidation attack with the chemical composition indicating a high Al, Ni, Pt and oxygen content.

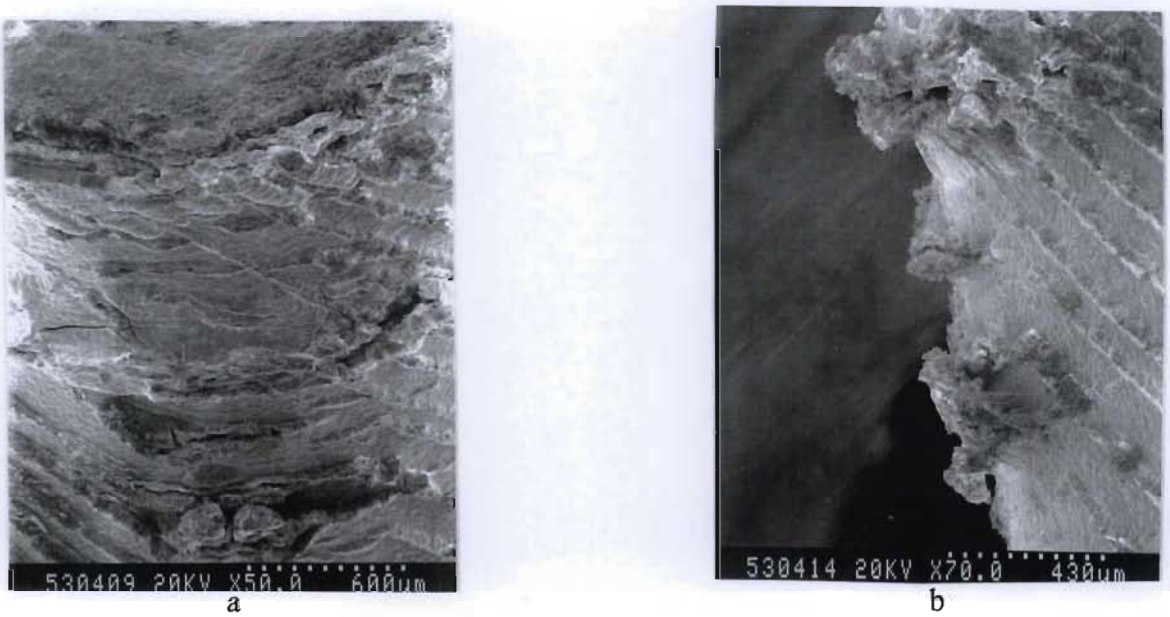

a b

Figure 3.64 : Cracking of TYPE II platinum aluminide coating close to the fracture surface due to HTLCF IN Ar + 5%SO_2 (S.R. 0.66%)

From the cross-sectional examination of the fatigue sample after HTLCF in a SO_2 bearing atmosphere, figure 3.65, it was evident that although the outer Pt rich layer was fairly resistant to sulphidation attack, however, it was very brittle and prone to cracking under mechanical loading. The NiAl and interdiffusion zones below the outer layer showed a lower resistance to sulphidation attack resulting in a "bell" shaped crack. The morphology of the cracks observed on the outer surface was revealed more graphically displayed in figure 3.65b. The sulphidation attack was concentrated below the Pt aluminide outer layer. This resulted in corrosion product build-up and internal sulphidation in this region. Eventually, the "pressure" of the corrosion product build-up caused the coating to be forced outwards. The substrate below the coating had also sustained extensive sulphidation attack. The morphology of the crack in the substrate indicated that there was a very broad corrosion "front" below the coating. This was due to the substrate being more resistant to crack initiation.

From figure 3.65 it can be seen that the NiAl rich zone and interdiffusion zone was more resistant to crack propagation. In these regions the cracks were branched and followed a more "jagged" path.

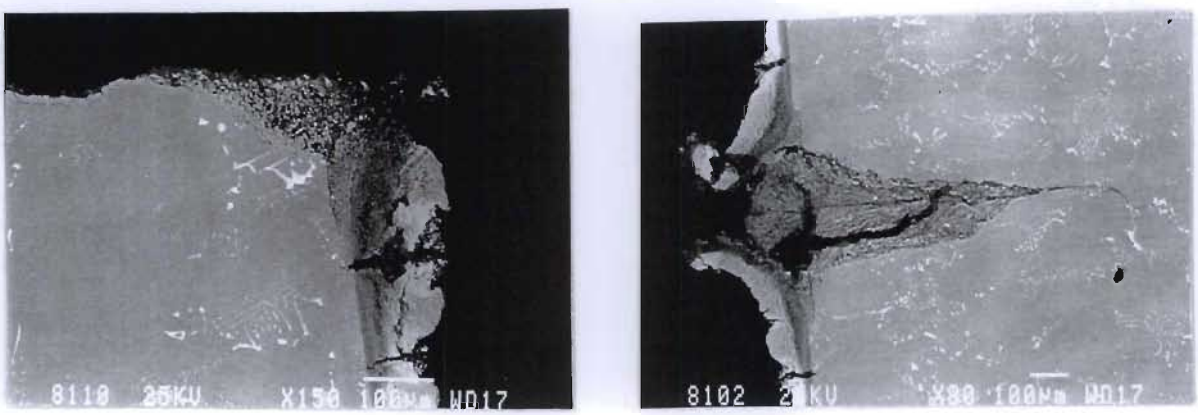

a b

Figure 3.65 : Cross-sectional analysis of TYPE II platinum aluminide coated MAR-M002 after HTLCF in SO_2 Containing environment (S.R. 0.66%)

Figure 3.66 shows the chemical analysis of a crack that had progressed into the substrate. The corrosion product close to the Pt rich outer layer of the coating was composed of mainly Al, Ni and oxygen with a small amount of sulphur. The scale was composed of essentially aluminium oxides. The regions adjacent to the crack were depleted of Al due to the corrosion process. The black region at the coating/corrosion product interface (figure 3.66 pt.Cblack) was made up of essentially Ni, Cr, and S with smaller amounts of Al, Co, Hf and W. This indicated that the sulphides of mainly Ni and Cr were present. The white regions in the crack in the substrate (figure 3.66 pt.E) were particles of the substrate which were depleted of the reactive elements Al and Cr. The black regions (Figure 3.66 pt.E) were corrosion product made up of essentially Cr, Ni, oxygen and S. Analysis of the crack edge in the substrate, showed these regions to be severely depleted of Cr (figure 3.66 pt.F). The corrosion product at the propagating crack tip was made up of essentially Ni, Cr and S (figure 3.66 pt.G).

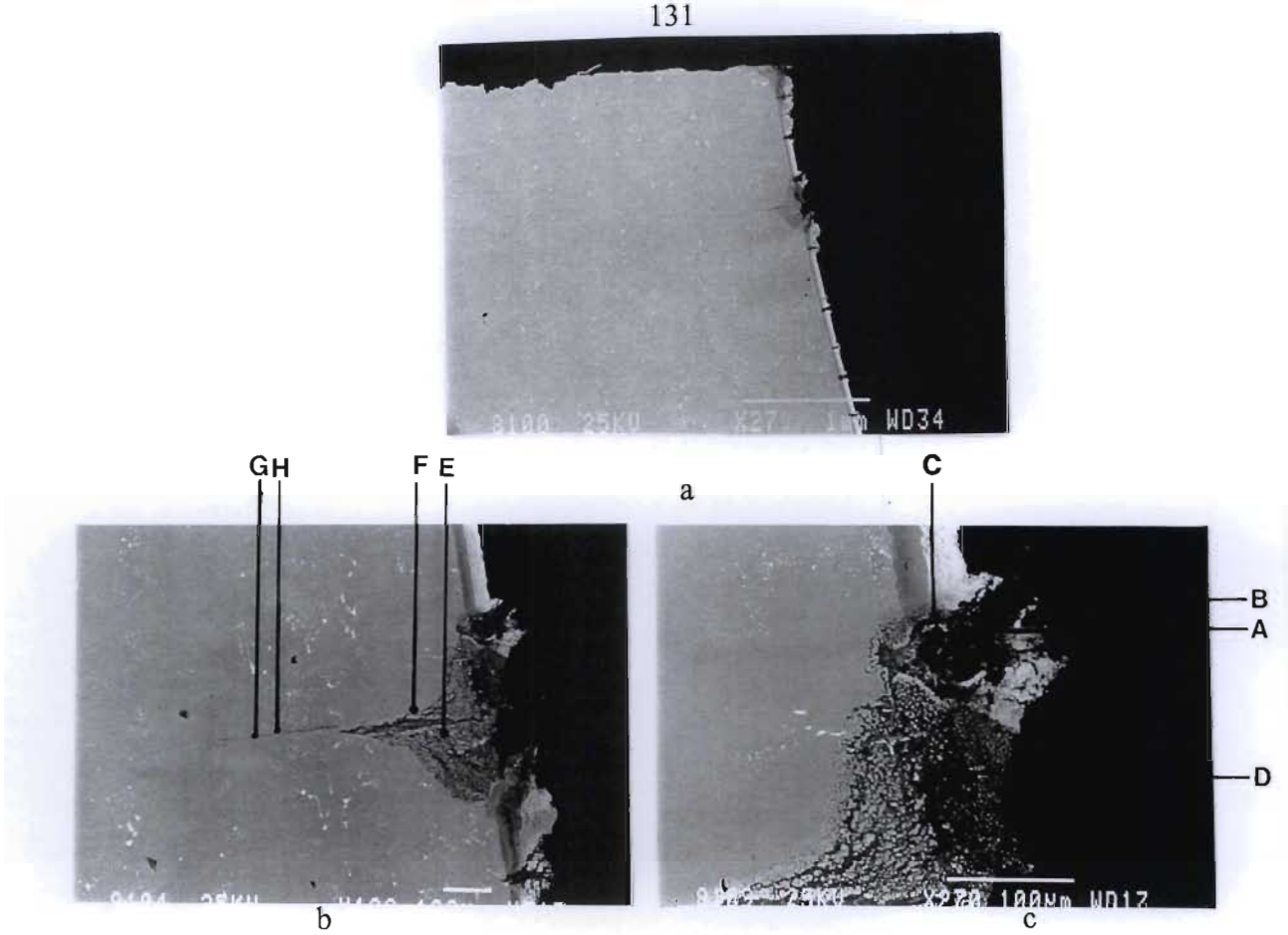

Elements	Weight percent									
	A	B	C white	C black	D	E white	E black	F	G	H
Al	37.19	7.39	6.64	6.70	8.48	3.87	1.55	2.69	5.15	6.65
Cr	1.42	0.45	3.94	12.50	3.34	3.99	36.07	0.39	13.00	7.48
Co	2.44	1.33	7.77	6.94	5.38	10.95	2.00	12.31	6.91	9.42
Ni	13.81	29.56	55.22	36.28	35.04	62.49	17.71	65.05	43.35	58.58
Ti	0.38	0.00	0.36	0.56	0.31	0.71	0.97	0.06	1.16	1.33
Zr	1.56	0.10	0.00	0.14	0.00	0.00	0.00	0.11	0.00	0.00
Hf	0.21	0.81	0.71	2.87	0.78	0.00	0.68	0.32	1.98	0.77
Ta	0.00	1.56	1.95	1.14	3.17	1.15	0.79	1.43	2.07	1.97
W	0.00	0.00	13.59	5.97	6.43	16.85	0.41	17.64	6.41	10.37
Pt	0.00	57.34	2.17	1.09	0.61	0.00	0.00	0.00	0.18	0.00
O	39.05	0.00	0.00	0.00	30.30	0.00	32.24	0.00	0.00	0.00
S	3.97	1.47	7.65	25.81	6.15	0.00	7.59	0.00	19.77	3.44

Figure 3.66 : Cross-section of TYPE II platinum aluminide coated MAR-M002 showing a fatigue crack that had propagated into the substrate after HTLCF in Ar + 5%SO_2 (S.R 0.66%)

X-ray diffraction of a TYPE II platinum aluminide coated sample exposed to Ar + 5%SO_2 at 870°C for 5 hours, is shown in figure 3.67. Typical phases that will be found in the corrosion scale on the coating are Al_2O_3, Ni_3S_2, Cr_2O_3 and Ni_7S_6.

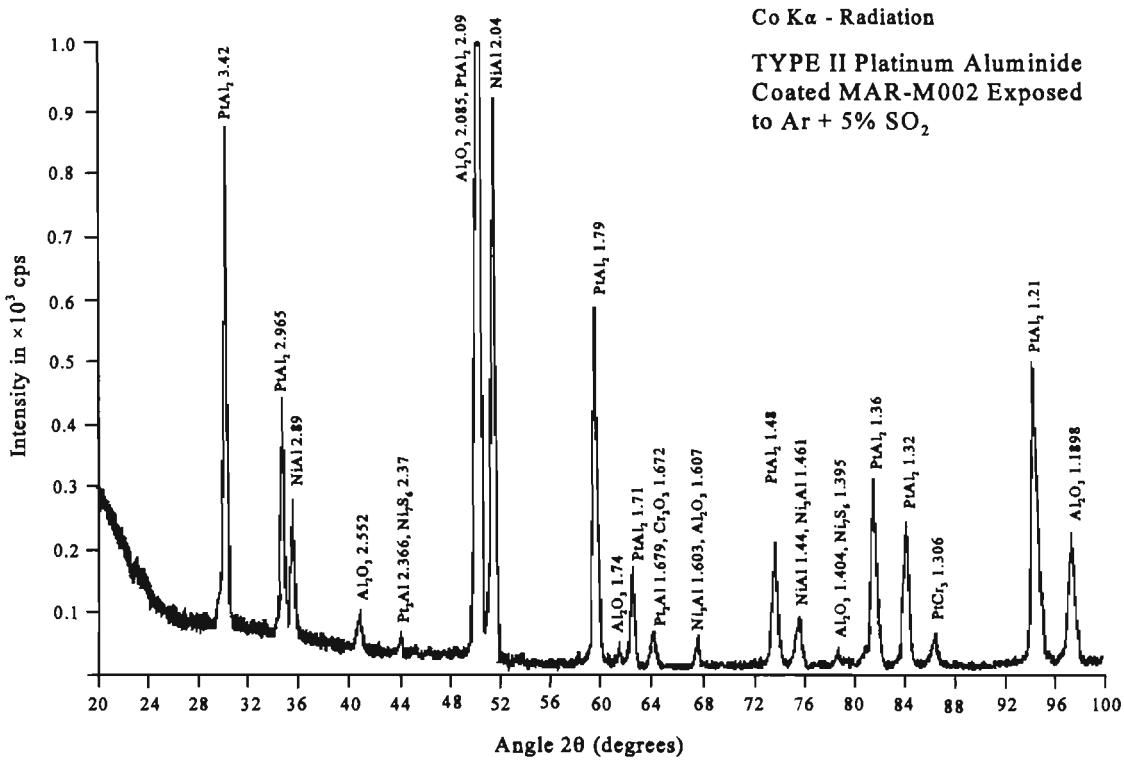

Figure 3.67 : X-ray diffraction analysis of TYPE II platinum aluminide coated MAR-M002 after exposure to Ar + 5% SO_2 at 870°C for 5 hours

3.2.3.5 2μm Platinum Aluminide Coated MAR-M002

HTLCF of 2μm platinum aluminide coated MAR-M002 in Ar + 5%SO_2 at a strain range of 0.66% produced a life of 606 cycles. Fractography analysis (figure 3.68) revealed evidence of sulphidation attack of the fracture surface and severe cracking of the coating close to the fracture surface. The cracking of the coating was primarily circumferential and perpendicular to the direction of loading. The morphology of the cracks (figure 3.69) were similar to that observed in the TYPE II platinum aluminide coated sample. Figure 3.69 showed evidence that the coating was forced outward. The indicated region in figure 3.68 shows "swelling" of the coating due to subsurface sulphidation attack. The brittle platinum rich outer layer cracked due to the swelling of the coating (figure 3.69) and mechanical loading.

a b

Elements	Weight percent				
	A	B	C	D	E
O	14.93	22.95	15.03	24.02	30.23
Al	5.10	0.12	4.41	17.99	16.04
S	4.67	3.88	3.14	10.76	1.44
Ti	2.22	0.06	1.64	0.21	1.56
Cr	10.31	26.51	6.09	3.08	7.30
Co	6.06	16.93	7.91	2.81	7.27
Ni	42.23	25.08	45.56	30.53	24.52
Zr	0.00	0.24	0.05	0.00	0.29
Hf	3.99	1.03	1.63	0.50	1.91
Ta	4.50	0.00	3.19	0.00	3.47
W	5.99	3.19	11.33	0.00	3.04
Pt	0.00	0.00	0.00	10.12	2.94

Figure 3.68 : Fracture surface of 2μm platinum aluminide coated alloy after HTLCF in AR + 5% SO_2 (S.R. 0.66%)

Chemical analysis of the fracture surface showed a high Cr, Ni, and oxygen content with a relatively small but significant amounts of sulphur present. The corrosion product on the crack on the external surface was composed of essentially Ni, Al, oxygen and sulphur. The region between the cracks showed a significantly lower sulphur content than the corrosion product on the crack edge.

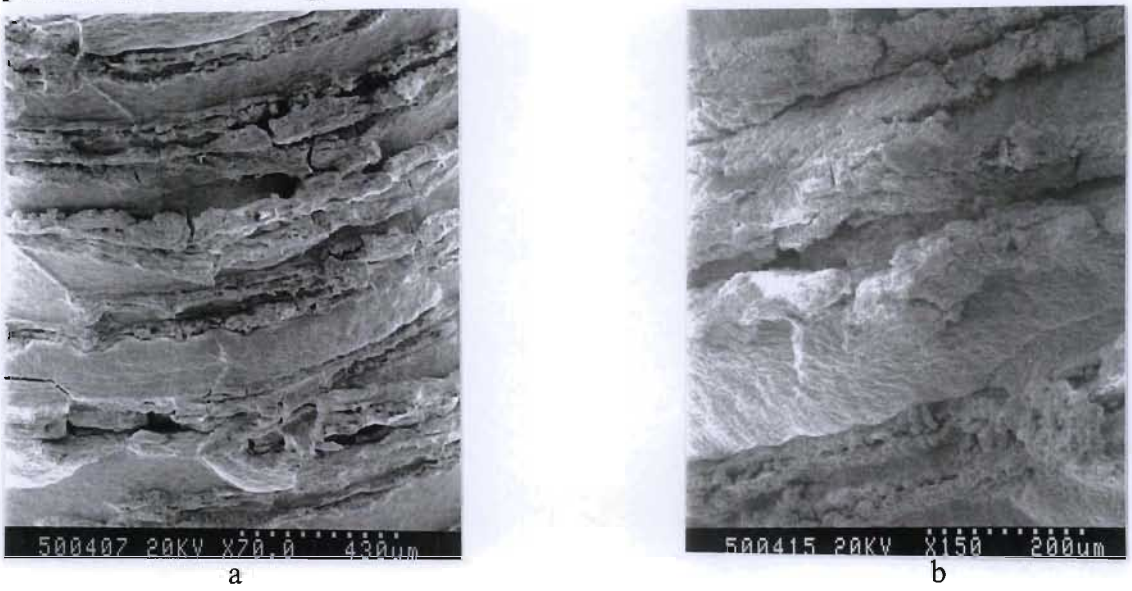

a b

Figure 3.69 : Cracking of the 2µm platinum aluminide coated MAR-M002 close to the fracture surface after HTLCF in SO_2 containing environment (S.R. 0.66%)

Cross-sectional analysis of the fatigue sample showed several cracks in the coating (figure 3.70). The morphology of the cracks were very similar to that observed in the TYPE II platinum aluminide coated sample. The structural difference in the coatings was that in the 2µm platinum aluminide coating the platinum rich outer layer was thinner than the TYPE II platinum aluminide coating. The nickel aluminide intermediate layer in the coating was found to be more susceptible to sulphidation attack. Once the platinum rich layer was breached the sulphidation attack proceeded at a much higher rate "laterally" along the NiAl layer rather than inwards towards the substrate. Figure 3.70a shows swelling of the coating due to the internal sulphidation attack. This process resulted "blistering" of the coating. The single phase NiAl layer was again shown to be more resistant to crack propagation with the cracks in the coating tending to branch in this region (figure 3.70). Since the corrosion proceeded "laterally" in the NiAl zone in the coating, the "corrosion front" encountered by the substrate was much broader with it eventually being concentrated at the crack tip.

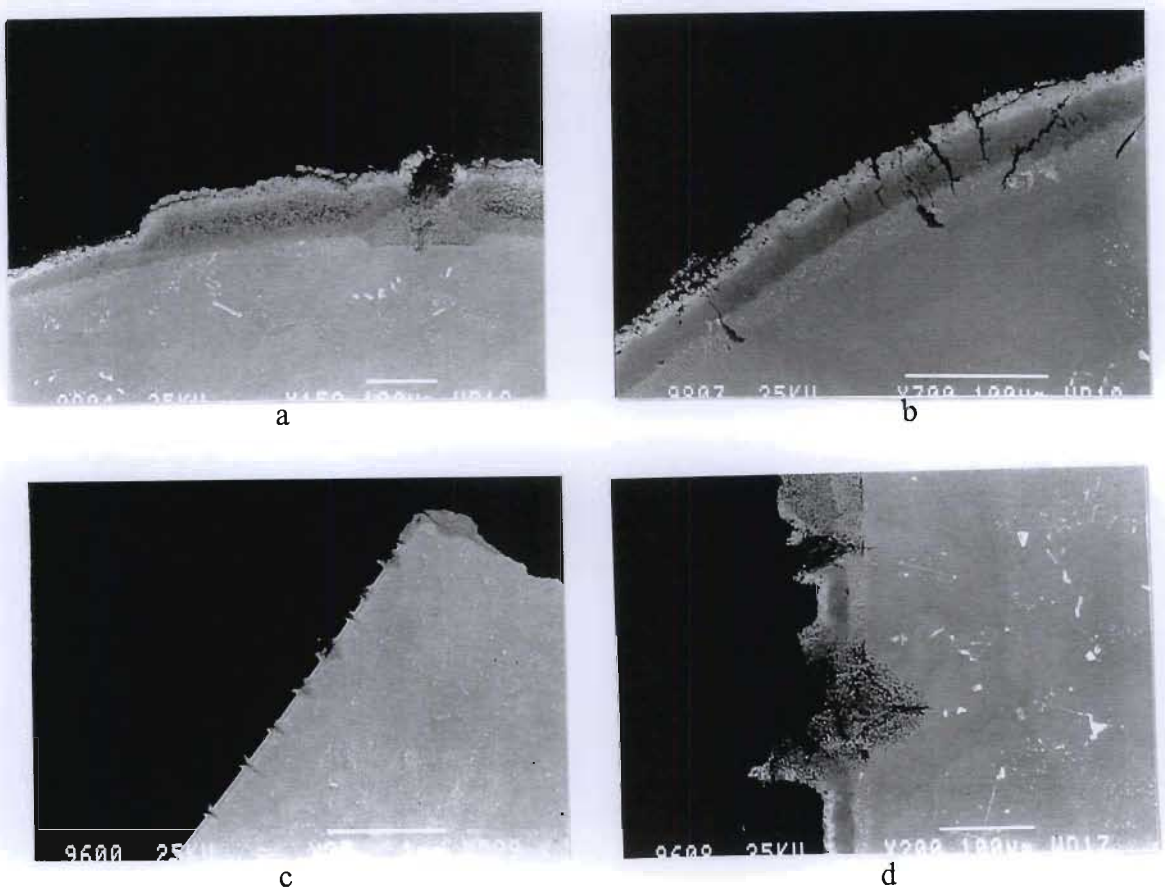

Figure 3.70 : Cross-sectional analysis of 2μm platinum aluminide coated MAR-M002 after HTLCF in SO_2 Containing environment (S.R. 0.66%)
a&b) Transverse cross-section
c&d) Longitudinal cross-section

Chemical analysis of the cross-section of a crack in the coating (figure 3.71) revealed that the corrosion product was composed of mainly aluminium, chromium and oxygen with smaller amounts of sulphur and elements of the base alloy. The sulphur content was significantly higher in the "porous" region with oxygen being virtually non-existent (figure 3.71 pt.E). The region of the coating adjacent to the crack was depleted of aluminum when compared with the bulk coating analysis. Analysis of the corrosion product in the interdiffusion zone (figure 3.71 pt.H) indicated a high nickel and oxygen content with a significant amount of sulphur present. From the quantitative analysis it can be seen that the corrosion product in this region was essentially nickel oxides and sulphides, with sulphides

Elements	Weight percent										
	A	B	C	D	E	F	G	H	I	J	K
Al	34.74	0.58	41.36	4.02	17.00	11.89	23.69	0.31	7.81	13.49	9.00
Cr	4.17	54.58	1.58	0.41	9.70	0.75	2.54	0.79	2.46	7.84	12.47
Ni	14.08	11.15	7.66	21.58	32.77	75.53	52.59	46.04	62.65	43.93	14.98
Pt	0.23	0.00	0.40	66.81	6.94	4.34	7.62	1.09	1.36	1.78	0.33
Co	3.34	2.61	2.11	2.25	3.97	5.55	8.15	5.85	5.13	7.87	9.37
Ti	0.93	1.72	0.22	0.00	0.54	0.33	0.48	0.00	0.91	2.52	1.29
Zr	0.00	0.00	0.33	0.00	0.00	0.00	0.00	0.47	0.00	0.23	0.52
Hf	0.61	0.57	0.39	0.00	1.78	0.47	0.00	0.00	1.54	4.44	0.07
Ta	1.05	0.18	0.20	1.41	0.97	0.00	3.31	0.00	3.40	5.95	2.36
W	0.71	0.00	0.00	3.52	1.78	0.00	1.61	0.40	10.50	11.97	16.56
O	39.36	25.04	43.24	0.00	0.00	0.00	0.00	20.50	0.00	0.00	28.11
S	0.78	3.57	2.51	0.00	24.55	1.14	0.00	24.54	4.24	0.00	4.96

Figure 3.71 : EDS analysis of a crack in the coating of 2μm platinum aluminide coated MAR-M002 after HTLCF in Ar + 5% SO_2 environment (S.R. 0.66%)

making up the major constituent. A significant feature was that the sulphide phases were found to be concentrated more towards the corrosion scale/substrate interface. This was evidence that the oxides were formed first with sulphur diffusing through the corrosion scale to the substrate.

X-ray diffraction analysis of the of a 2μm platinum aluminide coated MAR-M002 disc sample exposed to Ar + 5%SO_2 at 870°C for 5 hours is shown in figure 3.72. The corrosion product was composed of Al_2O_3 and Cr_2O_3 oxides and in smaller quantities Ni_3S_2, CrS, NiS, Al_2S_3, Cr_3S_4, and Ni_7S_6. From this analysis it was evident that the coating had a higher tendency to form oxides rather than sulphides on the external surface.

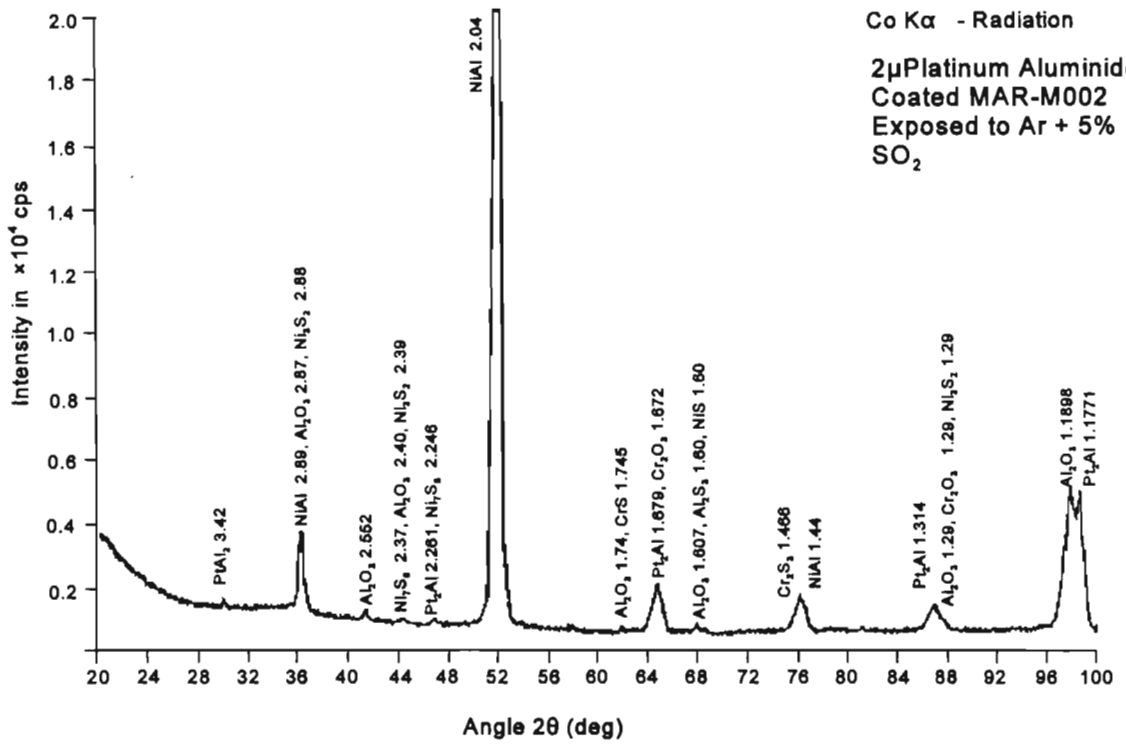

Figure 3.72 : X-ray diffraction analysis of a 2μm platinum aluminide disc sample after exposure to Ar + 5% SO_2 at 870°C for 5 hours

3.2.3.6 Platinum Coated MAR-M002

The platinum coated MAR-M002 fatigue sample failed after 271 cycles under the combined effect of HTLCF and SO_2 containing environment. The presence of the platinum coating did not influence the corrosion-fatigue life significantly compared to the uncoated alloy. The fracture surface (figure 3.73) showed evidence of sulphidation attack. High magnification of the fracture edge displayed evidence of delamination of the coating (figure 3.73b) due to the combined effect of fatigue loading and sulphidation attack. Chemical analysis of the corrosion product on the fracture surface showed that it was made of mainly Cr, Ni, sulphur and oxygen. AES analysis of the fracture surface (figure 3.74) confirmed the presence of oxygen in the corrosion product, and showed that it was made up of mainly Cr, Ni, Al, S and oxygen.

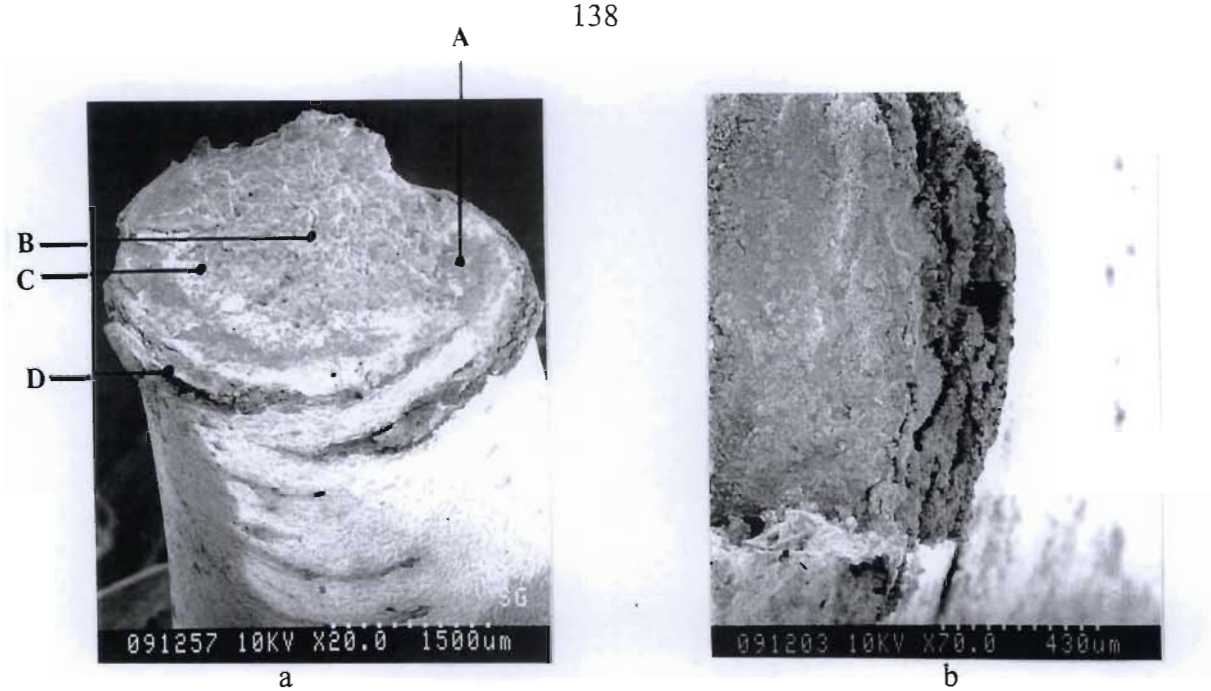

a b

Elements	Weight percent			
	A	B	C	D
O	18.05	21.45	22.53	18.93
S	10.84	2.51	7.84	3.94
Ti	2.20	2.09	2.40	0.95
Cr	17.85	7.65	25.67	15.51
Co	3.57	5.69	3.84	6.83
Ni	36.94	36.11	28.99	38.05
Al	1.05	2.83	0.44	3.63
Zr	3.30	2.27	0.47	1.36
Fe	0.12	0.38	0.03	0.40
W	3.03	7.79	1.05	3.69
Ta	2.24	5.51	2.11	2.33
Hf	0.82	3.27	0.26	1.56
Pt	0.00	0.00	0.00	2.80

Figure 3.73 : a) Fracture surface of platinum coated MAR-M002 after HTLCF in SO_2 bearing atmosphere (S.R. 0.66%)

b) High magnification showing delamination of coating.

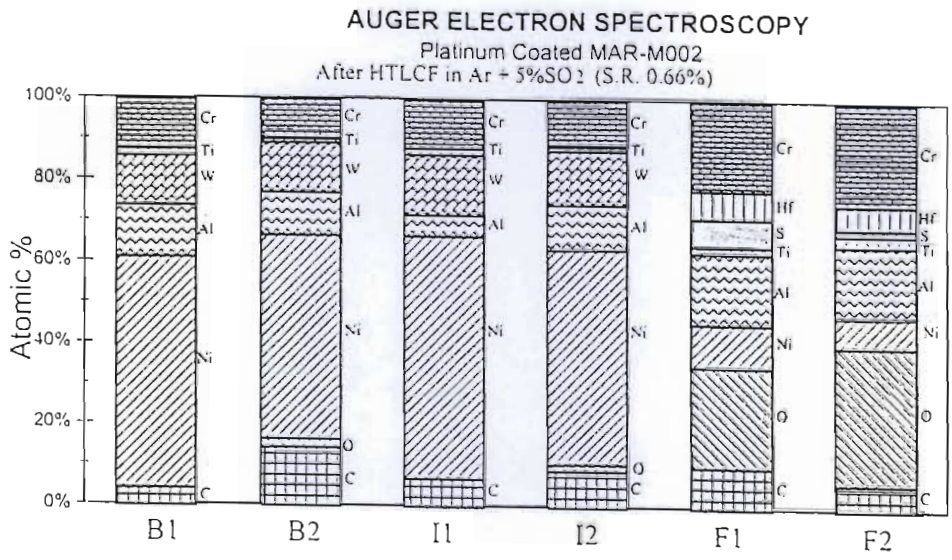

Figure 3.74 : AES analysis of the fracture surface of platinum coated MAR-M002 after HTLCF in Ar + 5%SO_2 (S.R. 0.66%)

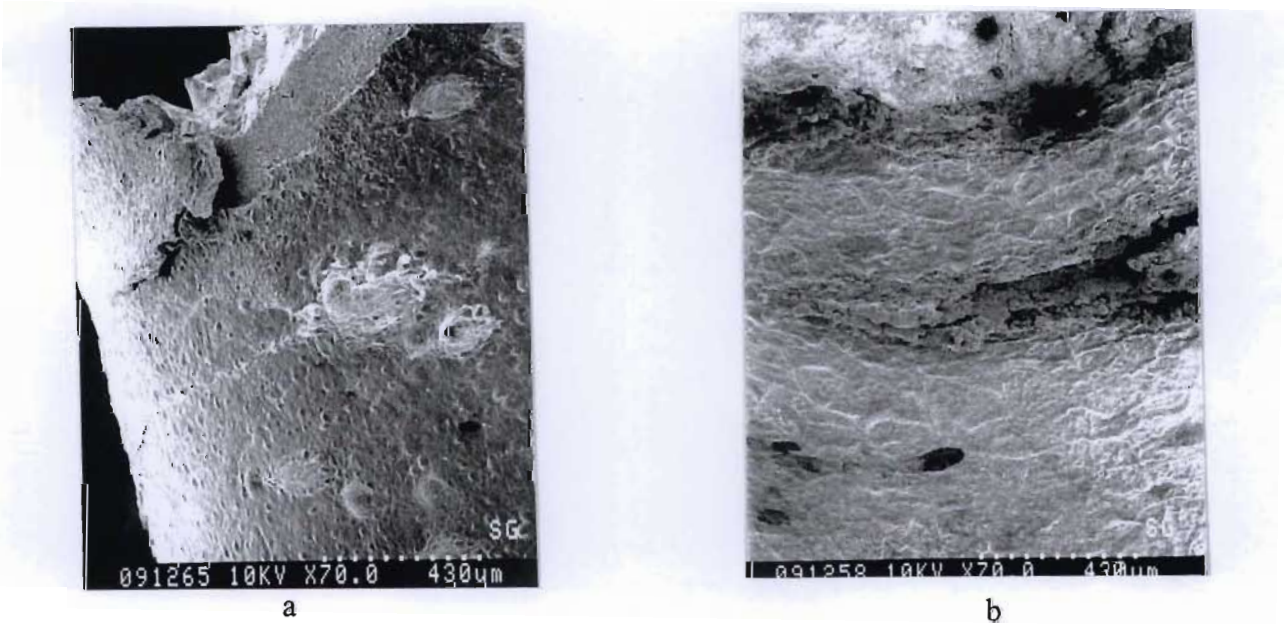

Figure 3.75 : Fractography of platinum coated MAR-M002 after HTLCF in SO_2 containing environment (S.R. 0.66%)

From the nature of the fracture surface it was evident that there was two major cracks propagating simultaneously which resulted in the final failure of the of the fatigue sample. The external surface close to the fracture revealed that the coating layer had "peeled" off in the region of the fracture (figure 3.75). No severe cracking of the coating was observed, however, there was evidence of "blistering" of the coating (figure 3.75a) due to the combined effect of sulphidation attack and mechanical loading. Figure 3.75b showed a "creased" effect on the coating on one half of the sample. The "bubble" like protrusions on the coating was evident as in the samples tested in argon and air atmospheres, indicating that this was a property of the coating and not due to the environment.

Cross-sectional analysis (figure 3.76) revealed little evidence of cracking of the coating. A significant feature observed, as in the previous platinum coated samples tested, was that the coating thickness had grown from approximately 17μm to approximately 50μm, due to the high temperature exposure of the sample. This demonstrated the high diffusivity of platinum. The longitudinal cross-section of the fracture surface showed that the coating had "peeled" away from the substrate at the coating-fracture interface.

Figure 3.76 & 77 showed that the sulphidation attack was concentrated in the γ' depleted zone. The corrosion processes proceeded along this region resulting in the coating peeling off. This image compliments the evidence shown on the fractography analysis shown in figure 3.75. The corrosion product in the "pores" was made up of essentially Ni, Cr and sulphur with no evidence of oxygen. A significant feature was that the corrosion product had a similar composition to that found on the uncoated alloy. The corrosion product on the external surface was made up mainly of chromium, nickel, sulphur and oxygen (figure 3.77). From the quantitative analysis it was very evident that it was made up mainly of oxides. The white region (point B) was made up of mainly nickel and platinum and was depleted of aluminium and chromium.

In certain regions of the coating the external surface of the coating did show sulphidation attack (figure 3.78). This, in general, had occurred close to the fracture surface. The "grey" region of the coating showed a higher susceptibility to sulphidation attack. This process produced "porous" regions. The dark regions or "pores" were made up of essentially Cr, Ni and sulphur, while the white regions (solid) was essentially nickel and platinum.

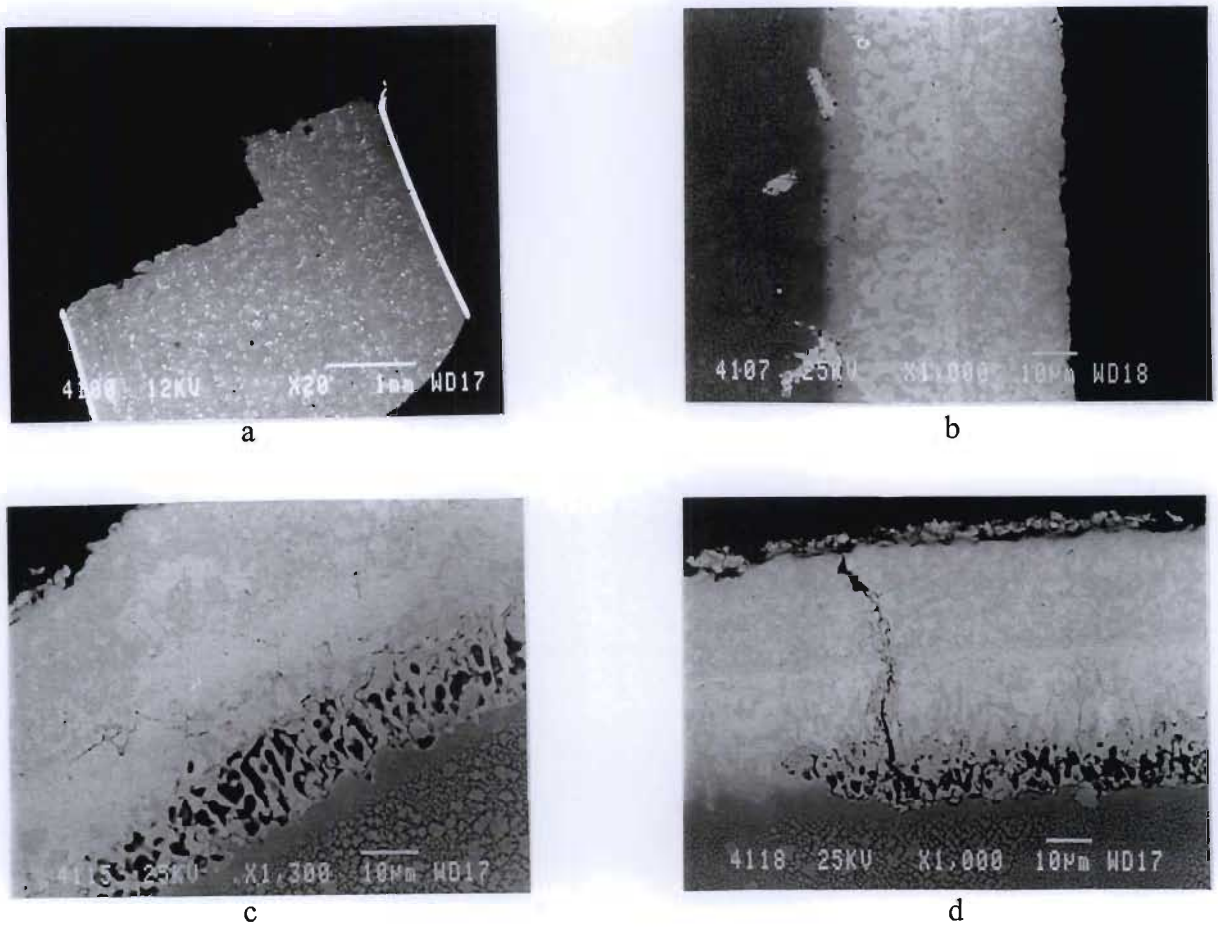

Figure 3.76 : Cross-sectional analysis of platinum coated MAR-M002 after HTLCF in SO_2 Containing environment (S.R. 0.66%)

a & b) Longitudinal cross-section

c & d) Transverse cross-section

X-ray diffraction analysis of platinum coated disc sample exposed to Ar + 5%SO_2 at 870°C for five hours is shown in figure 3.79. It can be seen that the coating was not very susceptible to sulphidation attack in the unstressed condition. From this analysis typical phases in the corrosion product on the coating was determined to be Cr_2O_3, Al_2O_3, $NiCr_2O_4$ Cr_2S_3, CrS_4, Ni_7S_6, TiS, Ni_3S_2 and CrS. The phases present in the substrate-coating interdiffusion zone will be more accurately determined using the corrosion test results obtained for the uncoated disc sample.

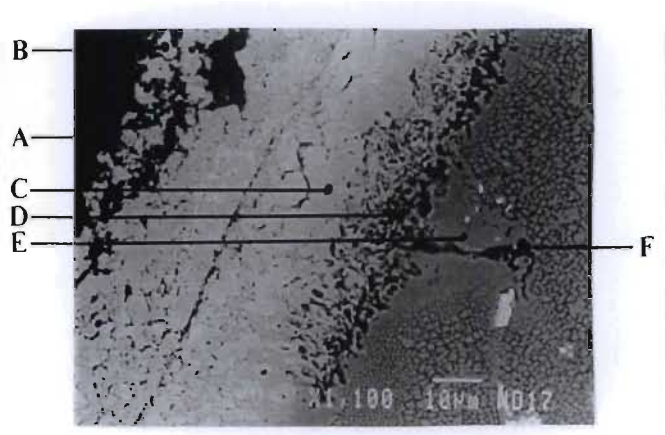

Elements	Weight percent					
	A	B	C	D	E	F
Ti	0.58	0.11	1.73	1.34	1.14	2.19
Cr	56.43	0.67	0.95	15.44	7.02	31.40
Co	3.43	7.50	2.23	5.89	10.50	4.40
Ni	3.53	33.62	27.22	33.32	63.81	17.36
Al	4.47	0.64	4.32	3.43	3.10	2.54
Zr	0.00	0.00	0.00	4.83	0.00	0.00
Hf	0.00	0.34	4.71	3.16	1.08	2.29
Ta	0.00	0.00	1.13	0.00	2.28	0.59
W	0.00	0.00	3.85	10.46	11.07	1.45
Pt	1.78	57.12	53.37	0.00	0.00	0.00
S	0.75	0.00	0.49	22.14	0.00	37.80
O	29.04	0.00	0.00	0.00	0.00	0.00

Figure 3.77 : Transverse cross-section of platinum coated MAR-M002 showing sulphidation attack of the external surface and internal sulphidation of the γ' depleted zone

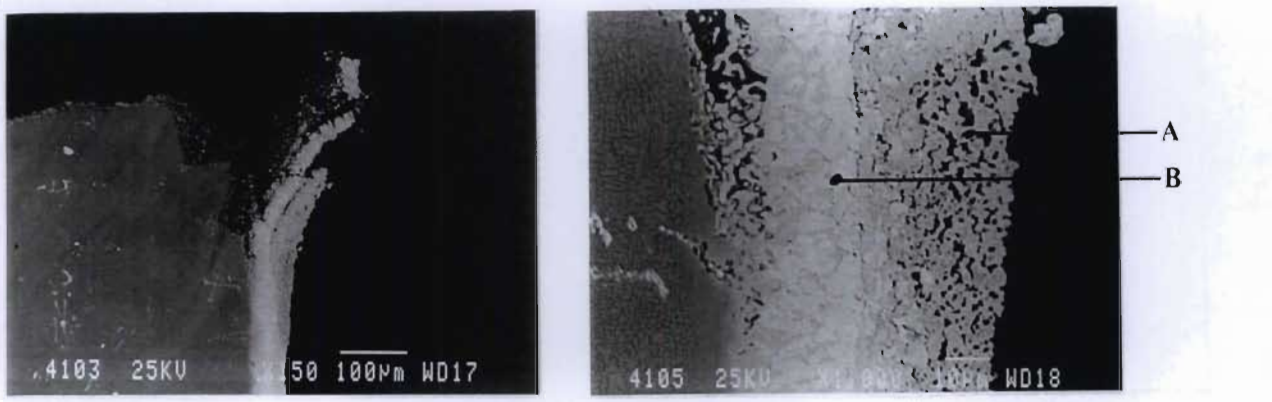

a b

Elements	Weight percent			
	A(solid)	A(pores)	Bw	Bg
Ti	0.83	1.47	1.12	0.17
Cr	4.89	27.42	1.81	5.86
Co	3.57	5.02	2.62	7.12
Ni	23.99	20.56	22.70	32.79
Zr	3.28	0.00	1.38	0.00
Hf	0.67	1.24	0.86	0.55
Al	3.16	0.00	3.69	1.83
Ta	0.00	0.06	2.75	0.25
W	1.37	0.00	4.94	8.28
Pt	57.33	10.78	58.12	42.11
S	0.91	33.46	0.00	1.03

Figure 3.78 : Internal sulphidation of the platinum coating due HTLCF in AR + 5%SO_2 (S.R. 0.66%)

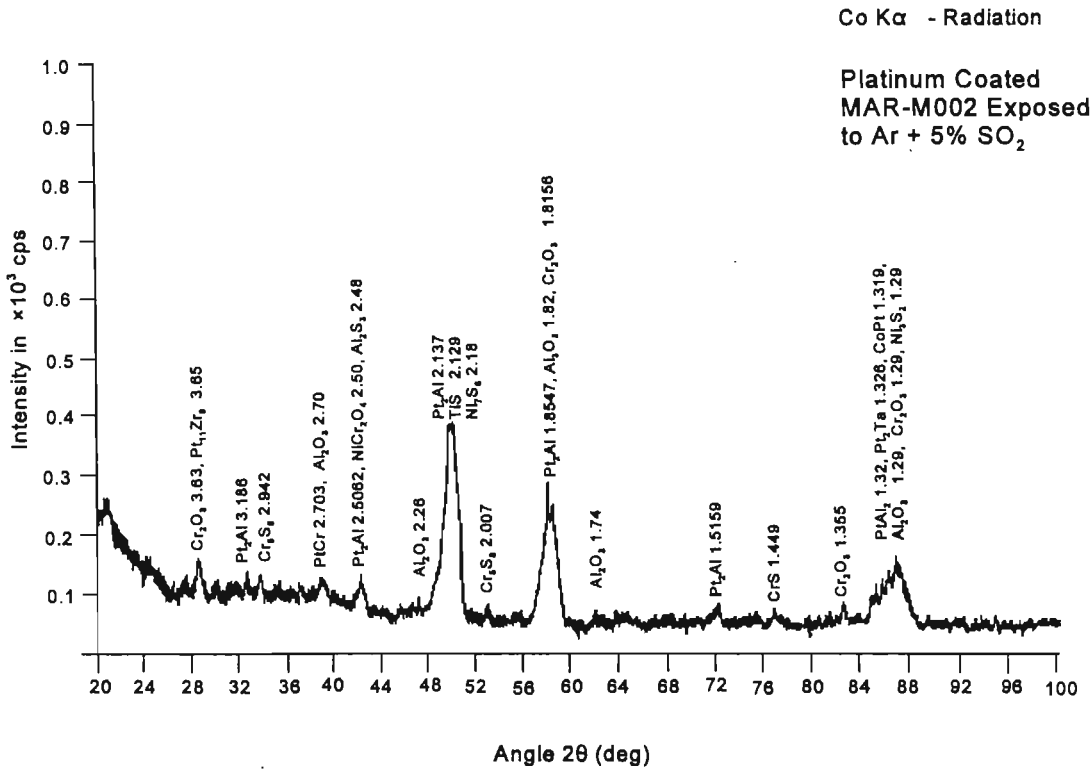

Figure 3.79 : X-ray diffraction analysis of platinum coated MAR-M002 after exposure to Ar + 5% SO_2 at 870°C for 5 hours

3.2.4 HTLCF in Ar + 5%SO_2 - Strain range of 0.38%

Due to the accelerated failures observed in the coated sample under the strain range of 0.66%, HTLCF in Ar + 5%SO_2 was performed on all the materials systems at a lower strain range of 0.38%. It was established that at the higher strain range that mechanical failure of the coatings played a key role in the final failure of the fatigue sample. At the lower strain range it was believed that the environment will play a more influential role in the failure mechanism. The tests were limited to the SO_2 bearing atmosphere due to the limited number of samples available.

3.2.4.1 Uncoated MAR-M002

HTLCF failure of uncoated MAR-M002 in Ar + 5%SO_2 at a strain range of 0.38% occurred after 9304 cycles. The lower strain range resulted in a 30 fold increase in the HTLCF life under sulphidation conditions when compared with similar tests performed at the higher strain range. Fractography analysis revealed severe sulphidation attack on the fracture surface and the external surface close to the fracture (figure 3.80). The fracture surface was covered with a "sponge" like corrosion product (figure 3.80b). The corrosion product on the external surface had cracked due to the combination of mechanical loading and sulphidation (figure 3.81a). The sulphidation attack below the corrosion scale forced the lips of the cracks outwards (figures 3.81b).

Chemical analysis of the corrosion product on the external surface close to the fracture (figure 3.80) indicated that it was composed of mainly aluminium and nickel oxides and sulphides. The corrosion product on the fracture surface was made up of mainly nickel and chromium oxides and sulphides. This was consistent with the tests performed at the higher strain range. Auger electron spectroscopy (figure 3.82), indicated that the corrosion product was made up of mainly Cr, S, Al, Ni and oxygen. The region just below the fracture surface (I_1 and I_2) showed no significant variation from the base metal. The AES analysis of the fracture surface complimented the EDS analysis and confirmed the presence of oxygen in significant quantities.

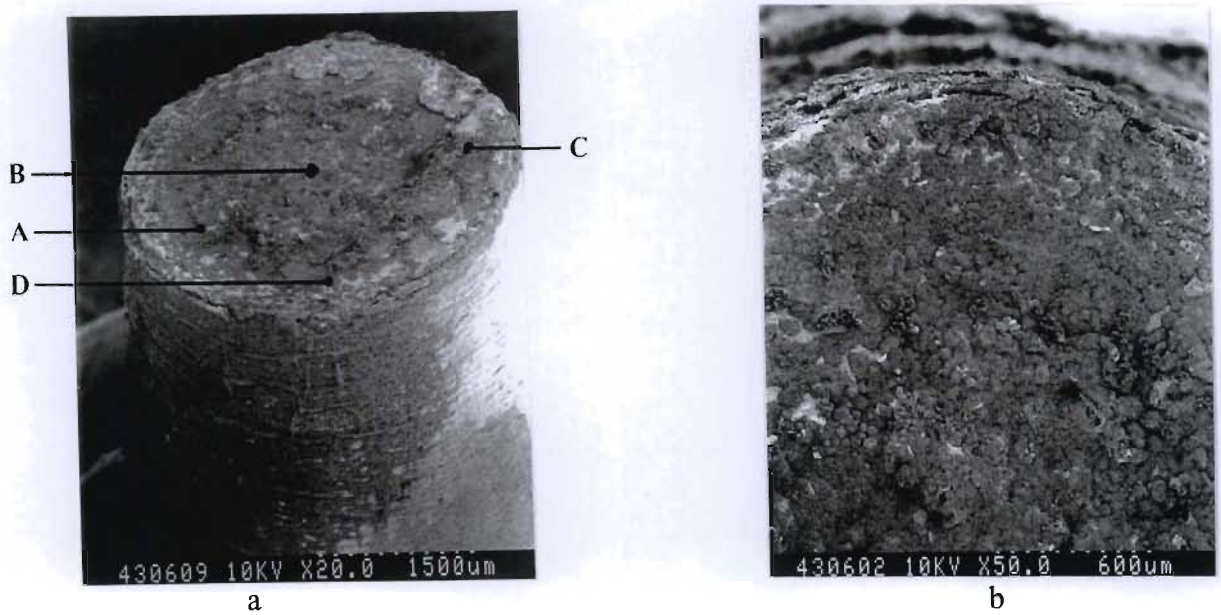

a b

Elements	Weight percent				
	A	B	C	D	External Surface
O	23.05	28.52	25.39	28.70	20.55
Al	2.26	1.12	1.92	0.44	36.90
Ni	32.35	25.85	31.44	23.99	33.57
Cr	21.20	25.92	15.55	28.75	2.12
Co	5.11	5.25	5.08	4.72	0.00
W	2.59	1.02	1.04	0.70	2.15
Ta	0.48	1.41	2.16	2.17	0.00
Hf	0.21	1.07	1.53	0.75	1.48
Ti	0.56	1.11	1.47	1.35	0.34
Zr	4.84	0.00	2.34	0.00	0.00
Fe	0.00	0.03	0.09	0.11	0.38
S	7.35	8.70	11.97	8.31	2.52

Figure 3.80 : Fracture surface of uncoated MAR-M002 after HTLCF in Ar + 5% SO_2 (S.R. 0.38%)

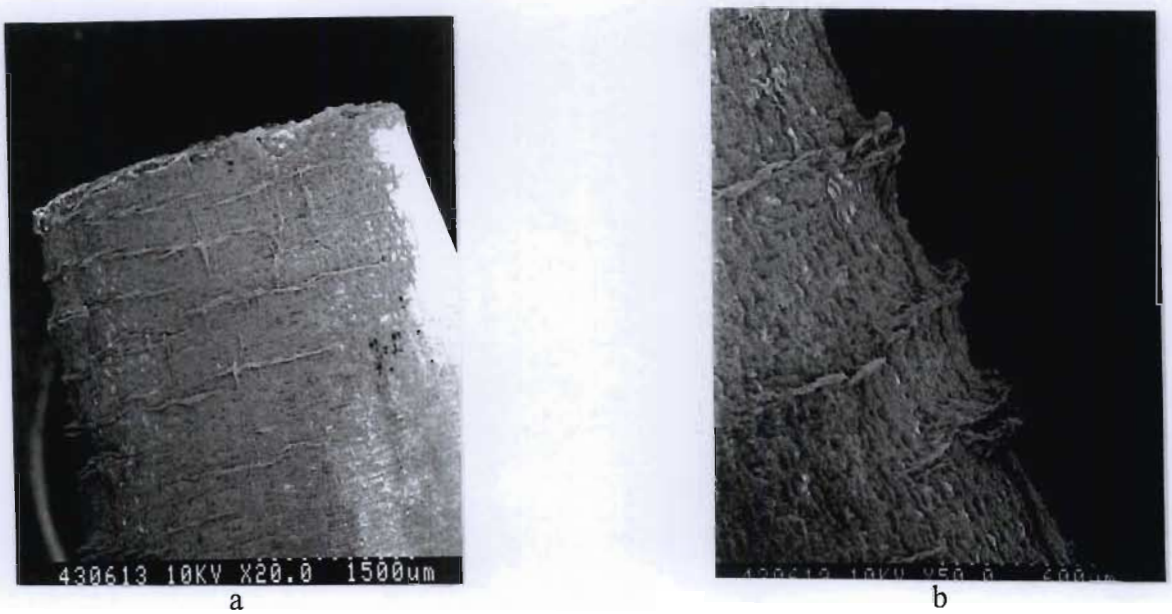

Figure 3.81 : Fractography of uncoated MAR-M002 after HTLCF in SO_2 containing environment showing corrosion on the external surface close to the fracture surface (S.R. 0.38%)

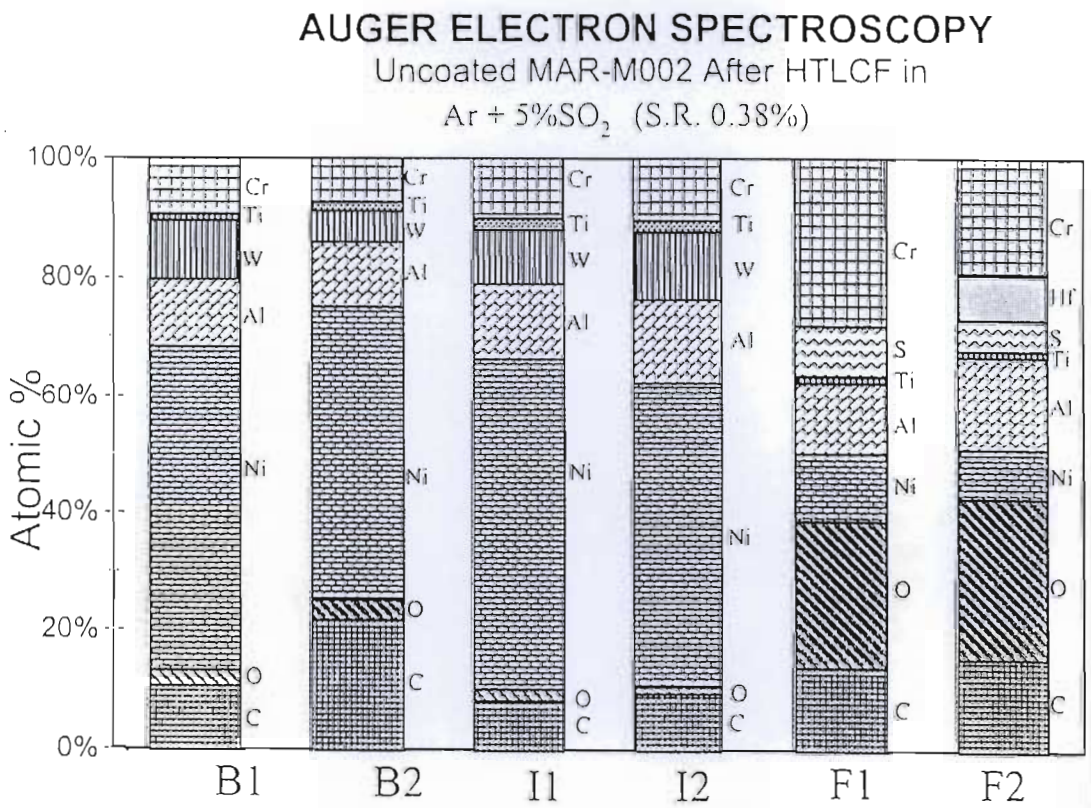

Figure 3.82 : AES analysis of the fracture surface after HTLCF of uncoated MAR-M002 in SO_2 containing environment (S.R. 0.38%)

Cross-sectional analysis of an uncoated fatigue sample after HTLCF in SO_2 bearing atmosphere at a strain range of 0.38% revealed severe sulphidation attack of the surface (figure 3.83 & 84). A significant feature, as observed in tests performed at the higher strain range, was that only one major crack had propagated to final failure. The corrosion product morphology on the surface was very similar to that observed in the tests performed at a strain range of 0.66%, indicating that the corrosion processes was not affected by the change in the mechanical loading. It is evident from figure 3.83 that the corrosion scale had "spalled" off in regions. The cracking of the corrosion scale (figure 3.83b) did not affect the corrosion process significantly.

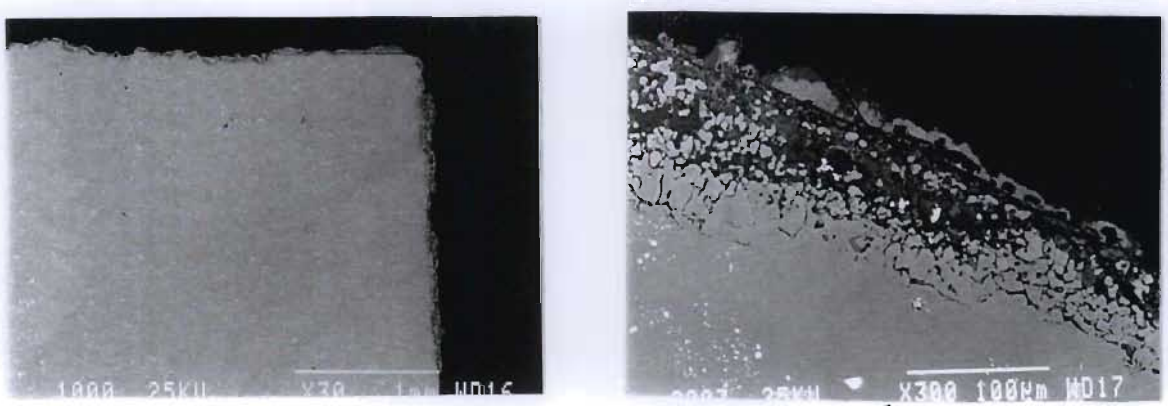

a b

Figure 3.83 : Cross-sectional analysis of uncoated MAR-M002 after HTLCF in SO_2 Containing environment (S.R. 0.38%)

The corrosion scale on the fracture surface (figure 3.84) was significantly thicker than that observed in the test performed at a strain range of 0.66%. However, the morphology of the scale was very similar. The corrosion scale was differentiated into three regions/zones according to their shading: (I) light grey region, (ii) dark grey region, and the (iii) black region. The chemical composition of these regions were discovered to vary significantly. The light grey region was composed mainly of Ta and oxygen with smaller amounts of Al, S, Cr, Ni, Ti, and Hf. The dark grey region was composed essentially of Cr, Ni, oxygen and sulphur. This region made up the major part of the corrosion product and formed the layer of the corrosion product that was exposed to the environment. The black region was made

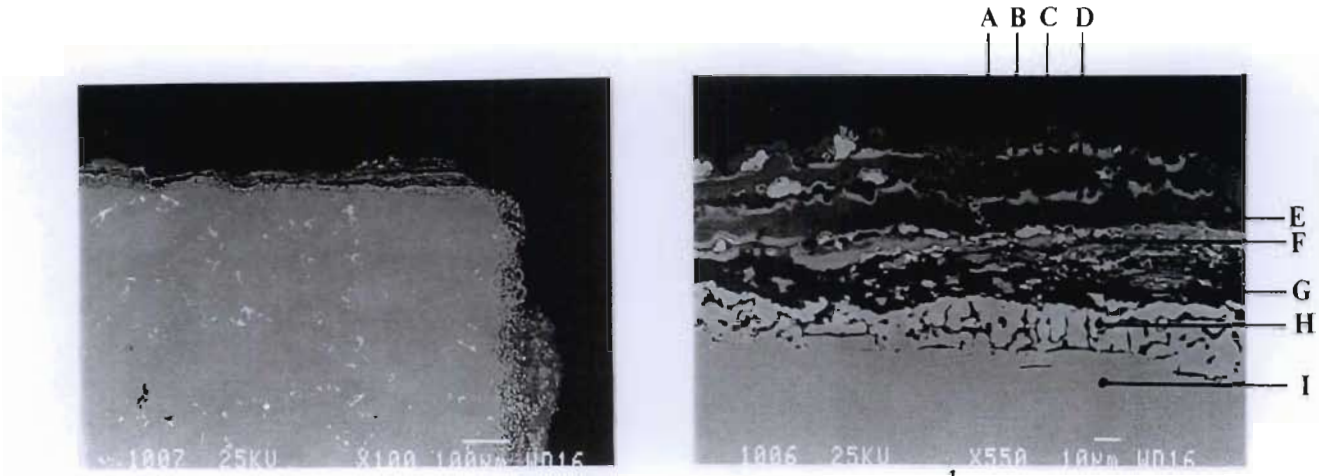

a b

Elements	Weight percent								
	A	B	C	D	E	F	G	H	I
Al	8.01	1.07	31.49	5.92	0.16	0.68	35.10	2.71	6.22
S	4.61	6.90	9.91	6.24	7.51	3.16	8.99	0.46	0.29
Cr	2.36	40.84	4.46	6.53	42.46	7.53	1.82	0.45	8.19
Co	1.43	2.38	4.37	1.70	2.58	1.19	2.46	12.62	8.98
Ni	10.81	15.64	18.01	14.34	16.73	10.64	21.99	69.99	60.97
Ta	29.06	1.01	0.00	29.47	0.57	41.73	1.30	0.00	1.81
Zr	0.00	0.39	0.17	0.20	0.29	0.00	0.28	0.11	0.18
Ti	10.08	1.68	0.77	12.03	1.55	18.96	0.28	0.17	1.20
W	0.00	0.32	0.00	0.00	0.46	0.00	0.00	13.49	10.91
O	23.89	28.94	29.63	20.75	27.68	16.10	27.77	0.00	0.00
Hf	4.75	0.84	1.20	2.81	0.00	0.00	0.00	0.00	1.24

Figure 3.84 : Corrosion product on the fracture surface after HTLCF of uncoated MAR-M002 in SO_2 bearing atmosphere (S.R 0.38%)

up of mainly Al, Ni, oxygen and sulphur. These regions were found in the middle of the corrosion scale and at the scale/substrate interface. The "porous" region below the corrosion scale shows clear evidence of internal sulphidation. The "pores" were filled with black corrosion product which was essentially composed of nickel sulphides (figure 3.84). The corrosion scale on the external surface close to the fracture was made up of a similar morphology to that found on the fracture surface.

3.2.4.2 Aluminide Coated MAR-M002

Aluminide coated MAR-M002 exposed to creep-fatigue loading and Ar + 5%SO_2 atmosphere at 870°C and creep-fatigue loading at a strain range of 0.38% failed after 6769 cycles. The fracture surface (figure 3.85) showed two distinct regions: a "smooth" region (where crack propagation occurred) and a "coarse" region (where final failure occurred). Sulphidation attack was manifested by the presence of dark sulphide phases on the fracture surface. The corrosion product on the "smooth" region was complex with significant amounts of a number of the alloying elements of the substrate, plus oxygen and sulphur. It was evident from that the main constituents were Ni, Cr and oxygen with a smaller but significant amount of sulphur being present. The coarse region showed only minor sulphidation attack and this was confirmed by the lower oxygen and sulphur content detected. AES of the fracture surface, region just below the fracture surface and bulk alloy (figure 3.86) showed that the corrosion product was composed of significant amounts of oxygen, Cr, S Ti, Al, Hf and Ni.

High magnification of the region close to the edge of the fracture surface (figure 3.85b) revealed delamination of the coating and the presence of "spongy" corrosion product. The external region close to the fracture showed severe deterioration of the coating. Swelling (figure 3.87a) and blistering of the coating (figure 3.87b) was observed. There was also evidence of localised sulphidation attack of the coating. The cracking of the coating was not as severe as that observed in the tests performed at the higher strain range. However, cracking of the coating in the region adjacent to the fracture surface was observed due to this region experiencing the highest stresses.

Cross-sectional analysis of an aluminide coated sample after HTLCF in AR + 5%SO_2 at a strain range of 0.38% showed severe damage to the coating (figure 3.88a). The coating immediately adjacent to the fracture surface was completely destroyed. The "blistering" of the coating was vividly displayed and the sulphidation of the coating was very evident. Internal sulphidation of the NiAl layer resulted in a "sponge" like effect with the "pores" being filled with corrosion product. This process plus the susceptibility of the interdiffusion zone to sulphidation resulted in the blistering of the coating.

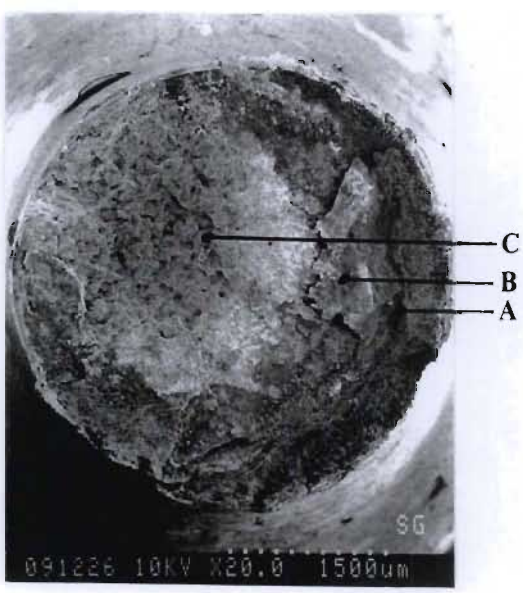

a

b

Elements	Weight percent		
	A	B	C
O	23.53	21.05	14.66
Al	3.21	3.32	2.98
Ni	37.40	41.51	46.52
Cr	8.98	8.30	7.13
Co	6.16	7.29	7.38
W	6.96	8.86	8.96
Ta	3.13	2.16	3.93
Hf	1.98	1.04	3.75
Ti	1.70	1.71	1.60
Zr	1.38	0.00	1.72
Fe	0.03	0.00	0.14
S	5.50	4.76	1.25

Figure 3.85 : Fracture surface of aluminide coated MAR-M002 after HTLCF in Ar + 5% SO_2 (S.R. 0.38%)

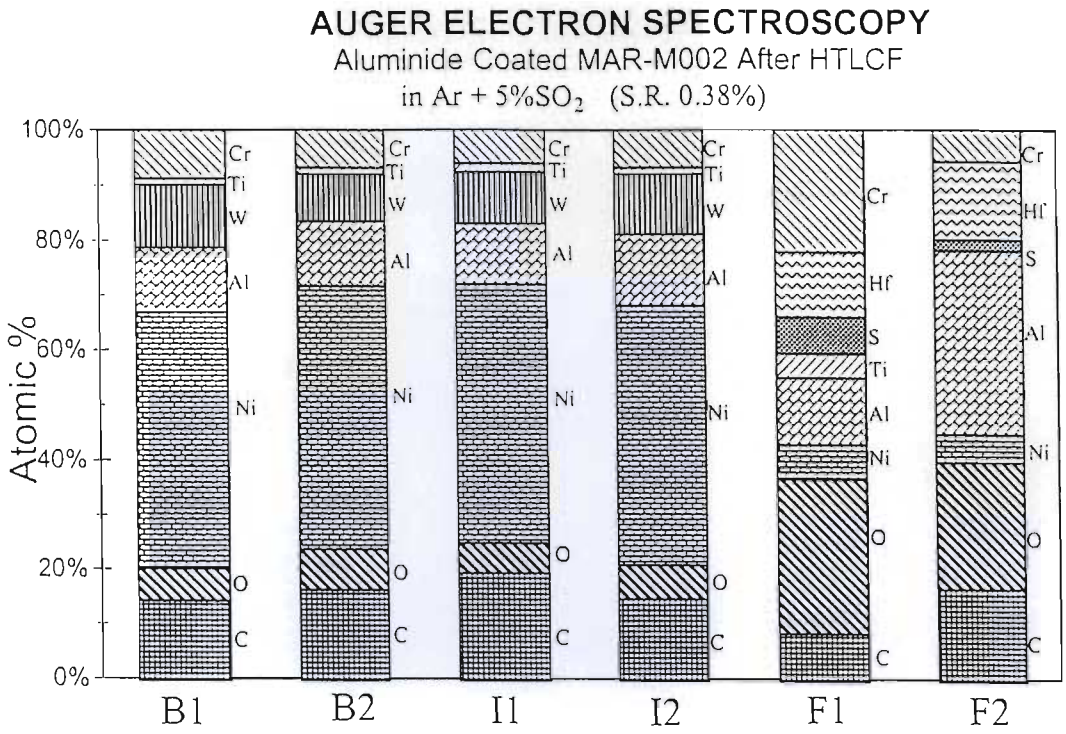

Figure 3.86 : AES analysis of the fracture surface an aluminide coated sample after HTLCF in SO_2 bearing atmosphere (S.R. 0.38%)

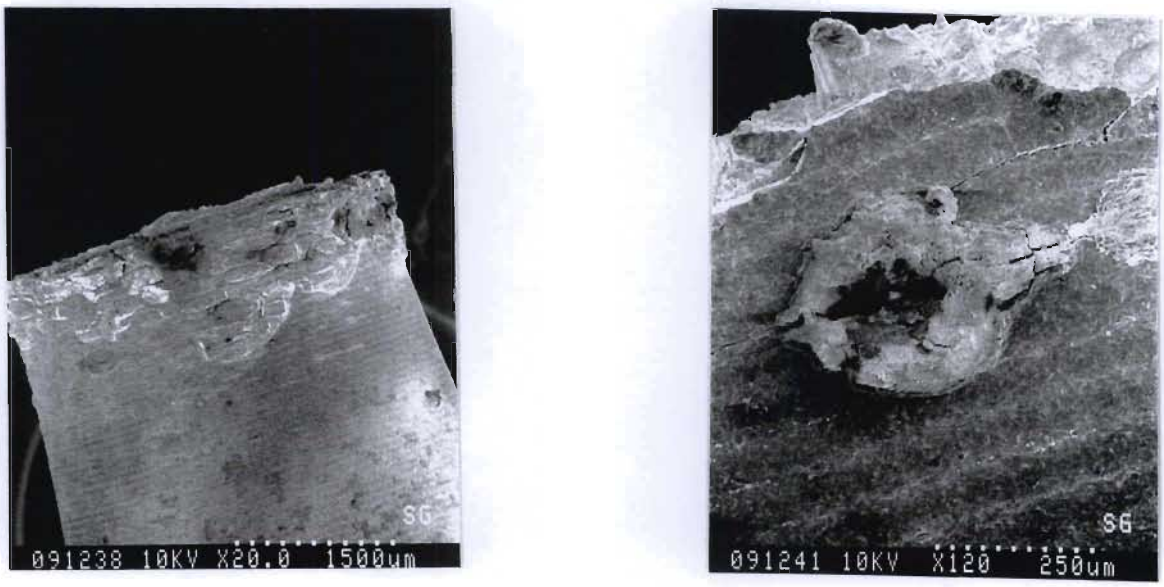

a b

Figure 3.87 : Fractography showing blistering of the aluminide coating after HTLCF in Ar + 5% SO_2 (S.R. 0.38%)

Chemical analysis of a blister in the coating (figure 3.89) showed that the corrosion scale on the outer region was made up of mainly Ni, Al, and oxygen with smaller amounts of S, Cr and W. The corrosion product in this region was essentially Al and Ni oxides and sulphides with Al being the dominant constituent. Chemical analysis of the "porous" region in the coating showed that this region was depleted of aluminium and the corrosion product was made up of mainly oxides.

The corrosion product on the coating was made up of essentially aluminium oxides and sulphides due to the high aluminium content in the NiAl layer (figure 3.90). This analysis also indicates that the aluminium was significantly more reactive under the environmental conditions tested. The region adjacent to the corrosion scale (figure 3.90) was depleted of aluminium, dropping by approximately 60% when compared with the as received coating. The NiAl layer was effectively leached of aluminium.

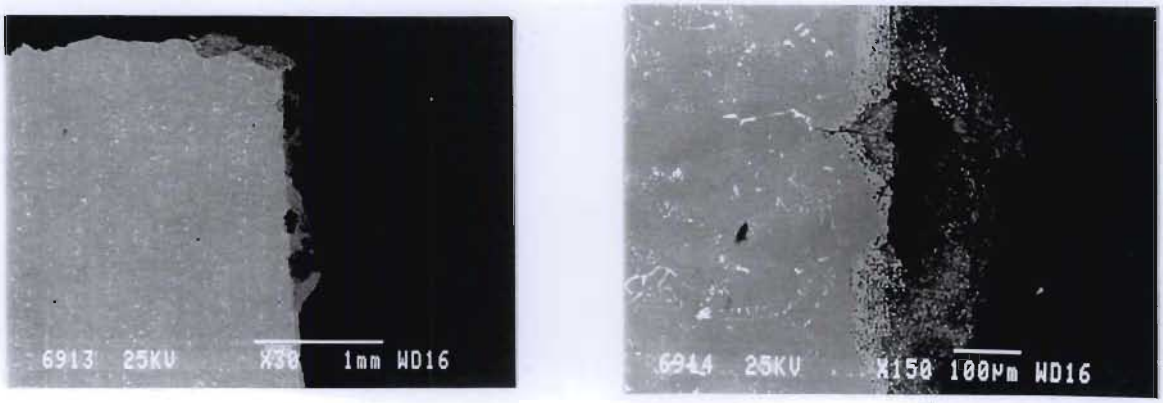

a b

Figure 3.88 : Cross-sectional analysis of aluminide coated MAR-M002 after HTLCF in SO_2 Containing environment (S.R. 0.38%)

Elements	Weight percent					
	A	B (pores)	B (solid)	C (corr.prod.)	C (solid)	D
O	31.62	0.55	1.33	33.05	1.45	45.26
Al	26.27	0.68	3.06	1.59	4.55	25.08
Ti	1.04	0.32	0.00	5.87	0.00	0.91
Cr	7.09	8.77	0.47	1.92	0.31	3.90
Co	1.19	11.98	12.74	3.70	8.60	1.26
Ni	18.72	69.49	68.77	33.04	71.18	13.86
Zr	0.59	0.00	0.07	8.47	0.44	0.22
Hf	1.86	0.92	0.00	4.90	0.00	0.95
Ta	1.43	1.81	1.54	0.90	2.88	0.75
W	4.20	5.06	11.94	1.01	10.08	0.26
S	5.99	0.41	0.08	5.53	0.51	7.55

Figure 3.89 : Chemical analysis of the blister in the aluminide coating after HTLCF in SO_2 (S.R. 0.38%)

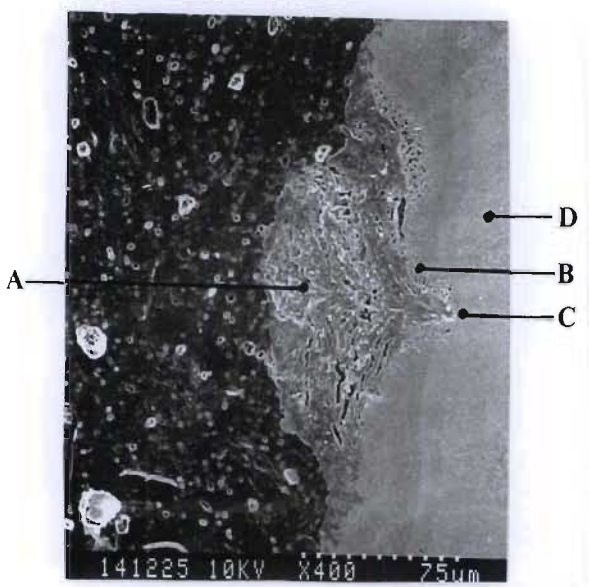

Elements	Weight percent			
	A	B	C	D
O	43.12	0.00	0.00	0.00
Al	32.24	7.77	7.57	5.77
S	5.29	0.38	0.45	0.00
Ti	0.36	0.35	1.88	1.94
Cr	4.33	1.01	3.19	3.51
Co	1.33	8.79	6.90	6.47
Ni	0.95	70.95	61.71	60.47
W	5.29	5.48	14.08	12.18
Zr	0.00	0.00	0.45	3.94
Hf	0.75	1.11	1.15	1.74
Ta	1.94	4.15	2.62	3.67

Figure 3.90 : Corrosion process in a crack that had developed in the aluminide coating after HTLCF in Ar + 5% SO_2 (S.R. 0.38%)

3.2.4.3 TYPE I Platinum Aluminide Coated MAR-M002

The life of TYPE I platinum aluminide coated MAR-M002 after HTLCF in Ar + 5%SO_2 at a strain range of 0.38% was significantly lower than that of the aluminide coated and uncoated samples tested under similar conditions. The number of cycles to failure was 1400, which was very similar to the samples tested at the higher strain range. The fracture surface (figure 3.91) was covered with dark corrosion product as a result of the sulphidation attack. There were two distinct regions on the fracture surface; the smooth region where crack propagation occurred and the coarse region where final failure occurred. The corrosion product on the fracture surface was made up of mainly Ni, Cr, S and oxygen (figure 3.91). A qualitative AES analysis of the fracture surface (figure 3.92) showed that there was a significant amount of oxygen and sulphur present in the corrosion product. (A quantitative analysis was not possible due to the contamination of the fracture surface with carbon.) The most prominent alloying elements present were Al and Ni with smaller amounts of Cr and Ti.

The coating showed evidence of a few severe cracks (figure 3.93) close to the fracture surface. Figure 3.93a indicated that the sulphidation attack was concentrated in the region where the coating was cracked. Corrosion product was evident around the edge of the fracture surface (figure 3.93b). The morphology of this corrosion product indicates that it was most probably in the liquid state during the test. The crack profile (figure 3.93b) revealed a structure very similar to that observed in the TYPE II platinum aluminide coated alloy. The evidence indicated that the corrosion processes inside the crack had forced the lips of the crack outwards.

Sulphidation attack of the coating was concentrated in the regions where the coating had failed (figure 3.94). The deterioration of the coating was most severe at the fracture surface/coating interface (figure 3.94). Severe internal sulphidation of the coating was evident. The interdiffusion/substrate zone was very susceptible to sulphidation and the corrosion proceeded more rapidly along this region than into the substrate. High magnification of the crack in the coating (figure 3.94b) revealed severe internal sulphidation of the coating along the crack edge resulting in "swelling" of the coating. The sulphidation attack progressed more rapidly "laterally" along the coating resulting in the widening of the crack.

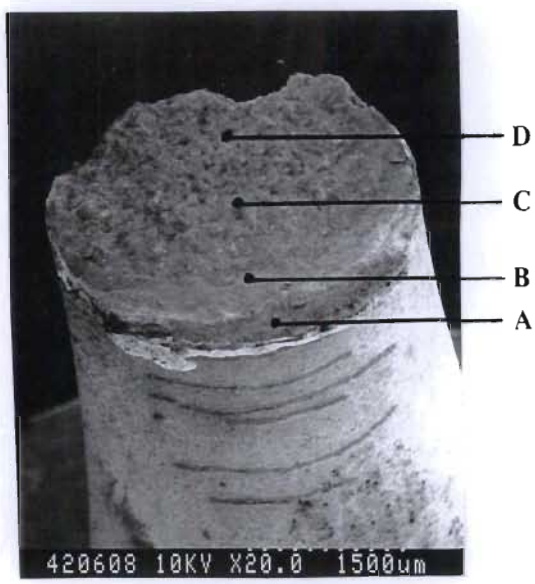

Elements	Weight percent			
	A	B	C	D
O	19.03	26.42	23.70	17.47
Al	3.37	0.67	1.19	3.87
Ni	34.67	30.95	27.66	41.17
Cr	14.94	20.59	19.23	8.12
Co	10.01	5.70	4.19	5.81
W	4.96	2.95	3.20	7.83
Ta	1.39	0.49	6.56	4.44
Hf	0.30	0.43	3.14	2.68
Ti	0.54	0.32	2.87	2.10
Zr	4.31	0.00	0.00	0.00
Fe	0.41	0.06	0.09	0.07
S	6.06	11.20	8.17	5.79
Pt	0.00	0.22	0.00	0.65

Figure 3.91 : Fracture surface of TYPE I platinum aluminide coated MAR-M002 after HTLCF in Ar +5% SO_2 (S.R. 0.38%)

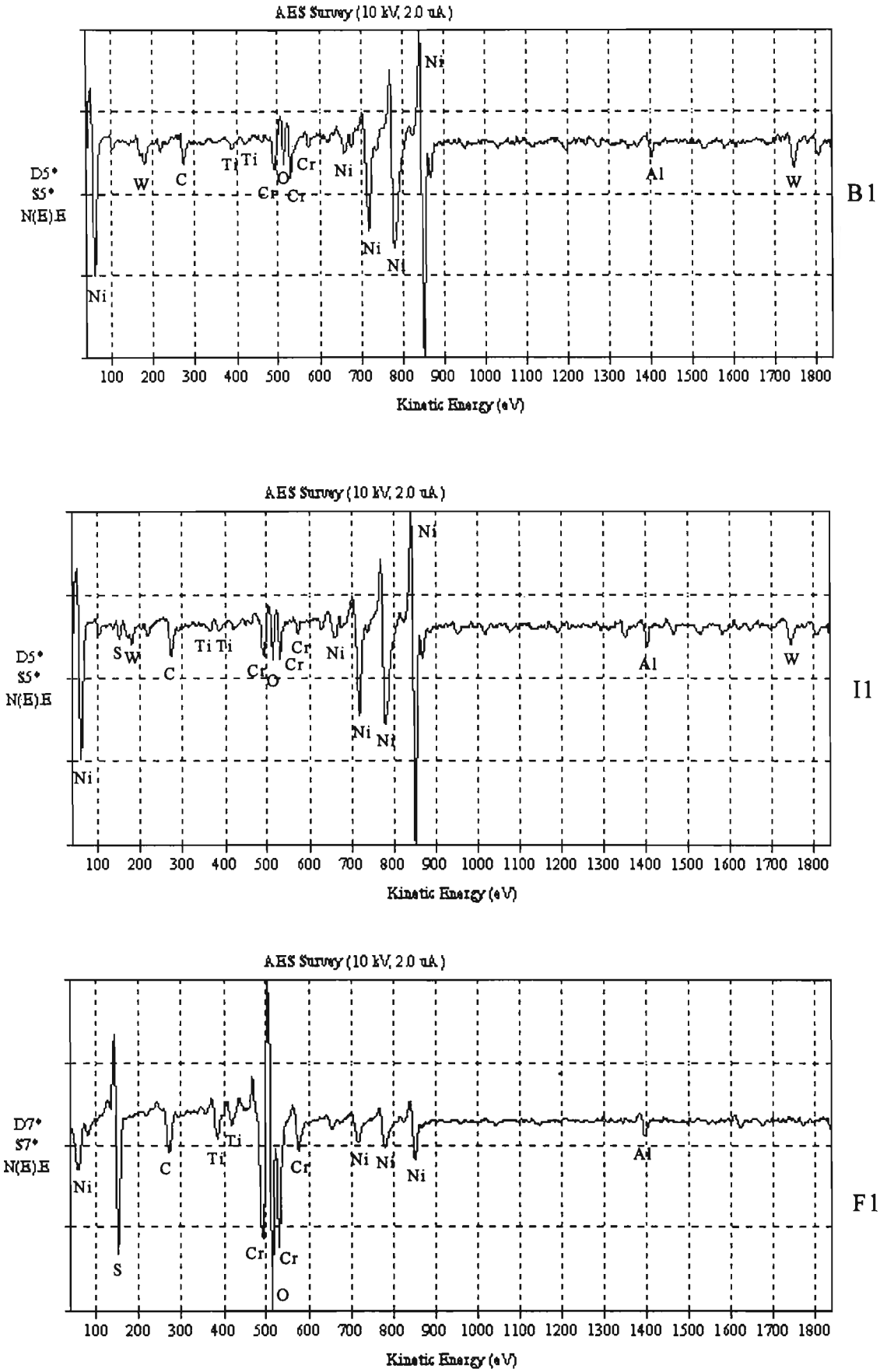

Figure 3.92 : AES analysis of the fracture surface of TYPE I platinum aluminide after HTLCF in SO_2 containing atmosphere (S.R. 0.38%)

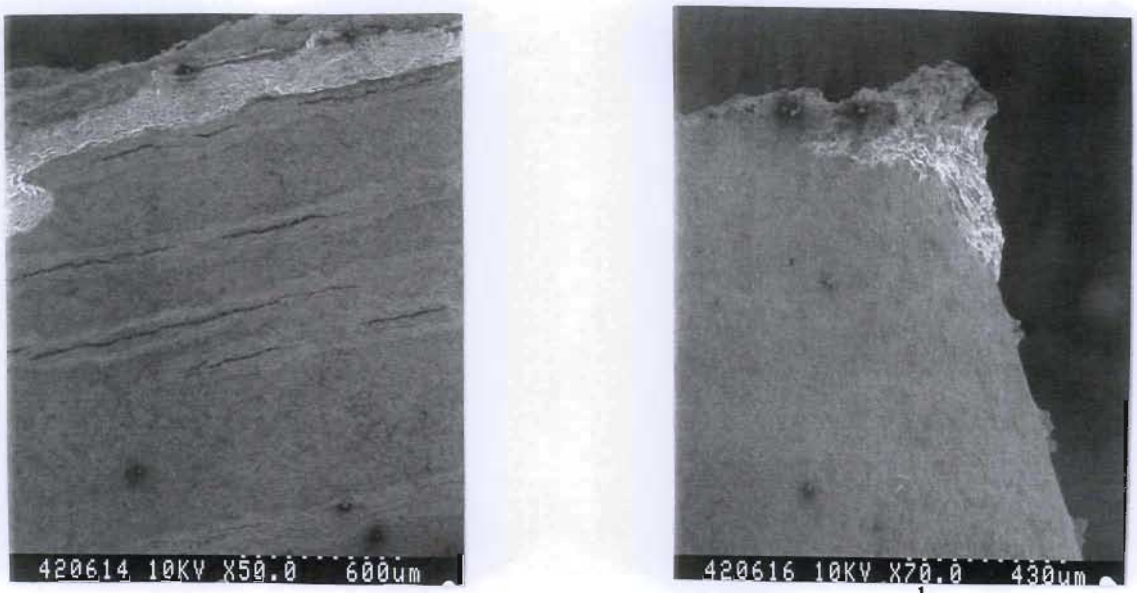

a b

Figure 3.93 : Fractography showing cracking and localized sulphidation of the TYPE I platinum aluminide coating after HTLCF in Ar + 5% SO_2 (S.R. 0.38%)

Chemical analysis of the region close to the fracture surface is shown in figure 3.95. The evidence indicated that the corrosion product on the outer region was composed of mainly Cr, Al, Ni, oxygen and sulphur. The edge of the fracture surface showed a more complex corrosion product morphology (figure 3.95). The outer layer of the corrosion product (figure

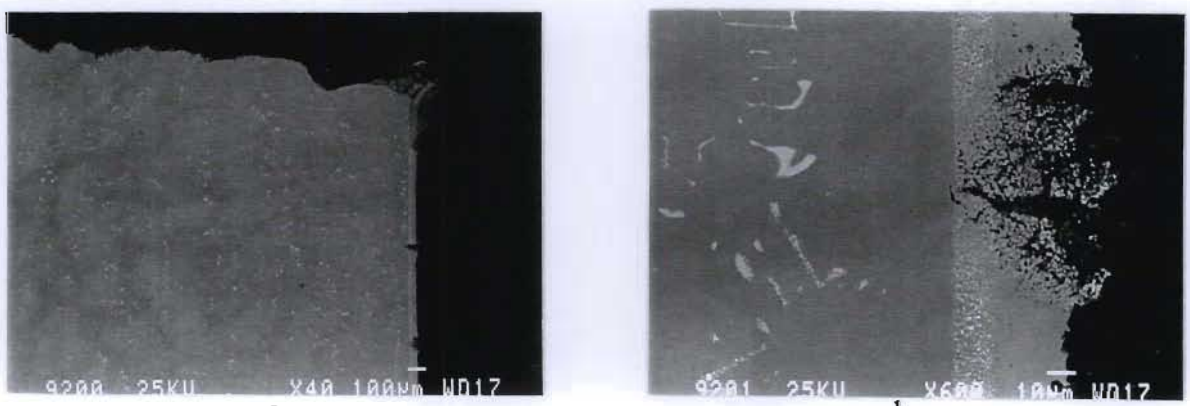

a b

Figure 3.94: Micrographs showing the morphology of cracks and corrosion -fatigue damage of the TYPE I platinum aluminide coating after HTLCF in Ar + 5% SO_2 (S.R. 0.38%)

3.95) was made up of principally Cr, Ni, Co, oxygen and sulphur. The region below this was a mixture of particles of the alloy and dark corrosion product. The dark corrosion product was made up of the alloying elements, Ti, Cr, Ni, Ta, Hf, and Al, and oxygen and

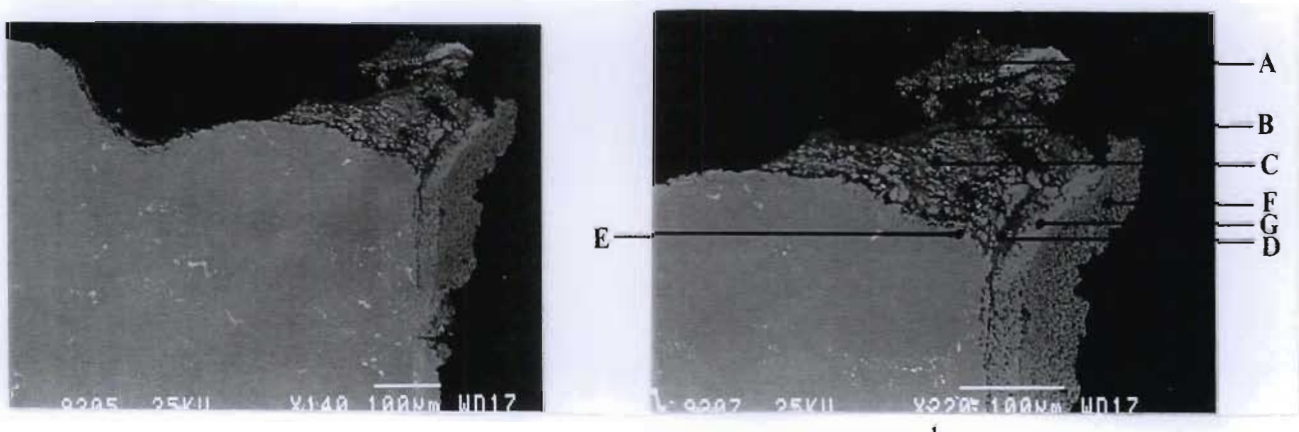

a b

Elements	Weight percent								
	A	B	C (dark)	C (light)	D	E	F (dark)	F (light)	G
Ti	2.55	0.22	5.77	0.01	9.16	0.48	0.33	0.00	0.02
Cr	7.77	35.12	15.39	1.20	18.45	3.51	15.02	0.77	0.22
Co	2.26	7.19	1.11	11.79	2.36	12.24	5.36	10.96	10.93
Ni	23.28	13.95	8.26	53.10	11.61	67.51	24.86	75.24	72.02
Ta	4.02	0.00	16.25	0.70	9.85	0.29	0.63	0.41	0.00
Hf	1.97	0.00	2.53	0.37	6.96	1.14	1.09	0.16	0.00
W	01.31	0.50	0.94	25.22	0.00	12.07	0.00	0.00	7.10
Zr	0.54	0.00	0.07	0.00	0.00	0.00	0.00	0.00	0.00
Al	16.94	0.00	9.30	0.17	6.38	2.76	11.65	4.32	3.39
Pt	0.19	0.00	0.00	0.00	0.29	0.00	1.88	8.15	6.32
O	28.53	38.91	39.81	7.43	30.18	0.00	0.00	0.00	0.00
S	10.63	4.10	1.47	0.00	4.78	0.00	39.18	0.00	0.00

Figure 3.95 : Chemical analysis of the coating close the fracture surface of a TYPE I platinum aluminide coated sample after HTLCF in SO_2 (S.R. 0.38%)

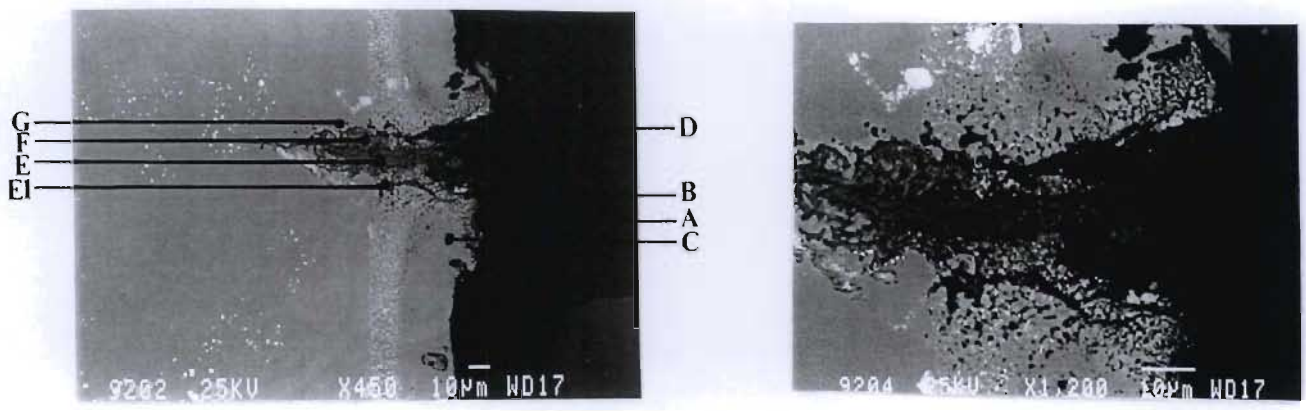

a b

Elements	Weight percent							
	A	B	C	D	E	E1	F	G
Ti	0.29	0.16	0.36	0.60	0.19	0.55	7.26	1.82
Cr	4.17	7.18	3.25	5.28	1.19	23.60	14.20	5.39
Co	2.89	2.14	6.79	1.49	23.64	2.58	1.55	8.47
Ni	11.02	28.24	55.76	5.61	51.83	8.97	5.64	63.54
Ta	0.00	0.71	0.00	0.35	0.13	0.33	7.33	1.79
Hf	0.00	1.04	0.00	0.52	0.61	0.00	0.79	0.90
W	0.21	0.00	1.01	0.45	0.06	0.67	15.52	10.70
Zr	1.27	2.47	0.00	0.56	0.00	0.25	0.00	0.00
Al	35.39	10.99	17.07	39.07	0.00	9.40	8.00	7.06
S	2.87	15.95	0.00	4.67	0.00	43.17	4.87	0.00
O	41.89	8.12	0.00	41.15	21.63	10.39	33.11	0.00
Pt	0.00	23.00	15.75	0.23	0.70	0.09	1.72	0.33

Figure 3.96 : Chemical analysis of crack through the TYPE I platinum aluminide coating after HTLCF in Ar + 5% SO_2 (S.R. 0.38%)

sulphur. The major constituents were Cr, Ni, Ta, Al and oxygen. This indicated that mainly the oxides of these elements were present. The "white" alloy particles were depleted of the reactive elements and were composed of mainly of Ni, Co, and W. The corrosion product in the "pores" in the coating was made up of the sulphides of Cr, Co, Ni, and Al with no oxygen evident. The "white" coating alloy was depleted of aluminium and Cr.

The corrosion product in the crack in the coating and on the external surface (figure 3.96) was composed of mainly aluminium oxides and sulphides. The black region in the coating adjacent to the corrosion scale (figure 3.96 pt. E1) was found to be essentially chromium sulphides with the oxygen content being insignificant. The corrosion product in the interdiffusion zone (figure 3.96 pt. E) was predominantly Ni, Co, and oxygen. As the corrosion-fatigue crack proceeded into the substrate the corrosion product became more complex with significant amounts of Ti, Cr, Ni, Ta, W, Al, oxygen and sulphur being detected. The distribution of sulphur and oxygen indicate that oxides are formed on the outer regions, with sulphides being formed in the scale/substrate interface. The corrosion front progressing into the alloy was fairly broad due to the sulphidation attack progressing "laterally" in the coating. The coating showed a high resistance to sulphidation attack with sulphidation attack being concentrated in the cracks.

3.4.2.4 TYPE II Platinum Aluminide Coated MAR-M002

TYPE II platinum aluminide coated MAR-M002 failed after 1668 cycles due to the combined effect of HTLCF (0.38% strain range) and Ar + 5%SO_2 at 870°C. There was no significant improvement in life when compared to similar tests performed on TYPE I platinum aluminide coated samples. However, there was approximately a three fold increase in life when compared to similar tests performed on TYPE II platinum aluminide coated MAR-M002 at a strain range of 0.66%.

The fracture surface was covered with dark corrosion product (figure 3.97). There were again two distinct regions on the fracture surface, i.e., a smooth region where crack propagation occurred and a coarse region where final failure occurred. Chemical analysis of the fracture surface showed that the corrosion product was made up of a mixture of oxides and sulphides of the alloying elements. Cr, Ni and Co were the most significant of the alloying elements present. The amount of aluminium became much more significant closer to the coating/fracture surface interface. This was due to the higher aluminium content in the coating. The composition of the corrosion product on the external surface close to the fracture was essentially Ni, Cr, Al, oxygen and sulphur and platinum. The aluminium content was significantly higher than that on the fracture surface. The corrosion product on the lip of the cracks showed a composition similar to that detected on the fracture surface

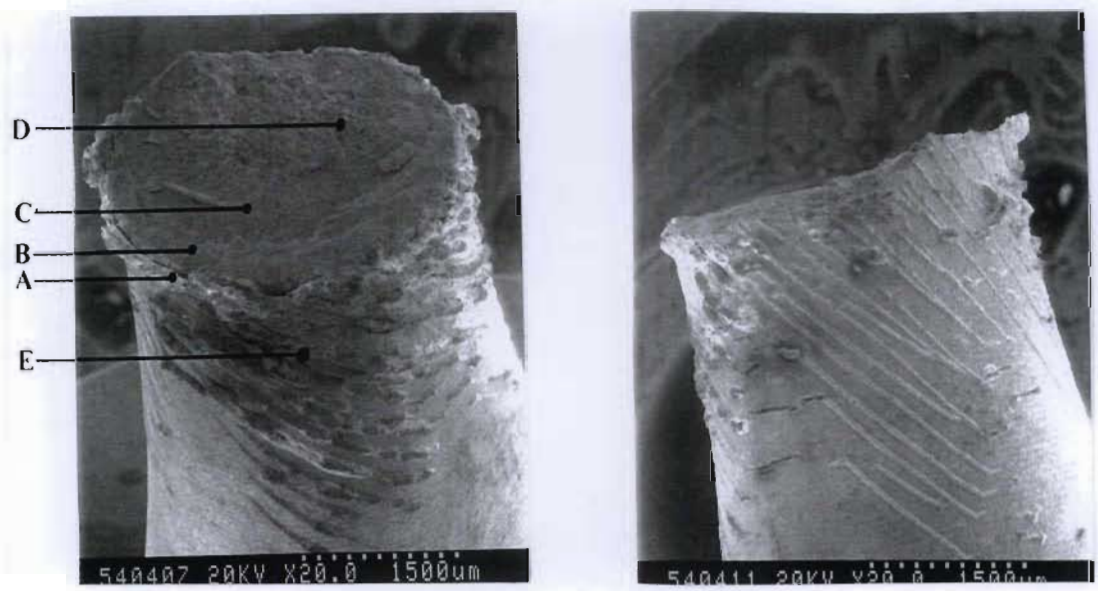

a b

Elements	Weight percent					
	A	B	C	D	E crack	Ecoat
O	27.60	17.16	15.50	18.58	24.75	31.57
S	2.83	6.09	8.14	11.75	5.94	0.21
Cr	9.48	21.49	26.27	18.48	29.75	3.36
Co	4.58	15.44	5.41	4.56	5.42	0.26
Ni	27.35	36.42	34.99	30.42	20.71	10.86
Zr	0.00	0.23	0.00	0.00	0.52	0.00
Hf	0.49	0.00	1.24	2.80	0.42	0.00
Ta	0.56	0.00	2.49	5.31	0.48	0.32
W	0.13	1.96	1.66	1.30	0.00	0.38
Ti	1.46	0.20	2.55	3.37	2.07	0.03
Pt	10.29	0.00	0.00	0.00	0.98	16.66
Al	15.22	1.02	1.74	1.45	8.97	36.36

Figure 3.97 : a) Fracture surface of TYPE II platinum aluminide coated MAR-M002 after HTLCF in Ar + 5%SO_2 (S.R. 0.38%)

b) Profile of the fracture surface showing cracking of the coating

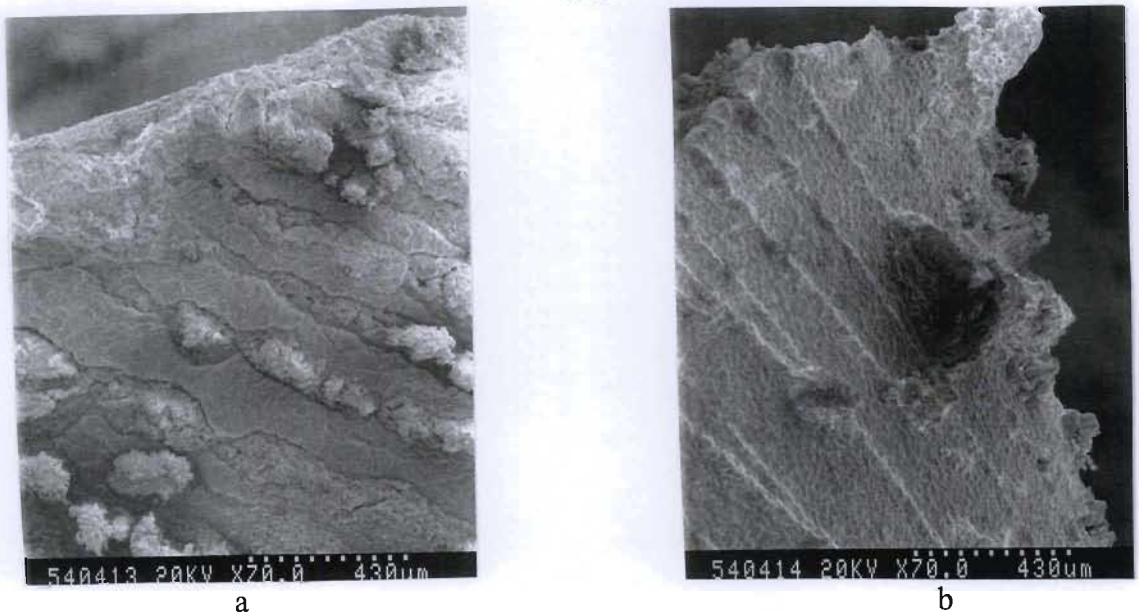

a b

Figure 3.98: Fractography showing severe cracking of the coating close to the fracture surface in TYPE II platinum aluminide coating after HTLCF in Ar + 5% SO_2 (S.R. 0.38%)

with a significantly higher aluminium content. The regions between the cracks was composed of Pt, Al, Ni and oxygen with the sulphur content being negligible. This indicated that if the coating was not damaged, it offered a high resistance to sulphidation attack.

The coating close to the fracture surface showed evidence of severe cracking and sulphidation attack (figure 3.97&98). Two modes of cracking was observed, namely, 45° to the direction of loading and circumferential cracks perpendicular to the direction of loading. The sulphidation attack was concentrated at the cracks in the coating. Swelling of the coating as a result of internal sulphidation was evident. The nature of the corrosion product, figure 3.98, indicated that it was in the molten state at the test temperature.

The coating close to the fracture was severely damaged (figure 3.99). The sulphidation attack below the platinum rich outer layer causing the coating to "swell", "blister" and spall off. The NiAl and interdiffusion zones were more vulnerable to sulphidation. The interdiffusion/substrate interface was most prone to sulphidation with the corrosion processes proceeding most rapidly along this region causing the coating to spall off, hence exposing the base metal (indicated regions in figure 3.99).

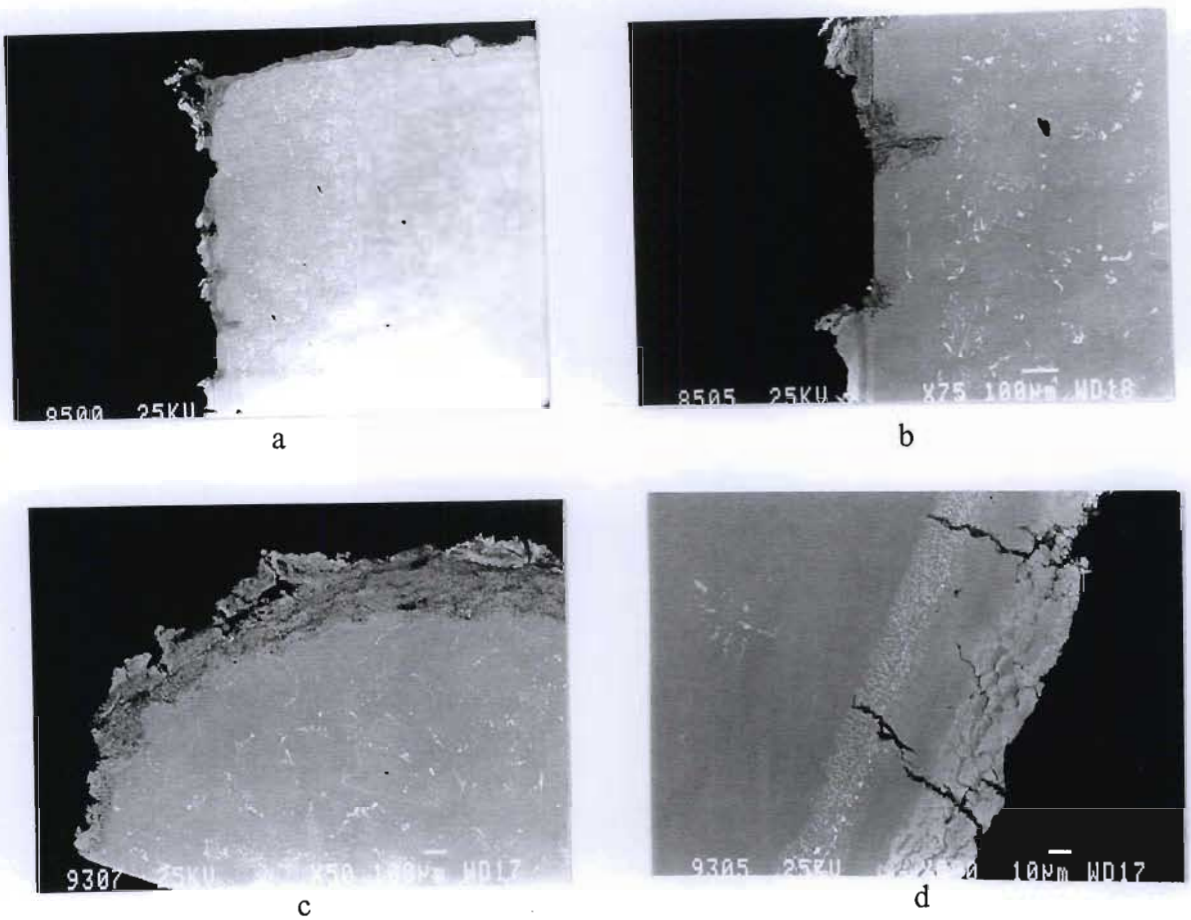

Figure 3.99: Longitudinal cross-section showing the morphology of cracks and corrosion -fatigue damage of the TYPE II platinum aluminide coating after HTLCF in Ar + 5% SO_2 (S.R. 0.38%)
a&b) Longitudinal cross-section
c&d) Transverse cross-section

The transverse cross-section of a TYPE II platinum aluminide coated sample shows regions in which the coating was completely destroyed followed by sulphidation attack of the substrate (figure 3.99). Closer examination of the coating (figure 3.99) revealed that there was a number of fine cracks in the platinum rich outer layer. It was also evident that this zone had grown in thickness producing a structure similar to that observed in the pure platinum coated samples. The cracks generally propagated in the grey regions with the white regions being more resistant to cracking. The NiAl middle zone again showed evidence of being more resistant to crack initiation and propagation.

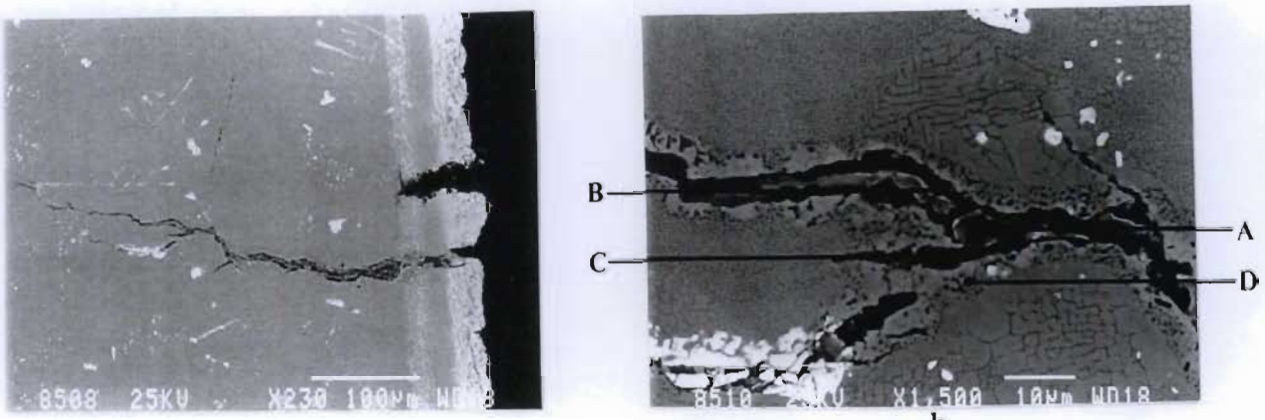

a b

Elements	Weight percent			
	A	B	C	D
Ti	4.23	13.89	1.10	0.24
Cr	39.93	14.95	13.30	0.99
Co	1.43	1.28	3.24	12.15
Ni	9.54	4.12	13.11	68.96
Al	0.66	2.89	22.62	2.45
Zr	0.20	0.00	0.13	0.00
Hf	1.28	5.66	4.11	0.53
Ta	2.52	23.08	1.97	0.98
W	1.62	1.04	2.57	13.03
S	5.47	13.72	15.82	0.66
O	33.12	19.37	22.04	0.00

Figure 3.100 : Chemical analysis of the corrosion product in the crack propagating in the substrate of TYPE II platinum aluminide coated MAR-M002 after HTLCF in Ar + 5%SO_2 (S.R. 0.38).

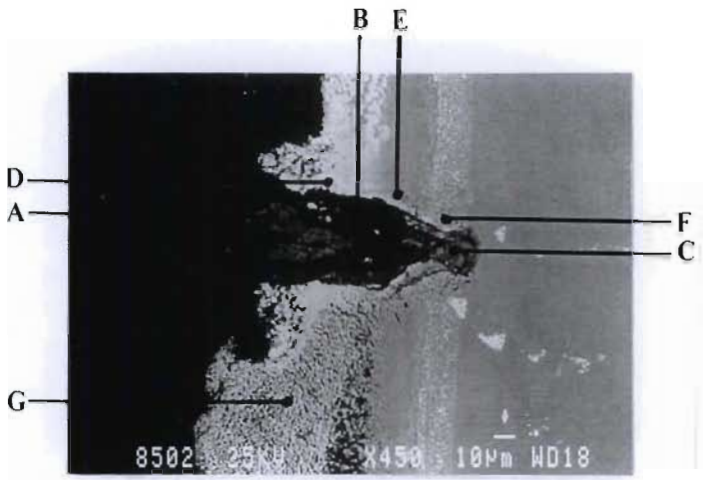

Elements	Weight percent						
	A	B	C	D	E	F	G
Ti	0.28	0.39	0.008	0.007	0.35	0.84	0.02
Cr	49.86	5.05	0.48	0.19	0.84	4.14	1.26
Co	5.51	0.47	10.37	1.25	3.66	5.31	3.47
Ni	6.81	1.53	44.03	21.59	50.37	26.99	45.20
Al	0.74	38.89	0.10	9.56	11.45	8.28	8.88
Zr	0.00	0.36	0.60	0.00	0.00	0.00	0.00
Hf	0.21	0.00	0.45	0.51	0.56	2.07	0.00
Ta	0.38	0.29	0.33	0.10	0.00	3.67	0.84
W	2.70	0.74	0.31	1.03	1.16	27.82	0.20
Pt	1.37	1.11	1.34	65.68	31.60	11.53	36.42
S	1.37	11.65	26.73	0.00	0.00	9.35	3.70
O	30.78	39.52	15.18	0.00	0.00	0.00	0.00

Figure 3.101 : Cross-section of TYPE II platinum aluminide coated MAR-M002 after HTLCF in Ar + 5% SO_2 showing chemical composition of the crack in the coating (S.R. 0.38%)

Crack propagation was transdendritic and branched (figure 3.100). γ' denuded regions along the crack edge was evident. The corrosion product along the crack edge in the substrate (figure 3.100) was made up of mainly Cr, Ni, Al, S and oxygen. Chromium was found to be the major constituent in the centre of the crack (grey corrosion product). The sulphides

were concentrated at the crack edge indicating that the more stable oxides formed initially followed by sulphur being transported inwards and the formation of sulphur bearing phases a the crack edge. The corrosion product was a mixture of the oxides and sulphides of various alloying elements with the reactive elements Al, Cr, and Ni being most prominent.

Figure 3.101 revealed that the corrosion product in the crack in the coating was made up of two distinct regions: the black region along the crack edge and the grey region in the centre of the crack. The grey region was made up of mainly Cr and oxygen with relatively small amounts of sulphur. The dark region was essentially a mixture of Al, oxygen and sulphur. At the crack tip (figure 3.101), the corrosion product was made up of mainly Co, Ni, S and oxygen with sulphur making up a significant proportion of the corrosion product. The coating adjacent to the crack was depleted of aluminium and chromium. The platinum aluminide (platinum rich white regions) phases were denuded along the crack edge.

3.4.2.5 2μm Platinum Aluminide Coated MAR-M002

Sulphidation attack was evident on the fracture surface of 2μm platinum aluminide coated MAR-M002, figure 3.102. The fracture surface consisted of the two regions typical of corrosion fatigue in sulphidation environment, i.e., the "coarse" region and "smooth" region. The number of cycles to failure was 1821, which was approximately 3 times the test performed on a similar sample and similar conditions at a strain range of 0.66%. However, this result was significantly lower than that observed in similar tests performed on aluminide and uncoated samples. The external surface close to the fracture showed severe damage to the coating, i.e., cracking and even spalling of the coating in regions. Chemical analysis of the corrosion product on the fracture revealed that it was made up of a mixture of oxides and sulphides of the substrate alloying elements with Ni and Cr being the major constituents. The corrosion product on the cracks on the external surface was made up of mainly chromium and nickel oxides and sulphides. The "undamaged" coating between the cracks showed less evidence of sulphidation with the EDS analysis indicating that it was made up mainly of aluminium oxides.

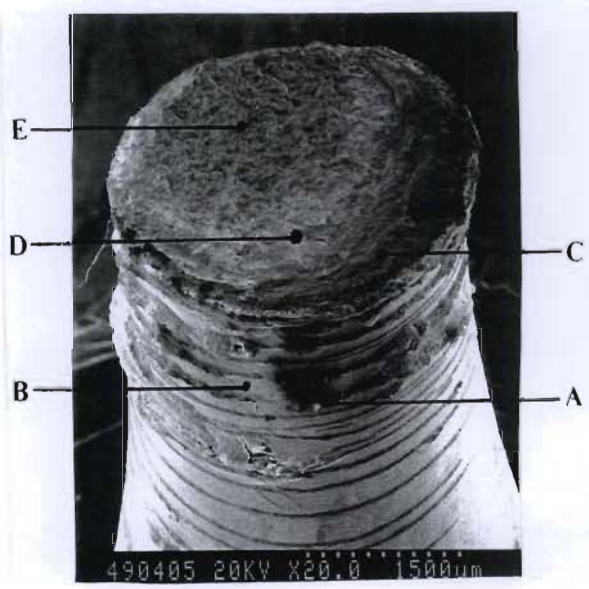

a

b

Elements	Weight percent				
	A	B	C	D	E
Ti	2.50	0.13	0.39	1.85	1.49
Cr	32.06	3.11	28.57	9.96	7.59
Co	6.09	0.39	11.72	6.38	8.23
Ni	19.57	13.89	21.21	42.69	52.41
Ta	1.71	0.00	0.00	3.35	5.84
Hf	0.71	0.04	0.47	2.37	3.47
W	0.39	0.61	3.18	6.81	8.06
Zr	0.35	0.00	0.00	0.03	0.12
Al	3.97	35.49	0.17	4.67	3.01
S	6.33	0.85	6.08	8.15	2.11
O	25.96	30.83	28.21	13.73	7.67
Pt	0.35	14.64	0.00	0.00	0.00

Figure 3.102 : a) Fracture surface of 2μm platinum aluminide after HTLCF failure in Ar +5% SO_2 (S.R. 0.38%)

b) Profile of fracture surface showing cracking of the coating.

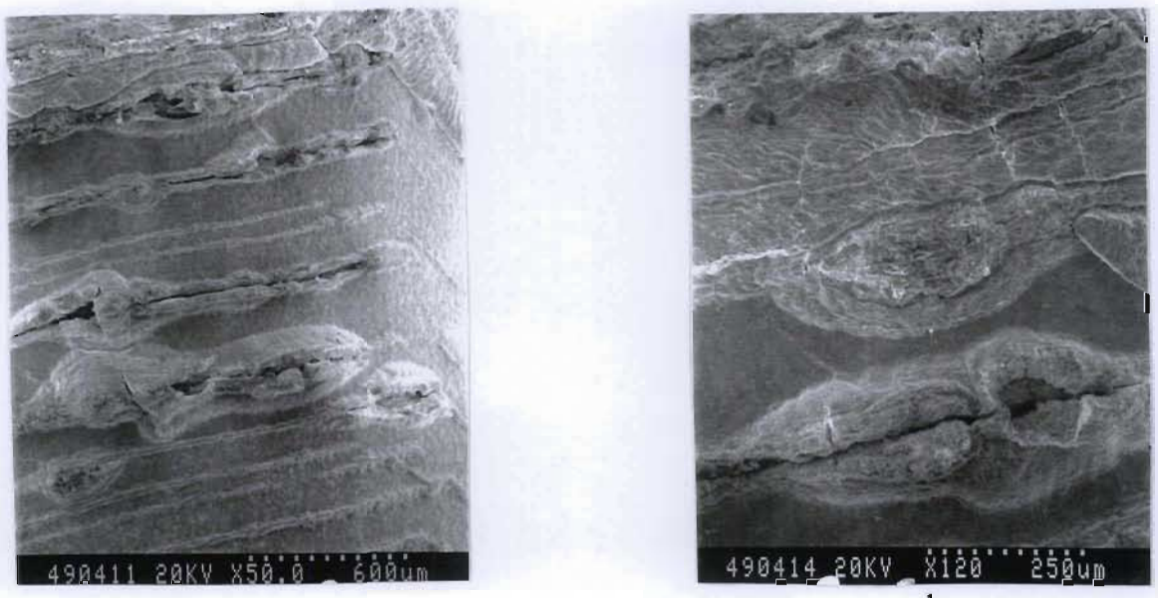

a b

Figure 3.103 : Fractography showing cracking of the coating close to the fracture surface in the 2μm platinum aluminide coating after HTLCF in Ar + 5% SO_2 (S.R. 0.38%)

It was evident that the coating was very brittle and prone to cracking (figure 3.102). Cracking of the coating occurred in two modes: one was circumferential cracks perpendicular to the loading direction and the other was cracks at approximately 45° to the loading direction. When the outer platinum rich layer was breached the sulphidation attack proceeded in the NiAl layer resulting in "swelling" of the coating in these regions. This process resulted in the lips of the cracks being forced outwards. Evidence of further cracking and spalling of the coating as a result of this process was also present (figure 3.103).

Cross-sectional analysis (figure 3.104) showed severe damage to the coating. The NiAl and Interdiffusion zones were prone to sulphidation attack. Sulphidation attack of this region occurred more rapidly once the brittle platinum rich zone had failed, resulting in severe internal sulphidation of the NiAl layer. This resulted in the swelling of the coating observed on the external surface. Spalling of the coating was also evident due to the delamination of the NiAl zone from the substrate. The corrosion processes were concentrated at the cracks in the coating indicating that the mechanical failure of the coating played a key role in the corrosion mechanism.

Chemical analysis of the cross-section close to the fracture (figure 3.105) showed that the corrosion products in the crack were made up of mainly oxygen, Ni, Cr and Al. It was evident that the main constituent of the corrosion product was oxides. The corrosion product in the "pores" in the coating was made up of essentially the sulphides of Ni and the NiAl zone was severely depleted of aluminium. Again "leaching" of the aluminium was instrumental in resulting in the "porous"nature of the coating.

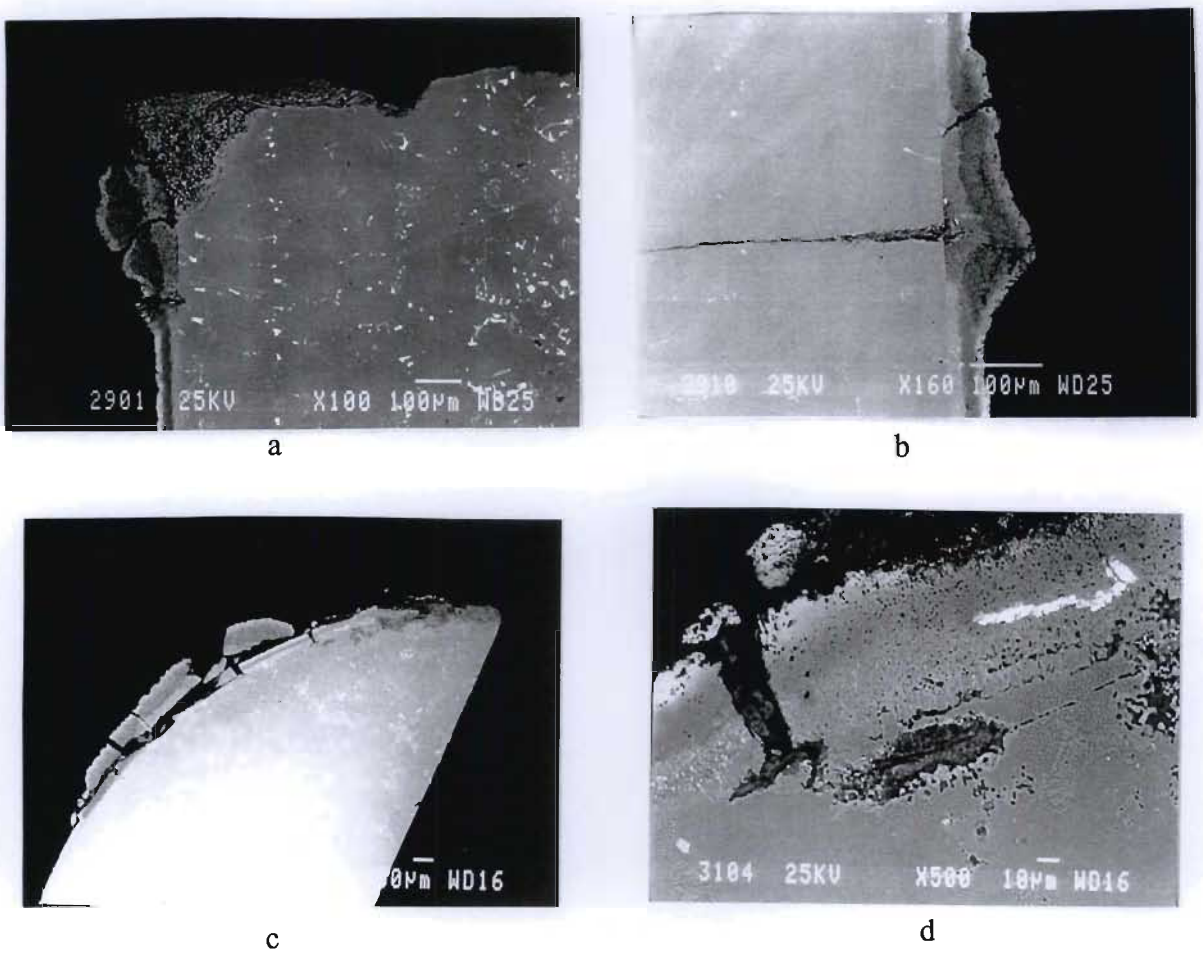

a b c d

Figure 3.104 : Metallography of 2µm platinum aluminide coated MAR-M002 after HTLCF in Ar + 5% SO_2 (S.R. 0.38%)

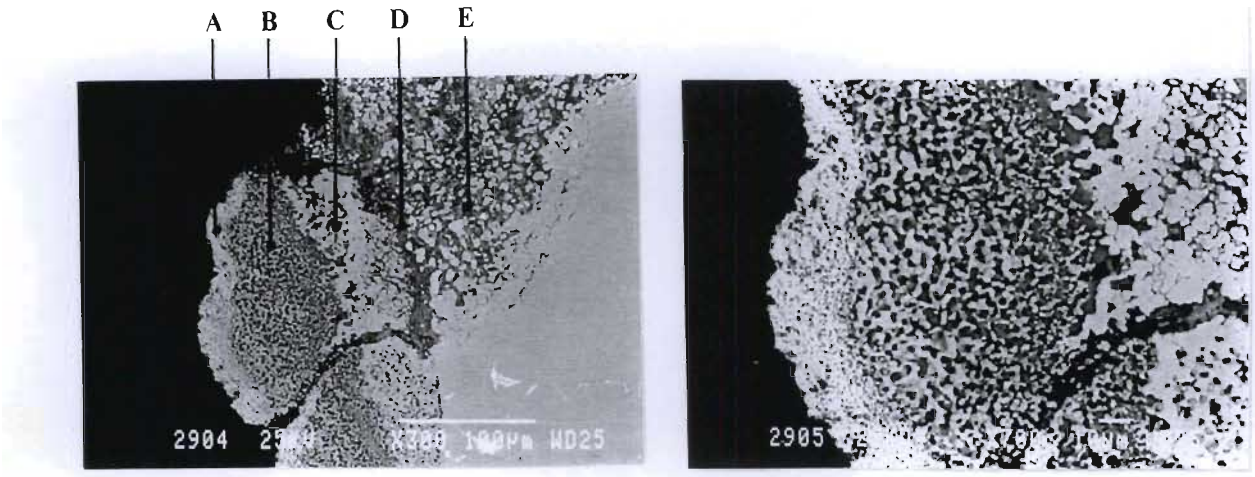

a b

Elements	Weight percent							
	A	B (pore)	B (solid)	C (pore)	C (solid)	D	E (corr.prod)	E (solid)
Co	2.94	7.19	11.77	5.56	11.77	2.68	3.00	11.86
Ni	58.02	35.88	72.11	26.37	72.11	16.70	20.82	59.85
Ti	0.00	0.04	0.07	0.06	0.07	6.51	7.04	0.23
Cr	0.45	16.50	1.33	12.30	1.33	16.45	12.20	2.63
Zr	0.00	0.00	0.00	0.31	0.00	0.40	0.18	0.52
Hf	0.57	1.86	0.00	2.19	0.00	3.91	4.53	0.19
Ta	1.48	2.30	0.00	1.80	0.00	6.34	6.85	0.59
W	0.77	1.46	1.71	2.17	3.98	0.00	0.37	20.60
Al	8.65	4.83	7.83	8.72	4.86	12.95	10.98	1.70
S	1.22	26.76	11.32	33.42	1.78	6.14	7.30	0.40
O	0.00	2.99	1.31	5.85	0.22	27.47	26.72	1.30
Pt	25.91	0.17	4.25	1.20	3.88	0.44	0.00	0.11

Figure 3.105 : Chemical analysis of the region close to the fracture surface showing internal sulphidation of the 2μm platinum aluminide coating (S.R. 0.38%)

3.4.2.6 Platinum Coated MAR-M002

The fracture surface of platinum coated MAR-M002 after HTLCF, at a strain range of 0.38%, in SO_2 bearing atmosphere is shown in figure 3.106. The surface was covered with dark corrosion product. The "smooth" region where crack propagation had occurred and the "coarse" region were final failure had occurred were evident. The number of cycles to failure was 3037. The "coarse" region where final failure had occurred was much smaller than that observed in the test performed at the higher strain range. The number of cycles to failure was about 11 times that observed at a strain range of 0.66%. However, the life of the platinum coated sample was approximately ½ that of the aluminide coated sample and ⅓ that of the uncoated sample. Chemical analysis of the fracture surface indicated that the corrosion product was made up of Cr, Ni, S and oxygen. Oxygen was very prominent in the surface analysis indicating a high presence of oxides in the corrosion product. The external surface close to the fracture revealed a higher resistance to sulphidation attack with the oxygen and sulphur contents being significantly lower than that observed on the fracture surface. Aluminium played a more prominent role since the amount of aluminium detected was much higher than that on the fracture surface.

AES analysis of the fracture surface (figure 3.107) indicated that the corrosion product was made up of mainly Cr, Ni, Al, Ti, sulphur and oxygen. The amount of oxygen was present in significant quantities, confirming the EDS analysis. There was some evidence of internal sulphidation of the of the substrate as can be seen by the sulphur detected in the region just below the fracture surface (figure 3.107). Close up examination of the fracture/coating interface showed evidence of peeling of the coating (figure 3.108).

The external surface close to the fracture showed little evidence of cracking. The coating was fairly resistant to sulphidation attack except in the regions immediately adjacent to the fracture surface (figure 3.108).

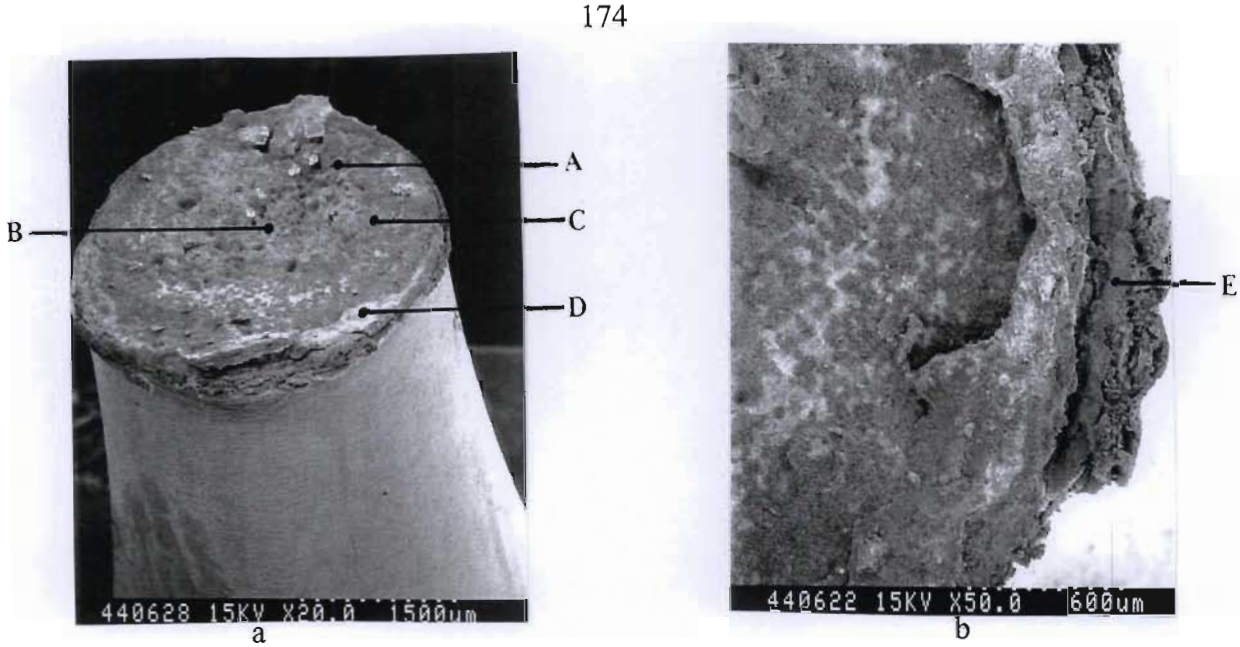

Elements	Weight percent					
	A	B	C	D	E	Ext. Surface
O	23.58	25.03	23.71	21.92	26.17	15.94
Al	2.48	1.16	2.14	6.42	0.75	32.88
Ni	33.30	28.89	29.50	39.26	28.50	40.45
Cr	17.29	18.56	17.50	10.62	26.10	3.66
Co	6.32	4.26	4.86	6.16	5.86	0.93
W	3.70	2.18	4.91	2.73	0.00	0.00
Ta	2.16	5.18	3.75	2.52	0.88	1.31
Hf	1.51	3.38	2.05	1.96	0.69	0.00
Pt	0.00	0.00	0.51	0.00	2.77	1.51
Ti	1.38	2.96	1.94	1.17	0.18	0.48
Zr	0.00	1.25	0.00	0.00	0.56	0.00
Fe	0.08	0.05	0.04	0.13	0.10	0.11
S	8.20	8.11	9.08	7.10	7.44	2.73

Figure 3.106 : Fracture surface of platinum coated MAR-M002 after HTLCF in Ar + 5%SO_2 (S.R. 0.38%)

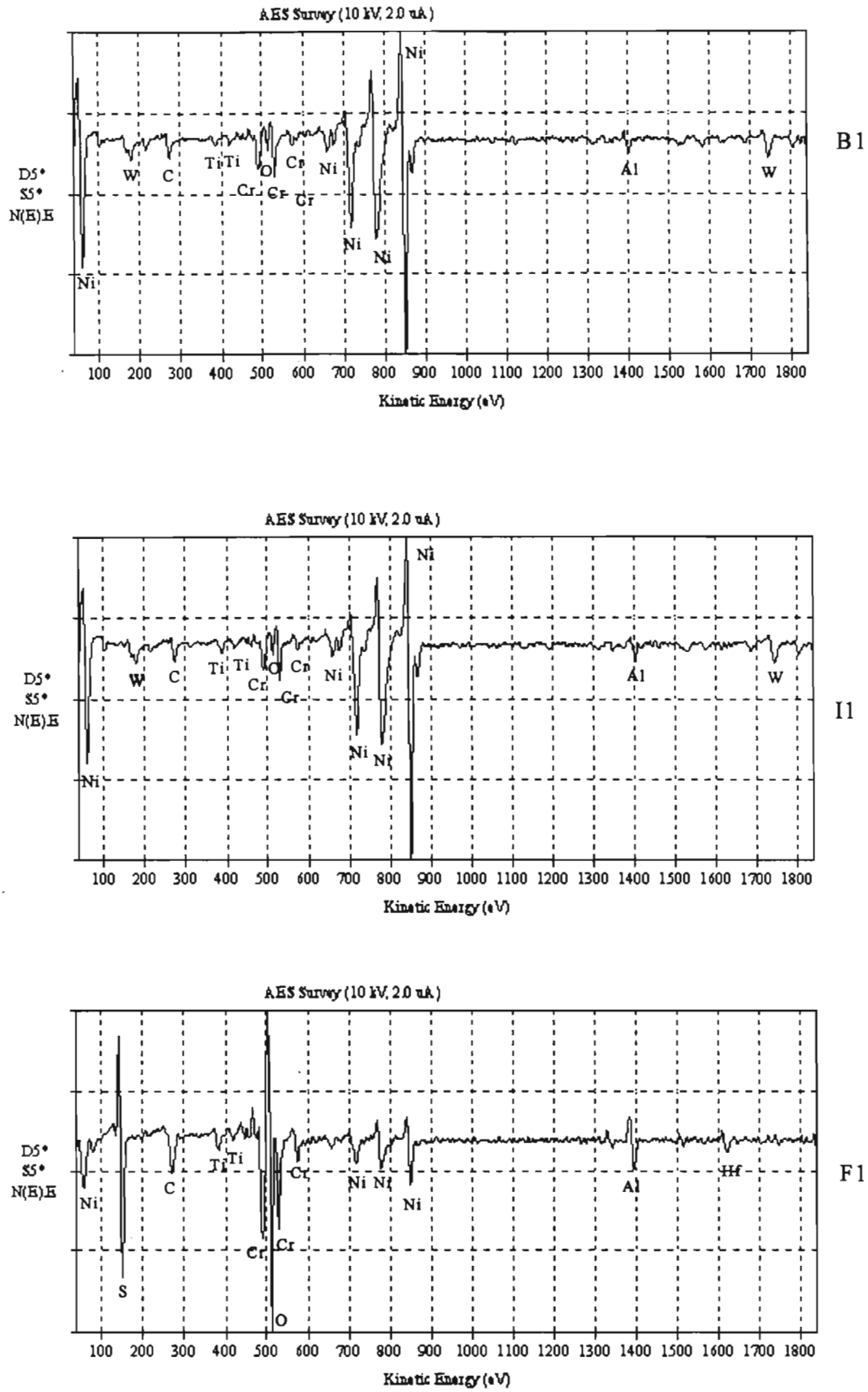

Figure 3.107 : AES analysis of the fracture surface of platinum coated MAR-M002 after HTLCF in Ar + 5% SO_2 (S.R. 0.38%)

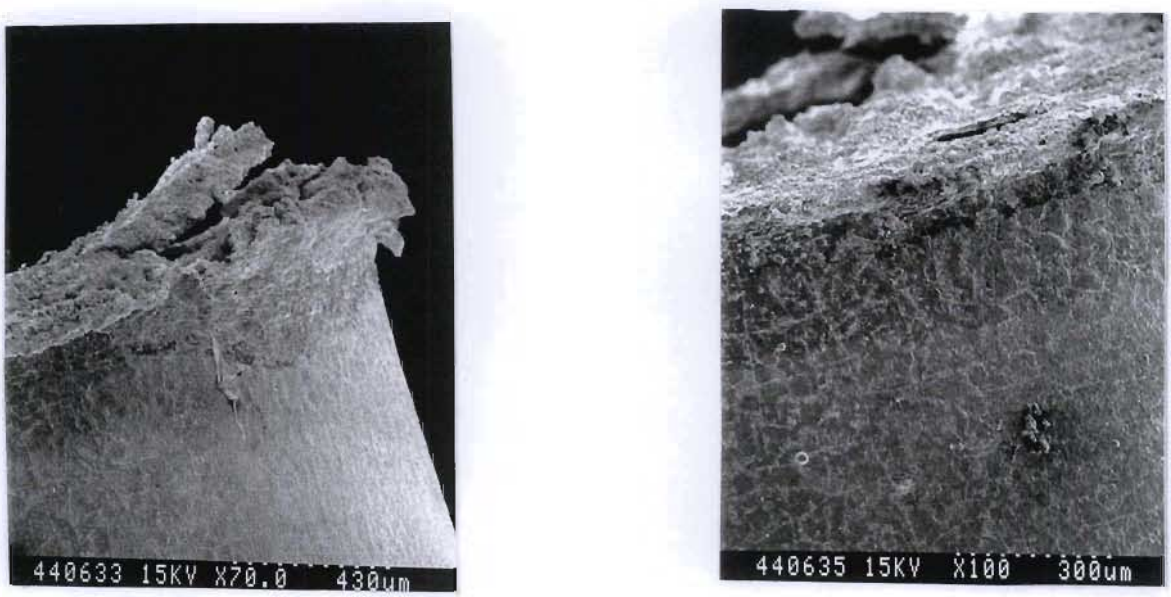

a b

Figure 3.108: Fractography of platinum coated MAR-M002 after HTLCF in Ar + 5% SO_2 (S.R. 0.38%)

Cross-sectional examination revealed that the coating thickness had grown to approximately 46 μm (figure 3.109). There was no evidence of severe cracking of the coating. The coating had peeled away from the substrate at the coating/fracture interface. It was evident that the γ' depleted zone was prone to sulphidation attack. The corrosion process proceeded more rapidly in this region than in the coating itself. High magnification of the region where the coating was peeling (figure 3.110) showed depletion of the "white phases" present in the coating. The cracks in the coating (figure 3.109) were branched and tended to propagate in the "grey" regions. There was also evidence of internal sulphidation (indicated in figure 3.109). Again, the evidence indicated that the grey region was more susceptible to sulphidation attack.

The corrosion product in the region where peeling of the coating occurred was in general composed of a mixture of oxides and sulphides of the alloying elements (figure 3.110a). The major constituents were Cr, Ni, sulphur and oxygen, with small but significant amounts of aluminium present. From the analysis of region A, figure 3.110a, it was evident that a large proportion of the of the corrosion product was made up of sulphides. Analysis of the corrosion product on the external surface (figure 3.110 pt.B) indicated that it was made up

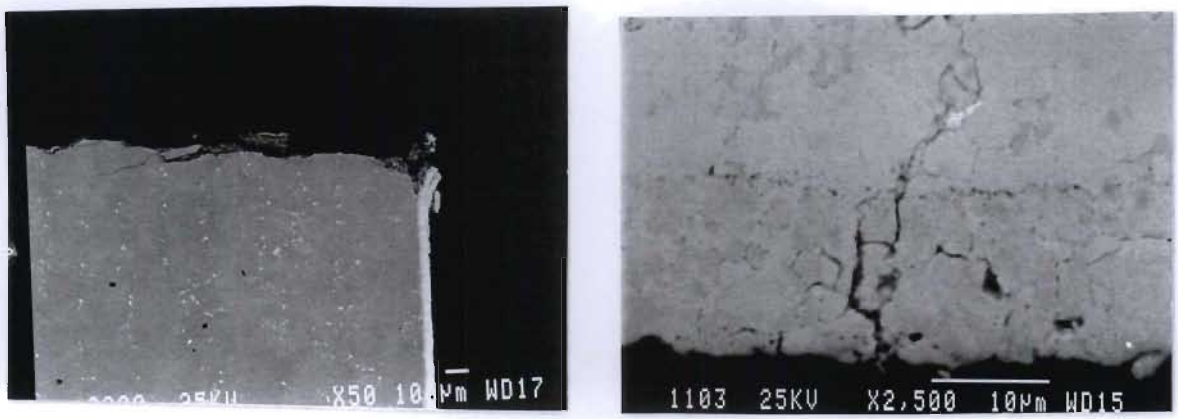

a b

Figure 3.109 : Cross-section of platinum coated MAR-M002 after HTLCF in Ar + 5% SO_2 (S.R. 0.38%)

of essentially Cr and Ni oxides and sulphides with the oxides being more prominent. The corrosion product inside the coating (figure 3.110 pt. C) was essentially composed of Ni, Hf, Ta, sulphur and oxygen with smaller amounts of other alloying elements. The regions adjacent to this point were depleted of the reactive elements Cr and Al. Corrosion product in the γ' depleted zone contained significant amounts of the refractory elements W, Ta and Ti and Ni, sulphur and oxygen.

Although the coating in general showed evidence of adequate sulphidation resistance, there were regions in which internal sulphidation was evident (figure 3.111a&b). This resulted in a "porous" type outer layer. The corrosion product in the "pores" was made up of the sulphides of Cr and Ni essentially with no evidence of oxides. The region adjacent to these "pores" was depleted of chromium. Figure 3.111b is a micrograph of a transverse cross-section showing corrosion process proceeding in the γ' depleted zone and internal sulphidation of the coating. The "pores" in the γ' depleted zone were filled with mainly Cr and Ni sulphides with no oxygen being detected.

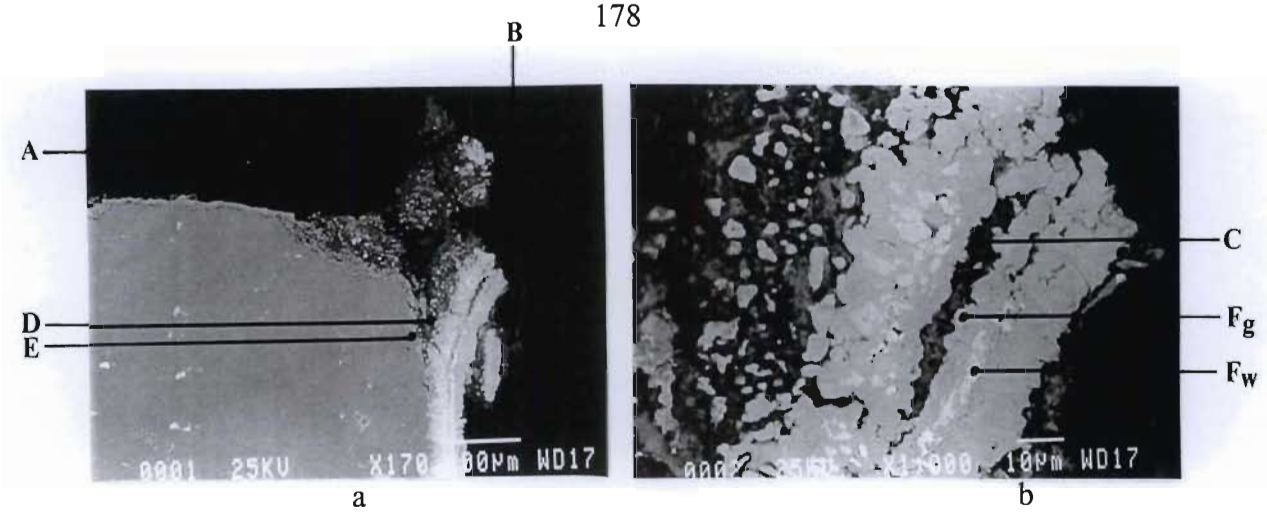

Elements	Weight percent						
	A	B	C	D	E	Fw	Fg
W	2.02	0.00	0.00	16.34	16.56	1.96	4.14
Cr	19.32	30.33	5.53	5.04	19.56	1.52	0.18
Co	4.29	1.75	3.11	1.36	5.68	2.34	7.38
Ni	24.64	17.02	23.03	13.07	42.00	28.08	42.00
Pt	0.00	0.40	2.76	0.00	0.00	53.87	40.40
Ta	3.14	1.95	8.31	14.80	5.53	3.67	2.74
Hf	3.36	2.86	12.67	1.15	1.48	1.99	0.70
Zr	0.00	0.66	2.15	0.10	3.82	0.07	0.00
Ti	2.13	2.11	3.84	9.49	1.21	1.42	0.12
Al	7.38	1.42	5.85	2.23	3.60	3.22	1.20
S	14.75	10.07	8.72	8.10	0.56	1.84	1.13
O	18.97	31.43	24.03	28.31	0.00	0.00	0.00

Figure 3.110 : Cross-section of platinum coated MAR-M002 after HTLCF in SO_2 showing peeling of coating and EDS analyses (S.R. 0.38%)

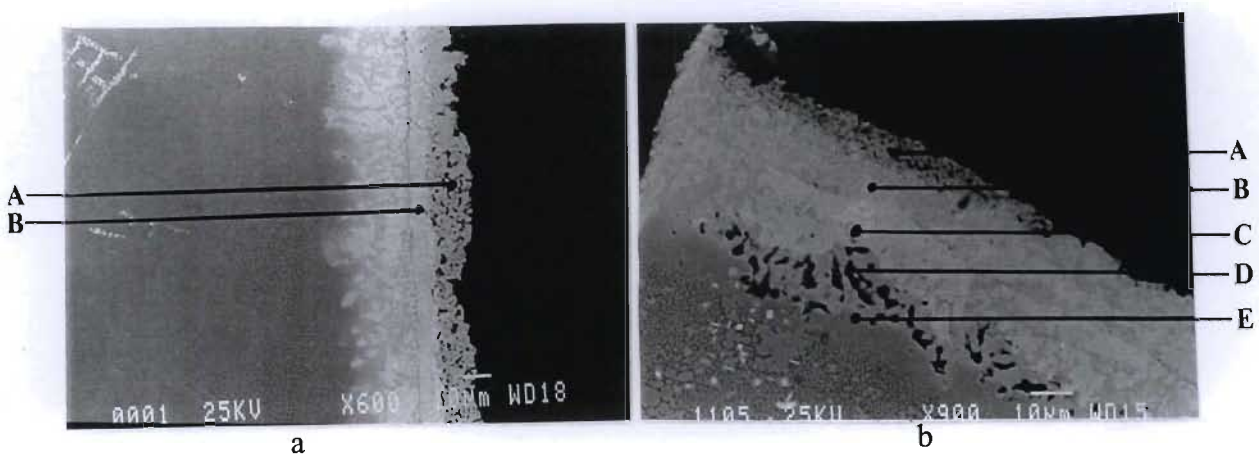

Elements	Weight percent		
	A (pore)	A (solid)	B
Al	0.00	2.20	3.64
Cr	19.98	1.85	5.03
Co	5.52	5.45	3.05
Ni	22.20	37.28	24.55
Pt	15.69	49.08	59.11
Ta	1.03	0.39	1.43
W	1.10	1.09	0.73
Hf	0.97	0.00	0.71
Zr	6.69	0.00	0.00
Ti	0.28	0.32	1.06
S	27.54	2.33	0.69
O	-	-	-

Elements	Weight percent				
	A (pore)	B	C	D	E
Al	3.54	3.50	0.96	0.46	1.93
Cr	16.06	2.80	0.85	28.38	7.04
Co	3.52	2.87	0.85	4.75	10.71
Ni	20.57	23.68	13.51	19.92	59.76
Pt	18.28	58.74	65.15	3.89	2.73
Ta	5.38	2.01	0.00	1.23	1.81
W	0.00	1.80	0.01	1.61	12.00
Hf	0.00	2.90	18.49	5.39	1.56
Zr	0.00	0.00	0.00	0.24	1.59
Ti	1.15	1.08	0.51	1.96	0.66
S	20.19	0.62	0.06	32.16	0.22
O	11.30	0.00	0.00	0.00	0.00

Figure 3.111 : Sulphidation of the external surface of the platinum coating after HTLCF in SO_2 (S.R. 0.38)

CHAPTER 4

4. DISCUSSION

4.1 Evaluation of the tested Materials Systems

4.1.1 Uncoated MAR-M002

The general analysis of the uncoated alloy indicated that there were no special features and the structure obtained was typical of that of a directionally solidified nickel-base superalloy. Dendritic grains had grown in the direction of solidification with the dendritic arms growing perpendicular to this direction.

The dendritic grain was made up of a high volume percent of cuboidal γ' produced during the aging heat treatment. The EDS analysis of the dendritic grain showed the typical γ' forming elements (Al,Ti and Ta) and solid solution strengthening elements (Cr, Co, W). It was evident that the carbide phases were concentrated in the interdendritic segregation zone. The carbide particles were of two forms, namely, large particles and smaller blocky carbides. The large carbide particles were made up of a mixture of Hf, Ta, W and Ti while the smaller blocky carbides were essentially Hf. These smaller blocky carbides had precipitated as fine random particles typical to that described in literature [19]. Another feature was that the γ-γ' eutectic structure was also concentrated at the interdendritic zone.

From the X-ray diffraction analysis it was evident that the principal phase present was $Ni_3(Al,Ti)$ γ' which conforms with the observations made in the microstructural analysis.

4.1.2 Aluminide Coated MAR-M002

The aluminide coating was produced by a packed cementation using the high temperature low activity (HTLA) process. The microstructure obtained consisted of three zones, namely, the coating layer, interdiffusion zone and base metal. In the HTLA process the aluminium activity is low and nickel diffuses outward at a higher rate than aluminium diffusing inwards and forms the NiAl coating zone. Due to the diffusion processes, there is always, to a certain extent, substrate alloying elements present in the coating layer which was evident in the chemical analysis of this layer. However, due to the low solubility of most alloying elements in the NiAl structure these elements will precipitated out as carbides, metals or topologically closed packed structures in the interdiffusion zone [82]. This was very evident in the EDS analysis of the interdiffusion zone showing a relatively high concentration of carbide forming elements W, Ti, Cr, and Ta and grain boundary strengthening elements Hf and Zr.

The coating layer was composed of essentially NiAl which was evident from the X-ray diffraction analysis. The presence of aluminium and chromium oxides was evident due to the enrichment of the coating layer with these elements.

4.1.3 TYPE I Platinum Aluminide Coated Mar-M002

The TYPE I platinum aluminide coating was produced by plating the sample with a 6-8μm layer of platinum followed by a HTLA aluminizing coating process and aging heat treatment. The microstructure obtained was similar to that of the aluminide coating consisting of three zones, namely, the coating layer, interdiffusion zone and base metal. Significant amounts of pack particles were observed in the coating layer. These were composed of essentially chromium rich particles and aluminium oxide (black particles). These particle were embedded in the coating during the aluminizing process.

The coating layer displayed a "single" phase structure with evidence of platinum rich particles being distributed randomly at the surface of the coating layer and platinum in solution in the coating. From the chemical analysis of different regions in the coating it was apparent that the platinum distribution in the coating was not consistent throughout the

sample. There was evidence of relatively high platinum content in some areas while other areas showed extremely small amounts of platinum. This phenomena could have occurred due to the platinum coating not being consistent on all surfaces of the sample analysed.

The final structure obtained was not typical of platinum aluminide coatings produce using the HTLA process, i.e., the presence of a $PtAl_2$ region on the outer region of the coating. Another feature that was significant was that of platinum existing in significant quantities in the interdiffusion zone. This had a important effect on the final morphology of the interdiffusion zone. Refractory elements were excluded from this region since platinum has the effect of reducing the diffusivity of these elements [106]. The absence refractory elements in the interdiffusion zone resulted in a columnar type structure with the TCP and carbides phases being virtually non-existent.

Although the typical coating structure was not obtained, Boone *et al* [108], did report variations in the coating morphology due to variations in the coating process parameters. The aluminium activity, which is difficult to control, plays a key role in the final microstructure. The aluminium activity of the pack could have increased and this would produce a "single" phase structure with platinum aluminide phases dispersed in it and platinum dissolved in the NiAl. From the microstructure obtained and the chemical analysis it was evident that the plating and aluminizing processes influenced the final microstructure significantly.

4.1.4 TYPE II Platinum Aluminide Coated MAR-M002

TYPE II platinum aluminide coated MAR-M002 was produced by the same method as the TYPE I platinum aluminide, however, the microstructure obtained was very different, with the morphology obtained being similar to that presented in literature [108]. The coating system consisted of a platinum rich outer region, a NiAl zone, interdiffusion zone and the substrate. The platinum rich outer zone consisted of a single phase, $PtAl_2$, layer and adjacent to this a two-phase region consisting of $PtAl_2$ and NiAl. The grey region in the platinum rich zone was essentially NiAl with platinum and $PtAl_2$ dissolved in it. The NiAl zone consisted of $PtAl_2$ and platinum "dissolved" in it.

The coating revealed a very low substrate alloy content. It was evident that platinum plays an important role in inhibiting substrate element diffusion into the NiAl zone.

The platinum content decreased as one moved towards the interdiffusion zone and was totally excluded from this region. This was in contrast to that observed in the TYPE I platinum aluminide coating where there were significant quantities of platinum in the interdiffusion zone. The interdiffusion zone revealed a composition and structure similar to that observed in the unmodified aluminide coating.

It must be noted that the TYPE I and TYPE II platinum aluminide coated samples were produced in different batches. This indicated that the difference in structures obtained was as a result of a variation in the coating process parameters.

4.1.5 2μm Platinum Aluminide Coated MAR-M002

This coating was produced due to the limitations of the platinum electroplating bath. A similar coating procedure was followed as for the TYPE I and TYPE II with the exception that the initial platinum coating was 2μm thick. The lower initial platinum coating thickness produced a coating with a very similar morphology to that of the TYPE II platinum aluminide, i.e., with the platinum rich outer zone, NiAl layer, interdiffusion zone and substrate. However, the platinum rich outer zone was not a continuous $PtAl_2$ layer but was a two-phase region of NiAl with platinum aluminide phases "dissolved" in it. This showed that the thickness of the initial platinum coating plays a significant role in the final phases produced and the microstructure of the coating. The lower platinum content applied was not sufficient to form a continuous $PtAl_2$ layer and the more stable phase under these conditions became Pt_2Al. The amount of platinum aluminide phases formed was significantly smaller when compared to that formed in the TYPE II platinum aluminide coatings. The overall thickness of the coating was also significantly thinner than the TYPE II platinum aluminide and was very similar to that observed in the conventional aluminide coating. Again as in the previous platinum aluminides discussed it was evident that platinum is very effective in inhibiting the diffusion of refractory elements into the coating. The NiAl single phase region contained platinum and platinum intermetallics of aluminium dissolved in it. There was also evidence of Al_2O_3 pack particles in the coating.

4.1.6 Platinum Coated MAR-M002

From literature and experiments performed it was established that platinum improved the high temperature corrosion properties of aluminide coated nickel-base superalloys. With this in mind it was decided to investigate the HTLCF properties of platinum coated nickel base superalloys without the aluminizing heat treatment. The samples were coated with a 4-6μm layer of platinum followed by a simulated aluminizing heat treatment and aging heat treatment. This heat treatment was in effect very similar to the prealuminizing heat treatments of platinum coated samples studied by Boone *et al* [115].

When the investigations of the platinum coated samples were undertaken it was done so under the assumption that the inert nature of platinum would provide effective protection against corrosion and also there would be sufficient ductility in the coating since platinum was being used as a "pure" metal. However, the interdiffussion and interaction of platinum with the substrate was not taken into account and became very evident in the microstructural analysis of these coated samples. The interdiffusion between the substrate alloying elements and platinum during the simulated heat treatment resulted in a coating thickness of approximately 17μm. SEM analysis of the coating revealed a "two" phase region consisting of "white" particles dispersed in a "grey" matrix. The "grey" region was rich in alloying elements and platinum, while the "white" regions were rich in nickel and platinum with a higher aluminium and titanium content. The microstructure obtained was similar to that observed by Boone *et al* [115]. It was also noted that platinum group metals had a high reactivity with Group IVB-VIB elements (Ti, Zr, Hf, Ta or W) [115]. Hence, there will exist selective interaction of platinum with substrate alloying elements. The outer region of the coating consisted of significant amounts of substrate alloying elements Al, Ti, Cr, Co, Ni, Hf, Ta and W. Below this region was a continuous layer of "white phase" rich in essentially Pt and Ni with significant amounts of Al, Ti, Cr and Co dissolved in it. The Cr, and Co content, however, was present in much smaller quantities than the "white" regions. This indicated that the platinum-aluminium and platinum-titanium intermetallic phases were concentrated in this region. The platinum intermetallics of Hf, Ta, W, Cr and Co were concentrated on the outermost region. From the chemical analysis of the coating it was postulated that platinum had diffused into the alloy at a higher rate than the alloying elements

diffusing out since platinum was detected in significant quantities to a depth of approximately 30μm.

The presence of platinum alters the microstructure of the substrate significantly, resulting in the dissolution/coarsening of the cuboidal γ' phase. This could have occurred due to platinum reacting selectively with titanium and aluminium and hence resulting in the depletion of these elements in the γ' phase. Platinum enhances the diffusion of aluminium and also has a high reactivity with Ti [115]. The presence of platinum hence increased the diffusion coefficient of Al and Ti in γ' and this in turn will result in an increase in the equilibrium molar concentration of aluminium in γ. Ripening of γ' is dependent on the diffusion coefficient of the γ' forming elements. If the diffusion coefficient of these elements are accelerated the γ' coarsening/depletion is accelerated. It was evident that platinum influenced the diffusion of aluminium and Ti which resulted in the γ' depleted zone. Nickel and cobalt platinum intermetallics are unlikely to form due to the high solubility of Ni and Co in platinum [174].

Another feature of the coating was the presence of porosity at the coating/substrate interface. Boone *et al* [115] noted Kirkendall porosity in the platinum coated samples which were exposed to prealuminizing heat treatments. This had occurred due to the preferential diffusion of certain alloying elements in the coating. This could explain the porosity present in the samples tested. The porosity could have also occurred due to contamination of the sample surface before the platinum coating was applied.

4.2 Failure Mechanisms of the Tested Materials Systems Under the Combination of HTLCF and Environment

Uncoated, aluminide coated, platinum aluminide coated and platinum coated MAR-M002 nickel-base super alloys were subjected to HTLCF in argon, air and Ar + 5%SO_2 at 870°C. The general result at a strain range of 0.66% indicated that the presence of the coating adversely effected the HTLCF in air and argon atmospheres (figure 4.1). However, in the sulphur containing environment the fatigue life was dependent on the coating system (figure 4.1). The aluminide and platinum coated alloys showed a decrease in fatigue life over the

uncoated alloy while the platinum modified aluminides showed an improvement in the fatigue life under the SO_2 environment. The margin of improvement was dependent on the coating morphology and platinum distribution in the coating. It was found that the mechanical properties of the coating was the factor that controlled the failure process in all the coating systems tested. In order to understand how the platinum aluminide coatings improved the life of the coated superalloys at high strain ranges it was necessary firstly to understand the failure mechanism of the coatings. This was analysed using the results obtained for the HTLCF tests performed in argon atmosphere since there was no active

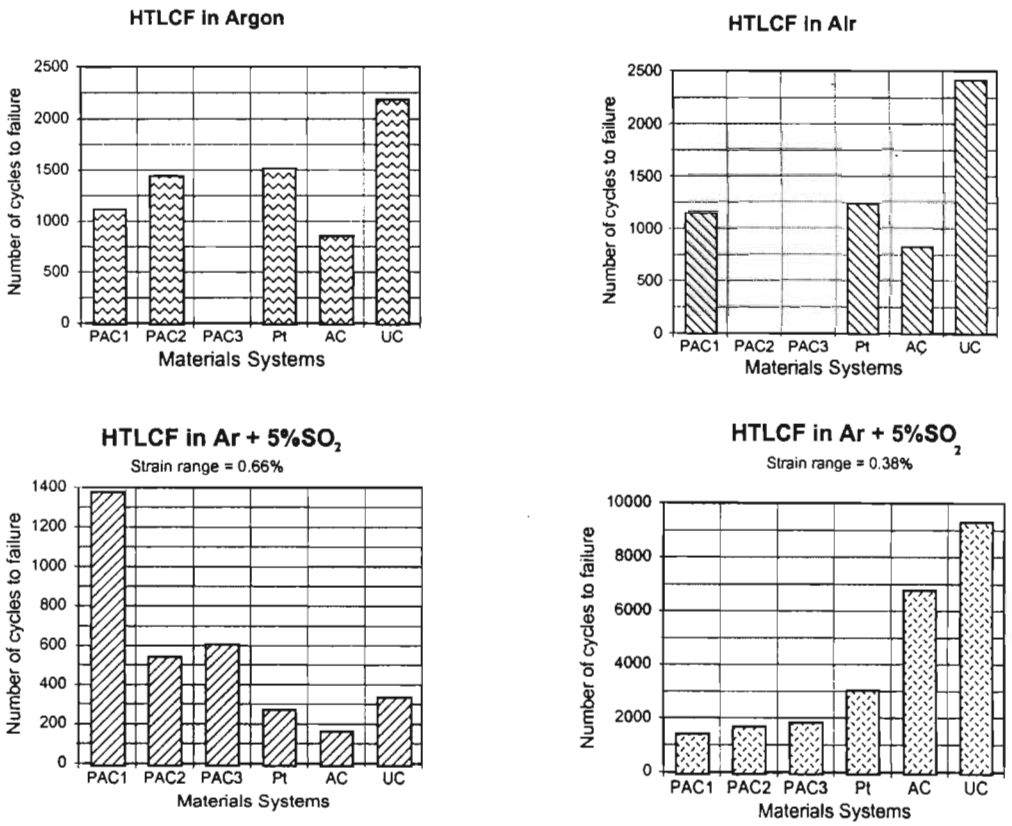

PAC1 = TYPE I Platinum Aluminide Coated MAR-M002
PAC2 = TYPE II Platinum Aluminide Coated MAR-M002
PAC3 = 2μPlatinum Aluminide Coated MAR-M002
Pt = Platinum Coated MAR-M002
AC = Aluminide Coated MAR-M002
UC = Uncoated MAR-M002

Figure 4.1 : Summary of HTLCF results

environment present. Any failure observed, was due purely to the mechanical failure of the coating. From these tests it became evident that the coating systems displayed fairly brittle mechanical properties and it was obvious that the strain range used was too large and resulted in mechanical failure of the coating very early in the fatigue tests. In order to allow the environment to play a more influential role in the failure mechanism HTLCF test were performed in only Ar + 5%SO_2 atmosphere at a strain range of 0.38%. Accelerated failure was observed in all the coating systems when compared to the uncoated alloy. Under these loading conditions the platinum aluminides performed very poorly when compared the aluminide coating. Although the platinum coating performed better than the platinum aluminide coated samples, it showed less resistance to fatigue loading than the aluminide coated material. Another factor that became very apparent from these tests was that the platinum content in the "single phase" type platinum aluminides (i.e TYPE I platinum aluminide) plays a significant role in the mechanical properties of the coating and hence the corrosion fatigue properties. The higher the platinum content the more brittle the coating.

All the final failures under fatigue loading occurred at a relatively high tensile load. This was independent of the coating system, environment and strain range being applied. This phenomena can be explained by the loading method used. The mechanical test rig used did not have the facility for strain control of the loading cycle, hence, in order to achieve this the displacement of the actuator piston was used to achieve the desired strain ranges. A LVDT was used to monitor the strain across the neck in order to ensure that the test was being performed at the desired strain range. However, once the critical crack length had been reached the strain across the neck of the sample began to increase rapidly and this could not be accommodated by the control of the actuator piston and hence this resulted in the failure of the samples at high tensile loads and not a gradual drop off in the tensile load. Since the tests were consistent for all the samples tested, and this problem only became apparent a few cycles before failure, the comparison of the results can be regarded as valid for the tests performed. This was a comparative study of the different coating systems and the main aim was to obtain the typical failure mechanisms of the coatings under the combination of SO_2 containing environment and fatigue loading.

4.2.1 Failure Mechanisms in Argon Atmosphere

The summary of the results obtained in inert argon atmosphere revealed that the uncoated alloy performed the best and the conventional aluminide coated alloy the worst. All the coating systems in general performed poorly in comparison with the uncoated alloy. Of the coating systems investigated, the pure platinum coating produced the best low cycle fatigue results.

The poor fatigue life of the coating systems could be ascribe to the unique mechanical properties of each coating, i.e., the inherent brittleness of the intermetallic phases formed during the coating process.

4.2.1.1 Failure of Uncoated MAR-M002

The HTLCF of uncoated MAR-M002 in argon was due to pure mechanical loading. The crack initiation had occurred preferentially at the interdendritic segregation zone due to the inherent weakness of this region under high temperature cyclic loading. The crack propagation was relatively straight and there was no evidence of crack tip blunting and/or branching of the crack. The sharp crack tip was due to the "sharpening" of the crack tip under compressive loading. In the absence of a reactive environment there was no corrosion product to prevent closure of the crack under compressive loading. Crack tip blunting due to environmental interaction ahead of the crack tip was also avoided. The presence of the sharp crack tip was conducive to crack propagation and hence failure.

4.2.1.2 Failure of Aluminide Coated MAR-M002

The aluminide coated superalloy may be regarded as a composite with the coating having very brittle properties and the substrate being fairly "ductile". Under tensile loads the NiAl coating fractured in a brittle fashion. It was evident that the failure of the coating had occurred early in the fatigue test. The crack was straight and propagated perpendicular to the direction of loading. The crack in the coating resulted in a high stress concentration point at the coating substrate interface (figure 4.2). Initiation of fatigue cracks in the substrate had

occurred at the points where the coating had failed, and did not show any preference to initiate at the interdendritic zones. The controlling factor in the HTLCF of the aluminide coating was the failure/cracking of the aluminide coating. Failure of the coating accelerated the initiation of fatigue cracks in the substrate and accelerated the failure of the material system. Fatigue crack propagation in the substrate proceeded as in the uncoated alloy.

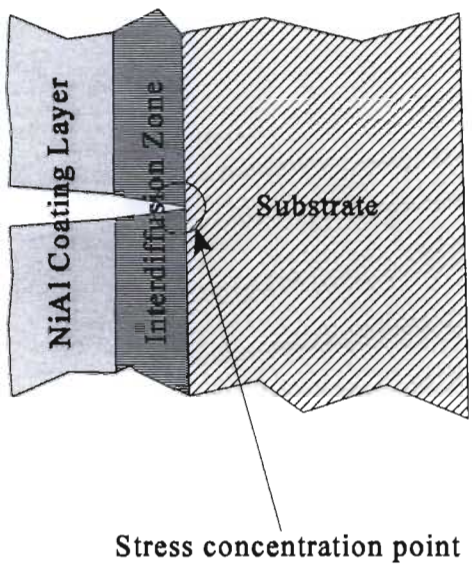

Figure 4.2: Brittle failure of aluminide coating due to mechanical loading

4.2.1.3 Failure of TYPE I Platinum Aluminide Coated MAR-M002

Although the TYPE I platinum aluminide coating had a similar morphology to the aluminide coated superalloy, the presence of platinum altered the mechanical properties of the coating significantly. It was apparent that the presence of platinum in the NiAl structure slowed down the crack propagation. An additional feature which also benefited the fatigue properties of the coating was the presence of pack particles in the coating. These particles had the effect of providing "barriers" to the crack propagation.

A schematic illustration of the failure mechanism for the TYPE I platinum aluminide coating is presented in figure 4.3. Brittle fatigue cracks were initiated on the surface. These cracks did not propagate at a high rate through the NiAl zone due to "obstructions" encountered in

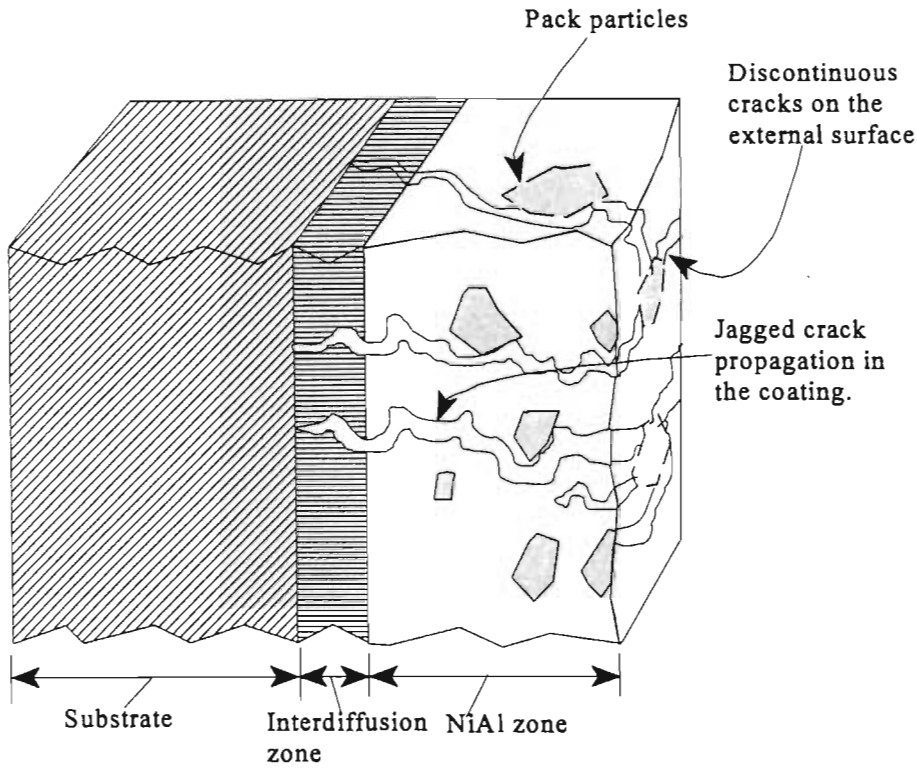

Figure 4.3 : Cracking of TYPE I platinum aluminide coated samples after HTLCF in argon

the NiAl crystal structure. This was deduced from the "jagged" path followed by the crack in the coating. When the propagating crack encountered particles in the coating the direction of the propagating crack direction changed due to the obstruction created by these particles. This had the effect of further slowing down the crack propagation through the coating. The crack formation around the circumference of the fatigue sample was also hindered by the presence of pack particles which resulted in the random discontinuous cracking observed on the external surface of the sample.

The increase in HTLCF life in argon atmosphere over the aluminide coating was due to the slower crack propagation of the fatigue crack through the coating. Once the crack had penetrated the coating, crack initiation sites at the coating/substrate interface was created. Crack initiation and propagation then proceeded in the substrate. Again as in the aluminide coating the fatigue life of the material system was controlled by the failure of the coating. Although the TYPE I platinum aluminide coating showed a higher resistance to fatigue crack propagation, the brittle nature of NiAl resulted in the lower life compared to the uncoated alloy.

4.2.1.4 Failure of TYPE II Platinum Aluminide Coated MAR-M002

The TYPE II platinum aluminide coated samples again showed an increase in HTLCF life over the conventional aluminides in the argon atmosphere. However, this coating also displayed a brittle nature with a network of cracks being observed on the external surface of the fatigue sample. This was due mainly to the presence of a continuous layer of brittle $PtAl_2$ on the external region of the coating. Fatigue cracks were initiated in the $PtAl_2$ on the surface of the coating.

Although this surface was very brittle, the NiAl layer beneath the $PtAl_2$ proved to be more resistant to crack propagation. The failure of the coating could be likened to laminated glass. The external brittle $PtAl_2$ layer fractured similar to glass but was held together by the NiAl layer which was more ductile and resistant to crack initiation and propagation (figure 4.4). The mechanical properties of the NiAl zone was altered by the presence of platinum which was probably in solid solution in the crystal structure and there may have been some $PtAl_2$ dispersed in this region. The platinum content in the NiAl zone played an important role in the mechanical properties of this region. The NiAl region immediately adjacent to the platinum rich outer layer was more susceptible to cracking than the low platinum content region.

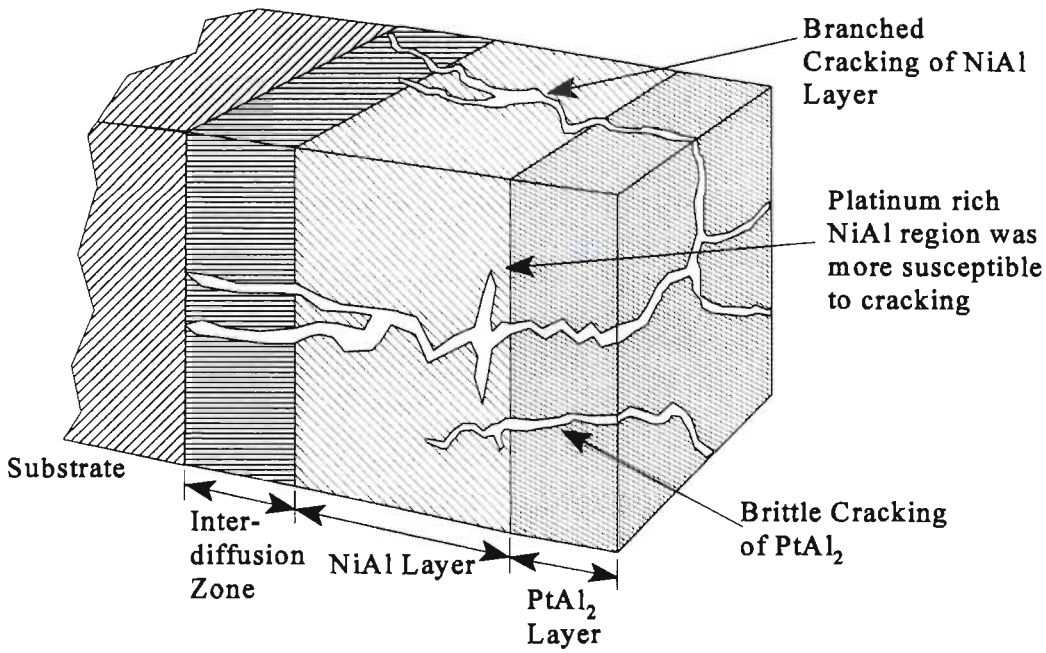

Figure 4.4 : Cracking of the TYPE II platinum aluminide coating after HTLCF in argon

The nature of the crack propagation indicated that there was a "crack blocking mechanism" present in the NiAl zone in the form of either discrete particles of $PtAl_2$ or platinum altering the NiAl crystal structure such that it changed the deformation process ahead of the crack tip. This resulted in the crack having to change its path and in doing so slowed the crack propagation. The crack "blocking" behaviour of the NiAl region resulted in the branching of the crack in certain areas.

Another feature that must be noted was the cracking of the NiAl layer just below the $PtAl_2$ region, parallel to the interdiffusion zone. This cracking had the effect of delaminating the $PtAl_2$ outer region, which was observed on the external surface as well as in the transverse cross-section.

The "45° cracks" observed in the fractography analysis was produced by the mechanism illustrated in figure 4.5. Once the propagating fatigue crack had penetrated the substrate to a sufficient depth, the tensile load did not act uniaxially on the material supporting the load. This resulted in a bending stress in the material under the tensile half of the fatigue cycle. The combination of tensile load and bending load resulted in the "45° cracking" of the brittle $PtAl_2$.

As in the TYPE I platinum aluminide coating the factor that was most influential on the

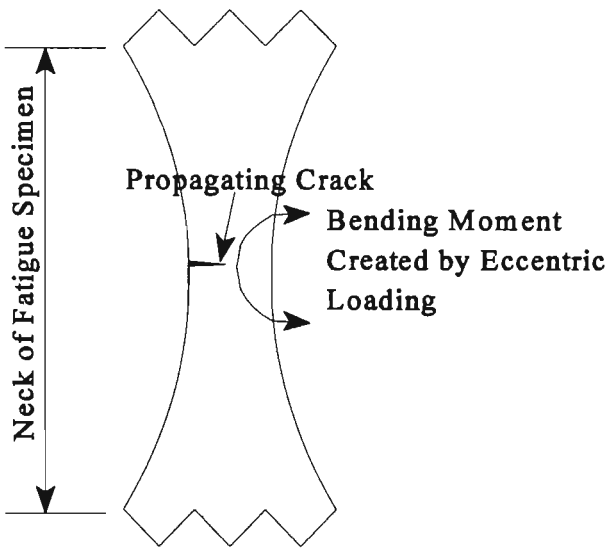

Figure 4.5 : Mechanism that may have produced the cracks in the coating at an angle of 45°

As in the TYPE I platinum aluminide coating the factor that was most influential on the failure mechanism was the modification of the NiAl region with platinum. This resulted in a crack "blocking" mechanism which slowed down the crack propagation and enhanced the overall fatigue life of the coating system under the inert argon environment.

Although this coating showed an improvement over the conventional aluminide and the TYPE I platinum aluminide it resulted in an accelerated failure when compared to the uncoated material. This was due mainly to the brittle nature of the coating which created fatigue crack initiation sites in the substrate. The crack propagation in the substrate proceeded as observed in the uncoated alloy.

4.2.1.5 Failure of Platinum Coated MAR-M002

The platinum coating produced the highest HTLCF life of the coating systems tested in argon. The cracking of the coating was not as severe as that observed in the aluminide coated samples. The platinum did, however, modify the surface of the fatigue sample resulting in embrittlement of the surface. In these samples, the formation of intermetallic phases with the substrate alloying elements caused embrittlement of the surface. Another feature was the continuing change in the surface properties due to the interdiffusion of platinum and alloying elements. The coating thickness had grown from 17μm in the as received condition to approximately 45μm after the HTLCF test in argon. As the high temperature exposure period increased the "white " regions became smaller discrete particles and the "grey" regions became more prominent. It was in this region that the intermetallics of the substrate alloying elements was concentrated, hence accounting for the brittleness of this region.

Cracks were initiated in the "grey" region due to its brittle nature. The fatigue crack also tended to propagate through this region (figure 4.6a). The platinum rich "white" regions acted as crack "stoppers", forcing the crack to propagate around these particles. This slowed down the crack propagation through the coating. In general, it was found that the crack initiation in the substrate had occurred in the interdendritic segregation zone, which was a similar behaviour to the uncoated alloy.

Another feature in the coating which probably contributed to its poor performance was the presence of porosity at the substrate/coating interface. This was most probably Kirkendall porosity which resulted from the preferential diffusion of certain alloying elements outwards. The porosity was most prominent in the regions where the fatigue cracks had been arrested at the dendritic grains.

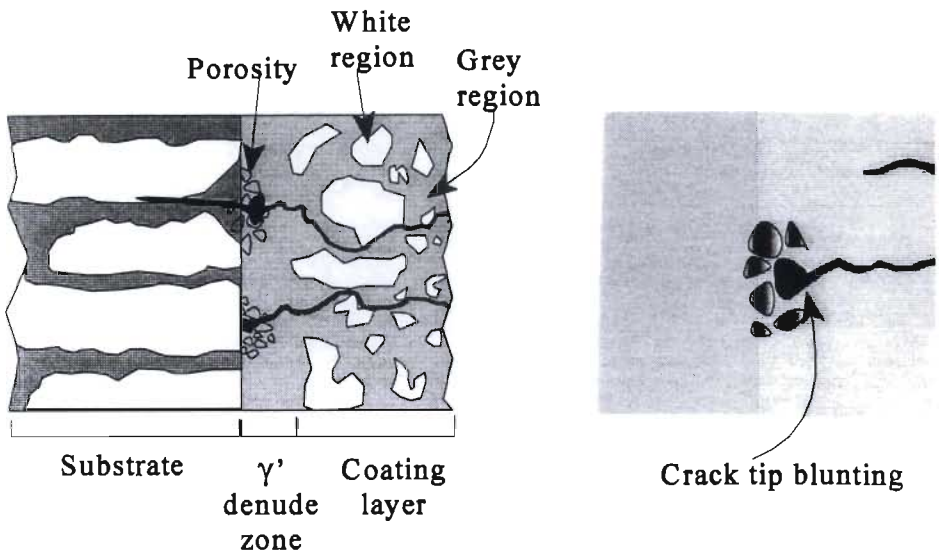

Figure 4.6 : a) Crack propagation through platinum coating after HTLCF in argon
b) Crack tip blunting due to porosity

From the characterization of the sample it was evident that the Kirkendall porosity is an inherent property of the coating, hence, this is going to be present even without fatigue loading. The extent of the porosity will be dependent on the exposure time of the specimen. Once the propagating fatigue crack "broke" into the porous region, the crack tip was blunted reducing the stress concentration at the crack tip (figure 4.6b). This resulted in the crack being arrested and the crack had to be "reinitiated" in order for propagation to proceed. Coalescence of these pores resulted in delamination of the coating.

From the HTLCF tests performed in argon it can be seen that the platinum coated sample formed the bridge between the aluminide and modified aluminides, and the uncoated samples. Platinum modified the material surface such that it retained a degree of ductility but was sufficiently brittle to initiate fatigue cracks earlier than that observed in the uncoated sample.

The failure of the sample was controlled by the initiation and propagation of the fatigue crack in the coating layer. However, in this case the interaction of the platinum with the substrate was very evident in the growth of the coating thickness. Another factor that must have contributed to the lower fatigue life when compared to the uncoated alloy was the dissolution of the γ' phase at the coating substrate interface. It was evident from these tests that the platinum did not serve the purpose it was supposed to; that was to provide a relatively "ductile" corrosion resistant layer.

4.2.2 Failure Mechanisms in Air Atmosphere

Due to the limited number of samples available HTLCF tests were only performed on the TYPE I platinum aluminide, platinum and aluminide coated samples, and the uncoated sample. From these results it was evident that the uncoated alloy performed the best and the aluminide coated sample the worst.

4.2.2.1 Failure of Uncoated MAR-M002

The uncoated alloy displayed a higher life under air environment compared to the argon atmosphere. It was apparent that the uncoated alloy was susceptible to oxidation. There was evidence of oxidation on the fracture surface and at the propagating crack tip. The corrosion product on the fracture surface was a mixture of oxides of the alloying elements of the substrate with nickel and oxygen being the most prominent.

The oxidation behaviour was believed to be of a similar mechanism to that described in literature [30] with a mixture of oxides forming initially until the more stable oxides, Cr_2O_3 and Al_2O_3 (figure 4.7) start to become more prominent. However, since the amount of aluminium and chromium was relatively small, it was not possible to maintain a continuous layer of these oxides, hence, making the alloy more susceptible to oxidation.

The crack initiation had occurred preferentially at the interdendritic zones on the external surface. The crack propagation was a mixed trans/interdendritic mode and branching and crack tip blunting was observed. This had occurred due to the synergistic effect of oxidation at the crack tip and mechanical loading. It was evident that nickel oxides were the prominent

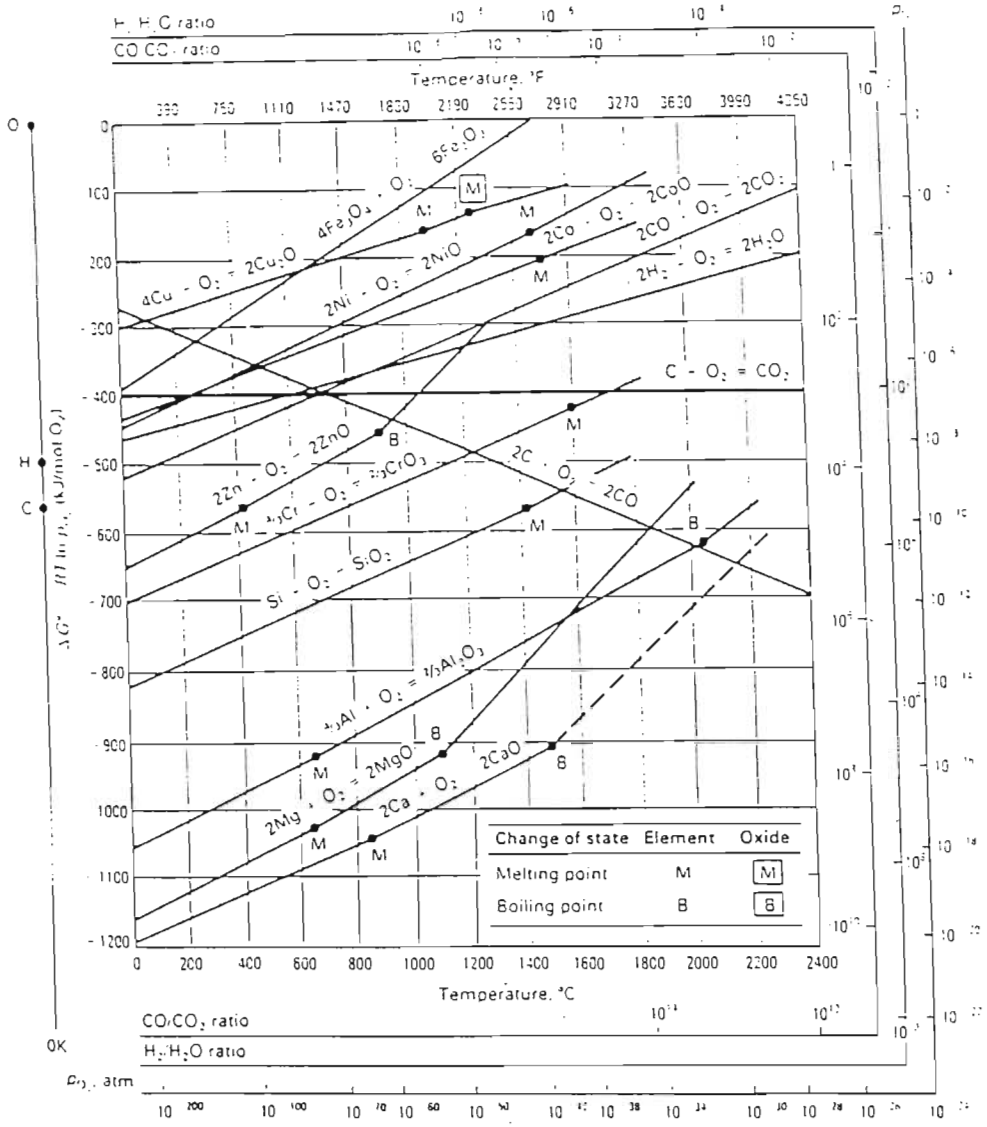

Figure 4.7 : Standard Gibbs free energy of formation of selected oxides as a function of temperature [176]

phase at the crack tip due to the high nickel content in the alloy. From the Gibbs Free energy curves for the formation of metal oxides (figure 4.7) it was obvious that the aluminium and chromium oxides were much more stable than nickel oxides, hence, even though these elements are present in relatively small quantities, they will be selectively oxidized. Internal oxidation of the crack tip resulted in embrittlement of this region [66]. Under the compressive cycles, cracking of the oxide created sites for branching to occur. The γ' depleted region adjacent to the crack edge resulted from the selective oxidation of aluminium. The failure mode, i.e, blunting of the crack tip and branching, has been reported in literature [66] and accounted for the increase in fatigue life over those performed in argon atmosphere.

4.2.2.2 Failure of aluminide coated MAR-M002

From literature and high temperature exposure tests performed in air it was evident that aluminide coatings were resistant to oxidation. The accelerated failure observed in air compared to the uncoated alloy was due mainly to the mechanical failure of the coating.

Once the coating fractured the air environment was transported to the crack tip in the coating where oxidation of the substrate proceeded (figure 4.8). Similar results were observed by Czech *et al* [171] where the creep rupture life was influenced by the cracking of the chrome-aluminide coating. The corrosion protection function of the coating was effectively bypassed due to the cracking of the coating. The cracks in the coating had the additional effect of creating stress concentration points at the coating/substrate interface which, combined with the materials susceptibility to oxidation accelerated the initiation of fatigue cracks in the substrate. The crack propagation in the substrate was of a similar mechanism to that observed in the uncoated alloy. The edge of the cracks in the coating showed no evidence of corrosion which was probably due to the formation of a stable Al_2O_3 early in the oxidation process. This indicated that the aluminide coating was not suitable under conditions of high stress due to its brittle nature. This type of coating will perform most effectively under conditions of much lower mechanical stresses.

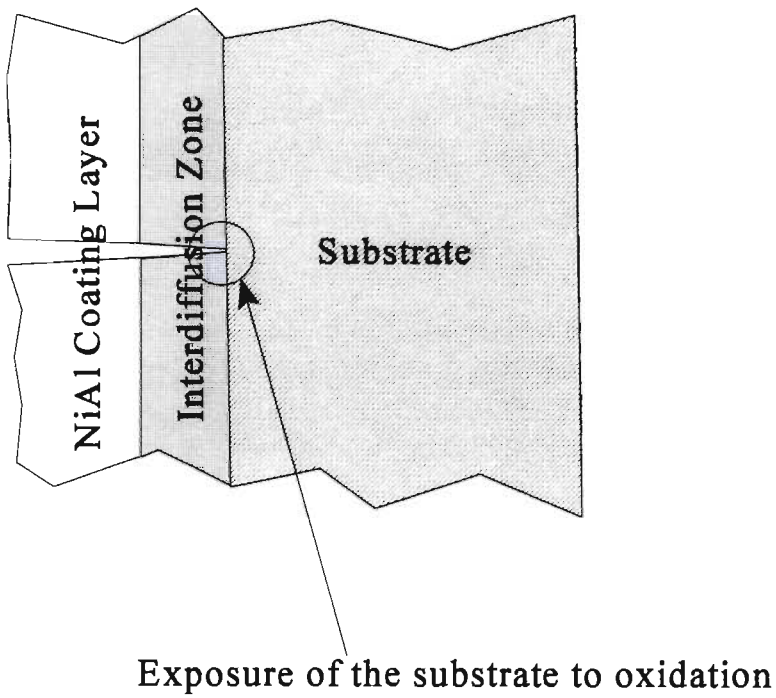

Figure 4.8 : HTLCF failure of the aluminide coated MAR-M002 in air

4.2.2.3 Failure of TYPE I Platinum aluminide coated MAR-M002

The failure of TYPE I platinum aluminide coated MAR-M002 in air atmosphere was again controlled by the failure of the coating due to mechanical loading. It was evident that the coating layer was significantly more resistant to oxidation than the substrate with no evidence of oxidation along the crack in the coating. The crack in the substrate did show evidence that the substrate had a higher susceptibility to oxidation.

The failure mechanism of the coating was the same as that described in the HTLCF failure in argon. Although the coating offers effective protection against oxidation, the brittleness of the coating lowers the overall life of the coated alloy. The improvement in fatigue life over the aluminide coating was mainly due to the improved mechanical properties of the coating. Again, once the crack had propagated through the coating, stress concentration points were created at the coating/substrate interface. This combined with the environment resulted in the crack initiation in the substrate.

4.2.2.4 Failure of Platinum Coated MAR-M002

The HTLCF life of the platinum coated sample in air atmosphere was lower than that observed in the argon atmosphere. In the HTLCF tests in argon atmosphere, it was established that the modification of the material surface with platinum resulted in the formation of brittle phases which assisted in the crack initiation and propagation. It was evident that the surface oxidation properties were also influenced by the presence of platinum. The relative brittleness of the coating surface facilitated the initiation of cracks but did not provide additional oxidation resistance.

Oxidation occurring at the crack tip altered the crack propagation mode through the coating with the results indicating a "straighter" crack through the coating. Although the white particles did show some resistance to crack propagation, they were not as effective as that observed in the argon atmosphere. The oxidation process occurring at the propagating crack tip depleted this region of the reactive elements (aluminium) resulting in the alteration of the chemical structure which in turn resulted in the change in the mechanical properties (figure 4.9). This resulted in the crack propagation in the coating being relatively straight. The γ'

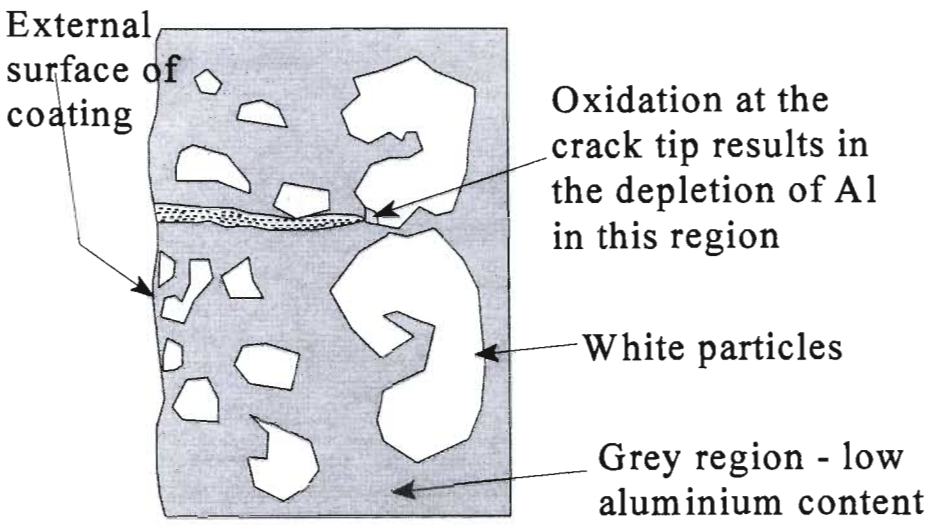

Figure 4.9 : Mechanism of fatigue crack propagation in the platinum coating in air atmosphere

depleted zone was shown to be the region most susceptible to corrosion; probably due to the reduced aluminium content in this region.

Once the fatigue crack had propagated through the coating the crack propagation in the substrate was the same as that observed in the uncoated sample. Crack initiation and propagation occurred preferentially in the interdendritic zone, proving this region to be most susceptible to HTLCF. The crack propagation mode in the substrate was trans-interdendritic.

The absence of porosity in this particular sample could have also played a significant role in decreasing the fatigue life when compared to the argon environment. It was noted that the porosity had a blunting effect on the fatigue crack tip, thereby slowing down the initiation of the fatigue crack in the substrate. In this sample there were no evidence of porosity, hence the crack blunting effect was absent. This allowed for the crack to propagate relatively unhindered into the substrate.

The general oxidation behaviour of the platinum modified surface indicated that although it was more susceptible to oxidation than the aluminide and modified aluminide coatings, it was more resistant than the substrate. However, the reduction in fatigue life over the uncoated sample was mainly due to the detrimental effect on the mechanical properties of the surface.

4.2.3 Failure Mechanisms in Ar +5%SO_2

The strain range selected for the HTLCF tests was 0.66% for all the environments tested. However, due to the aggressive nature of the sulphidation attack, the HTLCF was accelerated with a severe reduction in the fatigue life with the exception of the TYPE I platinum aluminide. The premature failure of the coated samples was attributed to the mechanical failure of the coating combined with the severe sulphidation attack. The mechanical failure of the coatings did not give a true reflection of the coatings sulphidation properties. It was hence decided to run a series of HTLCF tests in the SO_2 containing environment at a lower strain range of 0.38% in order to establish a more accurate representation of the sulphidation properties of the coating.

Failure in Ar + 5%SO_2 was composed of an incubation period followed by crack initiation and propagation. The incubation period was the initial sulphidation attack prior to crack initiation in the substrate (this included the crack initiation and propagation through the coating). Crack initiation was considered as when the fatigue crack was initiated in the substrate. From the results obtained, it was established that the incubation period controlled the fatigue life of the materials system. This was controlled by the combination of sulphidation and fatigue failure of the coating.

4.2.3.1 Failure of Uncoated MAR-M002

An accelerated failure was observed in the SO_2 containing environment. The substrate was susceptible to the sulphidation attack with severe sulphidation of the external surface close to the fracture and fracture surface being observed. It was apparent from the chemical analysis that the corrosion product was made up of oxides and sulphides due to the SO_2 breakdown via the following reaction:

$$SO_2 \rightarrow S + O_2$$

The HTLCF in Ar + $_5$%SO_2 consisted of the incubation period, crack initiation and crack propagation stages. During the incubation period severe sulphidation of the external surface occurred resulting in a "layered" structure (figure 4.10) with each layer having distinctive

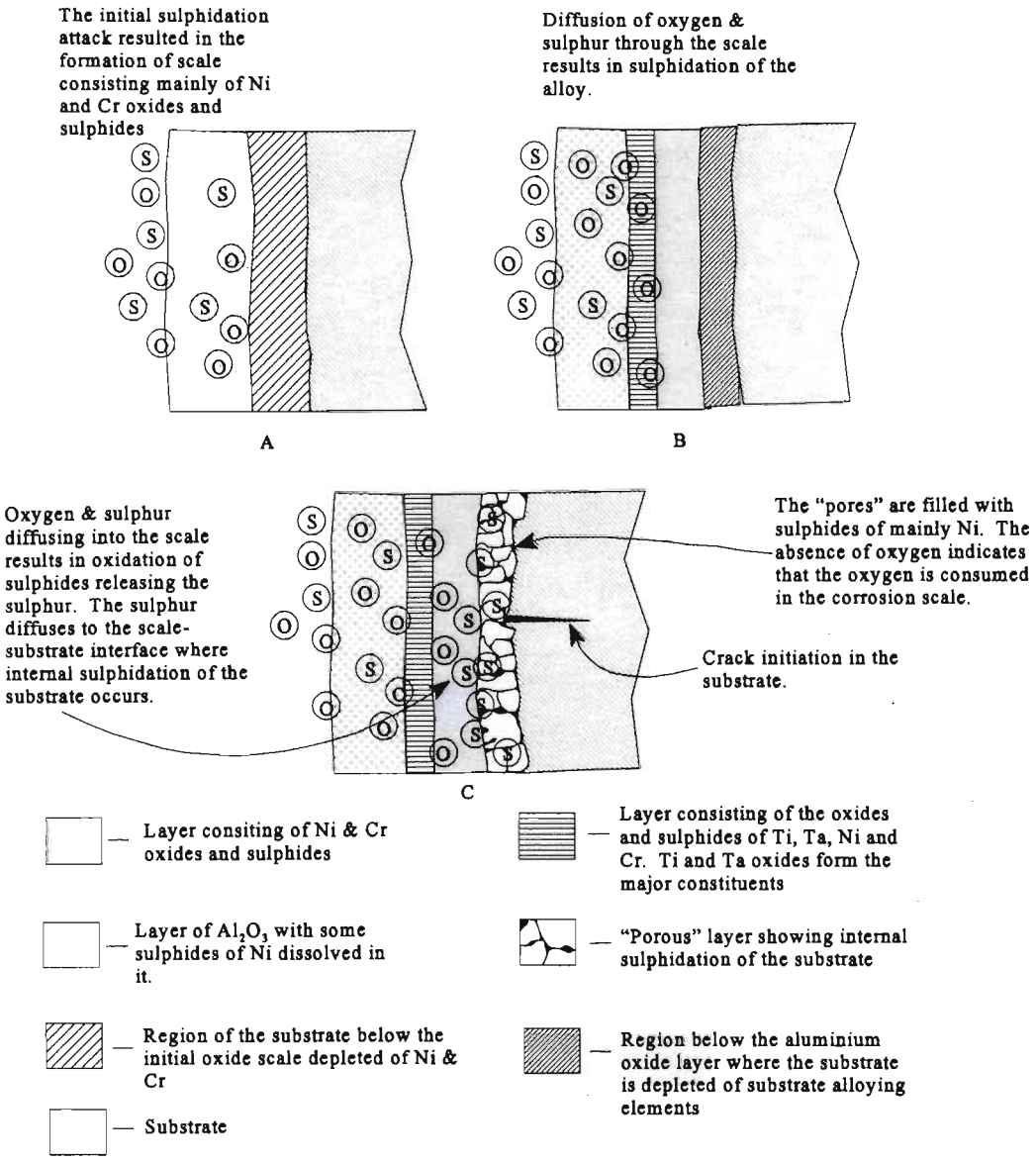

Figure 4.10 : Mechanism of sulphidation of the uncoated MAR-M002 after HTLCF in Ar + 5%SO_2

chemical properties. The mechanism of the corrosion process was as follows (Refer to figure 4.10):

The initial sulphidation attack resulted in the formation of a scale consisting of mainly Ni and Cr oxides and sulphides. The alloy below this corrosion scale became depleted of these elements (figure 4.10a). The diffusion of oxygen and sulphur through the scale resulted in the oxidation of this region. The oxidation mechanism will be the same as that observed in the case of alloys. Initially a mixture of oxides of the alloying elements will form followed by formation of the more stable oxide phases at the substrate-corrosion scale interface. This resulted in the "continuous" Al_2O_3 below a layer rich in Ti and Ta oxides (figure 4.10b). It must be noted that although the oxidation reaction was predominant, there was a significant

amount of sulphides also present due to the oxygen partial pressure not being sufficiently high for the formation of a protective oxide scale. The morphology of the corrosion scale was very similar to that presented for alloy CMSX-4 tested in air at 100°C for 1000 hours [151], hence, it was observed that the sulphidation mechanism was very similar to that of oxidation.

The Ni and Cr content was higher at the external region of the scale due to the tendency for the ions of these elements to diffuse outwards to the environment/scale interface. Sulphur and oxygen diffused into the scale in significant quantities. This resulted in the oxygen reacting with the sulphides present in the corrosion product which released the sulphur [175]. The sulphur released during this oxidation reaction, combined with that diffusing into the scale at the environment/scale interface, diffuses through the scale to the scale/substrate interface. The oxygen was consumed in the corrosion scale, hence, the corrosion product at the scale substrate interface consisted of only sulphides. The formation of low melting point nickel sulphides was due mainly to the depletion of the reactive elements Cr and Al from the substrate due to oxidation. This resulted in the "porous" region below the scale, and the γ' depleted zone. The sulphidation attack had the effect of reducing the effective cross-sectional area and creating stress concentration points on the surface which resulted in the accelerated crack initiation in the sample. Once the crack was initiated, it was evident that crack propagation was controlled by the sulphidation attack at the crack tip. The EDS analysis of the corrosion product at the crack tip indicated that the sulphide content at the crack tip was made up essentially of Ni and Cr and there was no evidence of oxides. The presence of low melting point Ni sulphides at the crack tip resulted in catastrophic sulphidation in the region which accelerated the crack propagation. The preferential sulphidation of the stable elements Al and Cr, depleted the alloy of these elements ahead of the crack. Since sulphur was present in sufficiently high quantities Ni sulphides were formed which enhanced the sulphidation attack. Under the combination of HTLCF and SO_2 environment, the diffusion of sulphur through the oxide scale was enhanced due to defects created in the corrosion scale. This allowed for the accelerated attack of the substrate.

From the HTLCF tests performed at a SR of 0.38% it was evident, from the corrosion scale morphology, that the sulphidation mechanism was the same. Due to the lower stress applied, the fatigue life was significantly increased. The corrosion scale produced was significantly thicker due to the longer exposure. There was evidence of the corrosion scale spalling off

in regions which was due to the combination of compressive stress build-up in scale and the mechanical loading of the sample. The mechanical loading again played a significant role in the transport of sulphur through the corrosion scale by creating defects in the oxide scale. The much increased life in the specimen was mainly due to the lower stress applied and hence, the increased time to crack initiation and the decrease in crack propagation rate. The sulphidation attack at the crack tip again controlled the fatigue crack propagation rate.

4.2.3.2 Failure of Aluminide Coated MAR-M002

HTLCF of aluminide coated MAR-M002 in the Ar + 5% SO_2 showed a severe reduction in fatigue life at the strain range of 0.66%. The number of cycles to failure was observed to be approximately 3 times that observed for similar tests performed [17]. This was mainly attributed to a change in the experimental apparatus which enabled more accurate control of the test environment. The mechanical properties of the coating played a significant role in the final failure of the fatigue sample. The cracking of the coating due to the high stresses resulted in the incubation period being effectively omitted. The cracking of the coating initiated the fatigue crack in the substrate. From this evidence it became apparent that the most significant aspect of the fatigue failure that was influenced by the sulphidation environment, was the crack propagation in the substrate. It has shown that the incubation period before the crack initiation in the substrate was the controlling factor in HTLCF in the SO_2 bearing atmosphere.

There were additional cracks observed in the coating which had not propagated into the substrate. These had occurred due to brittle failure of the coating but there was insufficient time for them to propagate into the substrate due to high propagation rate of the initial fatigue crack. Sulphidation attack in cracks present in the coating occurred by the following mechanism (figure 4.11):

SO_2 filled the crack once the coating had fractured and stagnation of gas occurred (figure 4.11a). The corrosion process that occurred was similar to that observed in the uncoated alloy (figure 4.11b). In this case, however, a mixture of Al and Ni oxides and sulphides fill the crack with aluminium oxide being more prominent. The sulphide phases again tended to form closer to the corrosion scale/coating interface indicating that oxides formed first and

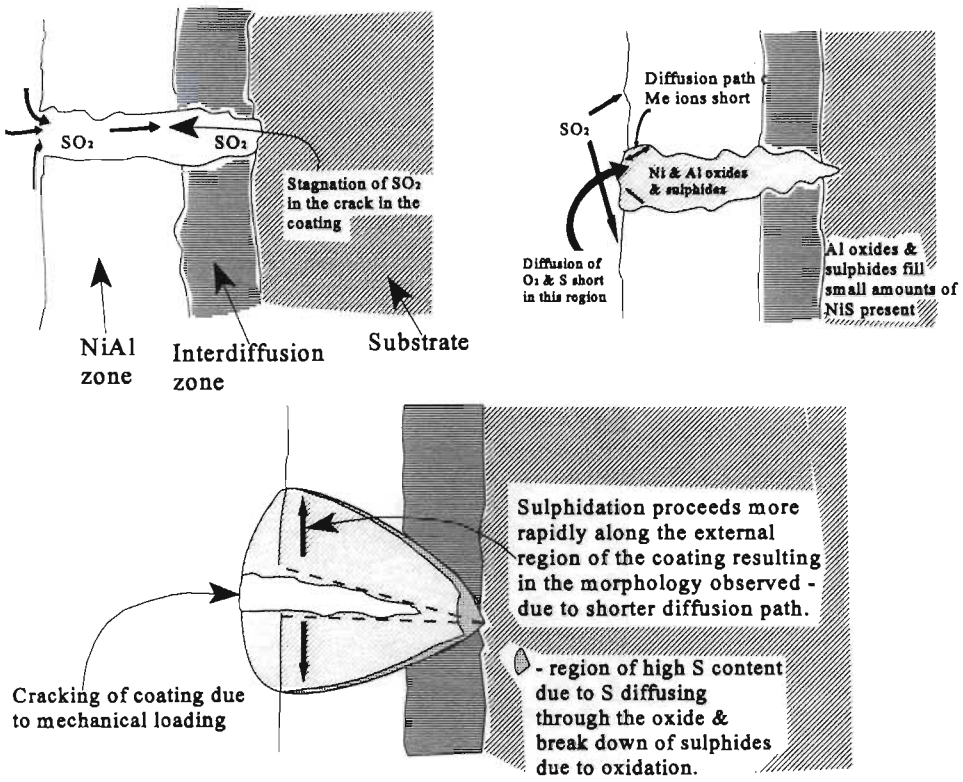

Figure 4.11 : Mechanism of corrosion that occurred in the cracks of the aluminide coating after HTLCF in Ar + 5%SO_2 at 870°C

sulphur was transported via the corrosion product towards this region. Transport of sulphur in the oxide layer was influenced by the mechanical loading which was evident in results. The diffusion path for the metal ions and gas ions was much smaller at the surface, hence resulting in higher corrosion rate at the external surface of the coating.

Another feature that was evident, was that the interdiffusion zone showed a higher susceptibility to sulphidation attack; probably due to the high refractory element content in this region. From literature, it was reported that refractory elements had a detrimental influence on the sulphidation resistance of Ni based superalloys [157].

The cracks were filled with oxides which should have "stopped" or slowed down the sulphidation attack of the substrate, however, due to the mechanical loading, cracking of the oxides occurred under the compressive loading cycle which provided a path for the SO_2 gas to be transported to the crack tip. The following failure mechanism for the failure of the Al coating under high strain conditions is proposed (figure 4.12):

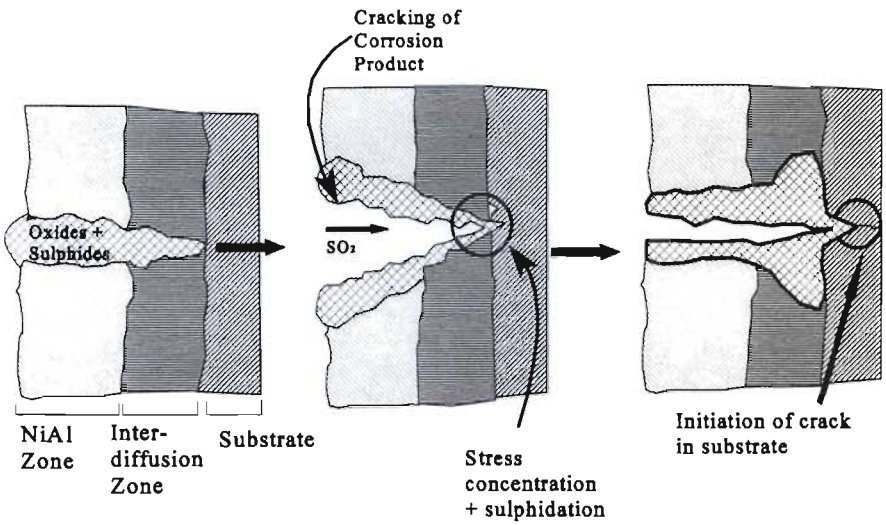

Figure 4.12 : Mechanism that resulted in the crack initiation in an aluminide coated MAR-M002 sample after HTLCF in Ar + 5%SO_2

the failure of the coating occurs via mechanical loading. The crack was filled with corrosion product (mainly oxides). Cracking of the corrosion product occurred during the compressive loads. This allowed gas to be transported to the crack tip during tensile loading. Sulphides in the corrosion scale were oxidized, releasing sulphur which was transported to crack tip. The interdiffusion zone which has a higher susceptibility to sulphidation allows sulphidation to proceed parallel to the substrate. The high stress concentration at the crack tip combined with the sulphidation attack initiated the fatigue crack in the substrate (figure 4.12)

The "porous" nature of the coating at the coating/fracture surface interface occurred by the "fluxing" process illustrated in fig. 4.13. The opening and closing of the crack under the cyclic loading resulted in spalling of the oxide scale from the fracture surface. Hence, the protective oxide scale was "eroded" away continuously. This resulted in the aluminium being depleted from the coating by the repeated sulphidation attack since aluminium was most reactive. This allowed for the diffusion of sulphur into the coating and the formation of the less stable, low melting point Ni sulphides.

Aluminide coated MAR-M002 exposed to HTLCF and SO_2 bearing atmosphere at a SR of 0.38% showed a much improved fatigue life. The failure mechanism of the material system was very different from that observed at the higher strain range, since the corrosion behaviour of the coating played a much more significant role in the corrosion-fatigue failure.

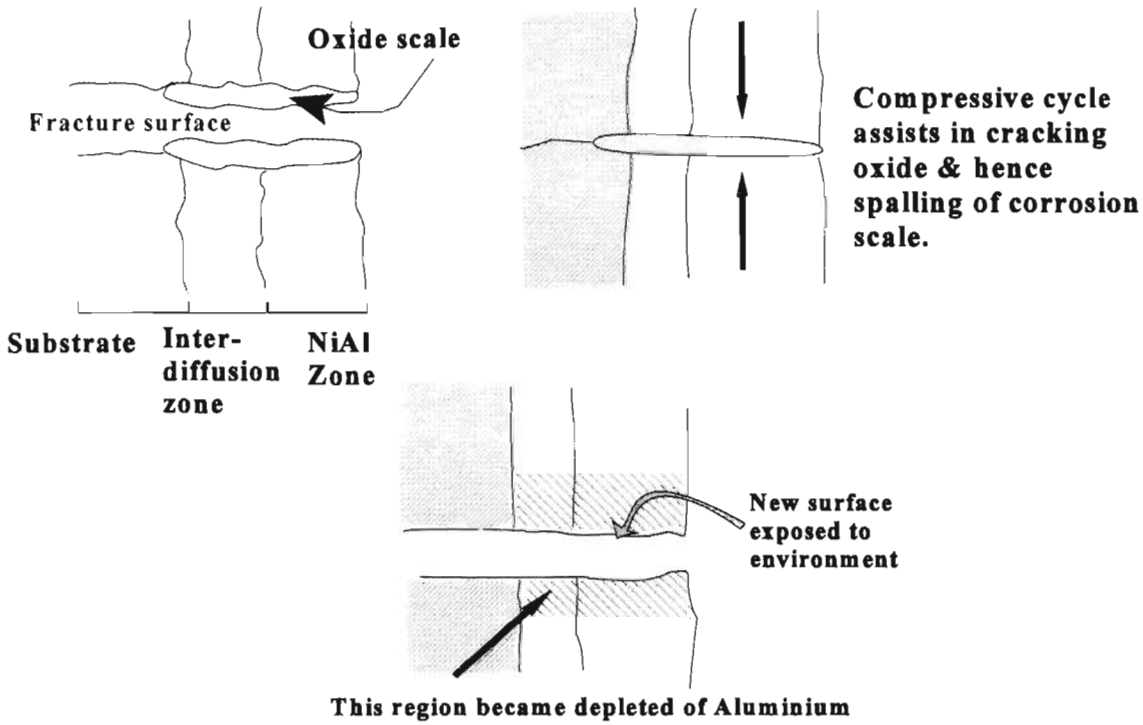

Figure 4.13 : Fluxing of aluminium from the aluminide coating due to the cyclic loading.

The inherent brittleness of the NiAl layer does initiate cracking in the coating but these cracks require a relatively high number of cycles for them to propagate to the substrate.

The sulphidation of the coating resulted in severe internal sulphidation and eventually "blistering" of the coating. It was very evident again that the mechanical failure of the coating was the critical step in the failure mechanism since the undamaged region of the coating did show that the coating offered significant resistance to sulphidation attack. The failure mechanism can be considered in the following context: incubation, crack initiation in the substrate and crack propagation in the substrate. The most significant of these stages was the incubation period.

The proposed blistering mechanism which occurred during the incubation period was as follows (fig. 4.14):

When fatigues cracks were initiated in the coating they became filled with the oxides and sulphides of Al and Ni. This effectively protected the propagating crack tip in the coating.

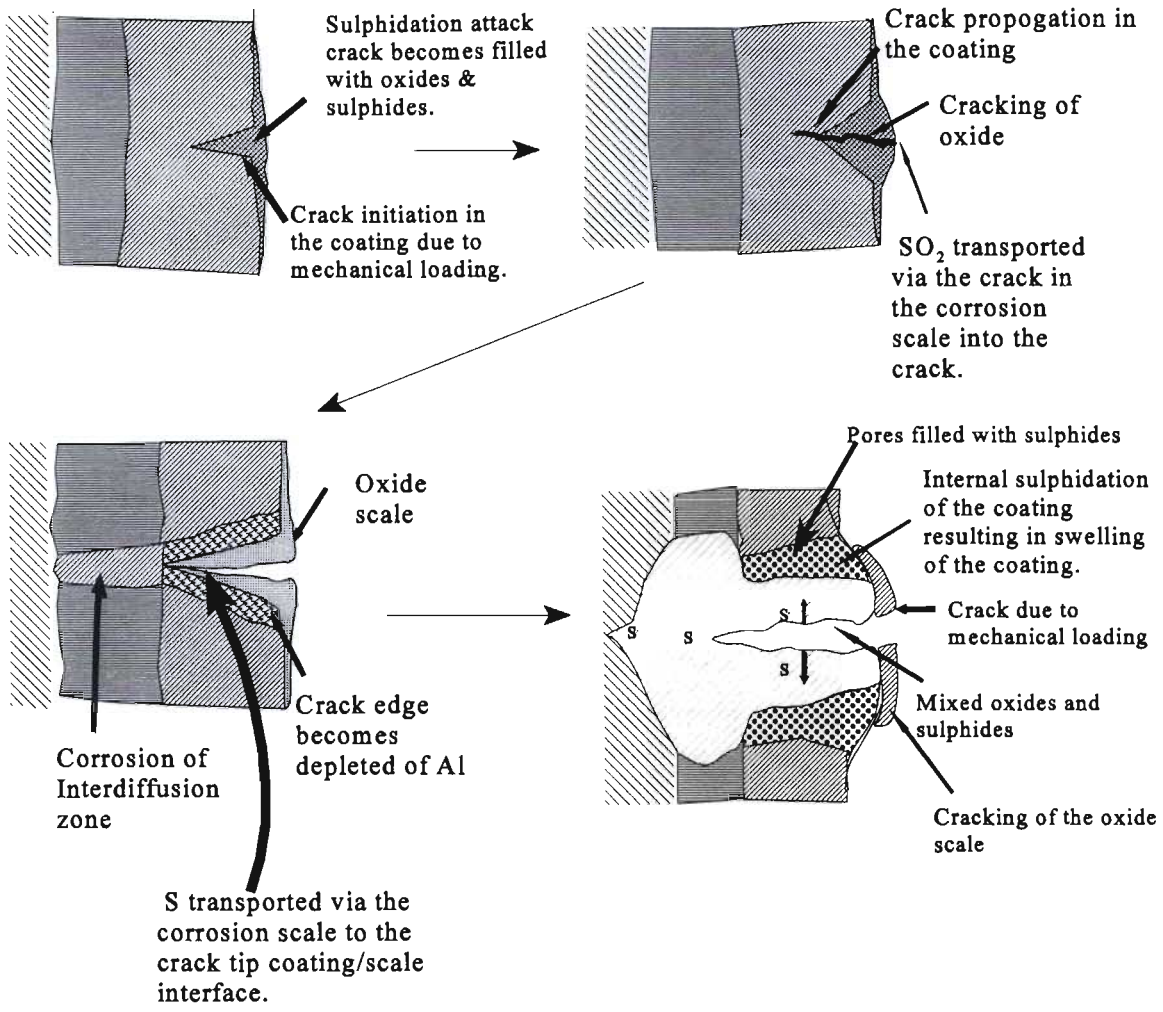

Figure 4.14 : Blistering mechanism that occurred during the HTLCF of aluminide coating MAR-M002 in Ar + 5%SO_2 at a strain range of 0.38 %

However, due to mechanical loading, the corrosion scale was cracked allowing the environment to penetrate the scale. This resulted in a "fluxing" mechanism. Every time a crack was created in the oxide "fresh" SO_2 was supplied into the crack creating a concentration gradient which allowed for the diffusion of alloying elements and the reagent, in this case sulphur and oxygen. This continual fluxing mechanism resulted in the depletion of aluminium in the region adjacent to the crack and resulted in internal sulphidation. The presence of low melting point nickel sulphides in the coating accelerated the sulphidation attack in this region which resulted in the "swelling" of the coating. The sulphidation processes proceeded more rapidly along the interdiffusion zone resulting in a relatively broad corrosion "front". This combined with the internal sulphidation resulted in the blistering of the coating. Crack initiation was accelerated when compared with the uncoated alloy due

to the crack in the coating creating a stress concentration point and concentration of the sulphidation attack to a small area. The stress concentration, however, was significantly lower than that observed in the tests performed at a strain range of 0.66% due to the broadening of the crack as a result of the sulphidation attack. Crack propagation in the substrate was similar to that observed in the uncoated alloy and was controlled by the sulphidation attack ahead of the crack tip.

From these results it was very apparent that the mechanical loading played a vital role in enhancing the sulphidation attack of the coating. Although a lower strain range was used, the brittle nature of NiAl resulted in the lower HTLCF life of the aluminide coating when compared to the uncoated alloy tested under similar conditions. However, the aluminide coating did show evidence of providing a higher resistance to sulphidation than the uncoated alloy.

4.2.3.3 Failure of TYPE I Platinum Aluminide Coated MAR-M002

The failure of TYPE I platinum aluminide coated MAR-M002 in Ar + 5% SO_2 environment produced similar lives for both the 0.66% and 0.38% strain ranges. Under the 0.66% strain range this coating showed a significant improvement over all the material systems tested, however, under the lower strain range it performed the worst.

This behaviour could be accounted for by one of the following two reasons:

1. There could have been contamination of the environment with air when the test was performed under the 0.66% strain range loading or
2. The platinum content in the coating was found to vary significantly in the samples tested even though the coating process was the same. The higher platinum content had the effect of embrittling the coating and making it prone to cracking under the mechanical loading. It was evident that in the sample tested at the strain range of 0.66%, the platinum content in the coating was significantly lower (a maximum of 10.28wt% was detected in the coating using EDS) than that observed in the sample tested at 0.38% S.R (a maximum of 23.00wt% was detected using EDS).

The latter was the most probable reason for the higher life experienced in the sample tested at the strain range of 0.66%.

The coating evidently displayed a "self healing" mechanism even though there was evidence of fatigue cracks in the coating. Due to the improvement in the mechanical properties, cracking of the coating did not occur immediately. General sulphidation of the coating surface covered the external surface with an oxide rich continuous corrosion scale (figure 4.15). Hence, when cracks did initiate in the coating they were protected from the environment. The sulphidation mechanism was the same as described previously with oxidation occurring first and sulphidation occurring at the corrosion scale/coating interface.

The corrosion scale remained "protective" as long as it was "undamaged". Once the oxide scale was cracked, sulphidation of the coating was concentrated in these regions. As long as the cracks in the coating were protected, the propagation mechanism in the coating was similar to that observed in the argon atmosphere. Once the oxide layer was breached

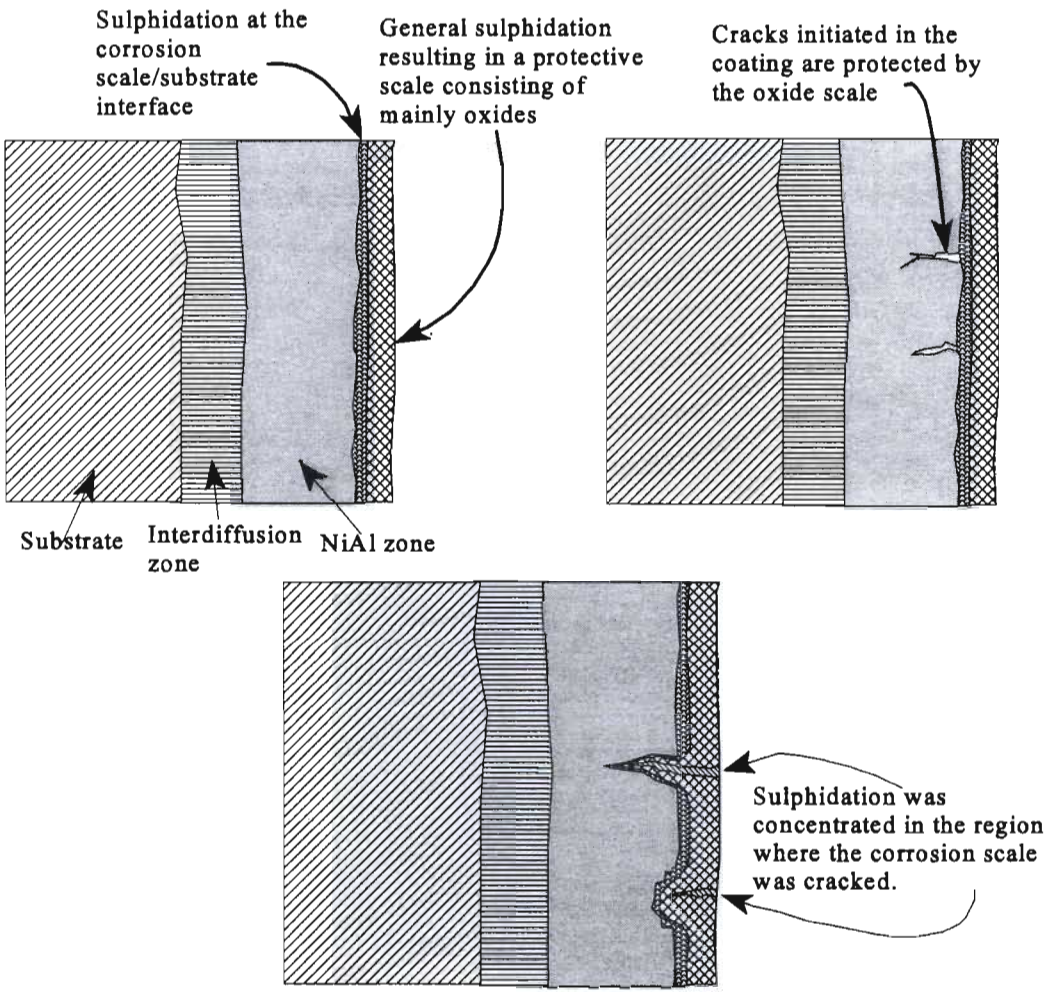

Figure 4.15: Self-healing mechanism of TYPE I platinum aluminide coated MAR-M002 after HTLCF in Ar + 5%SO_2 (S.R. 0.66%)

sulphidation at the crack tip controlled the crack propagation in the coating. Crack initiation in the substrate occurred at stress concentration points where the crack had penetrated the coating. Again crack propagation in the substrate was as that observed in the uncoated alloy. From this result, it was concluded that the increase in the incubation period (i.e time to crack initiation in the substrate) was the reason for the improved corrosion fatigue life in Ar + 5%SO_2 at the higher strain range.

The unstressed TYPE I platinum aluminide coated sample exposed to SO_2 bearing atmosphere at 870°C showed no evidence of severe sulphidation attack and also the XRD analysis of this sample showed little variation from the as received results. This indicated that in the unstressed condition the corrosion scale provided adequate protection against sulphidation.

HTLCF failure of TYPE I platinum aluminide coated MAR-M002 at a SR of 0.38% in SO_2 containing environment showed a very different failure mechanism when compared to that observed in the tests performed at 0.66% SR. It was obvious that the initial brittle failure of the coating had occurred in a relatively low number of cycles and the crack propagation through the coating was very rapid hence penetrating the coating fairly briskly. It was evident that the platinum content in the coating (max. of 23.00wt%) was relatively high when compared to the sample tested at 0.66% SR (max. of 10.28wt%). This probably resulted in the formation of a higher concentration of brittle platinum rich phases in the coating layer which effectively embrittled the coating.

The other feature which also was very different from the 0.66% SR test was the absence of the corrosion scale. This indicated that the coating was significantly more resistant to sulphidation attack, forming an adherent corrosion resistant oxide layer which effectively blocked the onset of sulphidation on the external surface. However, once the coating had cracked, SO_2 was concentrated in the regions where the coating had failed preventing the formation of a protective scale.

The following mechanism describes the corrosion process within the crack in the coating: Once the coating was cracked, SO_2 stagnated in the crack and the ensuing corrosion process filled the crack with oxides and sulphides (figure 4.16 a). The oxides layer failed due to the

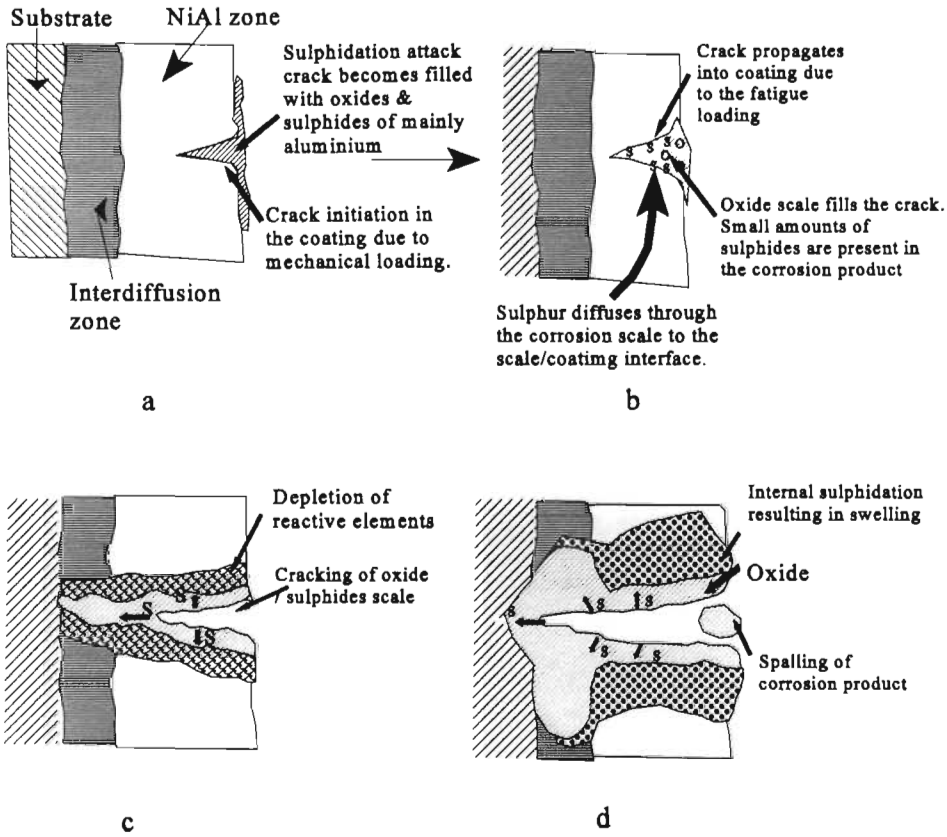

Figure 4.16 : HTLCF failure mechanism of TYPE I platinum aluminide coated MAR-M002 in SO_2 containing environment at a strain range of 0.38%.

mechanical loading creating the "fluxing" effect described for the aluminide coating (figure 4.16c). This process depletes the coating of reactive elements and enhances the internal sulphidation of the coating due to sulphur being transported to the corrosion scale/coating interface (figure 4.16). The internal sulphidation of the coating resulted in the formation of low melting point nickel sulphides, hence, causing "swelling" of the coating. The interdiffusion zone again was most susceptible to sulphidation resulting in a wide corrosion "front" proceeding into the substrate, beneath the coating. The build up of corrosion product in the substrate and interdiffusion zone contributed to forcing the coating outwards. It was apparent that the platinum content in the TYPE I platinum aluminide was critical to its mechanical and corrosion properties. The higher the platinum content the more brittle the coating and failure occurred relatively rapidly, even under low strain ranges. The higher platinum content also improved the sulphidation resistance of the coating but the detrimental effect on the mechanical properties resulted in an overall reduction of the HTLCF in Ar + 5% SO_2 when compared to the aluminide coating tested at the 0.38% strain range.

4.2.3.4 Failure of TYPE II Platinum Aluminide and 2μmPlatinum Aluminide Coated MAR-M002

The TYPE II and 2μm platinum aluminide coatings produced very similar lives for the HTLCF failure in Ar +5% SO_2. It was significant that the 2μm platinum aluminide coating showed a higher HTLCF life in both the strain ranges tested producing an average increase in HTLCF life of approximately 10% (i.e. 11% for the 0.66% SR and 9% for the 0.38% SR). The failure mechanism in both the coatings was similar due to the similar coating morphologies.

At this point it is important to note the distribution of platinum in the NiAl layer of the coatings. The platinum content was significantly lower in the NiAl zone than that observed in the outer region of these coatings and also lower than that observed in the TYPE I platinum aluminide coating. It was noted from the tests in Ar that platinum present in relatively small amounts in NiAl improves its mechanical properties significantly. Once the platinum intermetallics of Al form due to the low solid solubility of Pt in NiAl embrittlement of the coating occurs. This feature, which became more apparent at the lower strain range, had a significant influence on HTLCF in the sulphidation environment.

The mechanism via which these coatings failed under HTLCF loading in Ar + 5%SO_2 was as follows (figure 4.17):
The brittle platinum aluminide phase on the external surface failed under mechanical loading. This allowed the SO_2 gas to stagnate in the cracks. The thermodynamics of the corrosion reaction ensured the formation of oxides and small amounts of sulphides. The corrosion product filling these cracks provided some protection, however, the mechanical loading resulted in the cracking of the corrosion product.

The corrosion mechanism resulted in the formation of a oxide scale initially and sulphur diffused via this scale to the scale/coating interface and the crack tip in the coating. At the crack tip, Al and Cr sulphides formed initially, however , due to high sulphur content these elements were depleted and low melting point nickel sulphides formed. This combined with mechanical loading enhanced the sulphidation attack and the crack propagation rate in the coating.

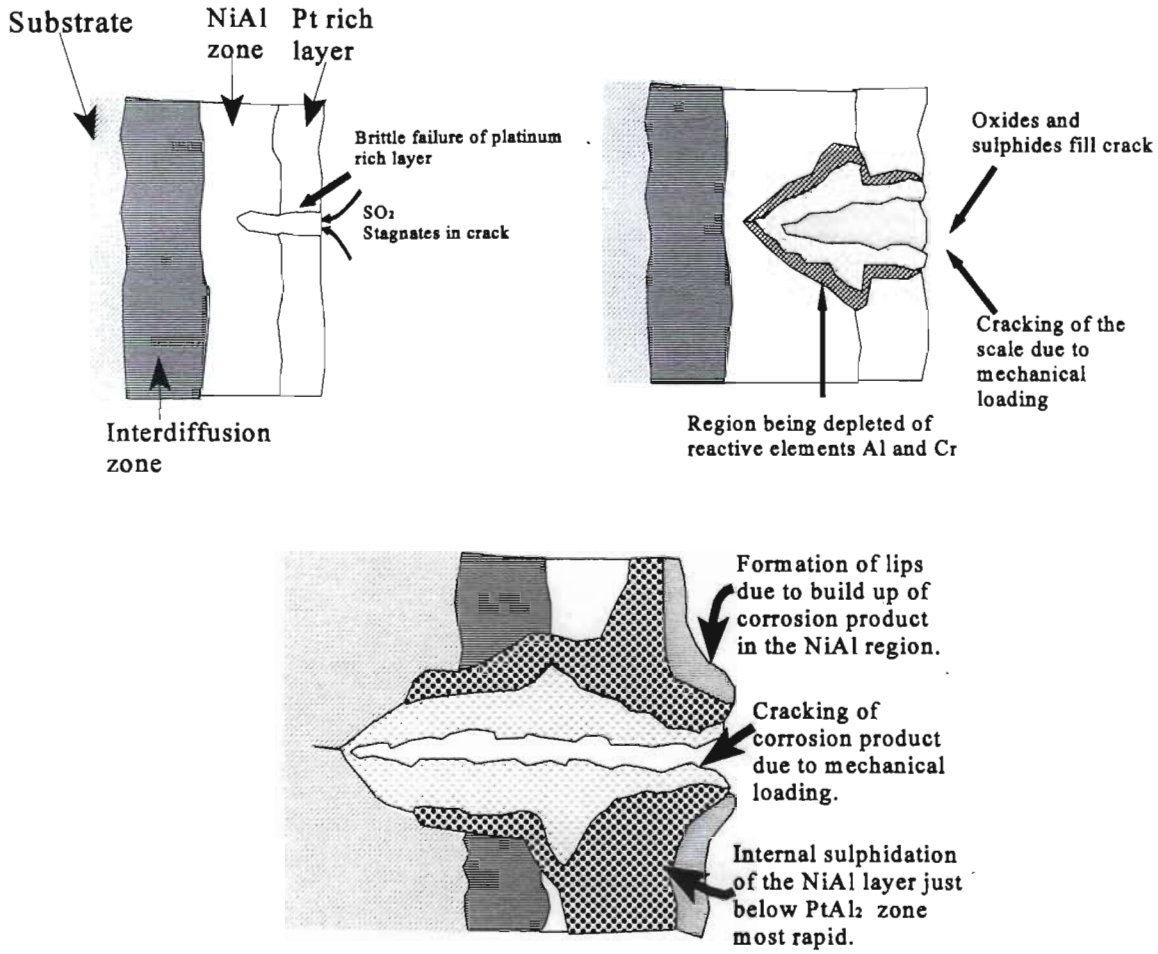

Figure 4.17 : Failure Mechanism of TYPE II platinum aluminide coating in SO_2 containing environment

The platinum rich outer layer of the coating proved to be much more resistant to sulphidation attack when compared to the NiAl layer. Although the NiAl layer was more resistant to crack propagation the sulphur containing environment accelerated the crack propagation rate. The sulphidation attack proceeded more rapidly along the NiAl zone and resulted in the "swelling" of the coating. The slower crack propagation rate in the NiAl region combined with the "self healing" properties resulted in the higher life when compared to the uncoated and aluminide coated samples tested at the strain range of 0.66%. This had the additional benefit of broadening the crack in the coating which resulted in the stress concentration of the crack through the coating being greatly reduced and delayed the crack initiation in the substrate.

The 2μm platinum aluminide coating displayed a similar mechanism of failure to the TYPE II platinum aluminide coating. This was deduced from the morphology of the cracks present

in the coating. The platinum rich outer layer again proved to be brittle and the source of crack initiation in the coating and NiAl layer again proved to be more susceptible to sulphidation attack. However, due to the initial thinner platinum coating applied that the outer platinum rich layer was thinner and it was no longer continuous $PtAl_2$ region but NiAl + Pt_2Al. The thinner NiAl - platinum layer proved to be more prone to sulphidation attack than the continuous $PtAl_2$ layer but the platinum modified NiAl zone was much greater than in the TYPE II platinum aluminide. It was this region that enhanced the coating life, due to the longer period required for crack propagation to occur through the NiAl zone.

The HTLCF tests at the lower strain range of 0.38% did not show as significant an improvement in fatigue life as that observed in the aluminide and uncoated alloys. This was mainly due to the presence of brittle platinum rich outer zone, which resulted in cracking of the coating early in the fatigue test. This combined with the SO_2 bearing atmosphere resulted in an accelerated fatigue failure when compared to the platinum coated, aluminide coated and uncoated alloy.

The mechanism of failure for both these materials systems proved to be similar to the higher strain range fatigue tests. However, the slower crack propagation (as a result of the lower loads) in the NiAl zone and longer time to crack initiation in the substrate resulted in very severe sulphidation of the NiAl layer. It was evident that the progression of sulphidation attack in this region was so rapid that it resulted in delamination of the TYPE II platinum coating in areas where two cracks were bridged. Another feature very evident in the TYPE II platinum aluminide coating was the break down of the single phase $PtAl_2$ zone into a two phase zone, due to the higher temperature exposure. This feature was also enhanced by the sulphidation attack in this region due to the selective oxidation of aluminium.

Delamination of the 2μm platinum aluminide coating was also observed due to similar processes as that in the TYPE II platinum aluminide coating. For both the coatings the sulphidation attack was concentrated in the regions where the coating had cracked. This had occurred due to the stagnation of the SO_2 gaseous environment in the crack and ensuing fluxing process that occurred. The significant conclusion from this result was that the platinum content in the coating plays a significant role in the mechanical properties and hence its corrosion-fatigue properties.

4.2.3.5 Failure of Platinum Coated MAR-M002

An accelerated failure was observed in the HTLCF tests performed in the SO_2 containing environment. At the higher strain range of 0.66%, the time to failure was lower than observed in the uncoated alloy but slightly greater than that observed in the aluminide coated material. The significant difference between the platinum aluminide samples and platinum coated samples was that the alloy surface was not enriched with aluminium, hence, the protection mechanism for the surface was derived by using the substrate alloying elements that had interacted with the platinum coating. The platinum modified surface enhanced the susceptibility to crack initiation (observed in tests performed in argon and air). Internal sulphidation of the coating showed that the corrosion product was essentially composed of Ni and Cr sulphides. The combination of the brittle coating layer and susceptibility of the coating to internal sulphidation resulted in the crack propagation in the coating to be fairly rapid and an early initiation of the fatigue crack in the substrate. The volumetric content of the more corrosion resistant platinum rich white phase diminished with high temperature exposure which further accelerated the sulphidation process. This occurred due to the interdiffusion of platinum and alloying elements of the substrate, and sulphidation. The γ' depleted zone, which was depleted of Al, was shown to be most susceptible to sulphidation attack. Once this propagating crack had entered this zone the sulphidation attack proceeded more rapidly along this region, than into the substrate.

The corrosion-fatigue failure of the platinum coated MAR-M002 sample occurred via the mechanism illustrated in figure 4.18. Crack initiation on the coating occurred in the grey region of the coating and propagated rapidly through this region to substrate/γ' depleted zone. The crack propagation through this region was accelerated due to the sulphidation attack at the crack tip. The white regions in the coating were ineffective as crack "stoppers" due to the sulphidation process altering the chemical composition of these regions and hence, the mechanical properties. The crack through the coating was relatively straight. Once the environment encountered the substrate, resistance to crack initiation and sulphidation was higher, however, the resistance of the γ' denuded zone to sulphidation was lower. The sulphidation attack proceeded more rapidly in this region than into the substrate. The corrosion product was made up of mainly oxides and small amounts of sulphides. This was consistent with the sulphidation mechanism observed in all samples tested, i.e., the oxidation

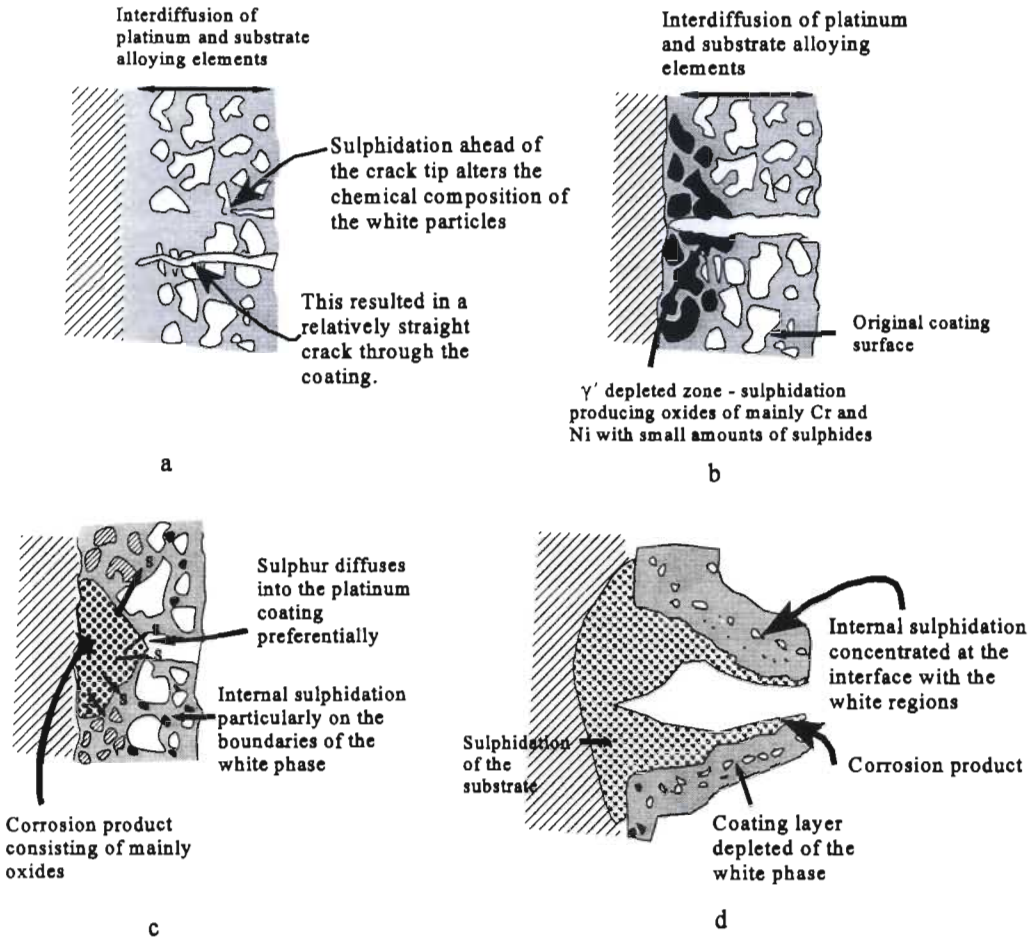

Figure 4.18: Failure mechanism of platinum coated MAR-M002 in SO_2 containing environment

reaction proceeded first followed by reaction with sulphur. The corrosion product was made up of significant quantities of Cr_2O_3 and NiO and significant amounts of Cr and Ni sulphides.

The presence of Ni oxides and sulphides would have reduced the "protective" nature of the initial scale formed. Oxygen diffusing through the scale was consumed first and also oxidised existing sulphides was oxidised, releasing the sulphur which diffused through the corrosion scale to the scale/substrate interface where sulphidation proceeded more rapidly. A significant feature was the diffusion of sulphur preferentially into the platinum layer than into the substrate resulting in internal sulphidation of the coating. The internal sulphidation of the coating was concentrated at the interfaces of the white particles in the coating and the original coating surface region. The accelerated sulphidation attack of the γ′ depleted zone played the instrumental part in the "peeling" of the coating. The combination of internal

sulphidation and sulphidation of the γ' depleted zone resulted in the swelling of the coating observed in the exterior surface of the fractography sample.

In the regions where internal sulphidation was more prevalent, the amount of white phase present was significantly reduced. This had occurred due to sulphur reacting firstly with the more thermodynamically stable sulphide forming elements, Al and Cr. This resulted in the Al being "drawn" out of the white regions effectively reducing the Al content in these regions which changed the structure. From the EDS analysis it was observed that this region was depleted of Al and Cr and effectively became a Ni/Pt alloy with some of the less reactive alloying elements dissolved in it.

The platinum coating produced a higher life compared to the aluminide coating mainly due to its higher resistance to crack initiation and propagation, and a lower life than the uncoated alloy due to the surface mechanical properties being altered. A significant feature was that the reduction in aluminium content in the coating played an important role in reducing the resistance to sulphidation attack.

The failure mechanism for HTLCF in SO_2 environment at the lower SR of 0.38% was the same as that observed for the higher strain range. At this strain range the life of the platinum coated sample was lower than the uncoated and aluminide coated samples but higher that the platinum aluminide coated samples. The reason for this behaviour was due to the combination of the alteration of the surface mechanical properties and corrosion properties. The platinum coating was more resistant to cracking than the platinum aluminides but less resistant than the uncoated alloy, however, it was susceptible to sulphidation attack.

The platinum intermetallics, in particular, where shown again to be extremely brittle and the lowering of the strain range did not slow down the crack initiation and propagation through the coating significantly. The reduction of aluminium content in certain regions of the coating (grey regions) resulted in the lowering of the sulphidation resistance and hence, enhanced corrosion-fatigue failure in sulphidizing atmospheres.

4.3 GENERAL DISCUSSION

From the HTLCF tests performed, it was determined that mechanical properties of the coating systems investigated played a key role in the failure mechanism. The poor resistance of the coatings to cracking must be attributed to the high DBTT of NiAl (868-1060°C) and $PtAl_2$ (870-1070°C) [10]. For the uncoated alloy the fatigue crack had to be initiated on the surface. In the case of the coated samples, cracks were initiated at the coating surface and propagated to the coating\substrate interface. This resulted in stress concentration points in this zone which resulted in crack initiation in the substrate.

The resistance of the aluminide and platinum modified aluminide coatings to crack initiation and propagation was found to be dependent on coating microstructure and platinum content. The aluminide coated samples revealed poor resistance to crack initiation and cracks were initiated readily at the surface at the higher strain range. The TYPE I platinum aluminide coatings revealed that crack initiation and propagation through the coating was dependent on the platinum content in the NiAl zone. It was noted for relatively high platinum content the susceptibility to cracking was increased. Although this point may be subjective in that the TYPE I coating was produced by a specific process condition and was not reproducible, the chemical analysis of the samples tested showed that there were significant differences in the platinum content in the NiAl zone between the samples. This was very apparent in the samples tested in the SO_2 bearing atmosphere. Since the environmental conditions were consistent for both the strain ranges, the test performed at the lower strain range was expected to produce a much higher life than that obtained. It was established that the there was a higher platinum content in the NiAl zone of the sample tested using the S.R. of 0.38%. The effect of platinum content on the mechanical properties also manifested itself in the TYPE II platinum aluminide where the NiAl zone adjacent to the $PtAl_2$ layer showed a higher tendency to crack. The TYPE II and 2μm platinum aluminide coatings showed that cracks had initiated in the platinum rich outer layer. This was due the presence of brittle platinum intermetallics. Crack initiation in the platinum coated samples had occurred in the grey region in the coating layer and cracks also tended to propagate in this region. Table 4.1 summarizes the resistance to crack propagation of the different regions in the coatings.

Under oxidation environment the failure of the coating controlled the overall life of the material. Crack propagation in the substrate was independent of the coating.

Table 4.1 : The resistance of the different regions in the coatings to crack propagation

Coating	Structure			
	Interdiffusion Zone	**NiAl**	**Pt Mod. NiAl**	**Pt_2Al**
Aluminide S.R. 0.66%	P	P		
S.R 0.38%	F	F		
Type I PAC S.R. 0.66%	F		F*	
S.R 0.38%	F		P*	
Type II PAC S.R. 0.66%	F		F	P
S.R 0.38%	F		F	P

	γ' depleted zone	**White region**	**Grey region**	
Platinum	F	G	P	

P - POOR

F - FAIR

G - GOOD

* - Mechanical properties dependent on platinum content

Under sulphidation environment, accelerated failures were observed, hence, tests at a lower strain range had to be performed in an attempt to eliminate the brittle failure of the coating. In general, the coatings did show evidence that in the absence of mechanical loading there would be a higher resistance to sulphidation attack.

The corrosion mechanism in the SO_2 environment was consistent for all the coatings and the uncoated sample tested. The corrosion mechanism involved the initial oxidation of the material, i.e. forming metal oxides. The thermodynamically stable oxides, i.e. oxides of Al and Cr, formed first. However, the oxygen pressure was not sufficiently high for only oxides to form and some sulphides did form in the corrosion scale. The sulphidation process normally was most prevalent at the corrosion scale/substrate interface. Hence, it was evident that if the coating was able to produce a protective oxide scale its resistance to sulphidation was much improved. If these oxides were coherent and continuous there was a higher resistance to sulphidation attack since the transport of sulphur through the scale becomes

more difficult. However, due to the mechanical loading and sulphides present, diffusion through the oxide scale was enhanced. The continuous cracking and spalling of the oxide scale due to the mechanical loading resulted in a "fluxing" mechanism which effectively depleted the coating of the reactive elements Al and Cr. This resulted in the formation of less stable oxides and sulphides, particularly that of nickel, which resulted in the high corrosion rate.

The production of the protective scale was dependent on the activity of aluminium and oxygen pressure. If the activity of aluminium was sufficiently high a protective Al_2O_3 scale would form. Platinum enhances the diffusion of aluminium to the surface and hence the activity of the aluminium during the corrosion reaction. This was evident in the HTLCF tests performed on platinum aluminides with relatively high platinum contents. In these samples, the sulphidation attack was concentrated in the regions where the coating had cracked.

The different regions in the coating also showed varying degrees of resistance to sulphidation attack. Table 4.2 summarizes the resistance of the different regions to sulphidation attack. These conclusions on the coating properties were based on the combination of mechanical loading and sulphidation attack.

Table 4.2 : The resistance of the different regions in the coatings to sulphidation

Coating	**Structure**			
	Interdiffusion Zone	**NiAl**	**Pt Mod. NiAl**	**Pt_2Al**
Aluminide	P	F		
Type I PAC	P		P	
Type II PAC	P		P	G

	γ' depleted zone	**White region**	**Grey region**	
Platinum	P	G	P	

P - POOR

F - FAIR

G - GOOD

CONCLUSIONS

1. The mechanical properties of the coatings influenced the overall fatigue properties. The coating mechanical properties were determined by the coating microstructure and composition. The NiAl and platinum aluminide layers were very brittle and fractured very easily under fatigue loading. This was mainly due to the tests being performed at the lower end of the DBTT range. The platinum aluminide layer showed a higher tendency to crack under mechanical loading than the NiAl layer. Platinum present in solid solution and/or dispersed as platinum aluminide particles in the NiAl zone had a beneficial influence on the mechanical properties of the NiAl zone by altering the crack propagation mechanism through the coating. However, this was only true for when the overall platinum content in the NiAl zone was relatively low.

2. The platinum coating was not effective as a ductile corrosion resistant layer. Interdiffusion and interaction with the substrate alloying elements resulted in embrittlement of the alloy surface, hence facilitating crack initiation. The absence of the aluminium enriched layer also made it ineffective for corrosion protection.

3. The aluminide coated alloy was susceptible to accelerated failure under the combination of sulphidizing environment and fatigue loading. This was due to a combination of the brittle nature of the coating plus the susceptibility of the NiAl zone to sulphidation. Lateral sulphidation at the "lip" of the cracks in the coating was mainly due to the short diffusion path for the corroding species through the corrosion scale. The susceptibility of the interdiffusion zone to sulphidation plus the severe internal sulphidation of the NiAl zone caused severe blistering of the coating when exposed to the sulphidizing environment for long periods (like in the case of the S.R. of 0.38%).

4. The presence of platinum in relatively small quantities in the NiAl zone significantly improved the corrosion fatigue properties of the TYPE I platinum aluminide coating by displaying a "self healing" mechanism. This mechanism was

unique to the TYPE I platinum aluminide coated sample tested at the 0.66% strain range and was not observed in the other samples tested. This feature of coating may be attributed to the coating's atypical microstructure and coating composition which also altered the mechanical properties of the coating.

5. TYPE II platinum aluminide coatings displayed adequate resistance to sulphidation attack as long as the $PtAl_2$ layer was not breached. However, once this region was cracked severe sulphidation of the NiAl zone occurred. For longer exposure times, like that observed in the 0.38% S.R. tests, this susceptibility of the NiAl to sulphidation resulted in delamination of the coating. Due to the brittle nature of the platinum aluminide phases, the platinum aluminide coatings did not show significant improvement in the HTLCF life under the sulphidizing conditions at the strain range of 0.38% when compared with the higher strain range.

6. The corrosion fatigue life, under the SO_2 containing environment, was controlled by the incubation period, i.e., the time before crack initiation in the substrate. The platinum aluminide coatings in general increased the incubation period which enhanced the overall fatigue life of the material system in the tests performed at a strain range of 0.66%. The increase in the incubation period was mainly due to the decrease in the crack propagation rate through the coating even though the cracking of the coating had occurred early in the fatigue test. In the tests performed at the strain range of 0.38%, the time to the first crack in the coating became more significant. The aluminide coating showed a higher resistance to cracking than the platinum aluminide samples tested and hence increased the incubation period significantly. Cracking of the platinum aluminide layer occurred early in the fatigue tests which resulted in a much smaller increase in the incubation period, hence, the lower life when compared to the aluminide coated sample.

8. The crack propagation in both the coating and substrate was controlled by the sulphidation attack at the propagating crack tip.

9. The sulphidation mechanism was independent of the material system. Oxidation proceeded first followed by sulphidation at the corrosion scale/substrate interface.

RECOMMENDATIONS

1. Since only a limited number of specimens were available a good statistical spread of data could not be obtained. It is recommended that in order to establish the life trends for the various environments a significant number of tests must be performed at different strain ranges.

2. The use of strain range partitioning method for life prediction requires the strain range versus life relationships for the four inelastic strain ranges, hence, these relationships need to be developed for the specific environments in order to apply these results for life prediction. These tests will also serve to indicate whether the SRP method can be applied to coated samples with confidence.

3. The strain range used for the fatigue tests should be reviewed. Tests at lower strain ranges, closer to typical operation conditions should be used. Since this would mean much longer tests, the testing technique should also be reviewed and higher frequencies may be considered in order to reduce the length of each test.

4. There was evidence from the tests performed on the 2μm platinum aluminide coating that the amount of platinum applied will play a significant role in the corrosion and fatigue properties of the alloy. A study on the effect of the initial platinum coating thickness versus the fatigue and corrosion properties should be investigated.

5. It would be useful to establish the fatigue crack propagation (FCP) rates through the coating structures and establish some correlation between the coating microstructure and composition to this property. This incorporates performing FCP tests on NiAl, $PtAl_2$ and platinum modified NiAl intermetallics.

REFERENCES

1. Benrey, R, "Taking the Heat", Chemtech, October, 1980, pp 595-597

2. Schneider, K. and Grünling, H.W., "Mechanical Aspects of High Temperature Coatings", Thin Solid Films, 107, 1983, pp395-416

3. Kolkman, H.J., "Creep, Fatigue and Their Interaction in Coated and Uncoated René 80", Materials Science and Engineering, 89, 1987, pp 81-91

4. Rhys-Jones, T.N. and Cunningham, T.P., "The Influence of Surface Coatings on the Fatigue Behaviour of Aero Engine Materials", Surface and Coatings Technology, 42, 1990, pp13-19

5. Castillo, R. and Willet, K.P., "The Effect of Protective Coatings on the High Temperature Properties of a Gamma Prime-Strengthened Ni-Base Superalloy", Metallurgical Transactions A, Vol. 15A, Jan. 1984, pp 229-236

6. Swadźba, L., Maciejny, A., Formanek, B. and Biedroń, J., "Microstructure and Resistance to Cracking of Modified Al-Si and Al-Cr Difffusion Coatings on Żs6k Nickel-based Superalloy", Surface and Coatings Technology, 54/55, 1992, pp84-90

7. Hancock, P., Chien, H.H., Nicholls, J.R. and Stephenson, D.J., "*In Situ* Measurements of the Mechanical Properties of Aluminide Coatings", Surface and Coatings Technology, Vol. 43/44, 1990, pp359-370

8. Kang, S.B., Kim, Y.G., Kim, H.M. and Stolhoff, N.S., "The influence of a Coating Treatment and Directional Solidification on the Creep Rupture Properties of a Nickel-Base Superalloy", Materials Science and Engineering, Vol. 83, pp 75-86

9. Totemeier, T.C., Gale, W.F. and King, J.E., "Fracture Behaviour of an Aluminide Coating on a Single Crystal Nickel Base Superalloy", Materials Science and Engineering, Vol. A169, 1993, pp19-26

10. Strang, A. and Lang, E., "Effect of Coatings on the Mechanical Properties of Superalloys", High Temperature Alloys for Gas Turbines 1982, Proceedings of a Conference held in Liège, Belgium, 4-6 October 1982, pp 469-506.

11. Wood, M.I., "Mechanical Interactions Between Coatings and Superalloys Under Conditions of Fatigue", Surface and Coatings Technology, Vol. 39/40, pp29-42

12. Bullock, E., Schuster, K. and Lang, E., "The Influence of Applied Coatings on the Creep Fracture of IN 738 LC", High Temperature Alloys for Gas Turbines 1982, Proceedings of a Conference held in Liège, Belgium, 4-6 October 1982, pp 779-789

13. Gayda, J., Gabb, T.P. and Miner R.V., " Isothermal and "Bithermal" Thermomechanical fatigue Behaviour of a NiCoCrAlY-Coated Single Crystal Superalloy", Superalloys 1988, Proceedings of the Sixth International Symposium on Superalloys, Seven Springs Mountain Resort, Pennsylvania,USA, 18-22 September 1988, pp 575-584.

14. Busso, E.P. and McClintock, F.A., "Thermal Fatigue Degredation of an Overlay Coating", Materials Science and Engineering, Vol. A161, 1993, pp165-179

15. Strangman, T.E., "Thermal-Mechanical Fatigue Life Model for Coated Superalloy Turbine Components", Superalloys 1992, Proceedings of the Seventh International Symposium on Superalloys, Seven Springs Mountain Resort, Pennsylvania, USA, 20-24 September 1988, pp 795-804.

16. Bressers, J., Menigault, J. and Rhys-Jones, T., "Thermo-Mechanical Fatigue of a Coated and Uncoated Nickel-Based Alloy", Report to Rolls-Royce, Report Number PNR90797, October 1990

17. Aghion, E, Govender, G, and Comins, N, "The Environmental Effect of SO_2 - Bearing Atmosphere on the Creep Fatigue Failure of Aluminide-coated MM-002 Nickel-base Superalloy At 870°C", Journal of Materials Science, Vol. 30, 1995, pp 2163-2170

18. Sims, C.T., "Superalloys: Genesis and Character", From Superalloys II, John Wiley & Sons Inc., 1987, pp 3-26.

19. Ross, E.W. and Sims, C.T., "Nickel-Base Alloys", From Superalloys II, John Wiley & Sons Inc., 1987, pp 97-133.

20. Duhl, D.N., "Single Crystal Superalloys", From Superalloys, Supercomposites and Superceramics, Academic Press Inc., 1989, pp 150-181.

21. Duhl, D.N., "Directionally Solidified Superalloys", From Superalloys II, John Wiley & Sons Inc., 1987, pp 189-214.

22. Hirschberg, M.H. and Halford, G.R., "Use of Strainrange Partitioning to Predict High-Temperature Low-Cycle Fatigue Life", NASA Report IND-8072, 1976.

23. Miller, D.A., Priest, R.H. and Elkson, E.G., "A Review of Material Response and Life Prediction Techniques under Fatigue-Creep Loading Conditions", High Temperature Materials and Processes, Vol. 6, Nos. 3/4, 1984, pp 155-194.

24. Thomas, G.B., Brossers, J. and Reynor, D., "Low Cycle Fatigue and Life Prediction Methods", High Temperature Alloys for Gas Turbines 1982, Proceedings of a Conference held in Liège, Belgium, 4-6 October 1982, pp291-317.

25. Atunes, V.T.A. and Hancock, P., "Strainrange Partitioning of MARM002 Over the Temperature Range 750^{0}C - 1040^{0}C", AGARD Conference, Aalberg, Denmark CP-243, April 1978.

26. Halford, G.R., Meyer, T.G., Nelson, R.S., Nissley, D.M. and Swanson, G.A., "Fatigue Life Prediction Modelling for Turbine Hot Section Materials", Journal of Engineering for Gas Turbines and Power, Vol. 11, April 1989, pp 279-285.

27. Aghion, E.E., Phase I Annual Report to the CSIR, Pretoria, South Africa, 1990.

28. Mrowec,s. and Weber, T.C., "Gas Corrosion of Metals", National Bereua of Standards and National Science Foundation, Washington D.C., 1978

29. Pettit, F.S. and Goward, G.W., "High Temperature Corrosion and Use of Coatings for Protection", Superalloys Source Book, ASM, 1984, pp 170-186.

30. Birks N. and Meier, G.H., "Introduction to High Temperature Oxidation of Metals", Edward Arnold (Publishers) Ltd., 1983.

31. Wood G.C. and Stott, F.H., "Oxidation of Alloys", Materials Science and Technology, July 1987, Vol. 3, pp 519-530.

32. Moon, D.P., "Role of Reactive Elements in Alloy Protection", Material Science and Technology, August 1989, Vol. 5, pp 754-764.

33. Smialedi, J.L. and Meier, G.H., "High-Temperature Oxidation", From Superalloys II, John Wiley and Sons Inc., 1987, pp 293-326.

34. Huntz, A.M., "Effect of Active Elements on the Oxidation Behaviour of Al_2O_3 - Formers", Proceedings of the European Colloqium, Petten, (N.H.), The Netherlands, 12-13 Dec. 1988, pp 81-109.

35. Bennet, M.J. and Moon, D.P., "Effect of Active Elements on the Oxidation Behaviour of Cr_2O_3-Formers", Proceedings of the European Colloqium, Petten, (N.H.), The Netherlands, 12-13 Dec. 1988, pp 111-129.

36. Jedlinski, J., "The Influence of Active Elements on the Stress-Relaxation in then Scale and Substrate of Alumina-Forming Alloys", Proceedings of the European Colloqium, Petten, (N.H.), The Netherlands, 12-13 Dec. 1988, pp 131-151.

37. Lai, G.Y., "High-Temperature Corrosion of Engineering Alloys", ASM International Publication, 1990.

38. Strafford, K.N. and Datta, P.K., "Design of Sulphidation Resistant Alloys", Materials Science and Technology, August 1989, Vol. 5, pp 765-779.

39. Brasunas, A.deS and Moran, J.J., Jnr, "High Temperature Corrosion", From Corrosion Basics An Introduction, National Association of Corrosion Engineers, 1984, pp 275-308.

40. Gesmundo, F., Young, D.J. and Roy, S.R., "The High Temperature Corrosion of Metals in Sulphidizing-Oxidizing Environments: A Critical Review", High Temperature Materials and Process, Vol. 8, No. 3, 1989, pp 149-190.

41. Luthra, K.L. and Worrell, W.L., "Simultaneous Sulphidation-Oxidation of Nickel at 603^{0}C in Argon-SO_2 Atmospheres", Metallurgical Transactions A, Vol. 9A, Aug. 1978, pp 1055-1061.

42. Lutjra, K.L. and Worrell, W.L., "Simultaneous Sulphidation-Oxidation of Nickel at 603^{0}C in SO_2 - O_2 - SO_3 Atmospheres", Metallurgical Transactions, Vol. 10A, May 1979, pp 621-631.

43. Haflan, B. and Kofstad, P., "The Reaction of Nickel with SO_2 + O_2/SO_3 at 500-900^{0}C", Corrosion Science, Vol. 23, No. 12, 1983, pp 1333-1352.

44. Quadakkers, W.J., Wasserfuhr, C., Khanna, A.S. and Nickel, H., "The Influence of SO_2 Additions on the Oxidation Behaviour of NiCrAl-Based Alloys in Air", Conference: UK Corrosion '88 - With Eurocorr, Vol. III, Brighton, UK, 305 Oct. 1988, pp 45-63.

45. Andersen, A. and Kofstad, P., "The Reaction of Ni-20Cr with SO_2 at 600-900^{0}C", Corrosion Science, Vol. 24, No. 8, 1984, pp 731-743.

46. Restall, J.E., "Surface Degradation and Protective Treatments", The Development of Gas Turbine Material, Meethan, G.W. (Editor), Applied Science Publishers Ltd., England, pp 259-290.

47. Stringer, J., "Hot Corrosion in Gas Turbines", MCIC Report, June 1972, Metals and Ceramics Information Center.

48. Pettit, F.S. and Meier, G.H., "Oxidation and Hot Corrosion of Superalloys", Superalloys 1984, Proceedings of the Fifth International Symposium on Superalloys, Seven Springs Mountain Resort, Pennsylvania, USA, 7-11 October 1984, pp 651-687.

49. Donachie, M.J., Bradley, E.F., Sprague, R.A. and Talboom, F.P., "Effects of Turbine Atmospheres on Sulphidation Corrosion", Source Book on Materials for Elevated Temperature Applications, ASME Publication 67-GT-2, USA, 1979, pp 34-45.

50. Lillerud, K.P. and Kofstad, "Sulfate-Induced Hot Corrosion of Nickel", Oxidation of Metals", Vol. 21, Nos. 5/6, 1984, pp 233-270.

51. Friend, W.Z., "Corrosion of Nickel and Nickel-Based Alloys", A Wiley-Interscience Publication, John Wiley and Sons Inc., New York, 1980, pp 445-449.

52. Conde, J.F.G., Erdos, E and Rahmel, A., "Mechanisms of Hot Corrosion", High Temperature Alloys for Gas Turbines 1982, Proceedings of a Conference held in Liège, Belgium, 4-6 October 1982, pp 99-148.

53. Jaffee, R.I. and Stringer, J., "High-Temperature Oxidation and Corrosion of Superalloys in the Gas Turbine" (A Review), Source Book on Materials for Elevated Temperature Applications, ASME Publication 67-GT-2, USA, 1979, pp 19-33.

54. Sequeira, C.A.C. and Hocking, M.G., "Hot Corrosion of Nimonic 105 in Sodium Sulphate-Sodium Chloride Melts", Corrosion-NACE, Vol. 37, No. 7, July 1981, pp 392-404.

55. Zuo, Y, Zhu, R. and Guo, M., "Hot Corrosion of Some Nickel-Based Superalloys Containing Niobium", Corrosion-NACE, Vol. 43, No. 1, January 1987, pp 51-55.

56. Reising, R.F., "Effects of Chromium, Molybdenum, and Tungsten on Sodium Sulphate-Induced High Temperature Corrosion of Nickel", Corrosion-NACE, Vol. 31, No. 5, May 1975, pp 159-163.

57. Floreen, S. and Kane, R.H., "An Investigation of the Creep-Fatigue-Environment Interaction in a Ni-Base Superalloy", Fatigue of Engineering Materials and Structure, Vol. 2, 1980, pp 401-412.

58. Gabrielli, F. and Pelloux, R.M., "Effect of Environment on Fatigue and Creep Crack Growth in Inconel X-750 at Elevated Temperature", Metallurgical Transactions A, Vol. 13A, June 1992, pp 1083-1090.

59. Duquette, D.J. and Gell, M., "The Effects of Environment on the Elevated Temperature Fatigue Behaviour of Nickel-Base Superalloys Single Crystals", Metallurgical Transactions, Vol. 3, July 1972, pp 1899-1905.

60. Lupinc, V., Onofrio, G. and Vimercati, G., "The Effect of Creep, Oxidation and Crystal Orientation on High Temperature Fatigue Crack Propagation in Standard and Raft-Like Gamma Prime CMSX-2", Superalloys 1992, Proceedings of the Seventh International Symposium on Superalloys, Seven Springs Mountain Resort, Pennsylvania, USA, 20-24 October 1992, pp 717-726.

61. Marchionni, M., Ranucci, D. and Picco, E., "High-Temperature Low-Cycle Fatigue Behaviour of IN738LC Alloy in Air and in Vacuum", High Temperature Alloys for Gas Turbines 1982, Proceedings of a Conference held in Liège, Belgium, 4-6 October 1982, pp 791-804.

62. Floreen, S. and Kane, R.H., "Effects of Environment on High Temperature Fatigue Crack Growth in a Superalloy", Metallurgical Transactions A, Vol. 10A, November 1979, pp 1745-1751.

63. Floreen, S. and Kane, R.H., "Elevated Temperature Fatigue Crack Growth in Incoloy Alloy 800 in Sulfidizing Environments", Metallurgical Transactions A, Vol. 13A, January 1982, pp 145-152.

64. Nazmy, M.Y., "The Effect Of Sulphur Containing Environment on the High Temperature Low Cycle Fatigue of a Cast Ni-Base Alloy", Scripta Metallurgica, Vol. 16, 1982, pp 1329-1332.

65. Hu, G.X., Zhou, I. and Zhang, Y.H., "Hot Corrosion of a Nickel-Base Superalloy in a SO_2-Air Environment Under Applied Load", International Symposium on High Temperature Corrosion of Alloys and Coatings for Energy Systems and Turboengines, 7-12 July 1986, Topic 8.

66. Aghion E.E., "The Effects of Sulphur-Containing Environment on High Temperature Fatigue Failure of a Nickel Base Superalloy", The 8th Biennial Conference on Fracture-ECF8, Fracture Behaviour and Design of Materials nand Structures, Torino, Italy, October 1990, pp 485-487.

67. Aghion, E.E., "The Mechanism of High-Temperature blistering of a Nickel-Based Superalloy Under Cyclic Loading and Sulphidizing Environment", Journal of Materials Science Letter II, 1992, pp 627-629.

68. Pieraggi, B., "Effect of Creep or Low Cycle Fatigue on the Oxidation or Hot Corrosion Behaviour of Nickel-Base Superalloys", Materials Science and Engineering, Vol. 88, 1987, pp 199-204.

69. Yoshiba, M and Miyagawa, O., "Strength Properties of a Nickel-Base Superalloy Subjected to Creep-Fatigue Interaction in Hot Corrosive Environment", Proceedings of the Japan-US Seminar on Superalloys, Susono, Japan, 7-11 December 1984, pp 141-149.

70. Grunling, H.W., Keienburg, K.H. and Schweitzer, K.K., "The Interaction of High Temperature Corrosion and Mechanical Properties of Alloys", High Temperature Alloys for Gas Turbines 1982, Proceedings of a Conference held in Liège, Belgium, 4-6 October 1982, pp 507-543.

71. Hoffelner, W. and Speidel, M.O., "Microstructural Aspects of Fatigue Crack Propagation of Cast Nickel Base Superalloys at 850^{0}C in Various Environments", Corrosion and Mechanical Stresses at High Temperatures, Applied Science Publishers, New York, USA, 1983, pp 275-287.

72. Feld, U., Rahmel, A., Schmidt, M. and Schorr, M., "Investigations on the Interactions Between Creep and Corrosion of Nickel Base Alloys in Sulphate Melts", Corrosion and Mechanical Stresses at High Temperatures, Applied Science Publishers, New York, USA, 1983, pp 171-196.

73. Yoshiba, M. and Miyagawa, O., "High Temperature Corrosion Fatigue and Grain Size Control in Nickel-Base and Nickel-Iron-Base Superalloys", Superalloys 1988, Proceedings of the Sixth International Symposium on Superalloys, Seven Springs Mountain Resort, Pennsylvania, 18-22 September 1988, pp 825-834.

74. Schutze, M. and Glaser, B., "The Role of Environmental Effects for the Mechanical Behaviour of Materials at High Temperatures", Proceedings of the 7th JIM International Symposium on Aspects of High Temperature Deformation and Fracture in Crystalline Materials, Nagoya, Japan, 28-31 July 1993, pp 561-567.

75. Nicholls, J.R. and Stephenson, D.J., "High Temperature Coatings for Gas Turbines", Metals and Materials, March 1991, pp 156-163.

76. Rhys-Jones, T.N., "Protective Oxide Scales on Superalloys and Coatings Used in Gas Turbine Blade and Vane Applications", Materials Science and Technology, Vol.4, May 1988, pp 421-430.

77. Kanao, H. and Doi, T., "Application of Corrosion Resistant Coatings to Gas Turbines", Welding Technique, Vol. 35, No. 4, 1987, pp 57-63.

78. Sivakumar, R. and Mordike, B.L., "High Temperature Coatings for Gas Turbine Blades: A Review", Surface and Coatings Technology, Vol. 37, 1989, pp 139-160.

79. Rickerby, D.S. and Winstone, M.R., "Coatings for Gas Turbines", Materials and Manufacturing Processes, Vol. 7, No. 4, 1992, pp 495-526.

80. Goeard, G.W., "Protective Coatings for High Temperature Alloys", Source Book on Materials for Elevated Temperature Applications, ASME Publication 67-GT-2, USA, 1979, pp 369-386.

81. Comassar, D.M., "Surface Coatings Technology for Turbine Engine Applications", Plating and Surface Finishing, Vol. 79, Part 7, July 1992, pp 20-26.

82. Wood, J.H. and Goldman, E.H., "Protective Coatings", From Superalloys II, John Wiley and Sons Inc., 1987, pp 359-384

83. Saunders, S.R.J. and Nicholls, J.R., "Coatings and Surface Treatments for High Temperature Oxidation Resistance", Materials Science and Technology, Vol. 5, August 1989, pp 780-798.

84. Duret, C., Davin, A., Marijnissen, G. and Pichoir, R., "Recent Approaches to the Development of Corrosion Resistant Coatings", High Temperature Alloys for Gas Turbines 1982, Proceedings of a Conference held in Liège, Belgium, 4-6 October 1982, pp 53-86.

85. Goward, G.W. and Cannon, L.W., "Pack Cementation Coatings for Superalloys: A Review of History, Theory, and Practice", Journal of Eng. for Gas Turbine and Power, Vol. 110, January 1988, pp 150-154.

86. Pichoir, R. and Hauser, J.M., "The Current Status of Coatings for High Temperature Applications", Paper obtained by correspondence with CSIR, pp 1-21.

87. Goward, G.W. and Boone, D.H., "Mechanisms of Formation of Diffusion Aluminide Coatings on Nickel-Base Superalloys", Oxidation of Metals, Vol. 3, No. 5, 1971, pp 475-495.

88. Andersen, P.J., Boone, D.H. and Paskiet, G.F., "A Comparison of the Effect of Inward and Outward Diffusion Aluminide Coatings on the Fatidue Behaviour of Nickel-Base Superalloys", Oxidation of Metals, Vol. 4, No. 2, 1972, pp 113-119.

89. Singheiser, L., Grunling, H.W. and Schneider, K., "Chemical Compatibility of Coated Systems at High Temperatures", Surface and Coatings Technology, Vol. 42, 1990, pp 101-117.

90. Bianco, R., Rapp, A. and Smialek, J.L., "Chromium and Reactive Element Modified Aluminide Diffusion Coatings on Superalloys: Environmental Testing", Journal of the Electrochem. Soc., Vol. 140, No. 4, April 1993, pp 1191-1203.

91. Saito, Y. and Onay, B., "Improvements of Scale Adherence on Heat-Resisting Alloys and Coatings by Rare Earth Additions", Surface and Coatings Technology, Vol. 43/44, 1990, pp 336-346.

92. Martinengo, P.C. and Carughi, C., "Investigation on the Effect of Yttrium and Cerium additions on the Corrosion resistance of Slurry Chromium Aluminized IN 738 LC Superalloy", Final Report, European Concerted Action-COST 50- Materials for Gas Turbines-I6, June 1979.

93. Jedlinski, J. and Mrowec, S., "The Influence of Implanted Yttrium on the Oxidation Behaviour of β-NiAl", Materials Science and Engineering, Vol. 87, 1987, pp 281-287.

94. Smeggil, J.G., "The Effect of Chromium on the High Temperature Oxidation Resistance of Ni:Al", Surface and Coatings Technology, Vol. 46, 1991, pp 143-153.

95. Tu, D.C., Lin, C.C., Liao, S.J. and Chou, J.C., "A Study of Yttrium-Modified Aluminide Coatings on IN 738 Alloy", J. Vac. Sci. Technol. A, Vol. 4. No. 6, Nov/Dec 1986, pp 2601-2608.

96. Swadzba, L., Formanek, B. and Maciejny, A., "Modified Heat-Resistant Protective Coatings for Nickel-Base Superalloys", Proceedings of the First European East-West

Symposium on Materials and Processes, Inderscience Enterprises ltd., UK, 1990, pp 155-169.

97. McMordie, B., "Slurry Aluminide Coating Processes for Gas Turbine Components at Over haul", Sermatech Review, No. 46-1, Fall 1993, pp 2-5.

98. Streiff, R. and Boone, D.H., "Corrosion Resistant Modified Aluminide Coatings", Journal of Materials Engineering, Vol. 10, No. 1, 1988, pp 15-26.

99. Gleeson, B., Cheung, W.H., Costa, W.D. and Young, D.J., "The Hot Corrosion Behaviour of Novel Co-Deposited Chromium-Modified Aluminide Coatings", Oxidation of Metals, Vol. 38, Nos. 5/6, 1992, pp 407-424.

100. Bianco, R. and Rapp, R.A., "Pack Cementation Aluminide Coatings on Superalloys: Codeposition of Cr and Reactive Elemnets", Journal of the Electrochem. Soc., Vol. 140, No. 4, April 1993, pp 1181-1190.

101. Gleeson, B., Cheung, W.H., Costa, W.D. and Young, D.J., "Co-Deposited Chromium-Aluminide Coatings and Their High-Temperature Corrosion Resistance", Copy of an article submitted for publication in the Proceedings of the 8th Asian-Pacific Corrosion Control Conference, Bangkok, Thailand, December 1993.

102. Duret, C. and Pichoir, R., "Protective Coatings for High Temperature Materials: Chemical Vapour Deposition and Pack Cementation Processes", Coatings for High Temperature Applications, Applied Science Punlishers Ltd., New York, USA, 1983, pp 33-78.

103. Godlewska, E. and Godlewski, K., "Chromaluminizing of Nickel and Its Alloys", Oxidation of Metals, Vol. 22, Nos. 3/4, 1984, pp 117-131.

104. Wing, R.G. and McGill, I.R., "The Protection of Gas Turbine Blades", Platinum Metals Review, Vol. 25, No. 3, 1981, pp 94-105.

105. Smith, J.S. and Boone, D.H., "Platinum Modified Aluminides-Present Status", The American Society of Mechanical Engineers, 1990, pp 1-10.

106. Jackson, M.R. and Rairden, J.R., "The Aluminization of Platinum and Platinum-Coated IN-738", Metallurgical Transactions A, Vol. 8A, 1977, pp 1697-1707.

107. Biss, V. and Strabel, G., "Metallographic Study of Platinum Modified Aluminide Coatings on IN-738 Base Metal", Field Metallography, failure analysis, and Metallography, Boston, Massachussetts, USA, 5-6 Aug. 1986, published by ASME International, 1987, pp 353-365.

108. Streiff, R., Cerclier, O. and Boone, D.H., "Structure and Hot Corrosion behaviour of Platinum-modified Aluminide Coatings", Surface and Coatings Technology, Vol. 32, 1987, pp 111-126.

109. Streiff, R. and Boone, D.H., "High Temperature Corrosion Resistance Platinum Modified Aluminide Coatings for Superalloys", International Congress on Metallic Corrosion, Vol. 2, Toronto, 3-7 June1984, pp 489-494.

110. Sun, J.H., Jang, H.C. and Chang, E., "Effects of pretreatments on structure and oxidation behaviour of d.c.-sputtered platinum aluminide coatings", Surface and Coatings Technology, Vol. 64, 1994, pp 195-203.

111. Tawancy, H.M., Abbas, N.M. and Rhys-Jones, T.N., "Role of Platinum in Aluminide Coatings", Surface and Coatings Technology, Vol. 49, 1991, pp 1-7.

112. Lin, K.L. and Hwang, C.M., "Interdiffusion of the aluminized and Pt-aluminized coatings on MAR-M247 superalloy", Surface and Coatings Technology, Vol. 56, 1992, pp 81-87.

113. Deb, P., Boone, D.H. and Streiff, R., "Platinum Aluminide Coating Structural Effects on Hot Corrosion Resistance at 900^0C", J. Vac. Sci. Technol. A, Vol. 3, No. 6, 1985, pp 2578-2581.

114. Deb, P., Boone, D.H. and Streiff, R., "Effects of Microstructural Morphology on the Performance of Platinum Aluminide Coatings", Surface Modifications and Coatings, Toronto, Ontario, Canada, 14-17 Oct. 1985, ASM, USA, 1986, (Met. A., 8611-72-0465) pp 143-159.

115. Boone, D.H., Deb, P., Purvis, L.I. and Rigney, D.V., "Surface Morphology of Platinum Modified Aluminide Coatings", J. Vac., Sci., Technol. A, Vol. 3, No. 6, 1985, pp 2557-2563.

116. Dust, M., Deb, P., Boone, D.H. and Shankar, S., "Structure and 700^{0}C Hot Corrosion Behaviour of Chromium Modified Platinum-Aluminide Coatings", J. Vac., Sci., Technol. A, Vol. 4, No. 6, 1986, pp 2571-2576.

117. Frances, M., Steinmetz, P., Duret, C. and Mevrel, R., "Hot Corrosion Behaviour of Low Pressure Plasma Sprayed NiCoCrAlY + Ta Coatings on Nickel-Base Superalloys", Congress ICMC, Los Angelos, 15-19 April 1985.

118. Mazars, P., Manesse, D. and Lopvet, C., "Degradation of MCrAlY Coatings by Interdiffusion", Presented at Gas Turbine Conference and Exhibition, Anaheim, California - May 31-June 4, 1987.

119. Huang, N.K., "X-ray Photoelectron Spectroscopy Studies on the Surface of NiCoCrAlY Coatings before and after High-Temperature Oxidation", Surface and Coatings Technology, Vol. 53, 1992, pp 65-69.

120. Irons, G. and Zanchuk, V., "Comparison of MCrAlY Coatings Sprayed by HVOF and Low Pressure Process", Thermal Spray Coatings : Research, Design and Applications, Proceedings of the 1993 National Thermal Spray Conference, Anaheim, CA, 7-11 June 1993, pp 191-197.

121. Schilke, P.W., Foster, A.D., Pepe, J.J. and Beltran, A.M., "Heat-resistant alloys and coatings play enabling roles in the development of more fuel-efficient stationary gas turbines", Advanced Materials and Processes, Vol. 4, 1992, pp 22-30.

122. Parker, D.W., "Thermal Barrier Coatings for Gas Turbines, Automotive Engines and Diesel Equipment", Materials and Design, Vol. 13, No. 6, 1992, pp 345-351.

123. Miller, R.A., Levine, S.R. and Hodge, P.E., "Thermal Barrier Coatings for Superalloys", Superalloys 1980, Proceedings of the Fourth International Syposium on Superalloys, Seven Springs Mountain Resort, Pennsylvania, USA, 21-25 September 1980, pp 473-480.

124. Borom, M.P. and Johnson, C.A., "Thermomechanical Behaviour and Phase Relationships of Plasma-Sprayed Zirconia Coatings", Surface and Coatings Technology, Vol. 54/55, 1992, pp 45-52.

125. Taylor, T.A., Appleby, D.L., Weatherill, A.E. and Griffiths, J., "Plasma-Sprayed Yttria-stabilized Zirconia Coatings: Structure-Property Relationships", Surface and Coatings Technology, Vol. 43/44, 1990, pp 470-480.

126. Taylor, T.A., "Thermal Properties and Microstructure of Two Thermal Barrier Coatings", Surface and Coatings Technology, Vol. 54/55, 1992, pp 53-57.

127. Brindley, W.J. and Miller, R.A., "Thermal Barrier Coating Life and Isothermal Oxidation of Low-Pressure Plasma-Sprayed Bond Coat Alloys", Surface and Coatings Technology, Vol. 43/44, 1990, pp 446-457.

128. James, A.S. and Matthews, A., "Developments in R.F. Plasma-Assisted Physical Vapour Deposition Partially Yttria-Stabilised Zirconia Thermal Barrier Coatings", Surface and Coatings Technology, Vol. 43/44, 1990, pp 436-445.

129. Joshi, S.V. and Srivastava, M.P., "On the Thermal Cycling Life of Plasma-Sprayed Yttria-Stabilised Zirconia Coatings", Surface and Coatings Technology, Vol. 56, 1993, pp 215-224.

130. Lih, W., Chang, E., Wu, B.C. and Chao, C.H., "The Effect of Pack-Aluminisation on the Microstructure of MCrAlY and the Performance of Thermal Barrier Coatings", Surface and Coatings Technology, Vol. 50, 1992, pp 277-288.

131. Pekshev, P.Y., Tcherniakov, S.V., Arzhakin, N.A. and Rutskin, V.V., "Plasma-Sprayed Multilayer Protective Coatings for Gas Turbine Units", Surface and Coatings Technology, Vol. 64, 1994, pp 5-9.

132. Nicholas, E.U. and Neal, P.A., Advanced Thermal Barrier Coated Superalloy Components, US Patent, Patent No. 5262245, 16 Nov. 1993.

133. Twigg, P.C. and Page, T.F., "The Temperature-Variant Hardness Response of Duplex TBCs", Thin Solid Films, Vol. 236, 1993, pp 219-224.

134. Sun, J.H., Chang, E., Wu, B.C. and Tsai, C.H., "The Properties and Performance of (ZrO_2-8wt.%Y_2O_3)/(chemically vapour-deposited Al Ọ)/(Ni-22wt%Cr-10wt.%Al-1wt.%Y) Thermal Barrier Coatings", Surface and Coatings Technology, Vol. 58, 1993, pp 93-99.

135. Petitbon, A., Boquet, L. and Delsart, A., "Laser Surface Sealing and Strengthening of Zirconia Coatings", Surface and Coatings Technology, Vol. 49, 1991, pp 57-61.

136. Jamarani, F., Korotkin, M., Lang, R.V., Ouellette, M.F., Yan, K.L., Bertram, R.W. and Parameswaran, V.R., "Compositionally Graded Thermal Barrier Coatings for High Temperature Aero Gas Turbine Components", Surface and Coatings Technology, Vol. 54/55, 1992, pp 58-63.

137. Ananthapadmanabhan, P.V., Sreekumar, K.P., Muraleedharan, K.V. and Venkatramani, N., "Plasma-Sprayed Composite Coatings for High Temperature Applications", Surface and Coatings Technology, Vol. 49, 1991, pp 62-66.

138. Qadri, S.B., Skelton, E.F., Kim, C., Harford, M.Z. and Lubitz, P., "Electron-beam Deposition of Zirconia Films stabilized in High Temperature Phases by Different Oxides", Surface and Coatings Technology, Vol. 49, 1991, pp 67-70.

139. Lih, W., Chang, E., Chao, C.H. and Tsai, M.L., "Effect of Pre-Aluminization on the Properties of ZrO_2-8wt.% Y_2O_3/Co-29Cr-6Al-1Y Thermal Barrier Coatings", Oxidation of Metals, Vol. 38, Nos. 1/2, 1992, pp 99-124.

140. Fritscher, K., Ratzer-Scheibe, H.J., Wirth, G. and Winstone, M.R., "Burner Rig Tests of Coated Single Crystal Superalloys at 1100^{0}C", High Temperature Materials for Power Engineering 1990, Proceedings of a Conference held in Ligièr, Belgium, September 1990, pp 1239-1248.

141. Peichl, L. and Johner, G., "High-Temperature Behaviour of Different Coatings in High-Performance Gas Turbines and Laboratory Tests", J. Vac. Technol. A, Vol. 4, No. 6, 1986, pp 2538-2592.

142. Swindels, N. and Rhys-Jones, T.N., "The High Temperature Corrosion of a Commercial Aluminide Coating on IN738-LC and MAR-M002 at 700^{0}C and 830^{0}C", Corrosion Science, Vol. 25, N0. 7, 1985, pp 559-576.

143. Russo, S.G., "Field Evaluation of Six Protective Coatings Applied to T-56 Turbine Blades after 2500 hours of Engine use", Department of Defence, Defence Science and Technology Organisation, Aeronautical Research Laboratory, Melbourne, Australia, Technical Report No. 27, April 1993, pp 1-17.

144. Cocking, J.L., Richards, P.G. and Johnston, G.R., "Comparative Durability of Six Coating Systems on First-Sage Gas Turbine Blades in the Engines of a Long- Range Maritime Patrol Aircraft", Surface and Coatings Technology, Vol. 36, 1988, pp 37-47.

145. Roode, M.V. and Hsu, L., "Evaluation of the Hot Corrosion Protection of Coatings for Turbine Hot Section Components", Surface and Coatings Technology, Vol. 37, 1989, pp 461-481.

146. Wood, J.H. and Swede, S.T., "Comparison of Coating Performance and Degradation Modes in Heavy-duty Land-based Gas Turbines", Surface and Coatings Technology, Vol. 61, 1993, pp 1-5.

147. Meetham, G.W., "Use of Protective Coatings in Aero Gas Turbine Engines", Materials Science and Technology, Vol, 2, 1986, pp 290-294.

148. Malik, M., Morbioli, R. and Huber, P., "The Corrosion Resistance of Protective Coatings", High Temperature Alloys for Gas Turbines 1982, Proceedings of a Conference held in Liège, Belgium, 4-6 October 1982, pp 87-98.

149. Godlewski, K. and Godlewski, E., "Effect of Chromium on the Protective Properties of Aluminides", Oxidation of Metals, Vol. 26, Nos. 1/2, 1986, pp 125-138.

150. Cocking, J.L., Johnston, G.R. and Richards, P.G., "Protecting Gas Turbine Components- The Relative Durability of a Conventional and a Platinum-Modified Aluminide Coating", Platinum Metals Rev., Vol. 29, No. 1, 1985, pp 17-26.

151. Gobel, M., Rahmel, A. and Schutze, M., "The Isothermal-Oxidation Behaviour of Several Nickel-Base Single -Crystal Superalloys With and Without Coatings", Oxidation of Metals, Vol. 39, Nos. 3/4, 1993, pp 231-261.

152. Streiff, R. and Boone, D.H., "Hot Corrosion Behaviour of Platinum Modified Coatings", 10th ICMC, Vol. 4, Sessions 14-19 held in Madras, India, 7-11 Nov. 1987, pp 3699-3707.

153. Meier, G.H. and Pettit, F.S., "High-Temperature Corrosion of Alumina-Forming Coatings for Superalloys", Surface and Coatings Technology, Vol. 39/40, 1989, pp 1-17.

154. Deb, P., Boone, D.H. and Manley, T.F., "Surface Instability of Platinum Modified Aluminide Coatings During 1100^{0}C Cycle Testing", J. Vac. Sci. Technol. A, Vol. 5, No. 6, Nov/dec 1987, pp 3366-3372.

155. Farrell, M.S., Boone, D.H. and Streiff, R., "Oxide Adhesion and Growth Characteristics on Platinum-Modified Aluminide Coatings", Surface and Coatings Technology, Vol. 32, 1987, pp 69-84.

156. Goebel, J.A., Barkalow, R.H. and Pettit, F.S., "The Effects Produced by Platinum in High Temperature Metallic Coatings", Report 79-40, Metals and Ceramics Information Centre, Colombus, Ohio, USA, 1979, pp 165-185.

157. Tawancy, H.M., Abbas, N.M. and Rhys-Jones, T.N., "Effect of Substrate Composition on the Oxidation Behaviour of Platinum-Aluminized Nickel-Base Superalloys", Surface and Coatings Technology, Vol. 54/55, 1992, pp 1-7.

158. Wu, W.T., Rahmel, A. and Schorr, M., "Role of Platinum in the Na_2SO_4-Induced Hot Corrosion Resistance of Aluminde Diffusion Coatings", Oxidation of Metals, Vol. 22, Nos. 1/2, 1984, pp 59-81.

159. Fountain, J.G., Golightly, F.A., Stott, F.H. and Wood, G.C., "The Influence of Platinum on the Maintenance of alpha-Al_2O_3 as a Protective Scale", Oxidation of Metals, Vol. 10, No. 5, 1976, pp 341-345.

160. Cooper, S.P. and Strang, A., "High Temperature Stability of Pack Aluminde Coatings on IN738LC",High Temperature Alloys for Gas Turbines 1982, Proceedings of a Conference held in Liège, Belgium, 4-6 October 1982, pp 249-260.

161. Meelu, M.C. and Loretto, M.H., "Development of High-Temperature Corrosion-Resistant Composite Coatings on Gas Turbine Hot end Components"", Materials and Designs, Vol. 14. No. 1, 1993, pp 53-55.

162. Nicholls, J.R., Lawson, K.J., Al Yasiri, L.H. and Hancock, P., "Vapour Phase Alloy Design of Corrosion-Resistant Overlay Coatings", Corrosion Science, Vol. 35, Nos. 5-8, 1993, pp 1209-1223

163. Gale, W.F., Totemeier, T.C., Whitehead, A.J. and King, J.E., "Microstructural Stability of Aluminide Coatings in Single Crystal Nickel-Base Superalloys", Surface Engineering, Vol. 1, Fundamentals of Coating Engineering, 1993, pp 45-66

164. Gale, W.F. and King, J.E., " Microstructural Degradation of Aluminide Coatings on Single Crystal Nickel Based Superalloys During High Temperature Exposure", Materials Science and Technology, Vol. 9, Sept. 1993, pp 793-798

165. Gale, W.F. and King, J.E., "Microstructural Development in Aluminide Diffusion Coatings on Nickel-Base Superalloy Single Crystals", Surface and Coatings Technology, 54/55, 1992, pp 8-12

166. Abraimov, N.V., "Effect of Composition and Structure of Aluminide Coatings on Their Plasticity", Protective Coatings on Metals, Vol. 12, 1986, pp 51-53

167. Wood, M.I. and Restall, J.E., "The Mechanical Properties of Coated Nickel Based Superalloy Single Crystal", High Temperature Alloys for Gas Turbines and Other Applications 1986, Proceedings of a Conference held in Liège, Belgium, 6-9 October 1986, pp 1215-1226

168. Holmes, J.W. and McClintock F.A., "Influence of Thermal Fatigue on Hot Corrosion of an Intermetallic Ni-Aluminide Coating", Superalloys 1988, Proceedings of the Sixth International Symposium on Superalloys, Seven Springs Mountain Resort, Pennsylvania, USA, 18-22 September 1988, pp 855-864.

169. Aghion, E., Walker, M. and Comins, N., "HTLCF Failure of Coated Nickel-Base Superalloy in H_2S Containing Atmosphere", Aspects of High Temperature Deformation and Frature in Crystalline Materials, Proceedings of the 7th JIM International Symposium, Nagoya, Japan, 28-31 July 1993, pp 577-582

170. Yoshiba, M., "Effect of Hot Corrosive Environment on the Mechanical Performance of Superalloys and Coating Systems", Aspects of High Temperature Deformation and Frature in Crystalline Materials, Proceedings of the 7th JIM International Symposium, Nagoya, Japan, 28-31 July 1993, pp 569-576

171. Czech, N., Eßer, W. and Schmitz, F., "Effect of Environment on Mechanical Properties of Coated Superalloys and Gas Turbine Blades", Materials Science and Technology, Vol. 2, March 1986, pp 244-249

172. Kim, S. and Weertman, J.R., "Investigation of Microstructural Changes in a Ferritic Steel Caused by High Temperature Fatigue", Metallurgical Transactions, Vol. 19A, 1988, pp 999-1007.

173. Gabb, T.P. and Dreshfiled, R.L., "Superalloy Data", Superalloys II, John Wiley and Sons, New York, 1987, pp 575-597.

174. Massalski, T.B., Murray, J.L., Bennett, L.H. and Baker, H., "Binary Alloy Phase Diagrams", American Society for Metals, August 1987, Metals Park, Ohio, USA.

175. American Society for Metals, "Metals Handbook, Volume 13, Corrosion", 9th Ed., Metals Park, Ohio, USA.